

Quantum dissipation and entanglement generation in photonic systems

Inauguraldissertation

zur

Erlangung des akademischen Grades eines

Doktors der Naturwissenschaften
(Dr. rer. nat.)

der

Mathematisch-Naturwissenschaftlichen Fakultät

der

Ernst-Moritz-Arndt-Universität Greifswald

vorgelegt von

Daniel Pagel

geboren am 18. März 1986

in Schwerin

Greifswald, 7. Juli 2015

Dekan: Prof. Dr. Klaus Fesser

1. Gutachter: Prof. Dr. Holger Fehske

2. Gutachter: Prof. Dr. Ulrich Zülicke

Tag der Disputation: 19. Oktober 2015

Contents

1	Summary	1
1.1	Introduction	1
1.2	Entanglement generation in short-time dynamics	2
1.3	Evolution of non-thermal preparations towards stationary states	9
1.4	Fluctuations and entanglement in the stationary state	13
1.5	Conclusions	19
2	Thesis Articles	21
2.1	Article I: Strongly entangled light from planar microcavities	23
2.2	Article II: Multipartite entangled light from driven microcavities	33
2.3	Article III: Equilibration and thermalization of the dissipative quantum harmonic oscillator in a nonthermal environment	43
2.4	Article IV: Nonequilibrium quantum fluctuation relations for harmonic systems in nonthermal environments	57
2.5	Article V: Nonclassical light from few emitters in a cavity	77
2.6	Article VI: Entangled light from driven dissipative microcavities	87
	Bibliography	99
	Scientific Contributions	101
	Declaration	103
	Acknowledgement	105

1 Summary

1.1 Introduction

This thesis deals with different quantum-mechanical and quantum-statistical methods as well as their application to problems in quantum optics. The development of these methods was motivated by the requirement to study dissipation in quantum optics [1, 2], e.g., for the construction of quantum computers [3–6]. Perfect control over the system state is needed, which is hard to realise because the necessary quantum coherence rapidly decays [7]. This decoherence is induced by the coupling of the system to reservoirs yielding modified system dynamics [8]. Recent experimental progress in the realisation of quantum computers shows, that the baths sometimes have to be treated as nonthermal environments [9–11].

The traditional modelling of decoherence through coupling of the microscopic system to environmental degrees of freedom has been focussed on thermal reservoirs [2, 8]. Nevertheless, structured nonequilibrium baths may lead to new and interesting phenomena such as the generation of an electrical current through the system that is induced by heat gradients [12, 13]. Alternatively, the open system may be used as an apparatus that measures properties of the environment [14].

The characteristics of the reservoir are reflected by the fluctuating forces that alter the dynamics of the open system [15]. In particular, the evolution becomes nonunitary because the fluctuating forces lead to damping of the system. The consequent loss of information, i.e., the transfer of quantum coherence into the surroundings, has to be suppressed for the construction of quantum computers.

The fundamental resource for quantum computation is quantum entanglement [7, 16–18], a kind of correlation between subsystems, that cannot be interpreted in terms of classical joint probabilities [19]. Especially in the multipartite situation with more than two subsystems, these nonclassical correlations exist in various forms. The most elementary examples of nonequivalent forms are given by Bell states in bipartite settings [20] and GHZ or W states in the multipartite case [21, 22].

The detection of entanglement is usually done with entanglement witnesses [23, 24]. A witness is an observable and can hence be measured in experiments. It has a non-negative expectation value for separable states, but exhibits negativities for entangled ones. To quantify the amount of entanglement within the state of a system, one has to find a proper entanglement measure [25–27]. The construction of entanglement measures from witnesses is possible, but requires the solution of an optimisation problem. Such a solution is already known for bipartite systems [27, 28], but remains open in the multipartite case [29].

Despite the experimental progress, the generation and control of entangled states is still a challenging task. From practical points of view an optical realisation in photonic systems is usually preferred. Common approaches are based on parametric down conversion in nonlinear crystals [30–32] or biexciton decay in quantum dots [33, 34].

Another prominent example employs the strong coupling between cavity photons and excitons and their parametric interactions in two dimensional semiconductor microcavities [35–38]. These systems can generate light entangled in polarisation, frequency, or photon number [39–43].

In this thesis we study the interplay between quantum dissipation and quantum entanglement generation in photonic systems (see Fig. 1). First, we show that semiconductor microcavities serve as sources of entangled light. Entanglement arises at short times because the different parametric scattering processes between cavity photons and semiconductor excitons are indistinguishable. Specifically, we demonstrate how bipartite branch entanglement and multipartite entangled photons in W states can be generated. We study the fundamental processes within the bosonic picture of interacting polaritons [40, 44] and analyse the entanglement properties using the Schmidt number [28, 45] and entanglement witnesses. At later times, dephasing of quantum states during the propagation of entangled light through media leads to a decrease of the available amount of entanglement.

Second, we study the dissipative dynamics of the quantum harmonic oscillator as a generic open system coupled to a harmonic oscillator bath. Because of the linearity of this model, the central oscillator density matrix can be constructed through evaluation of linear expectation values and variances of the position and momentum operators. The initial preparation enters only the initial expectation values such that we can allow for general initial bath preparations. Our focus is on the long-time behaviour of the central oscillator and we show that equilibration is generic and prevented only in situations where undamped oscillations exist. The additional requirements for thermalisation of the central oscillator are formulated as a hierarchy of conditions. While it is true that equilibration occurs through dephasing of quantum states, the results obtained for the dissipative oscillator go beyond the scope of arguments related to ensemble averages.

Third, we analyse the stationary states of three different photonic systems. The stationary state of the dissipative harmonic oscillator is shown to obey a generalised nonequilibrium fluctuation dissipation relation. We identify regimes of nonclassical light emission from few emitters in a cavity and emphasise that the usual quantum optical treatment entirely fails at predicting regimes of different photon statistics. The light emitted from a continuously pumped semiconductor microcavity is proven to be entangled even at infinitely long times. These studies are based on the computation of correlation functions, which requires methods from quantum optics and open systems.

1.2 Entanglement generation in short-time dynamics

We start with the description of parametric scattering in semiconductor microcavities. The exciting laser field with frequency near the fundamental band gap of the semiconductor coherently generates electron-hole pairs (excitons). The exciton motion is dominated by the Coulomb interaction and leads to scattering between the mixed exciton-photon modes (polaritons). Our goal is the characterisation of particular parametric scattering processes that lead to the generation of internal polariton entanglement (articles I and II).

The polariton motion leads to an ultrafast electric polarisation as a source of light that is emitted by the microcavity. The emitted photons serve as a probe of the internal

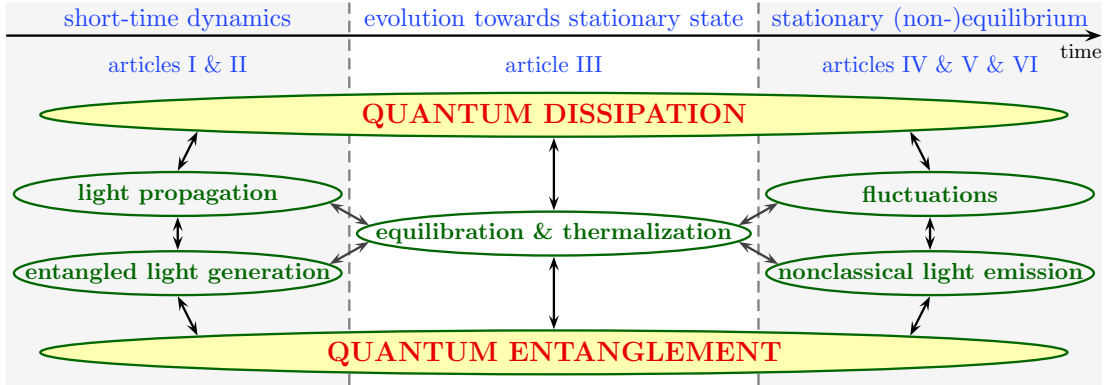


Fig. 1: Illustration of the interplay between quantum dissipation and entanglement generation. The physical aspects studied in this thesis are printed in green ellipses.

entanglement properties. To verify their entanglement we use the Schmidt number and entanglement witnesses.

The scattering of polaritons by other polaritons, phonons, and defects, as well as the propagation of the emitted light through media leads to polarisation decay and loss of optical coherence. While the losses through the cavity mirrors and the coupling to lattice vibrations are neglected, we study the decay of the initially available amount of entanglement when the light propagates through different linear media.

Parametric scattering in semiconductor microcavities We review the bosonic description of planar microcavities [40, 44]. This approach can easily be used to investigate polariton parametric scattering in momentum space [39].

The two-dimensional semiconductor system is described through an electron-hole Hamiltonian with Coulomb interaction [44]. A bound eigenstate of this Hamiltonian is an exciton with binding energy E_b and radius R_X . In the limit of low exciton density, the system may be treated as an ideal gas of bosons. Because there is a small but finite overlap of the exciton constituents, we have to include an effective repulsion between the fermionic exciton constituents. The mapping of the fermionic electron-hole Hamiltonian onto the bosonic exciton Hamiltonian is called the Usui transformation [46, 47]. The four-operator Coulomb terms transform into a sum of products of bosonic exciton operators to all orders. For the description of parametric scattering the Hamiltonian is truncated at the second order of the exciton density. The result includes the (two-dimensional) wave-vector dependent exciton kinetic energy $E_X(\mathbf{k})$ and all two-body interaction terms.

The excitons of the crystal are coupled to cavity photons with dispersion $E_C(\mathbf{k})$. Transformation of the dipole electron-hole-photon interaction Hamiltonian into the bosonic space yields a harmonic exciton-photon interaction and a saturation term accounting for the fermionic nature of the system [40, 44]. The coupling strength Ω_R of the harmonic exciton-photon interaction is called the Rabi frequency.

For the description of parametric scattering, the unitary Hopfield transformation [48] from semiconductor excitons and cavity photons to lower ($j = 1$) and upper ($j = 2$) polaritons $p_{j\mathbf{k}}$ with dispersions $E_j(\mathbf{k})$ is applied to the harmonic parts of the Hamiltonian.

This transformation leads to the polariton kinetic energy

$$H_P = \sum_{j,\mathbf{k}} E_j(\mathbf{k}) p_{j\mathbf{k}}^\dagger p_{j\mathbf{k}}, \quad (1)$$

and the polariton-polariton interaction

$$H_{PP} = \frac{1}{2} \frac{R_X^2}{A} \sum_{j_1, j_2, j_3, j_4} \sum_{\mathbf{k}, \mathbf{k}', \mathbf{q}} V_{\mathbf{k}, \mathbf{k}', \mathbf{q}}^{j_1 j_2 j_3 j_4} p_{j_1 \mathbf{k} + \mathbf{q}}^\dagger p_{j_2 \mathbf{k}' - \mathbf{q}}^\dagger p_{j_3 \mathbf{k}'} p_{j_4 \mathbf{k}}. \quad (2)$$

In this equation, A is the sample surface and the effective branch-dependent interaction potential $V_{\mathbf{k}, \mathbf{k}', \mathbf{q}}^{j_1 j_2 j_3 j_4}$ is given in Eq. (8) of article I.

The polariton dispersions $E_1(\mathbf{k})$ and $E_2(\mathbf{k})$ are schematically shown in Fig. 2 (solid lines) together with the dispersions $E_C(\mathbf{k})$ and $E_X(\mathbf{k})$ of the cavity photons and the excitons (dashed lines) for different values of the normalised detuning $\delta = [E_C(0) - E_X(0)]/(2\Omega_R)$. The strong coupling of exciton and cavity photon modes leads to the anticrossing of the polariton branches. The parameter $2\Omega_R$ determines the distance $E_2(\mathbf{k}) - E_1(\mathbf{k})$ at the crossing of exciton and cavity photon modes and is thus called polariton splitting. For large values of $|\mathbf{k}|$ the polariton modes are equal to the separated exciton and photon modes. For small $|\mathbf{k}|$, the strength of the exciton-photon mixing depends on the detuning δ .

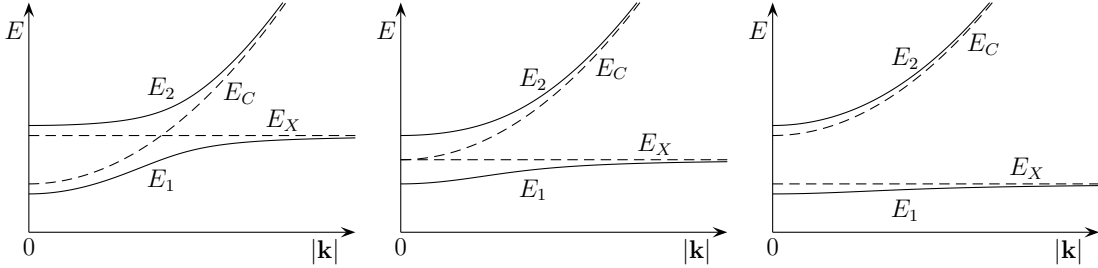


Fig. 2: Schematic dispersion relations of excitons, cavity photons, and lower and upper polaritons for (left) $\delta < 0$, (centre) $\delta = 0$, and (right) $\delta > 0$.

The idea for the generation of entanglement is, that the peculiar form of the polariton dispersions allows for energy and momentum conserving scattering processes between polaritons that lead to the generation of entangled polariton pairs. Because of the large photon component of the polaritons, these parametric processes can easily be stimulated by external pump lasers. We discussed two different pump configurations in articles I and II.

In the branch entanglement scheme of article I, a pump-pulse train, where all pump wave-vectors are aligned in the same direction but have different amplitudes, excites the upper polariton branch. This setup is illustrated for a single pump in the left part of Fig. 3. The pumped polaritons (solid black circles) scatter into states belonging to different branches (open black circles) and branch entanglement arises since both paths (indicated by the green lines) are indistinguishable. The total emission of this setup is visualised in the right part of Fig. 3, where the pumped mode (p, \mathbf{k}_p) is marked with a cross. The possible energy and momentum conserving scattering processes of two pumped polaritons into pairs of signal/idler polaritons lead to the two rings.

Entanglement arises at the crossings of these rings (the process shown in the left part of Fig. 3) and the entangled signal (s , \mathbf{k}_s) and idler (i , \mathbf{k}_i) modes are marked with crosses.

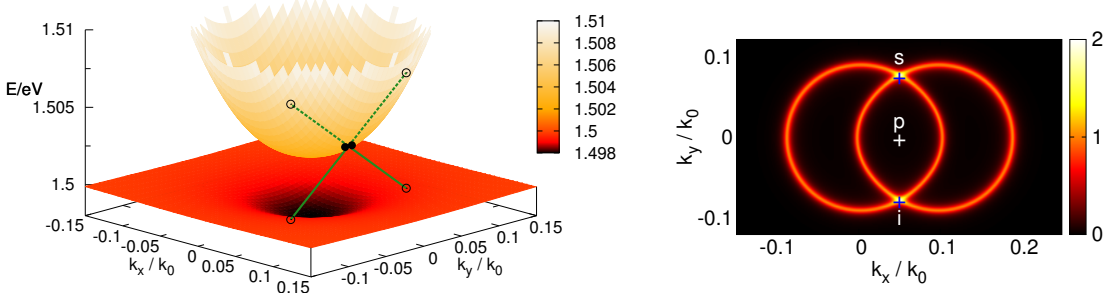


Fig. 3: Illustration of the branch entanglement generation in semiconductor microcavities. The left panel visualises the interbranch polariton pair scattering process that leads to entangled signal/idler polaritons. The right panel shows the emission of the system in momentum space.

A thorough theoretical description of these processes for a pump-pulse train of N individual pumps leads to the generation of N branch entangled polariton pairs in the state (see article I for details)

$$|\psi_N\rangle = \prod_{n=1}^N \left(\alpha_n p_{1\mathbf{k}_{sn}}^\dagger p_{2\mathbf{k}_{in}}^\dagger + \sqrt{1 - \alpha_n^2} p_{2\mathbf{k}_{sn}}^\dagger p_{1\mathbf{k}_{in}}^\dagger \right) |\text{vac}\rangle. \quad (3)$$

Here, $|\text{vac}\rangle$ denotes the polariton vacuum and $p_{j\mathbf{k}_{sn}}^\dagger$ ($p_{j\mathbf{k}_{in}}^\dagger$) creates a signal (idler) polariton in branch j that belongs to a scattering process driven by pump $n = 1, \dots, N$. The parameters α_n [see Eq. (18) of article I] depend on the properties of the semiconductor material. They influence the entanglement properties of $|\psi_N\rangle$. We have a product of true Bell states only if all $\alpha_n^2 = 1/2$. If one $\alpha_n^2 = 0$ or $\alpha_n^2 = 1$ the state of the corresponding polariton pair is separable, i.e., not entangled. In all other cases, each state within the product (3) is an entangled superposition of two product states.

For a single pump ($N = 1$), the violation of a corresponding Bell inequality can be quantified by the von Neumann entropy [49] $S = -\alpha_1^2 \ln \alpha_1^2 - (1 - \alpha_1^2) \ln(1 - \alpha_1^2)$ of the reduced signal polariton state. A true Bell state has $S = \ln 2$ and a separable state has $S = 0$. The value $S/\ln 2$ as a function of the normalised detuning δ and the ratio of polariton splitting to exciton binding energy $p_s = 2\Omega_R/E_b$ is plotted in Fig. 4. We remark that δ and p_s characterise the semiconductor material. The state described by Eq. (3) is a true Bell state on a specific line in the (δ, p_s) plane and for $p_s \rightarrow 0$. The state of the polariton pair is an entangled Bell-like state [20] with $S \in (0, \ln 2)$ for values of δ and p_s apart from these lines (see article I).

The second scenario presented in article II consists of four pumps with wave-vectors of equal amplitude that excite the lower polariton branch. The incident angles of all pumps are below the magic angle [36, 50], i.e., the scattering of two polaritons is suppressed, when they are generated by the same pump. Because the pumped lower polaritons can not scatter into the upper branch we can omit the upper polaritons in our description. In particular, we chose the four pump wave-vectors $\mathbf{k}_{p1} = (k_p, k_p)$,

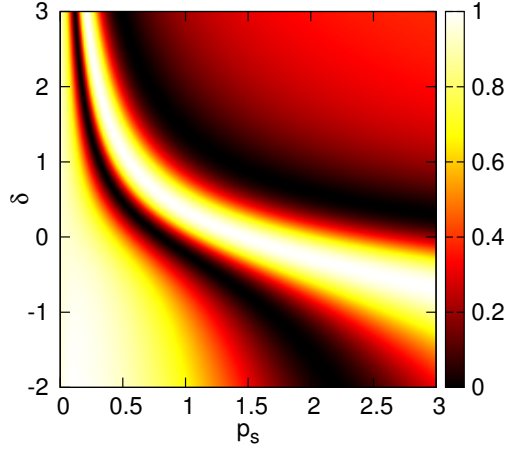


Fig. 4: Magnitude of $S/\ln 2$ in the (δ, p_s) plane for $N = 1$.

$\mathbf{k}_{p2} = (-k_p, k_p)$, $\mathbf{k}_{p3} = (-k_p, -k_p)$, and $\mathbf{k}_{p4} = (k_p, -k_p)$. The total emission for this scenario in momentum space is depicted in Fig. 5. Pair scattering processes of polaritons that are created by oppositely arranged (neighbouring) pumps with $|\mathbf{k}_{pn} + \mathbf{k}_{pm}| = 0$ ($|\mathbf{k}_{pn} + \mathbf{k}_{pm}| = 2k_p$) contribute to the circle(s) with radius $\sqrt{2}k_p$ (k_p). Because of the common idler mode at $\mathbf{k}_i = 0$, the four corresponding signal modes at $\mathbf{k}_{s1} = (0, 2k_p)$, $\mathbf{k}_{s2} = (-2k_p, 0)$, $\mathbf{k}_{s3} = (0, -2k_p)$, and $\mathbf{k}_{s4} = (2k_p, 0)$ are entangled. In the theoretical description (see article II), after taking the partial trace over the idler mode, the state of the signal modes emerges as

$$|\psi_W\rangle = \frac{1}{2}(|1, 0, 0, 0\rangle + |0, 1, 0, 0\rangle + |0, 0, 1, 0\rangle + |0, 0, 0, 1\rangle). \quad (4)$$

Here, $p_{1\mathbf{k}_{sn}}^\dagger |\text{vac}\rangle = |0, 1, 0, 0\rangle$ with the 1 being at the n th position. The state (4) is a four-partite entangled pure state, called the W state.

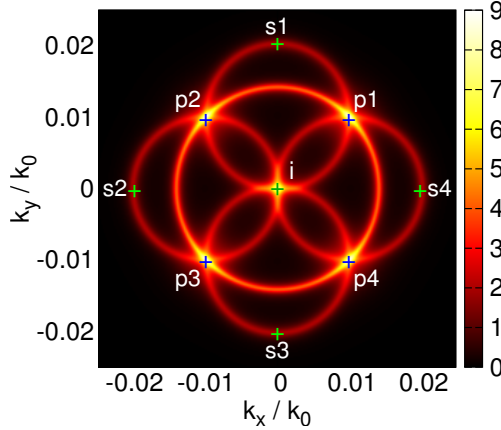


Fig. 5: Illustration of the microcavity emission for $N = 4$ and $k_p = 0.01k_0$.

Entanglement of emitted light To obtain the state of the emitted light we have to couple the intracavity polariton scattering dynamics to an extracavity field and determine the parametric luminescence. It is well known that there is a correspondence between the properties of the polaritons within the cavity and the emitted photons outside the cavity [38–40]. In particular, due to energy and momentum conservation, the emitted photon has both the energy and the in-plane momentum of the corresponding polariton. In addition, the emitted photons carry the internal polariton entanglement properties (see articles I and II), such that the states of the emitted photons are equal to the states (3) and (4).

To verify the bi- and multipartite entanglement of the emitted photons we use entanglement witnesses [23, 51]. The idea is to test if the state ρ under consideration is an element of a certain class of states. For example, the state ρ is entangled if and only if there exists a Hermitian operator L with the property [29, 52]

$$\langle L \rangle = \text{Tr} \rho L > f(L), \quad (5)$$

where $f(L) = f_{\text{sep}}(L) = \sup\{\langle \phi | L | \phi \rangle : |\phi\rangle \text{ separable state}\}$ is the maximum expectation value of L within the class of separable states [51]. Following this recipe, the choice $f(L) = f_r(L) = \sup\{\langle \phi | L | \phi \rangle : |\phi\rangle \text{ Schmidt rank } r \text{ state}\}$ leads to a condition for the bipartite state ρ to have a Schmidt number [28, 45] greater than r [52]. In the multipartite case we must distinguish between partially entangled (not fully separable) and fully entangled (not partially separable) states and the corresponding entanglement criteria are based on the functions $f_{\text{part}}(L) = \sup\{\langle \phi | L | \phi \rangle : |\phi\rangle \text{ partially separable state}\}$ and $f_{\text{full}}(L) = \sup\{\langle \phi | L | \phi \rangle : |\phi\rangle \text{ fully separable state}\}$ [29]. A witness can be constructed from $[f(L)\mathbb{I} - L]$, where \mathbb{I} denotes the identity operator.

The calculation of the different values of the function $f(L)$ is based on the solution of generalised eigenvalue equations [29, 52]. In the bipartite case the function $f_r(L)$ is determined from the Schmidt number eigenvalue equation

$$L|\psi_r\rangle = g|\psi_r\rangle + |\chi\rangle, \quad (6)$$

where $|\chi\rangle$ is a biorthogonal perturbation. The value g is the Schmidt number eigenvalue and the vector $|\psi_r\rangle$ is the Schmidt number eigenvector. The largest Schmidt number eigenvalue is the value of the function $f_r(L)$. Analogously, the values of the functions $f_{\text{part}}(L)$ and $f_{\text{full}}(L)$ in the N -partite case are calculated from the solution of separability eigenvalue equations $L|\psi\rangle = g|\psi\rangle + |\chi\rangle$, where $|\chi\rangle$ is an N -orthogonal perturbation. Now, g is the multipartite separability eigenvalue and $|\psi\rangle$ is the multipartite separability eigenvector. The largest multipartite separability eigenvalue determines the value of $f_{\text{full}}(L)$ and $f_{\text{part}}(L)$, respectively. We note that the value of the function $f_{\text{part}}(L)$ in general depends on the chosen decomposition of the combined Hilbert space and to obtain the value of the function $f_{\text{part}}(L)$ we have to consider all possible partial decompositions of the combined Hilbert space.

We use these relations for the states (3) and (4) of the emitted light in the two considered scenarios. For the frequency entangled photons in the state (3) we decompose the total Hilbert space into two parts containing the signal and idler photons, respectively. To determine the Schmidt number of the state $\rho = |\psi_N\rangle\langle\psi_N|$, we consider the projection $L = |\psi_N\rangle\langle\psi_N|$ and obtain $\langle L \rangle = \langle\psi_N|L|\psi_N\rangle = 1$. It can easily be shown, that the value of $f_r(L)$ is smaller than one, if there exist more than r values $\alpha_n \neq 0, 1$.

In conclusion, the considered pure state $|\psi_N\rangle$ in Eq. (3) has a Schmidt number of 2^N , in the general case that all $\alpha_n \neq 0, 1$ for $n = 1, \dots, N$. Considering the four mode W state $\rho = |\psi_W\rangle\langle\psi_W|$ from Eq. (4) and choosing $L = \rho$ we obtain $f_{\text{full}}(L) = 27/64$ and $f_{\text{part}}(L) = 3/4$. Because the left hand side of the entanglement criterion in Eq. (5) evaluates to one, we can prove partial and full entanglement of $|\psi_W\rangle$.

Propagation of entangled light Once the photons are emitted from the cavity, they are subject to the environment. The propagation of entangled light through media can be described by realistic loss models [53, 54]. This may include losses during the outcoupling of the field from the cavity [55], and the subsequent propagation through lossy media. Of special importance are turbulent media since they describe the typical propagation of light in the atmosphere [56].

A propagation of light in different linear media leads to dephasing, i.e., the decrease of the initially available amount of entanglement (see article I). The argument is, that the different dispersion relations of the media lead to different optical path lengths. To obtain the photon state measured by a detector at a fixed distance from the microcavity, one has to average over the different arrival times. In practice, the resulting statistics depends on the details of the dispersive properties of the different media representing the propagation channels. Such a treatment must be based on an experimental analysis of the used channels. To demonstrate the basic principles, we suppose an equally distributed difference of the arrival times in the interval $[t_1, t_2]$. The Schmidt number of the resulting state as a function of $\Delta t = t_2 - t_1$ for different values of the normalised detuning δ and the ratio of polariton splitting to binding energy p_s is given in Fig. 4 of article I. Since the microcavity is pumped by three beams with different wave-vectors aligned in the same direction, the maximal possible Schmidt number of the emitted radiation is $2^3 = 8$. An increasing dephasing due to the increase of Δt , yields a decreasing Schmidt number. The jumps of the value of the guaranteed Schmidt number from r to $r - 1$ occur for values of Δt where the corresponding witness fails to identify a Schmidt number larger than r . For a fixed value of Δt the Schmidt number strongly depends on the properties, δ and p_s , of the planar microcavity. For $\Delta t \rightarrow \infty$ the state becomes separable.

Our description of the short-time dynamics of semiconductor microcavities captures parametric scattering as the mechanism to generate entangled light. The entanglement properties of the emitted light can be tuned by varying the parameters of the semiconductor material. Dephasing, e.g., during the unitary propagation of light through different linear media, diminishes the initially available amount of entanglement. Nevertheless, because our approach neglects the losses through the cavity mirrors and the coupling to lattice vibrations, the inclusion of quantum dissipation is needed for a description of the emission under realistic experimental conditions. An interesting question is, if the entanglement generation in semiconductor microcavities can survive in the long-time limit when the system is coupled to the environment.

1.3 Evolution of non-thermal preparations towards stationary states

We now turn to the dissipative dynamics at long times. Our focus is on equilibration as the irreversible evolution of a system towards a stationary state as well as on the additional requirements for thermalisation. General arguments relate equilibration to dephasing by noting that the nondiagonal density matrix elements $\rho_{m,n}(t)$ in the system energy eigenbasis $H|n\rangle = E_n|n\rangle$ oscillate $\propto e^{i(E_m - E_n)t}$ [57–61]. In the thermodynamic limit, one can expect that only the diagonal terms $m = n$ survive for $t \rightarrow \infty$, such that a stationary state is obtained. Although this argument explains the origin of equilibration, it neither makes a statement about equilibration of a finite part of the total system nor about the emergence of a thermal state out of an initial preparation. Here, we study the microscopic model of the dissipative quantum harmonic oscillator [62–67] with general nonthermal preparations of the harmonic oscillator bath. Because this model allows for an exact analytical solution we can explicitly study the reason why equilibration of the central oscillator may fail and discuss the stationary state in the long-time limit. More details can be found in article III.

Prerequisite for equilibration The Hamiltonian for the dissipative quantum harmonic oscillator, $H = H_S + H_B + H_{SB}$, is the sum of the contribution of the central oscillator,

$$H_S = \frac{1}{2} \left(P^2 + \Omega^2 Q^2 \right), \quad (7)$$

the contribution of the harmonic oscillator bath,

$$H_B = \frac{1}{2} \sum_{\nu=1}^N \left(P_\nu^2 + \omega_\nu^2 Q_\nu^2 \right), \quad (8)$$

and the linear interaction term

$$H_{SB} = Q \sum_{\nu=1}^N \lambda_\nu Q_\nu. \quad (9)$$

In these expressions, the position and momentum operators Q_ν, P_ν fulfil the canonical commutation relation $[Q_\mu, P_\nu] = i\delta_{\mu\nu}$. The size of the coupling constants λ_ν is restricted by a positivity condition (see Eq. 8 of article III). It guarantees that the normal modes of the total Hamiltonian H have real frequencies, such that H is bounded from below [68]. We assume factorising initial states $\rho(0) = \rho_S(0) \otimes \rho_B(0)$ corresponding to the choice of isolated systems that are brought into contact at $t = 0$. We keep the initial bath distribution $\rho_B(0)$ arbitrary and do not necessarily assume thermal equilibrium.

The central oscillator density matrix $\rho_S(t)$ is obtained through solution of the Heisenberg equations of motion for the operators $Q(t)$ and $P(t)$. The central piece of information is the solution of the classical equation of motion

$$\ddot{u}(t) = -\Omega^2 u(t) + \int_0^t K(t - \tau) u(\tau) d\tau. \quad (10)$$

In this homogeneous integro-differential equation the damping kernel $K(t)$ emerges from the coupling to the bath as a combination of coupling constants and bath frequencies [Eq. (12) of article III]. The relevant solution $u(t)$ follows through Fourier transformation of a function $F(\omega)$, which has poles at the eigenfrequencies of the total system plus environment. Hence, for a finite number N of bath oscillators, $u(t)$ is a quasiperiodic function. Equilibration of the central oscillator requires the thermodynamic limit $N \rightarrow \infty$. In this limit, the characteristics of the bath are reflected by the bath spectral function $\gamma(\omega)$, which, for finite N , is a combination of coupling constants and bath oscillator frequencies [see Eqs. (28)–(30) of article III]. The Fourier transform $F(\omega)$ of the function $u(t)$ then follows from the analytic continuation $\Gamma(z)$ of the bath spectral function $\gamma(\omega)$ into the upper half of the complex plane,

$$F(z) = \left(\Omega^2 - z^2 + \Gamma(z) \right)^{-1}. \quad (11)$$

Because the only stationary solution of equation (10) is $u(t) \equiv 0$, the prerequisite for equilibration of the central oscillator is the condition $u(t) \rightarrow 0$ for $t \rightarrow \infty$, which is fulfilled if and only if $F(z)$ has no isolated poles.

As an explicit example for the violation of the prerequisite $u(t) \rightarrow 0$ for $t \rightarrow \infty$ we consider the infinite chain of harmonic oscillators (see Fig. 6) [69–73]. Oscillators in the right ($n \geq 1$) and left ($n \leq -1$) half of the chain, with frequency Ω_b , are coupled to their neighbours ($n \pm 1$) with spring constant k_b . They form the harmonic oscillator bath for the central oscillator at $n = 0$, with oscillator frequency Ω and coupling k to the oscillators at $n = \pm 1$. We introduce the dimensionless model parameters $\Omega_r = \Omega/\Omega_b$, $\kappa = 2k_b/\Omega_b^2$, and $\kappa_b = 2k/\Omega_b^2$ with $0 \leq \kappa_b \leq 1$, and use the normalised quantity $\bar{\omega} = \omega/\Omega_b$. In the thermodynamic limit, the bath spectral function emerges as

$$\gamma(\bar{\omega})/\Omega_b^2 = \frac{2}{\pi} \frac{\kappa^2}{\kappa_b^2} \sqrt{\kappa_b^2 - (1 - \bar{\omega}^2)^2} \quad \text{for} \quad |1 - \bar{\omega}^2| \leq \kappa_b. \quad (12)$$

Important is that $\gamma(\bar{\omega}) = 0$ for $|1 - \bar{\omega}^2| > \kappa_b$. We note that we assume identical initial conditions for both sides of the chain and thus exclude the possibility of stationary non-equilibrium states with finite heat flow between the right and left half-infinite chain.

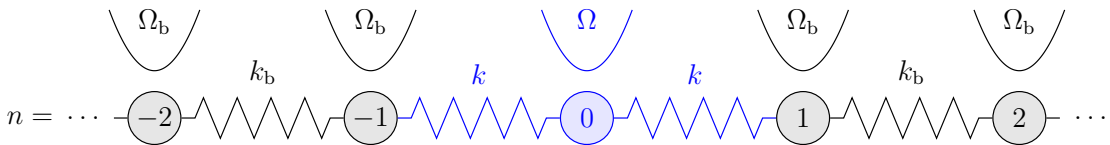


Fig. 6: Sketch of the infinite linear harmonic chain.

According to Eq. (11), to exclude the possibility of isolated poles of $F(z)$, we have to compare the functions $\bar{\omega}^2 - \Omega_r^2$ and $\text{Re} \Gamma(\bar{\omega} + i0^+)$ in regions where $\text{Im} \Gamma(\bar{\omega} + i0^+) = 0$. From the qualitative behaviour of $\Gamma(\bar{\omega} + i0^+)$, shown in Fig. 7, we first deduce that the function $\bar{\omega}^2 - \Omega_r^2$ must have a slope larger than that of $\text{Re} \Gamma(\bar{\omega} + i0^+)$ as well as a root within the interval $\bar{\omega} \in [\sqrt{1 - \kappa_b}, \sqrt{1 + \kappa_b}]$. This immediately yields the basic restrictions

$$\kappa \leq \kappa_b \quad \text{and} \quad |1 - \Omega_r^2| \leq \kappa_b \quad (13)$$

for the absence of isolated poles of $F(z)$. The second inequality guarantees that the central oscillator frequency Ω_r fulfils $\gamma(\Omega_r) > 0$. If this is fulfilled, equilibration is always possible for sufficiently small κ . Since $\kappa_b \leq 1$, it restricts the admissible parameters to the rectangle $(\kappa_b, \Omega_r^2) \in [0, 1] \times [0, 2]$. The admissible parameter combinations for equilibration of the harmonic chain that follow from a closer inspection of the involved quantities are shown in Fig. 8 [see Eq. (77) of article III].

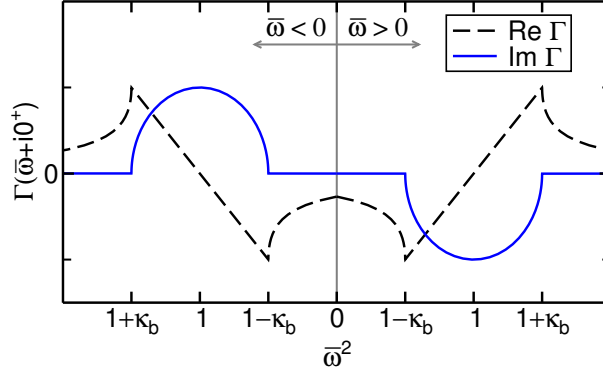


Fig. 7: Real (black dashed curve) and imaginary (solid blue curve) part of $\Gamma(\bar{\omega} + i0^+)$.

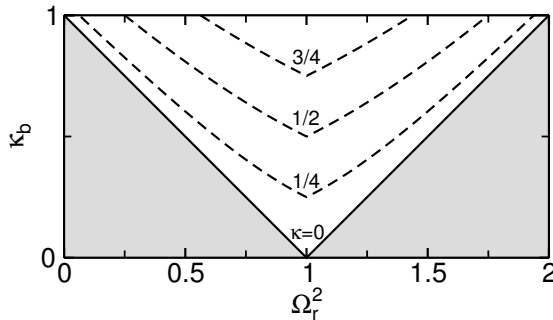


Fig. 8: Diagram of the admissible parameter space for equilibration of the infinite linear chain. The white triangular region above the solid black lines is the maximal set of allowed parameter combinations. Outside of this region an isolated pole exists even in the weak damping limit $\kappa \rightarrow 0$. For $\kappa > 0$, the region of admissible parameters shrinks as depicted by the dashed black curves.

In summary, the condition $u(t) \rightarrow 0$ for $t \rightarrow \infty$ is the prerequisite for equilibration of the central oscillator. In the weak damping limit, this condition is equivalent to $\gamma(\Omega) > 0$ (taking the thermodynamic limit for granted). This expresses the basic fact that equilibration occurs through energy exchange with the environment, which is not possible for an isolated oscillator with $\gamma(\Omega) = 0$. We note that a small value of $\gamma(\Omega)$ can result in long transients that prevent equilibration over the observation time.

Quantum equilibration and the conditions for thermalisation The construction of the propagating function, that maps any initial state $\rho_S(0)$ onto $\rho_S(t)$, can be done using only that an initial Gaussian state of the joint central oscillator and bath system remains a Gaussian state during time evolution with the Hamiltonian H . This

construction is possible in three steps (see article III). Assuming that the corresponding classical solution $u(t)$ is known, the dynamics of the central oscillator operators $Q(t)$ and $P(t)$ is calculated. This allows for the evaluation of linear expectation values and variances of the position and momentum operators in the thermodynamic limit. The parameters of the most general ansatz for the propagating function, that maps an initial Gaussian state $\rho_S(0)$ onto a Gaussian state $\rho_S(t)$ for $t \geq 0$, are fully specified through the mapping of linear and quadratic expectation values. The resulting propagating function is valid for arbitrary initial states $\rho_S(0)$. In this way, the full solution for the dynamics of the central oscillator is obtained without explicit consideration of non-Gaussian $\rho_S(t)$. We note that the propagating function is usually calculated in the position representation [65], which obscures the clear formal structure obtained using the Wigner function [74] in a conveniently simple derivation (see article III).

The result for the propagating function allows us to study the behaviour of the central oscillator density matrix $\rho_S(t)$ in the long-time limit $t \rightarrow \infty$. Assuming that the prerequisite $u(t) \rightarrow 0$ for $t \rightarrow \infty$ (taking the thermodynamic limit for granted) is fulfilled, the position and momentum expectation values vanish in the long-time limit (see Sec. IV.A of article III). In addition, the central oscillator variances converge to stationary values. Specifically, the mixed variance vanishes and the stationary position and momentum variances Σ_{QQ}^∞ and Σ_{PP}^∞ are fully determined by the frequency resolved energy distribution $\check{\mathcal{E}}(\omega)$ of the initial bath state. Equilibration of the central oscillator then follows from the observation that the long-time limit of the propagating function is a Gaussian state. In other words, the stationary state ρ_S^∞ is Gaussian and depends through the values Σ_{QQ}^∞ and Σ_{PP}^∞ on the initial bath state but is independent from the initial central oscillator state. This proves equilibration for general initial central oscillator states. In particular, the stationary state is Gaussian also for non-Gaussian initial states.

Because only Σ_{QQ}^∞ and Σ_{PP}^∞ are non-zero, the asymptotic stationary state ρ_S^∞ can be interpreted as the thermal equilibrium state of some harmonic oscillator. The effective oscillator frequency Ω_∞ and temperature T_∞ associated with ρ_S^∞ are

$$\Omega_\infty^2 = \frac{\Sigma_{PP}^\infty}{\Sigma_{QQ}^\infty}, \quad T_\infty = \frac{\Omega_\infty}{2} \operatorname{arcoth}^{-1} \left(2 \sqrt{\Sigma_{QQ}^\infty \Sigma_{PP}^\infty} \right). \quad (14)$$

Generally, Ω_∞ is not equal to the central oscillator frequency Ω . The condition $\Omega_\infty = \Omega$ is equivalent to equipartition of kinetic and potential energy $\langle P^2 \rangle = \Sigma_{PP}^\infty = \Omega^2 \Sigma_{QQ}^\infty = \Omega^2 \langle Q^2 \rangle$, which is achieved in the limit of weak damping. Then,

$$\Omega_\infty^{(\text{WD})} = \Omega, \quad T_\infty^{(\text{WD})}(\Omega) = \frac{\Omega}{2} \operatorname{arcoth}^{-1} \frac{2\check{\mathcal{E}}(\Omega)}{\Omega}, \quad (15)$$

such that the stationary state ρ_S^∞ is a thermal equilibrium state of the central oscillator. The temperature $T_\infty(\Omega)$ is determined by the energy $\check{\mathcal{E}}(\Omega)$ of the bath oscillator at frequency Ω in the initial state, but it still is a function of Ω . Full thermalisation requires that T_∞ is independent of Ω . According to Eq. (15) this leads to the condition

$$\check{\mathcal{E}}(\omega) = \frac{\omega}{2} \coth \frac{\omega}{2T_\infty}. \quad (16)$$

Note that this is a condition on the sum of initial bath kinetic and potential energies, and not on the individual functions. Therefore, any initial bath preparation that fulfils

condition (16) results in the same stationary state as the thermal bath at the respective temperature. Thermalisation is well possible in non-thermal environments, even those far from thermal equilibrium.

In summary, we have a hierarchy of conditions for equilibration and thermalisation: The central oscillator equilibrates whenever $u(t) \rightarrow 0$ for $t \rightarrow \infty$. The stationary state is always a Gaussian and thermal state. Equipartition of kinetic and potential energy occurs precisely at weak damping. The asymptotic temperature T_∞ is independent of the central oscillator frequency under the additional condition (16) on $\check{\mathcal{E}}(\omega)$.

1.4 Fluctuations and entanglement in the stationary state

So far, we considered the dynamics of bosonic systems for short times and their asymptotic approach to equilibrium. Combining these results, we analyse the properties of the stationary state with respect to fluctuations, nonclassicality, and entanglement. This analysis requires the calculation of different correlation functions.

Generalised nonequilibrium fluctuation relation for the dissipative oscillator

Fluctuation relations [75–78] build on the connection between the response of a physical system in thermal equilibrium to a weak externally applied force and the fluctuations in the system without the external force. In linear response theory this relation is expressed in form of the quantum fluctuation-dissipation theorem [79–83]

$$\Psi(\omega) = \frac{1}{2i} \coth\left(\frac{\omega}{2T}\right) \Phi(\omega), \quad (17)$$

which relates the Fourier transform $\Psi(\omega)$ of the symmetric equilibrium correlation function of an observable to the Fourier transform $\Phi(\omega)$ of the (antisymmetric) response function of this observable. Since the relation (17) is valid for a system in thermal equilibrium at temperature T only, systematic advancements are necessary.

Having in mind the hierarchy of conditions for equilibration and thermalisation of the dissipative oscillator, the validity of related fluctuation relations in case of nonthermal equilibrium or for stationary nonequilibrium states has to be scrutinised. Both issues are addressed for the dissipative harmonic oscillator in article IV. The latter situation requires the extension of the dissipative oscillator model to multiple baths to allow for finite heat flows in the stationary state. Here, we consider the generalisation of the fluctuation dissipation relation (17) to the situation of nonthermal equilibrium.

To proof the validity of a proportionality relation between the Fourier transforms of the symmetric correlation function for the central oscillator position,

$$\Psi(t, s) = \frac{1}{2} \langle Q(t)Q(t+s) + Q(t+s)Q(t) \rangle, \quad (18)$$

and the antisymmetric response function,

$$\Phi(t, s) = \frac{1}{i} \langle Q(t)Q(t+s) - Q(t+s)Q(t) \rangle, \quad (19)$$

we insert the solution for $Q(t)$. The thermodynamic limit $N \rightarrow \infty$ and the long-time limit $t \rightarrow \infty$ are performed employing the relations given in Sec. 2 of article IV. The

subsequent Fourier transformation yields the result

$$\Psi(\omega) = \frac{1}{i} \frac{\check{\mathcal{E}}(\omega)}{\omega} \Phi(\omega). \quad (20)$$

This relation generalises the thermal fluctuation dissipation theorem (17). It is valid for the stationary state of the central oscillator at arbitrary coupling strengths and bath preparations. The requirement is to have equilibration of the dissipative oscillator, i.e., we must have $u(t) \rightarrow 0$ for $t \rightarrow \infty$. The explicit form of the stationary state does not enter this relation. It is rather determined by the frequency-resolved energy distribution of the initial bath state $\check{\mathcal{E}}(\omega)$. A comparison with the thermal result in Eq. (17) shows that in the considered nonthermal situation the thermal energy distribution $\check{\mathcal{E}}_{\text{th}}(\omega) = (\omega/2) \coth \omega / (2T)$ has to be exchanged by the general bath energy distribution. This shows that not only the stationary state but also the fluctuations within the stationary state do only depend on the sum of the initial potential and kinetic bath energies and not on the individual functions.

Nonclassicality of cavity light The symmetric and antisymmetric correlation functions from the preceding paragraph contain products of two operators. In contrast, the Glauber $g^{(2)}$ function [84] is a correlation function that contains products of four operators. It is employed in quantum optics and determines statistical properties. In particular, it can be used to analyse the statistics of the photons emitted from quantum optical systems.

We study the Glauber $g^{(2)}$ function that characterises the light generated by a few emitters in a cavity at strong light-matter coupling. Specifically, we identify temperature and coupling regimes where nonclassical light [85, 86] is emitted. To capture the dissipative dynamics of the emitter-cavity system, we used the full input-output formalism [87–89] and Markovian master equation [2, 15, 90–93] without further approximations (see article V). We contrast our results with the predictions of the commonly used quantum optical master equation and show that it entirely fails at predicting different regimes of photon statistics.

The system of N two-level emitters interacting with a single cavity mode is described by the Dicke Hamiltonian [94],

$$H = \omega_c a^\dagger a + \omega_x \sum_{j=1}^N \sigma_+^{(j)} \sigma_-^{(j)} + g \sum_{j=1}^N (a^\dagger \sigma_-^{(j)} + a \sigma_+^{(j)}) + g' \sum_{j=1}^N (a \sigma_-^{(j)} + a^\dagger \sigma_+^{(j)}), \quad (21)$$

where $a^{(\dagger)}$ is the annihilation (creation) operator of a cavity photon with frequency ω_c and $\sigma_-^{(j)}$ ($\sigma_+^{(j)}$) is the corresponding lowering (raising) operator for the j th emitter with transition energy ω_x . We consider the resonant case $\omega_0 = \omega_c = \omega_x$. The emitter-cavity coupling strengths g for the corotating interaction terms and g' for the counterrotating terms are allowed to be different. Of particular interest are the Tavis-Cummings limit with $g' = 0$ and the Dicke limit with $g' = g$ [95, 96].

We couple the emitter-cavity system to the environment. The statistics of the emitted photons can be computed through a standard input-output formalism (see article V), which leads to the projected cavity-environment coupling operator

$$\dot{X}_- = \sum_{m,n \geq m} (E_n - E_m) |m\rangle \langle m| (a^\dagger - a) |n\rangle \langle n|, \quad (22)$$

where $|n\rangle$ are the eigenstates of the Dicke Hamiltonian (21) with $H|n\rangle = E_n|n\rangle$. The correlation functions of \dot{X}_- describe the emission from the cavity. Specifically, the second order Glauber function [84] at zero time delay reads

$$g^{(2)}(0) = \lim_{t \rightarrow \infty} \frac{\langle \dot{X}_+(t)\dot{X}_+(t)\dot{X}_-(t)\dot{X}_-(t) \rangle}{\langle \dot{X}_+(t)\dot{X}_-(t) \rangle^2}. \quad (23)$$

We note that evaluation of $g^{(2)}(0)$ requires diagonalisation of the Hamiltonian (21).

To obtain the dynamics $\dot{X}_-(t)$ we use the full Markovian master equation [2, 15, 90–93]. Compared with the explicit solution of operator equations of motion for the dissipative oscillator, this approach is justified because of the weak emitter-environment and cavity-environment couplings [1, 2]. In addition, we assume a thermal environment such that—according to the results from Sec. 1.3—full thermalisation of the emitter-cavity system is expected. The Glauber function $g^{(2)}(0)$ then follows from the numerical diagonalisation of the Dicke Hamiltonian (21) as a thermal expectation value.

The results for the Glauber function $g^{(2)}(0)$ for $N = 1, 2, 3$ emitters determine the statistics of the photons emitted by the cavity (see Fig. 9). For $g^{(2)}(0) = 1$ the emitted photons have a Poissonian distribution, while $g^{(2)}(0) > 1$ indicates super-Poissonian statistics. Thermal light has $g^{(2)}(0) = 2$ and $g^{(2)}(0) < 1$ indicates nonclassical light with sub-Poissonian photon statistics. Clearly distinguished regimes of emission can be identified in Fig. 9. In particular, regions with $g^{(2)}(0) < 1$, that stretch out along the vertical axis, indicate the emission of nonclassical light with sub-Poissonian photon statistics at low temperatures and moderate-to-strong light-matter coupling. The regime of strongly super-Poissonian photon statistics [$g^{(2)}(0) \gg 2$], visible in the Dicke limit in panels (a–c), is pushed back in favour of a second sub-Poissonian region that continues towards ultrastrong coupling in the Tavis-Cummings limit in panels (d–f). The emission of nonclassical light in the first sub-Poissonian region is observed equally in the Dicke and Tavis-Cummings limits.

The distinctive features of the Glauber function persist when varying the number of emitters, but the regions are shifted to smaller couplings g as the number of emitters increases from one to three. The similarity between $g^{(2)}(0)$ for $N = 1, 2, 3$ emitters (see Fig. 9) can be expressed as an approximate relation between the respective emitter-cavity coupling g . In the Dicke limit ($g' = g$), we find that the features of $g^{(2)}(0)$ follow the scaling $g \propto 1/N$. In the Tavis-Cummings limit ($g' = 0$), this scaling is $g \propto 1/\sqrt{N}$. Interestingly, the proper scaling of g depends on the presence of counterrotating interaction terms in the Hamiltonian. This difference is in contrast to the semiclassical theory where the mean cavity photon number in the steady state scales $\propto N$ both in the Dicke and Tavis-Cummings limits. Not surprisingly, the Glauber function $g^{(2)}(0)$ is more sensitive to the details of light-matter coupling than the semiclassical theory that neglects quantum correlations in favour of a mean-field approximation.

It is instructive to compare these results with the predictions from the usually employed quantum optical master equation [1, 2]. In this equation, terms for the emitter-environment and cavity-environment couplings appear independently. The coupling of emitters and cavity is completely neglected in the dissipative terms of the master equation. Specifically, the quantum optical master equation does not distinguish between energy-increasing and energy-decreasing transitions, such that it can lead to unphysical predictions, e.g., the emission out of the ground state. Results for the Glauber func-

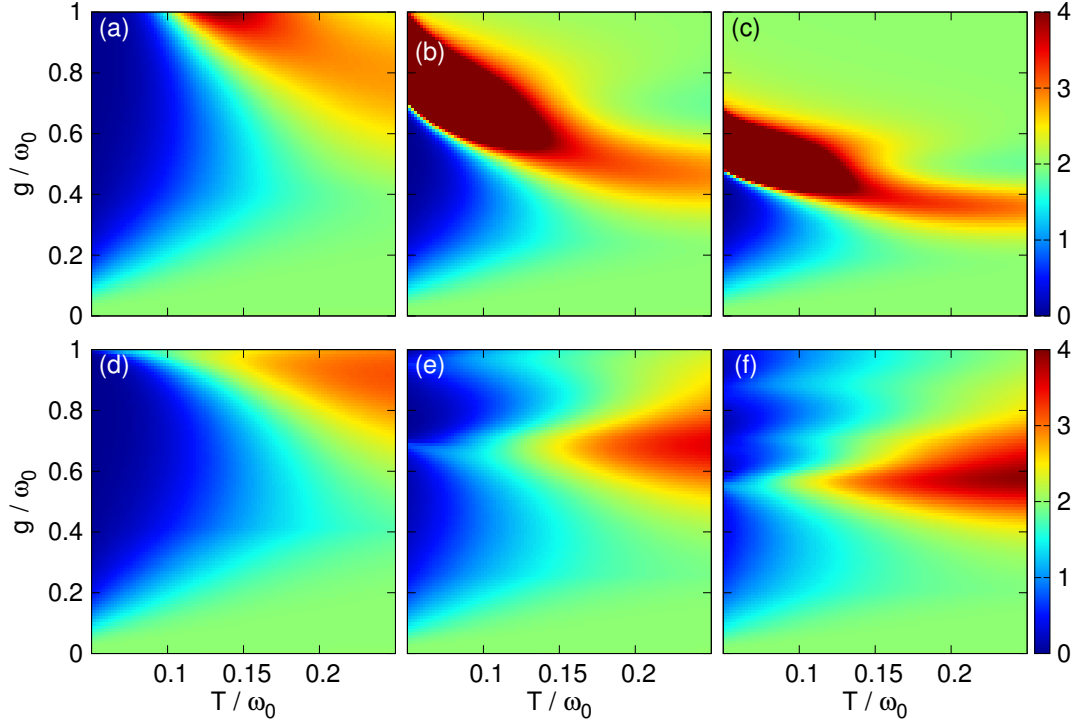


Fig. 9: Glauber function $g^{(2)}(0)$ as a function of temperature T and coupling strength g for (left) $N = 1$ emitter, (middle) $N = 2$ emitters, and (right) $N = 3$ emitters. The results are given for (a–c) $g' = g$ and (d–f) $g' = 0$. Note that all values $g^{(2)}(0) \geq 4$ are assigned the same dark red colour in the density plots.

tion in the Dicke limit $g' = g$ obtained with the quantum optical master equation are shown in Fig. 10. The quantum optical master equation does not predict the emission of nonclassical light with sub-Poissonian photon statistics in any part of the parameter space. The situation does not improve in the Tavis-Cummings limit $g' = 0$, where the quantum optical master equation gives $g^{(2)}(0) = 2$ independent of the number of emitters N , the coupling strength g , or the temperature T .

In summary, the features of the Glauber function (see Fig. 9) occur at smaller values of the individual emitter-cavity coupling strength when the number of emitters is increased. In this sense, the generation of nonclassical light is easier with more emitters. The reason is that all emitters interact with the same cavity mode leading to enhanced resonant emission and (re)absorption of cavity photons. While it may not be surprising that the quantum optical master equation fails at strong emitter-cavity coupling it is remarkable that it fails to capture any features of the Glauber function. This failure highlights the importance of using the correct master equation not only for strong light-matter coupling but also if one is interested in properties following from higher-order correlation functions, e.g., the photon statistics obtained from the second order Glauber function.

Stationary entanglement generation in semiconductor microcavities So far, we neglected the coupling to the environment in the description of the semiconductor

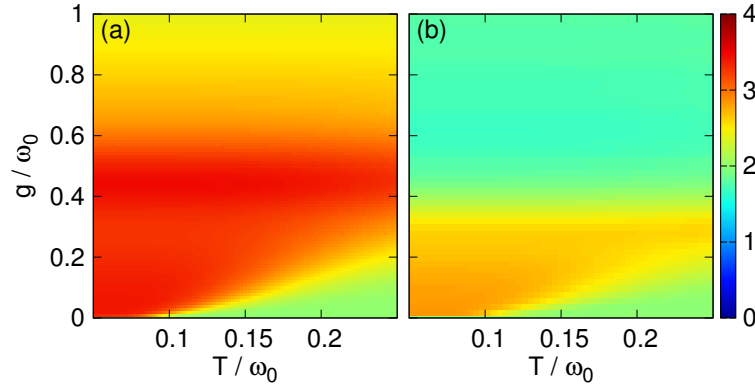


Fig. 10: Glauber function $g^{(2)}(0)$ computed with the quantum optical master equation, shown as a function of temperature T and coupling strength g for $g' = g$. The results are given for (a) $N = 1$ emitter and (b) $N = 2$ emitters.

microcavity with the four pump configuration that leads to the generation of four-partite entangled polaritons in a W state. Now, we include internal decoherence induced by the losses through the cavity mirrors and the coupling to lattice vibrations. This allows us to study the transfer of internal polariton entanglement to external photon entanglement under realistic experimental conditions. In this way, we answer the question if entanglement generation can survive the long-time limit in dissipative dynamics. These issues are addressed in article VI.

Our study is based on the Heisenberg equations of motion for the polariton operators,

$$\frac{d}{dt}p_{j\mathbf{k}} = -iE_j(\mathbf{k})p_{j\mathbf{k}} - iR_{j\mathbf{k}}^{\text{NL}}, \quad (24)$$

where, according to Eq. (2), $R_{j\mathbf{k}}^{\text{NL}}$ is the nonlinear contribution:

$$R_{j\mathbf{k}}^{\text{NL}} = \frac{1}{2} \frac{R_x^2}{A} \sum_{j_2, j_3, j_4} \sum_{\mathbf{q}, \mathbf{q}'} \left(V_{\mathbf{q}, \mathbf{q}', \mathbf{k}-\mathbf{q}}^{j, j_2, j_3, j_4} + V_{\mathbf{q}, \mathbf{q}', \mathbf{q}'-\mathbf{k}}^{j_2, j, j_3, j_4} \right) p_{j_2 \mathbf{q} + \mathbf{q}' - \mathbf{k}}^\dagger p_{j_3 \mathbf{q}'} p_{j_4, \mathbf{q}}. \quad (25)$$

We note that a similar equation of motion with equal operators but modified prefactors in $R_{j\mathbf{k}}^{\text{NL}}$ is obtained within the dynamics-controlled truncation formalism [97–100]. In this approach, no explicit bosonisation of the system Hamiltonian is performed. Instead, equations of motion for generalised Hubbard (transition) operators are derived and truncated at a certain order of the external field. Specifically, the mean-field Coulomb interaction terms are equal in the two approaches but the phase-space filling terms differ by a factor of about two [100]. This difference is a consequence of the polariton nature: In our approach, polaritons are bosonic particles, whereas within the dynamics-controlled truncation formalism they do not obey Bose-Einstein statistics.

The quantity of interest is the signal/idler photon density matrix that can be measured in experiments. This quantity can be computed through a tomographic reconstruction [42, 101], which is based on the evaluation of multi-time correlation functions of polariton operators. The losses through the cavity mirrors and the coupling to lattice vibrations are introduced through coupling of the semiconductor microcavity to an Ohmic thermal environment. Within the Langevin approach one has to add effective

damping rates and a noise background to the equation of motion (24). The resulting equation of motion can analytically be solved in the limit of a continuous pumping with identical pumps (see article VI). As a basis, we choose the four states $|1_i, 1_{sn}\rangle$ for $n = 1, \dots, 4$, where $|1_x\rangle$ denotes the state of a photon in channel $x = i, s1, \dots, s4$. The matrix elements $\rho_{m,n} = \langle 1_i, 1_{sm} | \rho | 1_i, 1_{sn} \rangle$ of the measured photon density matrix can be combined in the matrix

$$\rho = \frac{X}{4} \begin{pmatrix} 1 & 1 & 1 & 1 \\ 1 & 1 & 1 & 1 \\ 1 & 1 & 1 & 1 \\ 1 & 1 & 1 & 1 \end{pmatrix} + \frac{1-X}{4} \begin{pmatrix} 1 & 0 & 0 & 0 \\ 0 & 1 & 0 & 0 \\ 0 & 0 & 1 & 0 \\ 0 & 0 & 0 & 1 \end{pmatrix}, \quad (26)$$

where $X \in [0, 1]$. This state is a mixture of a pure (fully entangled) W state and a (not entangled) identity state, where the parameter X is the weight of the fully entangled W state in the mixture. The state ρ is fully entangled (fully separable) for $X = 1$ ($X = 0$). For any finite $X > 0$, ρ is entangled. In this sense, X can be taken as an entanglement measure, which quantifies the violation of a corresponding Bell inequality.

X as a function of the pump intensity Δ and the noise background N_b is shown in Fig. 11. We note that the pump intensity is limited by a stationarity condition that guarantees the convergence of polariton populations to stationary values in the long-time limit. The fully entangled pure W state is obtained for vanishing noise background. This result is in accordance with the previous one, where losses through the cavity mirrors and the coupling to lattice vibrations are neglected. Interestingly, even for a finite noise background $N_b > 0$ the pure W state can be generated if the pump power is high enough. This observation shows, that the entanglement generation in semiconductor microcavities can survive the long-time limit under realistic experimental conditions if the system is continuously pumped. Lowering the pump power at fixed N_b leads to a decrease of entanglement. Nevertheless, a small but finite amount of entanglement remains if the pump power is finite.

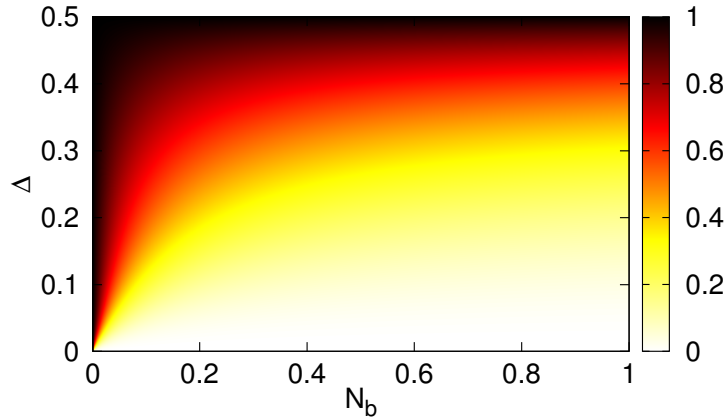


Fig. 11: Amount of entanglement in the state ρ [Eq. (26)] quantified by X as a function of the pump intensity Δ and the noise background N_b .

In summary, we showed that not only the stationary state but also the fluctuations of the central oscillator within the stationary state depend only on the initial bath

energy distribution, which generalises the well known thermal fluctuation-dissipation theorem to the case of stationary nonequilibrium. In addition, depending on the coupling strength and the bath temperature, emitters in a cavity can emit nonclassical light with sub-Poissonian statistics. For the analysis of this property the full Markovian master equation must be employed because the quantum optical master equation entirely fails at predicting the features of the Glauber function. Finally, we showed that a continuously pumped semiconductor microcavity generates entangled light even under realistic experimental conditions.

1.5 Conclusions

The realistic description of the physical processes in quantum optical systems requires careful investigation of the interplay between quantum dissipation and entanglement generation. In this thesis, we have considered from a microscopical perspective the entanglement generation in semiconductor microcavities at short times, the dissipative evolution of the quantum harmonic oscillator towards a stationary state, and the nonclassical properties of the asymptotic states of different photonic systems (see Fig. 12).

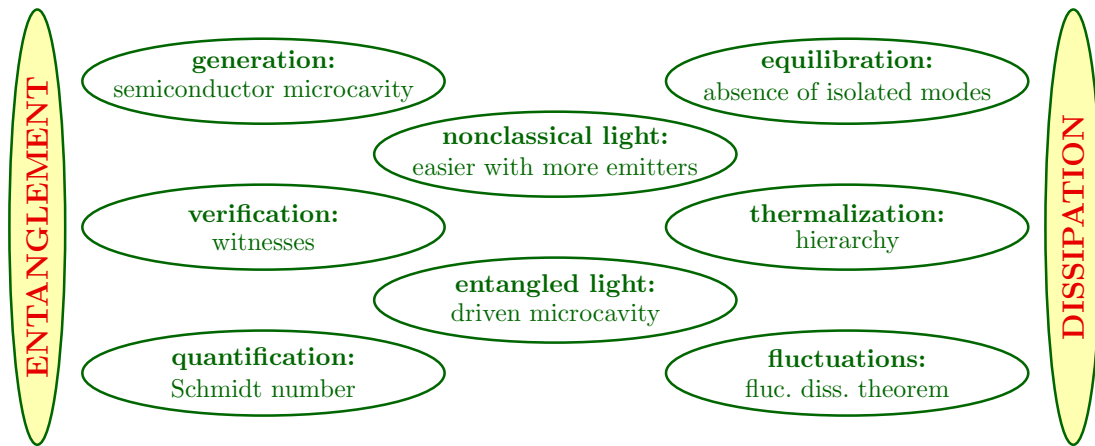


Fig. 12: Illustration of processes in quantum optics applications. The physical aspects studied in this thesis are printed in green ellipses.

In our description of two-dimensional semiconductor microcavities we showed that two different pump configurations can be used to stimulate parametric scattering processes between polaritons that lead to the generation of internal polariton entanglement. A moving polariton induces an ultrafast electric polarisation as a source of light that serves as a probe of the internal entanglement properties. The identification of the non-classical correlations of the emitted photons is based on entanglement witnesses that can also be used for the quantification of entanglement, e.g., in terms of the Schmidt number. The simultaneous creation of multiple branch entangled photon pairs renders it possible to generate an arbitrary number of entangled qubit states. By adjusting the number of pump beams and their spectral properties, one can optimize the Bell-type correlations within one or more of those entangled qubits.

Quantum dissipation can be studied in a microscopic setting with the well known model of a central oscillator coupled linearly to a bath of harmonic oscillators. We showed that equilibration of the central oscillator is the generic behaviour, which is prevented only in situations in which the classical oscillator equation of motion possesses undamped oscillatory solutions. Because of its localised spectral function, the infinite linear harmonic chain is an example for this behaviour. Thermalisation of the central oscillator depends on additional conditions. Equipartition of kinetic and potential energies requires the weak damping limit but is independent on the initial condition. The initial bath preparation enters the asymptotic temperature. Essential for the thermalisation of several oscillators is, that the asymptotic temperature is independent of the central oscillator frequency, which is fulfilled if the initial bath energy distribution matches that of a thermal state. Nevertheless, because this condition involves the sum of kinetic and potential energy, full thermalisation is possible in environments with nonthermal individual energy distributions, even in those far from thermal equilibrium. We showed, that even in the absence of full thermalisation the fluctuations of the central oscillator follow a generalised fluctuation dissipation theorem that reduces to the well know thermal result whenever the central oscillator thermalises in the strict sense.

Photonic systems such as two-level emitters in a cavity or semiconductor microcavities are employed in quantum optics applications. The realistic theoretical description of the physical processes requires the use of methods from quantum optics as well as from the field of quantum dissipation. Our focus was on the correct theoretical description of the emission from systems with strong coupling. The analysis of the light generated by emitters in a cavity reveals a non-trivial dependence of the photon statistics on the light-matter coupling and temperature. Clearly identifiable parameters regimes with sub- and super-Poissonian photon statistics appear at strong and ultrastrong coupling, and lie immediately next to each other. We provided an approximate rule to relate the emission characteristics for a single emitter to those obtained for few emitters under an appropriate scaling of the emitter-cavity coupling. In accordance with this rule, the generation of nonclassical light is easier with more emitters. The outright failure of the quantum optical master equation at predicting any of the features observed in the emission statistics shows that using the correct master equation is essential in all situation. Including internal dissipation channels we showed that a continuously driven semiconductor microcavity generates entangled light even at infinitely large times. The entanglement generation is thus robust against decoherence under realistic experimental conditions. Because the pair correlations between polaritons can sustain over long times and distances in these solid-state devices, a microcavity is a highly efficient source of entangled light and therefore well suited for quantum optics applications.

2 Thesis Articles

Author Contribution

Article I:

Strongly entangled light from planar microcavities, D. Pagel, H. Fehske, J. Sperling, and W. Vogel, *Phys. Rev. A* **86**, 052313 (2012). Copyright (2012) by the American Physical Society.

D. Pagel, H. Fehske, J. Sperling, and W. Vogel outlined the scope and strategy of the calculation. The calculation was performed by D. Pagel. D. Pagel and J. Sperling wrote the manuscript which was edited by all authors.

Article II:

Multipartite entangled light from driven microcavities, D. Pagel, H. Fehske, J. Sperling, and W. Vogel, *Phys. Rev. A* **88**, 042310 (2013). Copyright (2013) by the American Physical Society.

D. Pagel, H. Fehske, J. Sperling, and W. Vogel outlined the scope and strategy of the calculation. The calculation was performed by D. Pagel. D. Pagel and J. Sperling wrote the manuscript which was edited by all authors.

Article III:

Equilibration and thermalization of the dissipative quantum harmonic oscillator in a nonthermal environment, D. Pagel, A. Alvermann, and H. Fehske, *Phys. Rev. E* **87**, 012127 (2013). Copyright (2013) by the American Physical Society.

D. Pagel, A. Alvermann, and H. Fehske outlined the scope and strategy of the calculation. The calculation was performed by D. Pagel. D. Pagel and A. Alvermann wrote the manuscript which was edited by all authors.

Article IV:

Nonequilibrium quantum fluctuation relations for harmonic systems in nonthermal environments, D. Pagel, P. Nalbach, A. Alvermann, H. Fehske, and M. Thorwart, *New J. Phys.* **15**, 105008 (2013). Copyright (2013) by the IOP Publishing Ltd and the Deutsche Physikalische Gesellschaft.

D. Pagel, P. Nalbach, A. Alvermann, H. Fehske, and M. Thorwart outlined the scope and strategy of the calculation. The calculation was performed by D. Pagel. D. Pagel and M. Thorwart wrote the manuscript which was edited by all authors.

Article V:

Nonclassical light from few emitters in a cavity, D. Pagel, A. Alvermann, and H. Fehske, *Phys. Rev. A* **91**, 043814 (2015). Copyright (2015) by the American Physical Society. D. Pagel, A. Alvermann, and H. Fehske outlined the scope and strategy of the calculation. The calculation was performed by D. Pagel. D. Pagel and A. Alvermann wrote the manuscript which was edited by all authors.

Article VI:

Entangled light from driven dissipative microcavities, D. Pagel and H. Fehske, *Phys. Rev. A* **92**, 022342 (2015). Copyright (2015) by the American Physical Society. D. Pagel and H. Fehske outlined the scope and strategy of the calculation. The calculation was performed by D. Pagel. D. Pagel wrote the manuscript which was edited by all authors.

Confirmed:

(Prof. Dr. Holger Fehske)

Greifswald, 21 October 2015

(Daniel Pagel)

Greifswald, 21 October 2015

Strongly entangled light from planar microcavities

D. Pagel and H. Fehske

Institut für Physik, Ernst-Moritz-Arndt-Universität Greifswald, 17487 Greifswald, Germany

J. Sperling and W. Vogel

Institut für Physik, Universität Rostock, 18051 Rostock, Germany

(Received 20 July 2012; published 9 November 2012)

The emission of entangled light from planar semiconductor microcavities is studied and the entanglement properties are analyzed and quantified. Phase matching of the intracavity scattering dynamics for multiple pump beams or pulses, together with the coupling to external radiation, leads to the emission of a manifold of entangled photon pairs. A decomposition of the emitted photons into two parties leads to a strong entanglement of the resulting bipartite system. For the quantification of the entanglement, the Schmidt number of the system is determined by the construction of Schmidt number witnesses. It is analyzed to which extent the resources of the originally strongly entangled light field are diminished by dephasing in propagation channels.

DOI: [10.1103/PhysRevA.86.052313](https://doi.org/10.1103/PhysRevA.86.052313)

PACS number(s): 03.67.Bg, 03.67.Mn, 42.50.Dv, 71.36.+c

I. INTRODUCTION

The interaction of light and matter is a fundamental issue connecting elements of quantum optics and solid state physics. It offers a wide range of quantum effects, for example, the emission of various kinds of nonclassical light. These phenomena sensitively depend on the interaction of light with the fundamental excitations of the crystal. The nonclassical correlations of such systems can be used for various applications, such as quantum information processing, quantum metrology, and quantum communication (see, e.g., [1,2]).

One of the most prominent quantum phenomena is entanglement. It has been studied since the very first ideas of nonlocal superpositions of wave functions arose [3,4]. Entanglement has been used to perform a number of classically impossible operations in theory and experiment, such as, quantum teleportation, secure communication, and distillation protocols [1,2]. The latter ones require copies of entangled mixed states to distill pure entangled states [5,6], namely, Bell states [7]. One problem is the feasibility of appropriate quantum memories to store and manipulate the individual, entangled copies [8,9]. Despite this, the determination of entanglement of, in general, mixed quantum states is still a challenging task.

Typically, quantum correlations are determined from measurements of correlation functions. Here, we aim to quantify the measured correlations in terms of entanglement. The tricky relation between entanglement and correlations was mainly analyzed for spin systems [10,11]. Various entanglement measures have been introduced [12,13] and compared numerically and analytically [14–17]. It has been shown that the evaluation of an entanglement measure, especially for mixed states beyond qubits, is a sophisticated problem.

In the first instance, it is convenient to quantify entanglement for pure states only. One example is the Schmidt number (SN) [18–20]. For pure entangled states the SN counts the number of required superpositions of local product states to express the given state. A generalization to mixed quantum states can be achieved by a convex roof construction [21]. The SN of a general quantum state can be determined by

making use of the method of SN witnesses [18,22]. Recently, an approach based on generalized eigenvalue equations—so-called SN eigenvalue equations—led to a general construction scheme for SN witnesses [23]. Note that such an approach does not exist for other entanglement measures. Another advantage of the determination of the SN via SN witnesses is that these witnesses represent experimentally accessible observables.

Common approaches for the generation of bipartite entangled states consider type-II parametric down conversion [24] or biexciton decay in quantum dots [25,26]. Another prominent example is based on parametric phenomena in two-dimensional semiconductor microcavities [27–34]. They are known to realize a strong coupling between cavity photons and excitons [28] resulting in an anticrossing of the mixed exciton-photon modes, called lower and upper polariton branches. The ground state of the polaritons has been studied with respect to general quantum properties [31] and entanglement [35]. Stimulated scattering processes of polaritons within the lower branch have been shown to result in a large angle-resonant amplification of the pump field [36,37] and to produce polarization entangled polariton pairs [32,34]. Scattering processes involving both polariton branches can lead to the emission of photon pairs, which are entangled with respect to the branch index [29,31].

In the present work we show that semiconductor microcavities can be used to generate strongly entangled photons and demonstrate how their entanglement can be identified. In our study, we apply different pump beams to the microcavity, which leads to the emission of a large number of entangled photon pairs. These pair correlations can be identified as a strong entanglement, if we decompose the emitted light into two ensembles of beams. The identification of these strong correlations is done using SN witnesses. We quantify the impact of a lossy channel on the strongly entangled systems by determining the SN. This procedure is closely connected to the solution of the SN eigenvalue equations. As a result, we show that different degrees of dephasing require different kinds of witnesses to detect strong entanglement.

We proceed as follows. In Sec. II, we briefly recapitulate the physical description of the polariton formation in planar

microcavities. The intracavity scattering dynamics leads to branch entangled polariton pairs, which will be discussed in Sec. III. The coupling of the polaritons to radiation modes considered in Sec. IV yields strongly frequency-entangled photons. We verify their correlations by the use of entanglement and SN witnesses. In Sec. V, we study the dephasing due to the propagation of the frequency-entangled radiation through a linear dispersive medium. Section VI presents our conclusions.

II. PLANAR MICROCAVITY MODEL

In this section, we briefly recapitulate the quantum Hamiltonian model for semiconductor microcavities. It is based on the bosonic picture of interacting excitons [29,38,39] and can easily be used to investigate polariton parametric scattering in momentum space. Another common approach is based on the dynamics-controlled truncation formalism [40–42] that can be written in terms of the T matrix [43].

In semiconductors the fundamental excitations are electron-hole pairs with radius R_X and binding energy $E_b = e^2/(2\epsilon R_X)$, with ϵ being the static dielectric constant of the crystal. Since excitons are composite particles made up of fermions, they have an internal structure. Moreover, we have to take into account an effective exciton-exciton interaction [38,39],

$$H_{XX} = 6E_b \frac{R_X^2}{A} \sum_{\mathbf{k}, \mathbf{k}', \mathbf{q}} b_{\mathbf{k}+\mathbf{q}}^\dagger b_{\mathbf{k}'-\mathbf{q}}^\dagger b_{\mathbf{k}} b_{\mathbf{k}'}. \quad (1)$$

In this equation $b_{\mathbf{k}}$ ($b_{\mathbf{k}}^\dagger$) are bosonic annihilation (creation) operators of excitons with wave vector \mathbf{k} and dispersion

$E_X(\mathbf{k})$, and A is the sample surface. Since we consider planar microcavities, all wave vectors in Eq. (1) shall be in plane. As a simplification, we assume dispersionless excitons $E_X(\mathbf{k}) = E_X$ and work in units where $\hbar = c = 1$.

Coupling the excitons of the crystal to in-plane cavity photons with dispersion

$$E_C(k) = E_C(|\mathbf{k}|) = E_C(0)\sqrt{1 + (k/k_0)^2}, \quad (2)$$

where $k_0 = E_C(0)$, we have to consider the exciton-photon interaction. The harmonic part of this interaction is given by

$$H_{XC} = \Omega_R \sum_{\mathbf{k}} b_{\mathbf{k}}^\dagger a_{\mathbf{k}} + \text{H.c.}, \quad (3)$$

where $2\Omega_R$ denotes the vacuum Rabi splitting and $a_{\mathbf{k}}$ ($a_{\mathbf{k}}^\dagger$) are bosonic annihilation (creation) operators of the cavity photons with in-plane wave vector \mathbf{k} . It leads to lower ($j = 1$) and upper ($j = 2$) polariton branches

$$E_j(\mathbf{k}) = \frac{1}{2}(E_C(k) + E_X \mp \sqrt{[E_C(k) - E_X]^2 + 4\Omega_R^2}), \quad (4)$$

which depend on the modulus $k = |\mathbf{k}|$ only.

Figure 1(a) schematically shows the polariton dispersions $E_1(\mathbf{k})$ and $E_2(\mathbf{k})$ (solid lines) as well as the dispersions $E_C(k)$ and E_X of the cavity photons and the excitons (dashed lines). Note the anticrossing of the polariton branches, which is due to the strong coupling of exciton and cavity photon modes. The parameter $2\Omega_R$ is oftentimes called polariton splitting, since it determines the distance $E_2(\mathbf{k}) - E_1(\mathbf{k})$ when the exciton and cavity photon modes are resonant, $E_C(k) = E_X$.

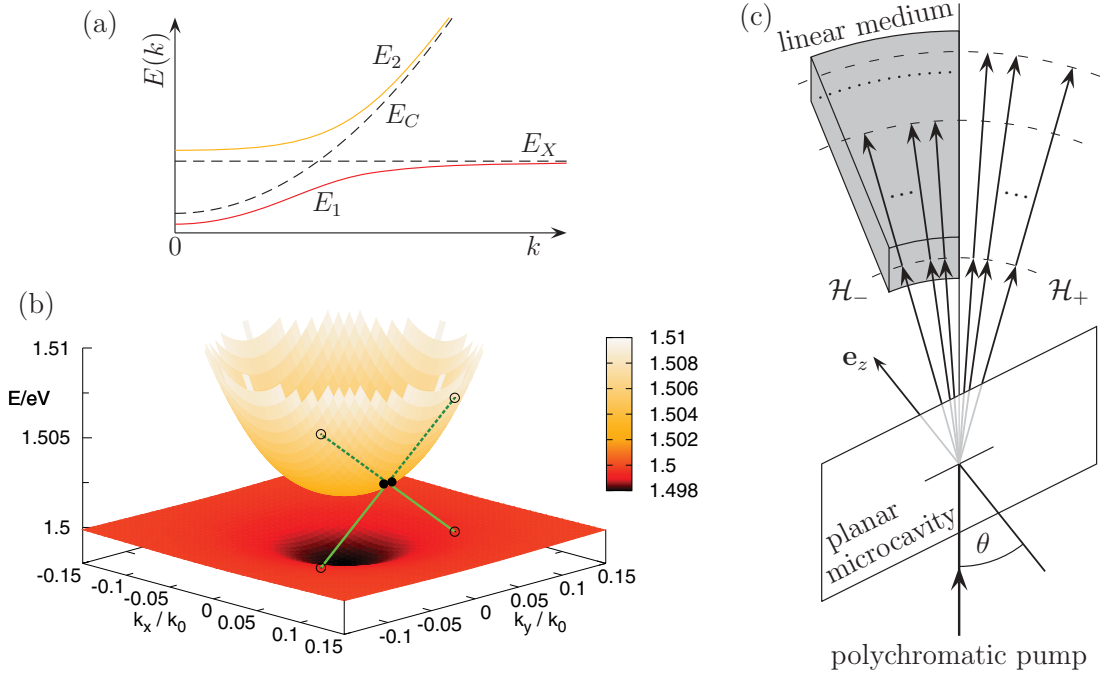


FIG. 1. (Color online) Sketch of the considered physical processes. The inset (a) shows the dispersion relations of the excitons, cavity photons, and polaritons. Part (b) visualizes the interbranch polariton pair scattering. Panel (c) depicts the emission and propagation of the emitted entangled light.

The anharmonic part of the total Hamiltonian of the exciton-photon interaction (saturation) is [37,38]

$$H_{XC}^{\text{sat}} = -\frac{1}{2} \sum_{\mathbf{k}, \mathbf{k}', \mathbf{q}} \frac{\Omega_R}{n_{\text{sat}} A} a_{\mathbf{k}+\mathbf{q}}^\dagger b_{\mathbf{k}'-\mathbf{q}}^\dagger b_{\mathbf{k}} b_{\mathbf{q}} + \text{H.c.}, \quad (5)$$

where $n_{\text{sat}} = 7/(16\pi R_X^2)$ is the exciton saturation density. Together with the exciton-exciton interaction H_{XX} , it gives rise to an effective polariton-polariton interaction

$$H_{PP} = \frac{1}{2} \sum_{\mathbf{k}, \mathbf{k}', \mathbf{q}} \sum_{\substack{j_1, j_2, \\ j_3, j_4}} \frac{R_X^2}{A} V_{\mathbf{k}, \mathbf{k}', \mathbf{q}}^{j_1 j_2 j_3 j_4} p_{j_1 \mathbf{k}+\mathbf{q}}^\dagger p_{j_2 \mathbf{k}'-\mathbf{q}}^\dagger p_{j_3 \mathbf{k}} p_{j_4 \mathbf{k}'}. \quad (6)$$

Here the $p_{j\mathbf{k}}$ ($p_{j\mathbf{k}}^\dagger$) are bosonic annihilation (creation) operators of polaritons in the lower or upper branch with in-plane wave vector \mathbf{k} . The effective branch-dependent potential $V_{\mathbf{k}, \mathbf{k}', \mathbf{q}}^{j_1 j_2 j_3 j_4}$ can be calculated through a unitary Hopfield transformation [44]

$$\begin{pmatrix} b_{\mathbf{k}} \\ a_{\mathbf{k}} \end{pmatrix} = \begin{pmatrix} M_{11\mathbf{k}} & M_{12\mathbf{k}} \\ M_{21\mathbf{k}} & M_{22\mathbf{k}} \end{pmatrix} \begin{pmatrix} p_{1\mathbf{k}} \\ p_{2\mathbf{k}} \end{pmatrix} \quad (7)$$

as

$$\begin{aligned} \frac{V_{\mathbf{k}, \mathbf{k}', \mathbf{q}}^{j_1 j_2 j_3 j_4}}{E_b} &= 12M_{1j_1 \mathbf{k}+\mathbf{q}} M_{1j_2 \mathbf{k}'-\mathbf{q}} M_{1j_3 \mathbf{k}} M_{1j_4 \mathbf{k}'} \\ &\quad - \frac{8\pi}{7} p_s (M_{2j_1 \mathbf{k}+\mathbf{q}} M_{1j_2 \mathbf{k}'-\mathbf{q}} M_{1j_3 \mathbf{k}} M_{1j_4 \mathbf{k}'} \\ &\quad + M_{2j_4 \mathbf{k}'} M_{1j_3 \mathbf{k}} M_{1j_2 \mathbf{k}'-\mathbf{q}} M_{1j_1 \mathbf{k}+\mathbf{q}}). \end{aligned} \quad (8)$$

In Eq. (8) we have introduced the ratio of polariton splitting to binding energy, $p_s = 2\Omega_R/E_b$. For the matrix elements of the Hopfield transformation one finds the relations

$$M_{22\mathbf{k}} = M_{11\mathbf{k}} = 1/\sqrt{1 + \rho_{\mathbf{k}}^2}, \quad (9)$$

$$M_{12\mathbf{k}} = -M_{21\mathbf{k}} = \sqrt{1 - M_{11\mathbf{k}}^2}, \quad (10)$$

where

$$\rho_{\mathbf{k}} = \frac{E_2(\mathbf{k}) - E_C(k)}{\Omega_R}. \quad (11)$$

Note that in contrast to the relations used in Ref. [29], the coefficient $M_{12\mathbf{k}}$ is always positive.

In Fig. 2 we show the dependence of the squared coefficients $M_{11\mathbf{k}}^2$ and $M_{12\mathbf{k}}^2$ on the modulus k of the wave vector \mathbf{k} for different values of the normalized detuning δ

$$\delta = \frac{E_C(0) - E_X}{2\Omega_R}. \quad (12)$$

For large values of k the coefficient $M_{11\mathbf{k}}^2 \rightarrow 1$, and consequently excitons and cavity photons do not mix. The polariton modes are equal to the separated exciton and cavity photon modes. For smaller k the value of $M_{11\mathbf{k}}^2$ depends on the detuning δ and the polaritons are a combination of excitons and cavity photons. This mixing is due to the strong coupling of excitons and cavity photons.

III. BRANCH-ENTANGLED POLARITONS

Since we are interested in the generation of entangled polariton pairs, we consider a situation where a pump laser

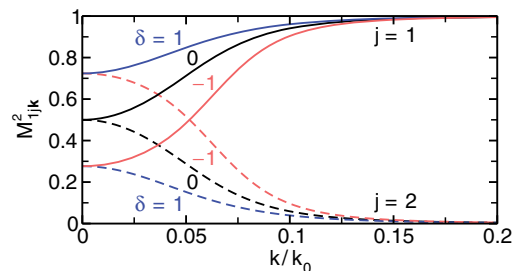


FIG. 2. (Color online) Coefficients of the Hopfield transformation matrix in Eq. (7), for the parameters $E_C(0) = 1.5$ eV and $\Omega_R = 2$ meV. The solid lines correspond to $M_{11\mathbf{k}}^2$ and the dashed ones to $M_{12\mathbf{k}}^2$. The color of the curves indicates the values of the normalized detuning δ . For large values of $|\mathbf{k}|$ the coefficient $M_{11\mathbf{k}}^2$ converges to one and $M_{12\mathbf{k}}^2$ vanishes.

stimulates scattering processes of polaritons. It was shown theoretically in Ref. [34] and experimentally in Ref. [32], using “which-way” experiments, that pumping the lower polariton branch can lead to the generation of polarization-entangled polariton pairs. Here we are interested in a different situation where the pump laser drives coherently the upper branch at a given wave vector \mathbf{k}_p , as illustrated by Fig. 1(b) for $\mathbf{k}_p = 0.05k_0 \mathbf{e}_x$, $E_C(0) = 1.5$ eV, $\Omega_R = 2$ meV, and $\delta = 0$. The pumped polaritons (solid black circles) scatter into states belonging to different branches, $j_1 \neq j_2$ (open black circles). In this setting, frequency or branch entanglement arises since both paths (indicated by the green lines) are indistinguishable, i. e., they are simultaneously phase matched. For strong pumping we approximately replace the annihilation operator $p_{2\mathbf{k}_p}$ by its mean-field value $\langle p_{2\mathbf{k}_p} \rangle$ and use $P_{2\mathbf{k}_p}^2 = \langle p_{2\mathbf{k}_p} \rangle^2 R_X^2/A$. This yields a parametric Hamiltonian

$$\begin{aligned} H_{PP}^{\text{par}} &= \frac{1}{2} \sum_{\mathbf{q}} P_{2\mathbf{k}_p}^2 (V_{\mathbf{k}_p, \mathbf{k}_p, \mathbf{q}}^{1222} p_{1\mathbf{k}_p+\mathbf{q}}^\dagger p_{2\mathbf{k}_p-\mathbf{q}}^\dagger \\ &\quad + V_{\mathbf{k}_p, \mathbf{k}_p, \mathbf{q}}^{2122} p_{2\mathbf{k}_p+\mathbf{q}}^\dagger p_{1\mathbf{k}_p-\mathbf{q}}^\dagger) + \text{H.c.} \end{aligned} \quad (13)$$

that approximates the polariton-polariton interaction Hamiltonian (6) for the scattering process of Fig. 1(b). Note that each pair of polariton creation operators has a different effective potential, such that we cannot factor out the effective potential as done in Ref. [29]. Additionally, there is a mean-field shift of the branch-dependent energy:

$$\tilde{E}_j(\mathbf{k}) = E_j(\mathbf{k}) + \Lambda_{\mathbf{k}, \mathbf{k}_p}^{j2} |P_{2\mathbf{k}_p}|^2, \quad (14)$$

where

$$\Lambda_{\mathbf{q}, \mathbf{k}_p}^{j2} = \frac{1}{2} (V_{\mathbf{q}, \mathbf{k}_p, 0}^{j2j2} + V_{\mathbf{k}_p, \mathbf{q}, 0}^{2j2j} + V_{\mathbf{q}, \mathbf{k}_p, \mathbf{k}_p-\mathbf{q}}^{2j2j} + V_{\mathbf{k}_p, \mathbf{q}, \mathbf{q}-\mathbf{k}_p}^{j22j}). \quad (15)$$

Assuming that the scattering wave vector \mathbf{q} fulfills the phase-matching condition for the considered interbranch polariton pair scattering process,

$$E_{2(1)}(\mathbf{k}_p + \mathbf{q}) + E_{1(2)}(\mathbf{k}_p - \mathbf{q}) = 2E_2(\mathbf{k}_p), \quad (16)$$

the Hamiltonian H_{PP}^{par} from Eq. (13) applied on the vacuum state $|\text{vac}\rangle$ generates branch-entangled pairs of polaritons in

the state

$$|\phi\rangle = (\alpha p_{1\mathbf{k}_p+\mathbf{q}}^\dagger p_{2\mathbf{k}_p-\mathbf{q}}^\dagger + \beta p_{2\mathbf{k}_p+\mathbf{q}}^\dagger p_{1\mathbf{k}_p-\mathbf{q}}^\dagger) |\text{vac}\rangle. \quad (17)$$

Here we introduced the parameters

$$\alpha = V_{\mathbf{k}_p, \mathbf{k}_p, \mathbf{q}}^{1222} [(V_{\mathbf{k}_p, \mathbf{k}_p, \mathbf{q}}^{1222})^2 + (V_{\mathbf{k}_p, \mathbf{k}_p, \mathbf{q}}^{2122})^2]^{-1/2}, \quad (18a)$$

$$\beta = V_{\mathbf{k}_p, \mathbf{k}_p, \mathbf{q}}^{2122} [(V_{\mathbf{k}_p, \mathbf{k}_p, \mathbf{q}}^{1222})^2 + (V_{\mathbf{k}_p, \mathbf{k}_p, \mathbf{q}}^{2122})^2]^{-1/2}, \quad (18b)$$

characterizing the properties of the material. In contrast to Ref. [29], the state $|\phi\rangle$ in Eq. (17) is not a Bell state (for $\alpha^2 \neq \beta^2$), which is due to the inequality of the effective branch-dependent potentials. As usual, $\alpha^2 + \beta^2 = 1$ ensures the normalization of $|\phi\rangle$.

In that the polariton energy dispersions $E_{1,2}(\mathbf{k})$ depend on k only, the phase-matching condition is fulfilled if

$$|\mathbf{k}_p + \mathbf{q}|^2 = |\mathbf{k}_p - \mathbf{q}|^2, \quad (19)$$

being equivalent to $\mathbf{q} \perp \mathbf{k}_p$. The second part of the phase-matching condition in Eq. (16) yields

$$E_C(|\mathbf{k}_p + \mathbf{q}|) + E_X = 2E_2(\mathbf{k}_p). \quad (20)$$

The solution of this equation gives the absolute value of the scattering wave vector \mathbf{q} :

$$|\mathbf{q}|^2 = \left(\frac{2E_2(\mathbf{k}_p) - E_X}{E_C(0)} \right)^2 - 1 - |\mathbf{k}_p|^2. \quad (21)$$

Because the sign of \mathbf{q} remains unspecified, the phase-matching condition is fulfilled for two equivalent interbranch polariton pair scattering processes. Entangled polaritons in the state (17) appear due to the indistinguishability of these scattering channels.

As we have mentioned above, the value of β influences the nonlocal character of $|\phi\rangle$, cf. Eq. (23). In case $\beta^2 = 1/2$, we have a true Bell state, and $|\phi\rangle$ is separable for $\beta^2 = 0$ or $\beta^2 = 1$. In all other cases, we have an entangled state as a superposition of two product states. Such states are referred to as Bell-like states. They violate a Bell inequality, but not maximally [7].

In Fig. 3 we plot the value of β^2 for the phase-matching scattering wave vector \mathbf{q} following from Eqs. (19) and (21) as a function of the normalized detuning δ and the polariton splitting to binding energy ratio p_s . From this figure we can deduce that the state described by Eq. (17) is a true Bell state only on a specific line in the (δ, p_s) plane. For values of δ and p_s apart from this line the state of the polariton pair is an entangled Bell-like state. Since δ and p_s are determined by the material, we are in the position to tune the entanglement properties of the polariton pairs. For example, we might consider materials, where the polariton splitting is of the order $2\Omega_R \sim 4$ meV, while the exciton binding energy approximately is $E_b \sim 10$ meV. Since the ratio of the anharmonic exciton-photon interaction to the exciton-exciton interaction, $[4\pi\Omega_R/(21E_b)]^2$, is of the order of 10^{-2} , it is a fairly good approximation to omit the anharmonic part of the exciton-photon coupling. The particular choice $p_s = 0$ causes a simpler effective branch-dependent potential

$$\frac{V_{\mathbf{k}, \mathbf{k}', \mathbf{q}}^{j_1 j_2 j_3 j_4}}{E_b} \approx 12M_{1j_1\mathbf{k}+\mathbf{q}}M_{1j_2\mathbf{k}'-\mathbf{q}}M_{1j_3\mathbf{k}}M_{1j_4\mathbf{k}'}, \quad (22)$$

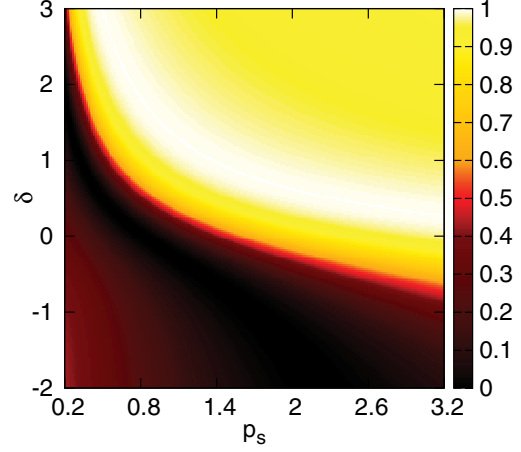


FIG. 3. (Color online) Magnitude of β^2 in the (δ, p_s) plane according to Eq. (18b) for $E_C(0) = 1.5$ eV, $E_b = 10$ meV, and $\mathbf{k}_p = 0.05k_0\mathbf{e}_x$. The phase-matching scattering wave vector \mathbf{q} follows from Eqs. (19) and (21).

$V_{\mathbf{k}_p, \mathbf{k}_p, \mathbf{q}}^{1222} = V_{\mathbf{k}_p, \mathbf{k}_p, \mathbf{q}}^{2122}$, and $\alpha^2 = \beta^2 = 1/2$. Obviously, such microcavities create polariton pairs in a Bell state configuration.

Another important effect results when we apply several pumps with different pump wave vectors $\mathbf{k}_{p1}, \mathbf{k}_{p2}, \dots$ to the microcavity. Motivated by experiments is a pump-pulse train, where all \mathbf{k}_{pn} , $n = 1, 2, \dots$ are aligned in the same direction but have different amplitudes. Then we have a phase-matching condition for each \mathbf{k}_{pn} . Accordingly, branch-entangled polariton pairs appear for all phase-matching scattering wave vectors \mathbf{q}_n following from Eqs. (19) and (21) by inserting the respective pump vector \mathbf{k}_{pn} . Then the state of N branch-entangled polariton pairs takes the form

$$|\psi\rangle = \prod_{n=1}^N (\alpha_n p_{1\mathbf{k}_{pn}+\mathbf{q}_n}^\dagger p_{2\mathbf{k}_{pn}-\mathbf{q}_n}^\dagger + \beta_n p_{2\mathbf{k}_{pn}+\mathbf{q}_n}^\dagger p_{1\mathbf{k}_{pn}-\mathbf{q}_n}^\dagger) |\text{vac}\rangle. \quad (23)$$

The normalization $\prod(\alpha_n^2 + \beta_n^2) = 1$ of this state follows from the property $\alpha_n^2 + \beta_n^2 = 1$ for each n .

IV. ENTANGLEMENT OF EMITTED LIGHT

A. Frequency-entangled photons

In the following, we consider the emission of entangled light from the microcavity. As shown in Ref. [29], the coupling of the intracavity polaritons to an external field can be described by the quasimode Hamiltonian

$$H_{FP}^{\text{ext}} = \sum_{j, \mathbf{k}} \int d\omega g(\omega) |M_{j2\mathbf{k}}|^2 a_{\omega, \mathbf{k}}^\dagger p_{j\mathbf{k}} + \text{H.c.} \quad (24)$$

with a frequency-dependent coupling $g(\omega)$. The creation operator $a_{\omega, \mathbf{k}}^\dagger$ describes an emitted photon with frequency ω and in-plane wave vector \mathbf{k} . The coupling of each branch to the external field is proportional to the photonic fraction $|M_{j2\mathbf{k}}|^2$. If the $|M_{j2\mathbf{k}}|^2$ are of comparable magnitude, the

branch entanglement of the polaritons transfers to a frequency entanglement of photon pairs in the state

$$|\psi\rangle = \prod_{n=1}^N (\alpha_n a_{n,-}^\dagger a_{n,+}^\dagger + \beta_n a_{n,-}^\dagger a_{n,+}^\dagger) |\text{vac}\rangle, \quad (25)$$

where the multi-indices are defined as

$$\begin{aligned} (n, \pm) &= (E_1(\mathbf{k}_{pn} + \mathbf{q}_n), \mathbf{k}_{pn} \pm \mathbf{q}_n), \\ (\bar{n}, \pm) &= (E_2(\mathbf{k}_{pn} + \mathbf{q}_n), \mathbf{k}_{pn} \pm \mathbf{q}_n). \end{aligned} \quad (26)$$

Obviously, $E_{1(2)}(\mathbf{k}_{pn} - \mathbf{q}_n) = E_{1(2)}(\mathbf{k}_{pn} + \mathbf{q}_n)$, for scattering wave vectors \mathbf{q}_n , fulfilling the phase-matching condition (16).

We now identify the entanglement of the multiple photon pairs as strong entanglement by changing the point of view according to Fig. 1(c). For this purpose, we decompose the compound Hilbert space \mathcal{H} of the emitted photons into two parties, $\mathcal{H} = \mathcal{H}_- \otimes \mathcal{H}_+$, where the subspaces \mathcal{H}_\pm contain all photons emitted with an in-plane wave vector $\mathbf{k}_{pn} \pm \mathbf{q}_n$, respectively. In Fig. 1(c), this yields two spatial subspaces for all photons emitted to the left-hand side or to the right-hand side. We choose this particular decomposition in order to quantify entanglement in possible which-way experiments. It is important to stress that other possible decompositions could be treated similarly, but they may give other outcomes [1,45]. Our particular decomposition is motivated from experimental accessibility. Consider, for example, the above-mentioned pump-pulse train, where all \mathbf{k}_{pn} are aligned in the same direction \mathbf{e}_p , but have different amplitudes. Then, according to the solution of the phase-matching condition (16) in Sec. III, all scattering wave vectors \mathbf{q}_n are perpendicular to the symmetry axis \mathbf{e}_p , i.e., photons with wave vectors $\mathbf{k}_{pn} \pm \mathbf{q}_n$ are spatially separated.

Let us describe this decomposition mathematically. We may introduce the states $|0\rangle_n$ for a photon with an energy $E_1(\mathbf{k}_{pn} + \mathbf{q}_n)$, and $|1\rangle_n$ for a photon energy $E_2(\mathbf{k}_{pn} + \mathbf{q}_n)$. With these definitions we get $a_{n,-}^\dagger a_{n,+}^\dagger |\text{vac}\rangle = |0\rangle_n \otimes |1\rangle_n$ and $a_{\bar{n},-}^\dagger a_{\bar{n},+}^\dagger |\text{vac}\rangle = |1\rangle_n \otimes |0\rangle_n$. Thus, the state $|\psi\rangle$ in Eq. (25) reads

$$|\psi\rangle = \prod_{n=1}^N (\alpha_n |0\rangle_n \otimes |1\rangle_n + \beta_n |1\rangle_n \otimes |0\rangle_n). \quad (27)$$

The expansion of this product yields a sum of 2^N product states

$$\begin{aligned} & \left(\prod_{n=1}^N |i_n\rangle_n \right) \otimes \left(\prod_{n=1}^N |1 - i_n\rangle_n \right) \\ &= |i_1, \dots, i_N\rangle \otimes |1 - i_1, \dots, 1 - i_N\rangle \end{aligned} \quad (28)$$

with $i_n \in \{0, 1\}$. The sequence $(i_n)_{n=1}^N$ can be understood as a binary representation of an integer m between 0 and $2^N - 1$, whereas the corresponding sequence $(1 - i_n)_{n=1}^N$ gives the complement integer $\bar{m} = (2^N - 1) - m$. As a result we obtain

$$|\psi\rangle = \sum_{m=0}^{2^N-1} \gamma_m |m, \bar{m}\rangle \quad (29)$$

with coefficients

$$\gamma_m = \prod_{n=1}^N [(1 - i_n)\alpha_n + i_n\beta_n]. \quad (30)$$

The expression $(1 - i_n)\alpha_n + i_n\beta_n$ equals α_n for $i_n = 0$ and β_n for $i_n = 1$. The normalization condition reads

$$\sum_{m=0}^{2^N-1} \gamma_m^2 = \prod_{n=1}^N (\alpha_n^2 + \beta_n^2) = 1. \quad (31)$$

Note that in the form of Eq. (29) $|\psi\rangle$ is no longer a multipartite product state, but a strongly entangled bipartite state.

B. Identification of strongly entangled states

To identify bipartite entanglement we use entanglement witnesses [46,47], or, more specifically, SN (Schmidt number) witnesses. For pure states the SN arises from the Schmidt decomposition of the state [2]. For example, if we consider the pure state $|\psi\rangle$, cf. Eq. (29), the SN is the number of nonzero coefficients γ_m . Thus, the SN quantifies the entanglement based on the quantum superposition of the product states $|m, \bar{m}\rangle$. SN witnesses can also be employed for mixed quantum states.

The construction of SN witnesses is a challenging task. Recently we have shown that one can use general Hermitian operators to identify the amount of entanglement [23]. A (in general mixed) quantum state has a SN greater than r if and only if there exists a Hermitian operator L with

$$\langle L \rangle = \text{Tr } \rho L > f_r(L), \quad (32)$$

where

$$f_r(L) = \sup\{\langle \psi_r | L | \psi_r \rangle : |\psi_r\rangle \text{ SN } r \text{ state}\}. \quad (33)$$

A SN witness can be constructed from $[f_r(L)\mathbb{I} - L]$. Obviously, the case $r = 1$ is equivalent to an entanglement test [47]. A possible way to identify the value of the function $f_r(L)$ is based on a generalized eigenvalue equation—the so-called SN eigenvalue equation—which takes the form

$$L|\psi_r\rangle = g|\psi_r\rangle + |\chi\rangle \quad (34)$$

with $|\chi\rangle$ being a biorthogonal perturbation, cf. [23]. The value g is the SN eigenvalue and the vector $|\psi_r\rangle$ is the SN eigenvector. The largest SN eigenvalue is the value of the function $f_r(L)$ for the SN test in Eq. (32). The case $r = 1$ delivers the separability eigenvalue equations [47], and we have shown that they also apply to the identification of entanglement via negative quasiprobabilities [48,49].

Now, let us measure the entanglement with respect to the chosen decomposition of the Hilbert space \mathcal{H} . To determine the SN of the state, we consider the projection $L = |\psi\rangle\langle\psi|$ and obtain $\langle L \rangle = \langle \psi | L | \psi \rangle = 1$. For the function $f_r(L)$ we get

$$f_r(L) = \max \{ \gamma_{m_1}^2 + \dots + \gamma_{m_r}^2 : m_i \neq m_j \text{ for } i \neq j \}, \quad (35)$$

which is the sum of the r largest squared Schmidt coefficients [23]. Due to the normalization of the state, $\sum_{m=0}^{2^N-1} \gamma_m^2 = 1$, the value of $f_r(L)$ is smaller than 1, if there exist more than r values $\beta_m \neq 0$. In conclusion, the considered pure state $|\psi\rangle$ has a SN of 2^N , in the general case that all $\alpha_n, \beta_n \neq 0$ for $n = 1, \dots, N$.

We conclude that the emitted light, which directly corresponds to the cavity-internal quantum state, is strongly entangled. In order to generate such a state, the quantum superposition of local states $|m, \bar{m}\rangle$, is required at least $r = 2^N$

times. These strongly entangled outputs verify the internal quantum correlation between the branch-entangled polaritons inside the cavity structure. However, in a more realistic scenario, we have imperfections causing a loss of quantum entanglement. For example, the initially strongly entangled state $|\psi\rangle\langle\psi|$ could undergo a dephasing. In the limiting case of full dephasing, the state ρ_{deph} becomes

$$\rho_{\text{deph}} = \sum_{m=0}^{2^N-1} \gamma_m^2 |m, \bar{m}\rangle\langle m, \bar{m}|, \quad (36)$$

and contains no interferences of the form $|m, \bar{m}\rangle\langle l, \bar{l}|$ for $l \neq m$. In this scenario, the SN equals the minimum value one for the separable state ρ_{deph} . This means that this state is useless for any protocol based on entanglement. In the following, we will study the amount of entanglement in the intermediate region between no and full dephasing.

V. DEPHASING

In quantum optics the role of losses is crucial and has to be considered carefully. On the one hand there are internal losses leading to branch-, wave-vector-, and excitation-density-dependent broadenings for the polariton modes. Examples are scattering with acoustic phonons [34,50], mixing with states of the exciton continuum [51], Coulomb induced parametric scattering [50], or losses through the cavity mirrors. On the other hand, there are external losses diminishing the initially available amount of entanglement. Once entangled radiation is emitted out of the cavity a major source for the loss of entanglement is dephasing [23,49]. We here aim to quantify this lossy channel, i.e., we neglect all internal losses and assume that the microcavity emits strongly entangled photons that shall be detected at a certain fixed distance.

A. Propagation through different linear media

In the bipartite setting under study, the two parts of the entangled radiation field would in general propagate through different media, cf. Fig. 1(c). In the case of pumping by a pulse train, already some small differences in the dispersive properties of the two media would lead to significant relative phase shifts and hence to an overall dephasing effect diminishing the entanglement between the output channels of the two transmission lines.

Let us assume two media with linear dispersions given by $\omega_{\pm}(k)$, where the index \pm indicates the propagation in \mathcal{H}_{\pm} , respectively. The Hamiltonian reads $H_{\text{deph}} = H_- + H_+$, where

$$H_{\pm} = \sum_{n=1}^N [\omega_{\pm}(E_{1n}) a_{n,\pm}^{\dagger} a_{n,\pm} + \omega_{\pm}(E_{2n}) a_{\bar{n},\pm}^{\dagger} a_{\bar{n},\pm}] \quad (37)$$

with the energies $E_{1n(2n)} = E_{1(2)}(\mathbf{k}_{pn} \pm \mathbf{q}_n)$. Recall that energies for wave vectors $\mathbf{k}_{pn} \pm \mathbf{q}_n$ are identical for phase-matching scattering wave vectors \mathbf{q}_n . These Hamiltonians are diagonal in the photon number basis, such that

$$H_{\pm}|m\rangle = E_{m,\pm}|m\rangle \quad (38)$$

with modified eigenvalues in the binary representation $(i_n)_{n=1}^N$ of the integer $m \in [0, 2^N - 1]$:

$$E_{m,\pm} = \sum_{n=1}^N [(1 - i_n)\omega_{\pm}(E_{1n}) + i_n\omega_{\pm}(E_{2n})]. \quad (39)$$

It is obvious that the vacuum can be expressed in the same way using the dispersion relation $\omega_{\text{vac}}(k) = k$.

The time evolution of the initially emitted radiation is

$$|\psi(t)\rangle = e^{-i(H_- + H_+)t} |\psi\rangle = \sum_{m=0}^{2^N-1} e^{-i(E_{m,-} + E_{m,+})t} \gamma_m |m, \bar{m}\rangle. \quad (40)$$

The spatial distances from the cavity to detectors in the left and right subspaces are assumed to be equal. However, the optical path lengths differ in both parties and depend on the frequency components of the propagating fields. Effectively, the arrival times at the detectors differ for the different field components created by the microcavity system. This leads to the exponential factor in Eq. (40) which takes into account the phase shift between the two parties of photons.

To obtain the photon state measured by the detectors, we have to average over the different arrival times to account for the different optical path lengths. In practice the resulting statistics depends on the details of the dispersive properties of both media representing the two propagation channels. Such a treatment must be based on an experimental analysis of the used channels, which is beyond the scope of the present paper. To demonstrate the basic principles, we simply suppose an equally distributed difference of the arrival times in the two channels. This yields

$$\begin{aligned} \bar{\rho}(t_1, t_2) &= \frac{1}{t_1 - t_2} \int_{t_1}^{t_2} dt |\psi(t)\rangle\langle\psi(t)| \\ &= \sum_{m,l=0}^{2^N-1} \gamma_m \gamma_l e^{-ix_{ml}(t_1+t_2)/2} \\ &\quad \times \text{sinc}\left(x_{ml} \frac{t_2 - t_1}{2}\right) |m, \bar{m}\rangle\langle l, \bar{l}|, \end{aligned} \quad (41)$$

with

$$\int_a^b e^{-ixt} dt = (b-a)e^{-ix(a+b)/2} \text{sinc}\left(x \frac{b-a}{2}\right), \quad (42)$$

where $x_{ml} = (E_{m,-} + E_{\bar{m},+} - E_{l,-} - E_{\bar{l},+})$, $\text{sinc}(y) = \sin(y)/y$. The state $\bar{\rho}(t_1, t_2)$ in Eq. (41) represents the structure of the density operator of entangled light suffering from dephasing. For $\Delta t = t_2 - t_1 \rightarrow \infty$ we obtain the separable state ρ_{deph} . All the correlations generated by the branch-entangled polaritons vanish in this extremal situation.

Clearly there is no dephasing if the photons in both Hilbert spaces \mathcal{H}_{\pm} propagate through the same medium, $\omega_{\pm}(k) = \omega(k)$, as it is perfectly realized in vacuum channels. Under such conditions, the sum

$$E_{m,\pm} + E_{\bar{m},\mp} = \sum_{n=1}^N [\omega(E_{1n}) + \omega(E_{2n})] \quad (43)$$

is independent of m such that $x_{ml} = 0$ for all $m, l \in [0, 2^N - 1]$. The difference in the optical path lengths only depends on the difference of the dispersion relations between left and right Hilbert space. Thus, without loss of generality, we can assume that we have a free-space propagation in \mathcal{H}_+ and a linear medium in \mathcal{H}_- as anticipated in Fig. 1(c).

B. Detection of strong entanglement

To quantify strong entanglement in the continuous-variable mixed state $\bar{\rho}(t_1, t_2)$ for finite Δt , we need to find a suitable test operator L . As we have seen in the case of pure states, the test operator should be closely related to the density operator in order to have a large value on the left-hand side of Eq. (32). On the other hand, the value $f_r(L)$ should be as small as possible. Together this means that we should use a test operator L in the form

$$L = \sum_{m, l=0}^{2^N-1} \Gamma_{m, l} |m, \bar{m}\rangle \langle l, \bar{l}|, \quad (44)$$

with the positive semidefinite matrix of coefficients

$$\mathbf{\Gamma} = (\Gamma_{m, l})_{m, l=0}^{2^N-1}. \quad (45)$$

As shown in Ref. [23], in such a case we can obtain the function $f_r(L)$ just by determining the largest eigenvalue of all $r \times r$ principal submatrices of $\mathbf{\Gamma}$.

To construct a suitable test operator we consider the given state $\bar{\rho}(t_1, t_2) = \sum_{m, l=0}^{2^N-1} \rho_{m, l} |m, \bar{m}\rangle \langle l, \bar{l}|$. Let $x^{(k)} = (x_m^{(k)})_{m=0}^{2^N-1}$ be the k th eigenvector of the coefficient matrix $(\rho_{m, l})_{m, l=0}^{2^N-1}$ for a nonzero eigenvalue. Then we choose L to be the projector in the subspace spanned by the vectors

$$|x^{(k)}\rangle = \sum_{m=0}^{2^N-1} x_m^{(k)} |m, m\rangle. \quad (46)$$

This means $\Gamma_{m, l} = \sum_k x_m^{(k)} x_l^{(k)*}$. Analogously to the case of a pure state we obtain

$$\langle L \rangle = \text{Tr} \bar{\rho}(t_1, t_2) L = 1. \quad (47)$$

As long as the subspace given by all $|x^{(k)}\rangle$ does not contain a SN r vector $|\psi_r\rangle$, for the projection L holds:

$$f_r(L) = \sup_{|\psi_r\rangle} \langle \psi_r | L | \psi_r \rangle < 1. \quad (48)$$

Hence we get a SN greater than r whenever $f_r(L) < 1 = \langle L \rangle$.

At this point, let us comment on the particular choice of the observable L . The fact that L is a projection guarantees a high verification rate of the SN test given by Eq. (32). The main advantage of using L , which depends on $\bar{\rho}(t_1, t_2)$, relates to the appearance of a large mean value $\langle L \rangle$ on the left-hand side of Eq. (32), representing the measurement outcome. By contrast, the right-hand side of the SN inequality test, for our choice, takes a comparably small value $f_r(L)$ because the projected subspace of L , by construction, has no SN r state in its range.

In Figs. 4 and 5, we plot the SN of the state $\bar{\rho}(t_1, t_2)$ depending on Δt for different values of the normalized

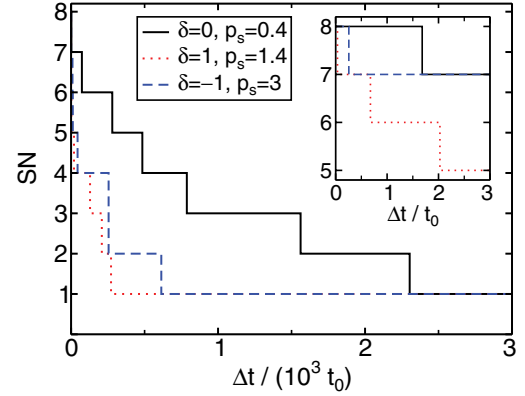


FIG. 4. (Color online) Amount of entanglement within the state $\bar{\rho}(t_1, t_2)$ depending on Δt and quantized by the SN. We apply three different pumps with wave vectors $\mathbf{k}_{pn} = 0.025nk_0\mathbf{e}_x$, $n = 1, 2, 3$ to the cavity. The system parameters are $E_C(0) = 1.5$ eV and $E_b = 10$ meV. The dispersion of the medium is chosen to be $\omega(k) = 0.5k$. Based on our units $\hbar = c = 1$, we choose a typical reference time scale $t_0 = 1$ eV. The inset shows the behavior for weak dephasing.

detuning δ and the ratio of polariton splitting to binding energy p_s . Figure 4 shows the case, where the microcavity is pumped by three beams with different wave vectors aligned in the same direction. Hence, the maximal possible SN of the emitted radiation is eight. Applying an additional pump, the maximal achievable amount of entanglement increases to 16 (see Fig. 5).

Both figures indicate that an increasing dephasing due to the increase of Δt , yields a decreasing SN. For $\Delta t = 0$ the SN of the state $\bar{\rho}(t_1, t_2)$ is equal to 2^N , which is the maximum value. The jumps of the value of the guaranteed SN from r to $r - 1$ occur for values of Δt where the corresponding witness fails to identify a SN larger than r . For a fixed value of Δt the SN strongly depends on the properties δ and p_s of the planar microcavity. A higher number of pump beams—and thus a higher initial SN—may significantly increase the range of Δt for which the state $\bar{\rho}(t_1, t_2)$ is still entangled (compare Figs. 4 and 5).

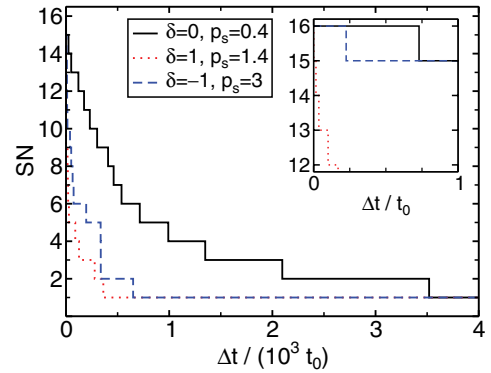


FIG. 5. (Color online) Amount of entanglement within the state $\bar{\rho}(t_1, t_2)$ for $N = 4$ different pumps. The parameters are the same as in Fig. 4, aside from the additional \mathbf{k}_{pn} for $n = 4$.

VI. CONCLUSIONS

We have discussed polariton scattering processes within planar semiconductor microcavities with a focus on the possible creation of entangled polariton pairs. In extension to previous works, we show that a polychromatic pumping of the upper polariton branch, as motivated by experiments, leads to a simultaneous creation of multiple branch-entangled polariton pairs. The coupling of the intracavity scattering dynamics to an external field then transfers these kinds of quantum correlations to frequency-entangled photon pairs. Since the entanglement properties of these photon pairs are determined by parameters of the device, the measurement of the photon correlations gives valuable information about the internal branch-entanglement within the microcavity.

The simultaneous creation of photon pairs renders it possible to generate an arbitrary number of copies of entangled qubit states ρ , of the form $\rho \otimes \rho \otimes \dots \otimes \rho$. Such kinds of states are desired to perform quantum operations based on entanglement, such as quantum teleportation. Usually the generation of such states requires that a source of entangled states produces at each time a state ρ , which will be stored in a quantum memory to obtain the desired number of copies. Here, the number of pump beams or the spectral properties of a pump-pulse train determine the maximal number of simultaneously available entangled qubits. By properly choosing the wave vectors of the

pump field, one can optimize the Bell-type correlations within one or more of those entangled qubits. Microcavities pumped with a single pulse of polychromatic light serve as generators of copies of entangled qubit states, making optical quantum memories superfluous. Decoherence due to the storage time in a quantum memory cannot occur.

If desired, the multipartite pair correlations can be mapped to strong bipartite entanglement. The quantification of such correlations can be done via the determination of the Schmidt number, which automatically quantifies the multipartite pair correlations and the branch entanglement in the microcavity. From our results follows that the Schmidt number of such an unperturbed system is maximal and it can be controlled by the properties of the pump field. A dephasing channel diminishes this resource of entanglement. However, we showed that a high amount of entanglement can be guaranteed for a certain range of parameters. By using a higher number of pump beams or properly designed pump pulses, one may not only increase the initially available amount of entanglement, but also its resistance against dephasing.

ACKNOWLEDGMENT

This work was supported by the Deutsche Forschungsgemeinschaft through SFB 652 by projects B5 and B12.

-
- [1] R. Horodecki, P. Horodecki, M. Horodecki, and R. Horodecki, *Rev. Mod. Phys.* **81**, 865 (2009).
 - [2] M. A. Nielsen and I. L. Chuang, *Quantum Computation and Quantum Information* (Cambridge University Press, Cambridge, 2010).
 - [3] A. Einstein, B. Podolsky, and N. Rosen, *Phys. Rev.* **47**, 777 (1935).
 - [4] E. Schrödinger, *Naturwiss.* **23**, 807 (1935).
 - [5] C. H. Bennett, G. Brassard, S. Popescu, B. Schumacher, J. Smolin, and W. K. Wootters, *Phys. Rev. Lett.* **78**, 2031 (1996).
 - [6] B. Hage, A. Sambrowski, J. DiGuglielmo, J. Fiurášek, and R. Schnabel, *Phys. Rev. Lett.* **105**, 230502 (2010).
 - [7] J. S. Bell, *Physics* (Long Island City, NY) **1**, 195 (1964).
 - [8] K. Hammerer, A. S. Sørensen, and E. S. Polzik, *Rev. Mod. Phys.* **82**, 1041 (2010).
 - [9] K. Jensen, W. Wasilewski, H. Krauter, T. Fernholz, B. M. Nielsen, A. Serafini, M. Owari, M. B. Plenio, M. M. Wolf, and E. S. Polzik, *Nucl. Phys.* **7**, 13 (2011).
 - [10] U. Glaser, H. Büttner, and H. Fehske, *Phys. Rev. A* **68**, 032318 (2003).
 - [11] F. Verstraete, M. Popp, and J. I. Cirac, *Phys. Rev. Lett.* **92**, 027901 (2004).
 - [12] V. Vedral, M. B. Plenio, M. A. Rippin, and P. L. Knight, *Phys. Rev. Lett.* **78**, 2275 (1997).
 - [13] L. Amico, R. Fazio, A. Osterloh, and V. Vedral, *Rev. Mod. Phys.* **80**, 517 (2008).
 - [14] J. Eisert and M. B. Plenio, *J. Mod. Opt.* **46**, 145 (1999).
 - [15] A. Miranowicz and A. Grudka, *J. Opt. B* **6**, 542 (2004).
 - [16] M. Plenio and S. Virmani, *Quant. Inf. Comput.* **7**, 1 (2007).
 - [17] J. Sperling and W. Vogel, arXiv:1004.1944.
 - [18] B. M. Terhal and P. Horodecki, *Phys. Rev. A* **61**, 040301 (2000).
 - [19] A. Sanpera, D. Bruß, and M. Lewenstein, *Phys. Rev. A* **63**, 050301 (2001).
 - [20] J. Sperling and W. Vogel, *Phys. Scr.* **83**, 045002 (2011).
 - [21] A. Uhlmann, *Open Syst. Inf. Dyn.* **5**, 209 (1998).
 - [22] D. Bruß, J. I. Cirac, P. Horodecki, F. Hulpke, B. Kraus, M. Lewenstein, and A. Sanpera, *J. Mod. Opt.* **49**, 1399 (2002).
 - [23] J. Sperling and W. Vogel, *Phys. Rev. A* **83**, 042315 (2011).
 - [24] P. G. Kwiat, K. Mattle, H. Weinfurter, A. Zeilinger, A. V. Sergienko, and Y. Shih, *Phys. Rev. Lett.* **75**, 4337 (1995).
 - [25] O. Benson, C. Santori, M. Pelton, and Y. Yamamoto, *Phys. Rev. Lett.* **84**, 2513 (2000).
 - [26] U. Hohenester, C. Sifel, and P. Koskinen, *Phys. Rev. B* **68**, 245304 (2003).
 - [27] C. Weisbuch, M. Nishioka, A. Ishikawa, and Y. Arakawa, *Phys. Rev. Lett.* **69**, 3314 (1992).
 - [28] R. Houdré, C. Weisbuch, R. P. Stanley, U. Oesterle, P. Pellandini, and M. Illegems, *Phys. Rev. Lett.* **73**, 2043 (1994).
 - [29] C. Ciuti, *Phys. Rev. B* **69**, 245304 (2004).
 - [30] W. Langbein, *Phys. Rev. B* **70**, 205301 (2004).
 - [31] C. Ciuti, G. Bastard, and I. Carusotto, *Phys. Rev. B* **72**, 115303 (2005).
 - [32] S. Savasta, O. Di Stefano, V. Savona, and W. Langbein, *Phys. Rev. Lett.* **94**, 246401 (2005).
 - [33] C. Diederichs, J. Tignon, G. Dasbach, C. Ciuti, A. Lemaître, J. Bloch, P. Roussignol, and C. Delalande, *Nature (London)* **440**, 904 (2006).
 - [34] S. Portolan, O. Di Stefano, S. Savasta, and V. Savona, *Europhys. Lett.* **88**, 20003 (2009).
 - [35] A. Auer and G. Burkard, *Phys. Rev. B* **85**, 235140 (2012).

- [36] P. G. Savvidis, J. J. Baumberg, R. M. Stevenson, M. S. Skolnick, D. M. Whittaker, and J. S. Roberts, *Phys. Rev. Lett.* **84**, 1547 (2000).
- [37] C. Ciuti, P. Schwendimann, B. Deveaud, and A. Quattropani, *Phys. Rev. B* **62**, R4825 (2000).
- [38] F. Tassone and Y. Yamamoto, *Phys. Rev. B* **59**, 10830 (1999).
- [39] C. Ciuti, P. Schwendimann, and A. Quattropani, *Phys. Rev. B* **63**, 041303 (2001).
- [40] V. M. Axt and A. Stahl, *Z. Phys. B* **93**, 195 (1994).
- [41] S. Savasta and R. Girlanda, *Phys. Rev. Lett.* **77**, 4736 (1996).
- [42] S. Portolan, O. Di Stefano, S. Savasta, F. Rossi, and R. Girlanda, *Phys. Rev. B* **77**, 195305 (2008).
- [43] R. Takayama, N. Kwong, I. Romyantsev, M. Kuwata-Gonokami, and R. Binder, *Eur. Phys. J. B* **25**, 445 (2002).
- [44] J. J. Hopfield, *Phys. Rep.* **112**, 1555 (1958).
- [45] P. Zanardi, D. A. Lidar, and S. Lloyd, *Phys. Rev. Lett.* **92**, 060402 (2004).
- [46] M. Horodecki, P. Horodecki, and R. Horodecki, *Phys. Lett. A* **223**, 1 (1996).
- [47] J. Sperling and W. Vogel, *Phys. Rev. A* **79**, 022318 (2009).
- [48] J. Sperling and W. Vogel, *Phys. Rev. A* **79**, 042337 (2009).
- [49] J. Sperling and W. Vogel, *New J. Phys.* **14**, 055026 (2012).
- [50] S. Portolan, O. Di Stefano, S. Savasta, F. Rossi, and R. Girlanda, *Phys. Rev. B* **77**, 035433 (2008).
- [51] D. S. Citrin and J. B. Khurgin, *Phys. Rev. B* **68**, 205325 (2003).

Multipartite entangled light from driven microcavities

D. Pagel and H. Fehske*

Institut für Physik, Ernst-Moritz-Arndt-Universität Greifswald, 17487 Greifswald, Germany

J. Sperling and W. Vogel

Institut für Physik, Universität Rostock, 18051 Rostock, Germany

(Received 23 July 2013; published 9 October 2013)

The generation and the characterization of multipartite entangled light is an important and challenging task in quantum optics. In this paper the entanglement properties of the light emitted from a planar semiconductor microcavity are studied. The intracavity scattering dynamics leads to the emission of light that is described by a four-partite W state. Its multipartite correlations are identified by using the method of entanglement witnesses. Entanglement conditions are derived, which are based on a general witness constructed from W states. The results can be used to detect entanglement of light that propagates through lossy and even turbulent media.

DOI: [10.1103/PhysRevA.88.042310](https://doi.org/10.1103/PhysRevA.88.042310)

PACS number(s): 03.67.Bg, 03.67.Mn, 42.50.Dv, 71.36.+c

I. INTRODUCTION

The phenomenon of quantum entanglement relies on the superposition principle of quantum physics. Since the pioneering works [1,2] this effect has been regarded as one fundamental discrepancy between the quantum and classical domains of nature. Nowadays, entanglement is considered to be a key resource for quantum information technologies (cf., e.g., [3–5]).

Quantum entanglement is defined as a kind of correlation between subsystems, which cannot be interpreted in terms of classical joint probabilities [6]. Especially in the multipartite scenario, these nonclassical correlations exist in various forms (for an introduction, see, e.g., [4,5]). The most elementary examples of nonequivalent forms are given by GHZ states [7] and W states [8]. Among many possible applications of entanglement, the best studied ones are quantum key distribution [9], quantum dense coding [10], and quantum teleportation [11].

Typically one can detect entanglement using so-called entanglement witnesses [12,13]. These observables are non-negative for separable states, but exhibit negativities for entangled ones. To quantify the amount of entanglement within a system [14–18] one has to find a proper entanglement measure, which can be constructed from entanglement witnesses. For bipartite systems the solution of such an optimization procedure is given [17,19]. In the multipartite case, the problem of finding an optimal entanglement measure is still unsolved. The construction of multipartite witnesses has been resolved only recently [20].

A system where the identification of multipartite entangled light becomes important is a two-dimensional semiconductor microcavity [21–25]. Here, an optical driving with a laser field at a frequency near the fundamental band gap of the semiconductor can coherently create excitons, i.e., bound states of electrons and holes. In the low density limit, excitons can be described as an ideal gas of bosons. For high densities one has to account for the fermionic nature of the exciton constituents, leading to effective exciton-exciton interactions

[26–30]. Within the microcavity, the strong coupling of cavity photons with semiconductor excitons leads to an anticrossing of the energy dispersions of the mixed exciton photon modes—so-called polaritons [31,32]. Polariton-polariton interactions arise from the Coulomb interaction within their electronic parts [26,28]. Due to this interaction, pumped polaritons can scatter into pairs of signal and idler polaritons, if energy and momentum are conserved. It has been shown, that the signal and idler polaritons can be in an entangled state [21,33–36].

While the generation of multipartite entanglement in planar microcavities is based on the strong coupling between the intracavity field and the semiconductor excitations, alternative generation schemes have been proposed in the literature. Realizations involving linear optics such as beam splitters rely on parametric light sources, e.g., squeezed light [37]. Examples for setups using nonlinearities are concurrent interactions in second-order nonlinear media [38], interlinked interactions in $\chi^{(2)}$ media [39], and down-conversion in parametric media [40].

In the present paper we demonstrate that multipartite entanglement can be created and identified in driven microcavities. In particular, we consider the emitted light from a planar semiconductor microcavity that is driven by four pumps. This leads to the generation of photons in a four-partite W state. The detection of their multipartite correlations is based on entanglement witnesses. This method requires the solution of the so-called multipartite separability eigenvalue equations [20], and we provide the full solution for a class of witnesses that is based on a generalized pure W state. This allows us to study the loss of entanglement of the emitted light when it propagates through lossy media.

We proceed as follows. In Sec. II we briefly recapitulate the bosonic description of planar microcavities and present the pump geometry that leads to the generation of polaritons in a W state. Their multipartite entanglement is verified in Sec. III. In Sec. IV we study the propagation of the emitted light through the atmosphere and its impact on the entanglement properties of the photons. We use the solution to the separability eigenvalue equations for a generalized pure W -state witness, obtained in Sec. IV B. Section V presents our conclusions.

*fehske@physik.uni-greifswald.de

II. SETUP FOR THE GENERATION OF ENTANGLED LIGHT

In this section, we give a short review of the description of planar microcavities in terms of bosonic polaritons [21,26,27]. This description can easily be used to investigate polariton parametric scattering in momentum space [21,36], and we propose a scenario that leads to the generation of polaritons in multipartite entangled states.

An alternative approach for the description of polariton scattering is based on equations of motion for the exciton and photon operators and is called dynamics controlled truncation formalism [41–43]. It was recently extended to double and triple cavities [35].

A. Bosonic description of planar microcavities

Our starting point is the bosonic description of two-dimensional semiconductor microcavities in the basis of excitons and cavity photons. The excitons are assumed to be dispersionless, i.e., $E_X(\mathbf{k}) = E_X$, whereas the photon energy E_C grows linearly with the modulus of the three-dimensional wave vector. Projected onto the two dimensions of the microcavity we obtain $E_C(k) = E_C(0)\sqrt{1 + (k/k_0)^2}$, where k is the modulus of the in-plane wave vector \mathbf{k} and $k_0 = E_C(0)$. As a simplification, we work in units where $\hbar = c = 1$.

The interaction of excitons and cavity photons can be separated into a harmonic and an anharmonic contribution [26,44]. In the harmonic approximation, we can perform a Hopfield transformation [45] to get new quasiparticles called polaritons. The Hamiltonian of noninteracting polaritons then reads

$$H_P = \sum_{j,\mathbf{k}} E_j(\mathbf{k}) p_{j\mathbf{k}}^\dagger p_{j\mathbf{k}}, \quad (1)$$

where $p_{j\mathbf{k}}^\dagger$ creates a polariton with in-plane wave vector \mathbf{k} in the lower ($j = 1$) or upper ($j = 2$) branch with energy $E_j(\mathbf{k})$. Figure 1 inset (a) schematically shows these functions (solid lines) together with the dispersions $E_C(k)$ and E_X of the cavity photons and excitons (dashed lines). For large values of k the polariton modes are equal to the separated exciton and cavity photon modes. For small k the strong coupling between the excitons and the photons of the planar microcavity leads to an anticrossing of the polariton dispersions.

A polariton pair interaction arises from the anharmonic exciton photon coupling and from the Coulomb interaction within the electronic part of the excitons and is given by [21,26,30]

$$H_{PP} = \frac{1}{2} \sum_{\mathbf{k}, \mathbf{k}', \mathbf{q}} \sum_{j_1, j_2, j_3, j_4} \frac{R_X^2}{A} V_{\mathbf{k}, \mathbf{k}', \mathbf{q}}^{j_1 j_2 j_3 j_4} p_{j_1 \mathbf{k} + \mathbf{q}}^\dagger p_{j_2 \mathbf{k}' - \mathbf{q}}^\dagger p_{j_3 \mathbf{k}} p_{j_4 \mathbf{k}'}. \quad (2)$$

In this equation R_X is the exciton radius, A is the sample surface, and $V_{\mathbf{k}, \mathbf{k}', \mathbf{q}}^{j_1 j_2 j_3 j_4}$ is the effective branch-dependent potential,

$$\begin{aligned} \frac{V_{\mathbf{k}, \mathbf{k}', \mathbf{q}}^{j_1 j_2 j_3 j_4}}{E_b} &= 12M_{1j_1 \mathbf{k} + \mathbf{q}} M_{1j_2 \mathbf{k}' - \mathbf{q}} M_{1j_3 \mathbf{k}} M_{1j_4 \mathbf{k}'} \\ &\quad - \frac{8\pi}{7} p_s (M_{2j_1 \mathbf{k} + \mathbf{q}} M_{1j_2 \mathbf{k}' - \mathbf{q}} M_{1j_3 \mathbf{k}} M_{1j_4 \mathbf{k}'} \\ &\quad + M_{1j_1 \mathbf{k} + \mathbf{q}} M_{1j_2 \mathbf{k}' - \mathbf{q}} M_{1j_3 \mathbf{k}} M_{2j_4 \mathbf{k}'}). \end{aligned} \quad (3)$$

Here, $E_b = e^2/(2\epsilon R_X)$ is the exciton binding energy with ϵ being the static dielectric constant of the crystal, and $p_s = 2\Omega_R/E_b$ is the ratio of polariton splitting to binding energy. The coefficients $M_{jj\mathbf{k}}$ follow from the Hopfield transformation as $M_{11\mathbf{k}} = M_{22\mathbf{k}} = 1/\sqrt{1 + \rho_{\mathbf{k}}^2}$ and $M_{12\mathbf{k}} = -M_{21\mathbf{k}} = \sqrt{1 - M_{11\mathbf{k}}^2}$, where $\rho_{\mathbf{k}} = [E_2(\mathbf{k}) - E_C(\mathbf{k})]/\Omega_R$.

B. Polariton parametric scattering

We consider an experimental setup that involves scattering processes within the lower polariton branch only. We choose a four-pump scheme, where the wave vectors \mathbf{k}_{pn} for $n = 1, \dots, 4$ of the pumps have equal amplitudes. The scattering of pumped polaritons into pairs of signal and idler is described by single-pump (signal at \mathbf{k} and idler at $2\mathbf{k}_{pn} - \mathbf{k}$) and mixed-pump (signal at \mathbf{k} and idler at $\mathbf{k}_{pn} + \mathbf{k}_{pm} - \mathbf{k}$ with $n \neq m$) parametric processes. Within the setup under study (see Fig. 1), the incident angles of the four pumps shall be below the magic angle [22,25], such that single-pump parametric scattering is negligible. In particular, we choose $\mathbf{k}_{p1} = (k_p, k_p)$, $\mathbf{k}_{p2} = (-k_p, k_p)$, $\mathbf{k}_{p3} = (-k_p, -k_p)$, and $\mathbf{k}_{p4} = (k_p, -k_p)$.

In Fig. 1 inset (b) we show the phase-matching function for this scenario. This function is given by

$$\begin{aligned} \Phi(\mathbf{k}) &= \sum_{n,m=1}^4 \gamma^2 \{ [E_1(k) + E_1(|\mathbf{k}_{pn} + \mathbf{k}_{pm} - \mathbf{k}|) \\ &\quad - 2E_1(\sqrt{2}k_p)]^2 + \gamma^2 \}^{-1}, \end{aligned} \quad (4)$$

where γ is the polariton broadening. Mixed-pump scattering processes of oppositely arranged pumps ($|\mathbf{k}_{pn} + \mathbf{k}_{pm}| = 0$) contribute to the circle with radius $\sqrt{2}k_p$ in Fig. 1 inset (b). The four mixed-pump processes of neighboring pumps ($|\mathbf{k}_{pn} + \mathbf{k}_{pm}| = 2k_p$) share a common idler mode at $\mathbf{k}_i = 0$, such that the four corresponding signal modes are expected to be entangled.

C. Emission of light

In the following we calculate the state of the emitted polaritons in the absence of noise or losses. Since we consider a setup, where the lower polariton branch is resonantly excited, we can neglect all processes where polaritons from the upper polariton branch scatter into some final states. Thus, we can assume $j_3 = j_4 = 1$ in the polariton pair interaction Hamiltonian, Eq. (2). Inspection of the polariton dispersions in Fig. 1 inset (a) shows that there is no energy and momentum conserving process, where two lower polaritons with incident angles below the magic angle scatter into one lower and one upper polariton. Hence, we can neglect all contributions from the upper polariton branch and approximate the polariton-polariton interaction Hamiltonian equation (2) by the parametric Hamiltonian

$$\begin{aligned} H_{PP}^{\text{par}} &= \frac{1}{2} \sum_{\mathbf{k}} \sum_{n,m=1}^4 V_{\mathbf{k}_{pn}, \mathbf{k}_{pm}, \mathbf{k} - \mathbf{k}_{pn}}^{1111} P_{1\mathbf{k}_{pn}} P_{1\mathbf{k}_{pm}} \\ &\quad \times p_{1\mathbf{k}}^\dagger p_{1\mathbf{k}_{pn} + \mathbf{k}_{pm} - \mathbf{k}}^\dagger + \text{H.c.}, \end{aligned} \quad (5)$$

where $P_{1\mathbf{k}_p}^2 = \langle p_{1\mathbf{k}_p} \rangle^2 R_X^2/A$ is a classical pump field. For the proposed parametric scattering process with $\mathbf{k}_i = 0$ and

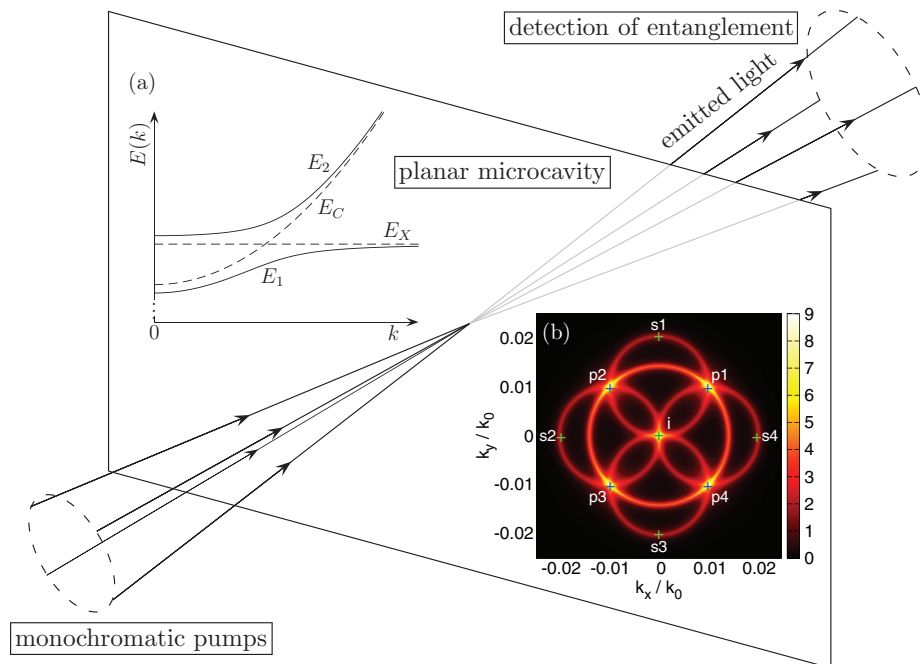


FIG. 1. (Color online) Sketch of the considered physical processes. The pumping of the planar microcavity leads to the emission of light whose multipartite entanglement is detected. Inset (a) shows the energy dispersion relations of the excitons, cavity photons, and polaritons. Inset (b) depicts the phase-matching function for $E_C(0) = E_X = 1.5$ eV, $\Omega_R = 2$ meV, and $\gamma = 10$ μ eV. The four pumps with $k_p = 0.01k_0$ are arranged on a cone.

$\mathbf{k}_{s1} = (0, 2k_p)$, $\mathbf{k}_{s2} = (-2k_p, 0)$, $\mathbf{k}_{s3} = (0, -2k_p)$, and $\mathbf{k}_{s4} = (2k_p, 0)$, the effective branch-dependent potential $V_{\mathbf{k}_{pn}, \mathbf{k}_{pm}, -\mathbf{k}_{pn}}^{1111}$ for neighboring pumps can be simplified, which yields

$$\begin{aligned} \frac{V_{\mathbf{k}_{pn}, \mathbf{k}_{pm}, -\mathbf{k}_{pn}}^{1111}}{E_b} &= 12M_{110}M_{112k_p}M_{11\sqrt{2}k_p}M_{11\sqrt{2}k_p} \\ &- \frac{8\pi}{7}p_s(M_{210}M_{112k_p}M_{11\sqrt{2}k_p}M_{11\sqrt{2}k_p} \\ &+ M_{110}M_{112k_p}M_{11\sqrt{2}k_p}M_{21\sqrt{2}k_p}), \end{aligned} \quad (6)$$

being independent of the directions of the respective wave vectors. In obtaining this equation we took into account that the coefficients $M_{j,j',\mathbf{k}}$ depend on the modulus k only. Consequently, we may take $V_{\mathbf{k}_p} = V_{\mathbf{k}_{pn}, \mathbf{k}_{pm}, -\mathbf{k}_{pn}}^{1111}$ and find

$$\begin{aligned} H_{pp}^{\text{par}} &= V_{k_p}(P_{1\mathbf{k}_{p1}}P_{1\mathbf{k}_{p2}}P_{1\mathbf{k}_i}^\dagger P_{1\mathbf{k}_{s1}}^\dagger + P_{1\mathbf{k}_{p2}}P_{1\mathbf{k}_{p3}}P_{1\mathbf{k}_i}^\dagger P_{1\mathbf{k}_{s2}}^\dagger \\ &+ P_{1\mathbf{k}_{p3}}P_{1\mathbf{k}_{p4}}P_{1\mathbf{k}_i}^\dagger P_{1\mathbf{k}_{s3}}^\dagger + P_{1\mathbf{k}_{p1}}P_{1\mathbf{k}_{p4}}P_{1\mathbf{k}_i}^\dagger P_{1\mathbf{k}_{s4}}^\dagger) + \text{H.c.} \end{aligned} \quad (7)$$

We now assume coherent pump polariton fields of equal amplitude, $P_{1\mathbf{k}_{pn}} = P_{1\mathbf{k}_{pm}} = P_{1\mathbf{k}_p}$ for $n, m = 1, \dots, 4$. Then, in the limit of low excitation intensity ($V_{k_p}|P_{1\mathbf{k}_p}|^2 t \ll 1$) [33], the Hamiltonian H_{pp}^{par} from Eq. (7)—when acting on a vacuum state—generates polaritons in the state

$$|\psi_{\text{out}}\rangle = \frac{1}{2}|1\rangle_i(|1\rangle_{s1} + |1\rangle_{s2} + |1\rangle_{s3} + |1\rangle_{s4}), \quad (8)$$

where we denote with $|1\rangle_x$ the state of a polariton in channel $x = i$ (idler), $s1, \dots, s4$ (signal). We now take the partial trace over the idler mode i to obtain the state ρ of the four signal fields

$$\rho = \text{Tr}_i|\psi_{\text{out}}\rangle\langle\psi_{\text{out}}| = |\psi\rangle\langle\psi|, \quad (9)$$

where

$$|\psi\rangle = \frac{1}{2}(|1,0,0,0\rangle + |0,1,0,0\rangle + |0,0,1,0\rangle + |0,0,0,1\rangle) \quad (10)$$

is a four-partite entangled pure state, called the W state. In the following, we denote this state as a four-mode W state. In a similar way one may generate not only four-mode, but also 2^N -mode W states.

To obtain the state of the emitted light we have to couple the intracavity polariton scattering dynamics to an extracavity field and determine the parametric luminescence. As is known from previous results [27,32,46] there is a correspondence between the properties of the polaritons within the cavity and the emitted photons outside the cavity. In particular, due to energy and momentum conservation, the emitted photon has both the energy and the in-plane momentum of the corresponding polariton. Since the coupling strength between an extracavity photon and an intracavity polariton depends on the energy and the modulus of the in-plane wave vector only, in the considered setup every (polariton) signal mode is equally coupled to a corresponding mode of the external field. Hence, we can assume that the emitted signal fields outside the microcavity are given by the state (8).

III. IDENTIFICATION OF MULTIPARTITE ENTANGLEMENT

In the bipartite case, several approaches for the identification and even for the quantification of entanglement exist (see, e.g., [3,4]). Examples are the relative entropy of entanglement [15] and Schmidt number witnesses for mixed states [12,47]. In the N -partite case with $N > 2$ we must distinguish between partially and fully entangled states. On the one hand, a pure quantum state is called partially entangled if it cannot be written as a product of states of each subsystem, i.e., it is not fully separable. On the other hand, if the state is not even partially separable, i.e., we cannot separate any subsystem, it is called fully entangled. These definitions can also be extended to mixed quantum states, since they can be written as classical mixtures of pure states.

For the identification of entanglement we use the method of multipartite entanglement witnesses [20]. A quantum state ρ is partially entangled if and only if there exists a Hermitian operator L with

$$\langle L \rangle = \text{Tr } \rho L > f_{\text{full}}(L), \quad (11)$$

where $f_{\text{full}}(L)$ is the maximum expectation value of L for fully separable states,

$$f_{\text{full}}(L) = \sup\{\langle \psi | L | \psi \rangle : |\psi\rangle \text{ fully separable}\}. \quad (12)$$

Accordingly, the state ρ is fully entangled if and only if there exists a Hermitian operator L with

$$\langle L \rangle = \text{Tr } \rho L > f_{\text{part}}(L), \quad (13)$$

where $f_{\text{part}}(L)$ is the maximum expectation value of L for partially separable states,

$$f_{\text{part}}(L) = \sup\{\langle \psi | L | \psi \rangle : |\psi\rangle \text{ partially separable}\}. \quad (14)$$

An entanglement witness can be constructed as $f_{\text{full/part}}(L)\mathbb{I} - L$, where \mathbb{I} denotes the identity [48].

The calculation of the values of the functions $f_{\text{full}}(L)$ and $f_{\text{part}}(L)$ is based on the solution of so-called separability eigenvalue (SE) equations [20]. In the N -partite case with the combined Hilbert space $\mathcal{H} = \bigotimes_{k=1}^N \mathcal{H}_k$ the maximum expectation value of L for fully separable states can be obtained from the solution of the equations

$$L_{\psi_1, \dots, \psi_{k-1}, \psi_{k+1}, \dots, \psi_N} |\psi_k\rangle = g |\psi_k\rangle \quad (15)$$

for $k = 1, \dots, N$. Here $|\psi_k\rangle \in \mathcal{H}_k$ are the normalized eigenstates of the reduced operator

$$\begin{aligned} & L_{\psi_1, \dots, \psi_{k-1}, \psi_{k+1}, \dots, \psi_N} \\ &= \text{Tr}_{1, \dots, k-1, k+1, \dots, N} [(\langle \psi_1 | \langle \psi_1 | \otimes \dots \otimes \langle \psi_{k-1} | \langle \psi_{k-1} | \\ & \quad \otimes \mathbb{I}_k \otimes \langle \psi_{k+1} | \langle \psi_{k+1} | \otimes \dots \otimes \langle \psi_N | \langle \psi_N | L], \end{aligned} \quad (16)$$

and the corresponding eigenvalue g ,

$$g = \langle \psi_1, \dots, \psi_N | L | \psi_1, \dots, \psi_N \rangle, \quad (17)$$

is called SE of L . The value of the function $f_{\text{full}}(L)$ then is

$$f_{\text{full}}(L) = \max\{g : g \text{ SE of } L\}. \quad (18)$$

The value of the function $f_{\text{part}}(L)$ in general depends on the chosen decomposition of the combined Hilbert space, which can be computed by the same form of equations [20]. In the

N -partite case $\mathcal{H} = \bigotimes_{k=1}^N \mathcal{H}_k$ a separation of \mathcal{H} into $K < N$ subsystems results in the SE equations

$$L_{\psi_1, \dots, \psi_{k-1}, \psi_{k+1}, \dots, \psi_K} |\psi_k\rangle = g |\psi_k\rangle \quad (19)$$

for $j = 1, \dots, K$. Note that the symbols $|\psi_k\rangle$ in Eq. (19) denote a state of the k th subsystem with $k \in [1, K]$, whereas in Eq. (15) it is used for a state of the k th mode with $k \in [1, N]$. To obtain the value of the function $f_{\text{part}}(L)$ we have to consider all possible partial decompositions of the combined Hilbert space. For every decomposition we calculate the maximum SE g . Then, $f_{\text{part}}(L)$ is the maximum of all these values.

As an example, let us consider the four-mode W state $|\psi\rangle$ from Eq. (10). A general pure state of the n th signal mode ($n = 1, \dots, 4$) is given by $|\psi_n\rangle = (\alpha_0^n)^* |0\rangle + (\alpha_1^n)^* |1\rangle$ with $|\alpha_0^n|^2 + |\alpha_1^n|^2 = 1$. We choose $L = \rho$ as the Hermitian test operator, such that $\langle L \rangle = \text{Tr } \rho L = 1$. From symmetry reasons we have to consider one component only, say the fourth one. The SE equation for full separability then reads $L_{\psi_1, \psi_2, \psi_3} |\psi_4\rangle = g |\psi_4\rangle$. We obtain

$$L_{\psi_1, \psi_2, \psi_3} = |\psi_{1,2,3}\rangle \langle \psi_{1,2,3}| \quad (20)$$

with

$$\begin{aligned} |\psi_{1,2,3}\rangle &= \frac{1}{2} (\alpha_0^1 \alpha_0^2 \alpha_0^3 + \alpha_0^1 \alpha_1^2 \alpha_0^3 + \alpha_1^1 \alpha_0^2 \alpha_0^3) |0\rangle \\ & \quad + \frac{1}{2} \alpha_0^1 \alpha_0^2 \alpha_0^3 |1\rangle. \end{aligned} \quad (21)$$

Since we are interested in nontrivial solutions of the SE equation, we find $|\psi_4\rangle = M |\psi_{1,2,3}\rangle$ with a normalization constant M . The corresponding eigenvalue g then is

$$g = \frac{1}{4} (|\alpha_0^1 \alpha_0^2 \alpha_0^3 + \alpha_0^1 \alpha_1^2 \alpha_0^3 + \alpha_1^1 \alpha_0^2 \alpha_0^3|^2 + |\alpha_0^1 \alpha_0^2 \alpha_0^3|^2). \quad (22)$$

The maximum g is obtained for $\alpha_0^1 = \alpha_0^2 = \alpha_0^3 = \sqrt{3}/2$ and we find

$$f_{\text{full}}(L) = \frac{27}{64}, \quad (23)$$

which obviously is smaller than one, such that the four-mode W state is shown to be partially entangled.

As mentioned above, the SE equations for partial separability depend on the chosen separation. In a first step, we consider the fourth mode as separated. The solution of the corresponding SE equation then yields the maximum expectation value $f_{\text{part}}^{123:4}(L) = 3/4$, where the superindex 123:4 indicates the chosen decomposition. For symmetry reasons permutations of this separation will result in the same value. For the remaining separations we find $f_{\text{part}}^{12:3:4}(L) = f_{\text{part}}^{12:34}(L) = 1/2$. Hence,

$$f_{\text{part}}(L) = \frac{3}{4}, \quad (24)$$

such that the four-mode W state $|\psi\rangle$ from Eq. (10) is not only partially but also fully entangled.

IV. ENTANGLEMENT IN THE PRESENCE OF LOSSES

In this section we study the propagation of entangled light through media which can be described by realistic loss models (cf. [49–51]). This may include losses during the outcoupling of the field from the cavity [52], and the subsequent propagation through lossy media. Of special importance are turbulent media since they describe the typical

propagation of light in the atmosphere [53]. In particular, we perform an entanglement test where the witness is based on a general pure W state. This allows us to study the effects of the lossy channel on the entanglement within the state of the signal fields.

A. Mixing with vacuum

We consider the case of a four-mode radiation field with up to one photon per mode. In a random loss model the initial pure state mixes with some vacuum contributions. A replacement scheme of this atmospheric propagation is a chain of beam splitters, which transmits a part of the incident light and scatters the remaining radiation. The scattered part of the light is given by the reflectivity $\sqrt{1-\eta}$ of the beam splitter and, in general, depends on the wave vector \mathbf{k} of the propagating light, i.e., the quantum efficiency is $\eta = \eta(\mathbf{k})$.

Mathematically, this process can be described by replacing the polariton creation operators $p_{1\mathbf{k}_{sn}}$ in the Hamiltonian equation (7) by a loss model of the output light $\sqrt{\eta_n}p_{\mathbf{k}_{sn}}^\dagger + \sqrt{1-\eta_n}b_n^\dagger$, where $\eta_n = \eta(\mathbf{k}_{sn})$ and b_n^\dagger creates a polariton in bath n . Note that the elaboration for polaritons instead of photons is justified through the equivalence of their respective momenta [33,46], as we already mentioned in Sec. II. The state of the emitted polaritons is then obtained by applying the resulting Hamiltonian onto the polariton vacuum. To obtain the state of the signal fields only, we take the partial trace over the idler mode and the bath degrees of freedom. The resulting state reads

$$\rho_{\text{mix}} = |\psi_{\text{mix}}\rangle\langle\psi_{\text{mix}}| + \frac{1}{4} \left(4 - \sum_{n=1}^4 \eta_n \right) |0,0,0,0\rangle\langle 0,0,0,0|, \quad (25)$$

where

$$|\psi_{\text{mix}}\rangle = \frac{1}{2} (\sqrt{\eta_1}|1,0,0,0\rangle + \sqrt{\eta_2}|0,1,0,0\rangle + \sqrt{\eta_3}|0,0,1,0\rangle + \sqrt{\eta_4}|0,0,0,1\rangle) \quad (26)$$

is a generalized four-mode W state. Let us also note that the turbulence model of losses is given by a probability distribution $\mathcal{P}(\eta_1, \dots, \eta_4)$ of the quantum efficiencies [53]. In the considered approximation this yields a replacement of the values η_n with the corresponding mean values.

B. General W -state witness

The mixed four-mode state ρ_{mix} from Eq. (25) can be written as the trace of a pure five-mode state over the fifth mode, i.e.,

$$\rho_{\text{mix}} = \text{Tr}_5 |W_5\rangle\langle W_5|. \quad (27)$$

Here,

$$|W_5\rangle = \frac{\sqrt{\eta_1}}{2} |1,0,0,0,0\rangle + \frac{\sqrt{\eta_2}}{2} |0,1,0,0,0\rangle + \frac{\sqrt{\eta_3}}{2} |0,0,1,0,0\rangle + \frac{\sqrt{\eta_4}}{2} |0,0,0,1,0\rangle + \frac{1}{2} \sqrt{4-\eta_1-\eta_2-\eta_3-\eta_4} |0,0,0,0,1\rangle \quad (28)$$

is a generalized five-mode W state. In order to detect entanglement within the state ρ_{mix} , i.e., in order to calculate the

right-hand sides of the conditions (11) and (13), it is therefore sufficient to consider a test operator based on a pure W state only. This property is known as the theorem of cascaded structures [20]. Since the right-hand sides of the entanglement conditions (11) and (13) are independent of the considered state, the results can be used to detect entanglement for any arbitrary state. Thus, we here consider the general test operator $L = |W_N\rangle\langle W_N|$ based on the generalized N -mode W state

$$|W_N\rangle = \sum_{i=1}^N \lambda_i |0, \dots, 0, 1, 0, \dots, 0\rangle, \quad (29)$$

where the λ_i for $i = 1, \dots, N$ are the weights of the respective modes.

1. Test for partial entanglement

As mentioned before, the value of the function $f_{\text{full}}(L)$ is obtained from the solution of the corresponding separability eigenvalue equations (15). For the state $|\psi_n\rangle$ of the n th subsystem we choose the parametrization $|\psi_n\rangle = (\alpha_0^n)^* |0\rangle + (\alpha_1^n)^* |1\rangle$ with the normalization $|\alpha_0^n|^2 + |\alpha_1^n|^2 = 1$. Explicitly, we get $L_{\psi_1, \dots, \psi_{k-1}, \psi_{k+1}, \dots, \psi_N} = |\psi_{1, \dots, k-1, k+1, \dots, N}\rangle\langle\psi_{1, \dots, k-1, k+1, \dots, N}|$ with

$$|\psi_{1, \dots, k-1, k+1, \dots, N}\rangle = \sum_{\substack{i=1 \\ i \neq k}}^N \lambda_i \alpha_1^i \prod_{\substack{j=1 \\ j \neq i, k}}^N \alpha_0^j |0\rangle + \lambda_k \prod_{\substack{j=1 \\ j \neq k}}^N \alpha_0^j |1\rangle \quad (30)$$

and

$$g = \left| \sum_{i=1}^N \lambda_i \alpha_1^i \prod_{\substack{j=1 \\ j \neq i}}^N \alpha_0^j \right|^2. \quad (31)$$

This expression has to be maximized over all α_0^n and α_1^n . We may decompose $\alpha_x^n = r_x^n e^{i\varphi_x^n}$ and $\lambda_n = |\lambda_n| e^{i\theta_n}$ for $x = 0, 1$ and $n = 1, \dots, N$ in polar coordinates, such that $r_1^n = \sqrt{1 - (r_0^n)^2}$. The definition $r_n = r_0^n$ and the maximization over all φ_x^n and θ_n then leads to the equation

$$g = \left(\sum_{i=1}^N |\lambda_i| \sqrt{1 - r_i^2} \prod_{\substack{j=1 \\ j \neq i}}^N r_j \right)^2. \quad (32)$$

We now have to maximize over $r_n \in [0, 1]$ for $n = 1, \dots, N$. At the borders $r_n = 0, 1$ the function in Eq. (32) assumes the solutions

$$g = 0, |\lambda_1|^2, \dots, |\lambda_N|^2. \quad (33)$$

If g has a local maximum for at least one $r_n \in (0, 1)$, the partial derivatives $\partial g / \partial r_n$ vanish at this point. This requirement leads to the N equations

$$|\lambda_n| = x_n \sum_{\substack{i=1 \\ i \neq n}}^N |\lambda_i| x_i \quad (34)$$

for $n = 1, \dots, N$, where we introduced the new variables $x_n = \sqrt{1 - r_n^2}/r_n \in (0, \infty)$. To obtain the global maximum of g we have to compare the solutions (33) with the local extrema determined from the solution of Eqs. (34).

For general choices of the weights λ_n for $n = 1, \dots, N$ Eqs. (34) have to be solved numerically. Analytical results can be obtained for an equal-weighted W state with $|\lambda_n| = 1/\sqrt{N}$ for all $n = 1, \dots, N$. Then, the solution of Eqs. (34) reads

$$x_1 = \dots = x_N = \frac{1}{\sqrt{N-1}}, \quad (35)$$

such that

$$g_{\max} = f_{\text{full}}(L) = \left(\frac{N-1}{N}\right)^{N-1}. \quad (36)$$

A more general but also analytically solvable situation arises, if we assume that all but one weights are equal, i.e., $|\lambda_1| = \dots = |\lambda_{N-1}| = \lambda$ and $|\lambda_N| = \lambda'$. Note that this situation corresponds to the choice of equal reflectivities $\eta_1 = \eta_2 = \eta_3 = \eta_4$ within the five-mode W state from Eq. (28). After some algebra, we get in the general N -mode case

$$g_{\max} = (N-1)\lambda^2 \left(\frac{(N-1)(N-2)\lambda^2}{(N-1)^2\lambda^2 - (\lambda')^2} \right)^{N-2}, \quad (37)$$

which is valid for $\lambda'/\lambda < \sqrt{N-1}$. If $\lambda'/\lambda \geq \sqrt{N-1}$ Eqs. (34) have no solution, such that $g_{\max} = \max_{n=1}^N |\lambda_n|^2$ taking the solutions (33) into account.

2. Test for full entanglement

To obtain the value of the function $f_{\text{part}}(L)$ we have to consider all possible separations of the Hilbert space. In a first step we study a general bipartite decomposition of the state $|W_N\rangle$. In particular, we consider the n subsystems with indices $k_1 < \dots < k_n$ as one party (system A) and the other $N-n$ subsystems with indices $k_{n+1} < \dots < k_N$ as the second party (system B). We then may write

$$|W_N\rangle = \sum_{i=1}^n \lambda_{k_i} |2^i, 0\rangle + \sum_{i=n+1}^N \lambda_{k_i} |0, 2^{i-n}\rangle, \quad (38)$$

where we introduced the abbreviations

$$|2^i, 0\rangle = \underbrace{|0, \dots, 0, 1, 0, \dots, 0\rangle}_{k_i-1} \quad (39)$$

and

$$|0, 2^{i-n}\rangle = \underbrace{|0, \dots, 0, 1, 0, \dots, 0\rangle}_{k_i-1} \quad (40)$$

in the form of two binary numbers for the states of the two parties. Note that, although the right-hand sides of Eqs. (39) and (40) look equal, they belong to different states. In Eq. (39) the mode k_i corresponds to a subsystem of system A ($i \in [1, n]$), whereas in Eq. (40) the k_i belongs to a subsystem of system B ($i \in [n+1, N]$).

We trace out the system A and obtain

$$\text{Tr}_A L = \sum_{i,j=n+1}^N \lambda_{k_i} \lambda_{k_j}^* |2^{i-n}\rangle \langle 2^{j-n}| + \sum_{i=1}^n |\lambda_{k_i}|^2 |0\rangle \langle 0|. \quad (41)$$

Since this expression already is the spectral decomposition, i.e., it is diagonal in the two states

$$|0\rangle, \quad \left(\sum_{i=n+1}^N |\lambda_{k_i}|^2 \right)^{-1/2} \sum_{i=n+1}^N \lambda_{k_i} |2^{i-n}\rangle, \quad (42)$$

we get two separability eigenvalues for the considered bipartition, such that

$$g_{\max} = \max \left\{ \sum_{i=1}^n |\lambda_{k_i}|^2, \sum_{i=n+1}^N |\lambda_{k_i}|^2 \right\}. \quad (43)$$

Note that the method of tracing out a system and reading of the separability eigenvalues from the result is valid only in the bipartite case ($N=2$) because in this situation the solutions (33) are the only ones.

The maximum of the values (43) is obtained for $n=1$, if we choose the mode with the smallest weight as system A , or for $n=N-1$, if we choose the $N-1$ modes with the largest weights as system A . The resulting eigenvalue is then the sum of the $N-1$ largest $|\lambda_i|^2$. In particular, in the case of equal weights we have $g_{\max} = (N-1)/N$, and in the case of all but one equal weights we have $g_{\max} = (N-1)\lambda^2$ if $\lambda > \lambda'$ and $g_{\max} = (N-2)\lambda^2 + (\lambda')^2$ if $\lambda < \lambda'$.

We now consider the general decomposition of the combined Hilbert space into K subsystems. We may write

$$|W_N\rangle = \sum_{n=1}^K \sum_{m=1}^{N_n} \lambda_m^{(n)} |0, \dots, 0, 2^m, 0, \dots, 0\rangle, \quad (44)$$

where N_n is the number of modes that are combined into subsystem n . Accordingly, $\lambda_m^{(n)}$ denotes the weight of the m th mode within subsystem n . The state $|0, \dots, 0, 2^m, 0, \dots, 0\rangle$ is a product of states of the n subsystems, where 0 denotes the respective vacuum state and 2^m denotes the state of one photon in mode m . To shorten the expressions we introduce

$$|a_n\rangle = \sum_{m=1}^{N_n} \lambda_m^{(n)} |2^m\rangle, \quad (45)$$

being the (unnormalized) state of the n th subsystem, such that

$$|W_N\rangle = \sum_{n=1}^K |0, \dots, 0, a_n, 0, \dots, 0\rangle. \quad (46)$$

Similar to the case of partial entanglement we have to solve the separability eigenvalue equations (19) and obtain $L_{\psi_1, \dots, \psi_{n-1}, \psi_{n+1}, \dots, \psi_K} = |\psi_{1, \dots, n-1, n+1, \dots, K}\rangle \langle \psi_{1, \dots, n-1, n+1, \dots, K}|$ with

$$\begin{aligned} |\psi_{1, \dots, n-1, n+1, \dots, K}\rangle = & \left(\sum_{\substack{i=1 \\ i \neq n}}^K \langle \psi_i | a_i \rangle \prod_{\substack{j=1 \\ j \neq i, n}}^K \langle \psi_j | 0 \rangle \right) |0\rangle \\ & + \left(\prod_{\substack{j=1 \\ j \neq n}}^K \langle \psi_j | 0 \rangle \right) |a_n\rangle. \end{aligned} \quad (47)$$

Hence, we can use

$$|\psi_n\rangle = (\alpha_0^n)^* |0\rangle + \frac{(\alpha_1^n)^*}{\sqrt{M_n}} |a_n\rangle \quad (48)$$

with $|\alpha_0^n|^2 + |\alpha_1^n|^2 = 1$ and $M_n = \langle a_n | a_n \rangle$ as parametrization for the state of the n th subsystem. The separability eigenvalue then follows as

$$g = \left| \sum_{i=1}^K \sqrt{M_i} \alpha_1^i \prod_{\substack{j=1 \\ j \neq i}}^K \alpha_0^j \right|^2. \quad (49)$$

Again, we can decompose $\alpha_x^n = r_x^n e^{i\varphi_x^n}$ for $x = 0, 1$ and $n = 1, \dots, K$ in polar coordinates such that $r_1^n = \sqrt{1 - (r_0^n)^2}$, define $r_n = r_0^n$, and obtain after maximization over the phases φ_x^n the relation

$$g = \left(\sum_{i=1}^K \sqrt{M_i} \sqrt{1 - r_i^2} \prod_{\substack{j=1 \\ j \neq i}}^K r_j \right)^2. \quad (50)$$

The solutions $g = M_n$ for $n = 1, \dots, K$ are obtained for $r_n = 0$ and $r_i = 1$ for $i = 1, \dots, K$ with $i \neq n$. For all other solutions we can compare Eq. (50) with Eq. (32) to see that the structure of both expressions is the same. It follows that the maximum separability eigenvalue in the case of full entanglement can be obtained from the general solution to Eq. (32) for partial entanglement if we replace the number of modes N by the number of subsystems K and the weights $|\lambda_i|$ by the values $\sqrt{M_i}$.

C. Analytical and numerical results

The general results from the last section allow us to identify the parameter range of the efficiencies η_n , for which the mixed signal state ρ_{mix} from Eq. (25) is partially and fully entangled. Choosing $L = \rho_{\text{mix}}$ we obtain for the left-hand side of all tests

$$\text{Tr } \rho_{\text{mix}} L = 1 - \frac{1}{2} \sum_{n=1}^4 \eta_n + \frac{1}{8} \left(\sum_{n=1}^4 \eta_n \right)^2. \quad (51)$$

Analytical results can be obtained for equal reflectivities, i.e., $\eta_n = \eta$ for all $n = 1, \dots, 4$. Because the moduli of the signal wave vectors \mathbf{k}_{sn} are equal in the considered scenario this assumption corresponds to a situation, where the reflectivities are isotropic. Then, we can use the result from Eq. (37) yielding

$$f_{\text{full}}(L) = \begin{cases} 1 - \eta, & 0 \leq \eta \leq 1/2 \\ 27\eta^4(5\eta - 1)^{-3}, & 1/2 < \eta \leq 1. \end{cases} \quad (52)$$

To determine the value of the function $f_{\text{part}}(L)$ we have to solve Eq. (50) for all relevant decompositions of the combined Hilbert space. Since we use the operator $L = |W_5\rangle\langle W_5|$ based on the pure five-mode W state from Eq. (28) instead of the mixed four-mode state ρ_{mix} from Eq. (25), the fifth mode should always be considered as a separated party. For the remaining four modes we have to allow for all possible decompositions. As a result, the maximum SE is obtained if we consider the fourth and the fifth mode as separated,

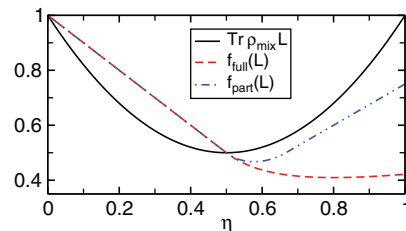


FIG. 2. (Color online) Left- and right-hand sides of Eqs. (11) and (13) as functions of $\eta = \eta_n$ for $n = 1, \dots, 4$. The state ρ_{mix} is partially entangled in regions where $\text{Tr } \rho_{\text{mix}} L > f_{\text{full}}(L)$ and fully entangled if $\text{Tr } \rho_{\text{mix}} L > f_{\text{part}}(L)$ with respect to the choice $L = \rho_{\text{mix}}$.

such that the states $|a_n\rangle$ from Eq. (45) are given by $|a_1\rangle = (\sqrt{\eta}/2)(|1,0,0\rangle + |0,1,0\rangle + |0,0,1\rangle)$, $|a_2\rangle = (\sqrt{\eta}/2)|1\rangle$, and $|a_3\rangle = \sqrt{1-\eta}|1\rangle$. It follows that $M_1 = 3\eta/4$, $M_2 = \eta/4$, and $M_3 = 1 - \eta$. After maximization of Eq. (50) for these values we obtain

$$f_{\text{part}}(L) = \begin{cases} 1 - \eta, & 0 \leq \eta \leq 1/2 \\ \frac{3\eta^2(\eta-1)}{13\eta^2-16\eta+4}, & 1/2 < \eta < 2/3 \\ 3\eta/4, & 2/3 \leq \eta \leq 1. \end{cases} \quad (53)$$

Note that according to our assumption of equal reflectivities the same result is obtained if one considers the first, second, or third together with the fifth mode as separated.

In Fig. 2 we show the results $f_{\text{full}}(L)$ and $f_{\text{part}}(L)$ from Eqs. (52) and (53) together with $\text{Tr } \rho_{\text{mix}} L$ from Eq. (51) as functions of η . We see, that we can detect entanglement for $\eta > 1/2$. The witness based on $L = \rho_{\text{mix}}$ does not distinguish between partial and full entanglement.

Numerically, we can also study the case of unequal reflectivities. As an example, we choose $\eta = \eta_n$ for $n = 1, 2, 3$ and $\eta' = \eta_4$. This choice corresponds to a nonisotropic situation, where the dependency of the reflectivity on the direction \mathbf{k}_{s4} differs from that of the other directions. In Figs. 3(a) and 3(b) we show the numerical results for the functions $\text{Tr } \rho_{\text{mix}} L - f_{\text{full}}(L)$ and $\text{Tr } \rho_{\text{mix}} L - f_{\text{part}}(L)$, respectively. We see, that these functions take positive values in some regions indicating that the state ρ_{mix} is partially or fully entangled.

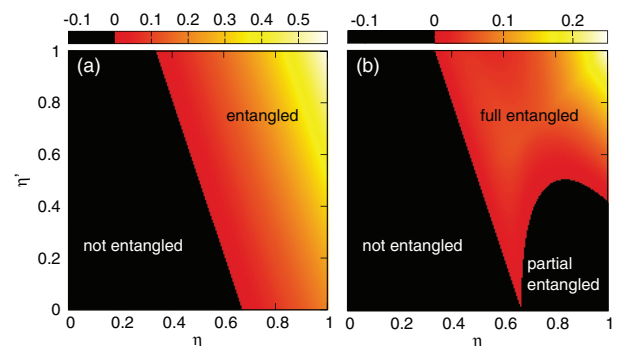


FIG. 3. (Color online) Contour plots of (a) $\text{Tr } \rho_{\text{mix}} L - f_{\text{full}}(L)$ and (b) $\text{Tr } \rho_{\text{mix}} L - f_{\text{part}}(L)$ as functions of $\eta = \eta_1 = \eta_2 = \eta_3$ and $\eta' = \eta_4$. The state ρ_{mix} is partially or fully entangled in regions where the respective function takes positive values.

From the test for partial entanglement—summarized in the left panel (a) of Fig. 3—we conclude that the state ρ_{mix} is not entangled within the black region and contains some entangled modes within the colored region. Panel (b) of Fig. 3 shows the corresponding results for the test for full entanglement. This panel shows an additional black region at the lower right corner, where the state ρ_{mix} is not fully entangled. Together with the results from panel (a) of Fig. 3 we conclude that the state ρ_{mix} is partially entangled in this additional black region and fully entangled within the remaining colored region.

V. CONCLUSIONS

We have studied the generation and the characterization of multipartite entanglement of light that is emitted from a planar semiconductor microcavity. Here, a monochromatic pumping of the lower polariton branch with four pumps arranged on a cone with opening angle below twice the magic angle leads to the emission of light in a four-mode W state. From an experimental point of view the most critical points in building the proposed setup are the realization of the pump geometry, the suppression of stray light, and the detection of the entangled output fields. Using linear optics, such as beam splitters and mirrors, our scheme requires careful adjustment of all optical paths. Recently, the authors of Ref. [54] proposed a multidimensional laser spectroscopy setup using spatial light modulators. Adapting this concept, it should also be possible to realize the required pump geometry. The stray light can be suppressed by means of spatial filtering [55], such that the setup under study can be experimentally realized [56]. In the context of the detection of entanglement, the advantage of our setup is that all pumps share the same frequency. In addition, all signal fields share the same frequency as well, which is different from the pump frequency however. This makes it possible to perform interference experiments or balanced homodyne detection of the four signal fields [57].

In our theoretical study, the identification of the multipartite entanglement of the light emitted from the microcavity is done by using the method of multipartite entanglement witnesses. We provide the solution for an entanglement test with a witness

based on a general N -mode W state. Using this solution, we characterize the light propagation through lossy channels regarding its entanglement properties. We showed that we can guarantee partial and full entanglement for certain ranges of loss. In our theoretical description the boundaries between these regions are sharp. In an experimental realization the distance between the left-hand side, $\text{Tr } \rho L$, and the right-hand side, $f_{\text{full/part}}(L)$, of the entanglement condition determines the maximum allowed fluctuations for a successful entanglement test.

From our results we can conclude, that in the case of a pure state the optimal entanglement witness is given by the state itself. Due to the theorem of cascaded structures [20], we may reduce the optimal test for mixed states to a pure test with one additional degree of freedom. This allows us to verify the entanglement of mixed states as well.

In particular, we deduce general criteria to decide whether an arbitrary N -mode state ρ is partially or fully entangled. For this purpose we constructed an appropriate test operator based on the N -mode W state itself. For every bipartite decomposition of the combined Hilbert space the corresponding boundary of the entanglement condition is readily calculated. Thus, we can perform a test for entanglement for every bipartite decomposition of the considered state. The full classification of the state ρ is the following. First, if there is no bipartite decomposition for which entanglement has been verified, then the state ρ under study is not entangled. Second, if there is at least one decomposition with a successful test, the state is at least partially entangled. Third, if any test is positive for any bipartite decomposition, the state is fully entangled. In the second case we can even identify which modes are entangled and which separate from all others. For this task we have to gradually repeat the bipartite tests within the two subsystems that are not entangled.

ACKNOWLEDGMENTS

We thank H. Stolz for valuable discussions. This work was supported by the Deutsche Forschungsgemeinschaft through SFB 652 by projects B5 and B12.

-
- [1] A. Einstein, B. Podolsky, and N. Rosen, *Phys. Rev.* **47**, 777 (1935).
 - [2] E. Schrödinger, *Naturwiss.* **23**, 807 (1935).
 - [3] M. A. Nielsen and I. L. Chuang, *Quantum Computation and Quantum Information* (Cambridge University Press, Cambridge, 2010).
 - [4] R. Horodecki, P. Horodecki, M. Horodecki, and R. Horodecki, *Rev. Mod. Phys.* **81**, 865 (2009).
 - [5] O. Gühne and G. Tóth, *Phys. Rep.* **474**, 1 (2009).
 - [6] R. F. Werner, *Phys. Rev. A* **40**, 4277 (1989).
 - [7] D. M. Greenberger, M. A. Horne, and A. Zeilinger, *Going Beyond Bells Theorem in Bells Theorem, Quantum Theory, and Conceptions of the Universe* (Kluwer Academic, Dordrecht, 1989).
 - [8] W. Dür, G. Vidal, and J. I. Cirac, *Phys. Rev. A* **62**, 062314 (2000).
 - [9] A. K. Ekert, *Phys. Rev. Lett.* **67**, 661 (1991).
 - [10] C. H. Bennett and S. J. Wiesner, *Phys. Rev. Lett.* **69**, 2881 (1992).
 - [11] C. H. Bennett, G. Brassard, C. Crepeau, R. Jozsa, A. Peres, and W. K. Wootters, *Phys. Rev. Lett.* **70**, 1895 (1993).
 - [12] M. Horodecki, P. Horodecki, and R. Horodecki, *Phys. Lett. A* **223**, 1 (1996).
 - [13] M. Horodecki, P. Horodecki, and R. Horodecki, *Phys. Lett. A* **283**, 1 (2001).
 - [14] V. Vedral, M. B. Plenio, M. A. Rippin, and P. L. Knight, *Phys. Rev. Lett.* **78**, 2275 (1997).
 - [15] V. Vedral and M. B. Plenio, *Phys. Rev. A* **57**, 1619 (1998).
 - [16] G. Vidal, *J. Mod. Opt.* **47**, 355 (2000).
 - [17] F. G. S. L. Brandao, *Phys. Rev. A* **72**, 022310 (2005).
 - [18] F. G. S. L. Brandao and R. O. Vianna, *Int. J. Quantum Inf.* **4**, 331 (2006).
 - [19] J. Sperling and W. Vogel, *Phys. Scr.* **83**, 045002 (2011).

- [20] J. Sperling and W. Vogel, *Phys. Rev. Lett.* **111**, 110503 (2013).
- [21] C. Ciuti, *Phys. Rev. B* **69**, 245304 (2004).
- [22] W. Langbein, *Phys. Rev. B* **70**, 205301 (2004).
- [23] C. Ciuti, G. Bastard, and I. Carusotto, *Phys. Rev. B* **72**, 115303 (2005).
- [24] A. Auer and G. Burkard, *Phys. Rev. B* **85**, 235140 (2012).
- [25] P. G. Savvidis, J. J. Baumberg, R. M. Stevenson, M. S. Skolnick, D. M. Whittaker, and J. S. Roberts, *Phys. Rev. Lett.* **84**, 1547 (2000).
- [26] F. Tassone and Y. Yamamoto, *Phys. Rev. B* **59**, 10830 (1999).
- [27] C. Ciuti, P. Schwendimann, and A. Quattropani, *Phys. Rev. B* **63**, 041303 (2001).
- [28] T. Östreich, K. Schönhammer, and L. J. Sham, *Phys. Rev. B* **58**, 12920 (1998).
- [29] T. Usui, *Prog. Theor. Phys.* **23**, 787 (1960).
- [30] G. Rochat, C. Ciuti, V. Savona, C. Piermarocchi, A. Quattropani, and P. Schwendimann, *Phys. Rev. B* **61**, 13856 (2000).
- [31] C. Weisbuch, M. Nishioka, A. Ishikawa, and Y. Arakawa, *Phys. Rev. Lett.* **69**, 3314 (1992).
- [32] R. Houdré, C. Weisbuch, R. P. Stanley, U. Oesterle, P. Pellandini, and M. Ilegems, *Phys. Rev. Lett.* **73**, 2043 (1994).
- [33] S. Savasta, O. Di Stefano, V. Savona, and W. Langbein, *Phys. Rev. Lett.* **94**, 246401 (2005).
- [34] S. Portolan, O. Di Stefano, S. Savasta, and V. Savona, *Europhys. Lett.* **88**, 20003 (2009).
- [35] L. Einkemmer, Z. Vörös, G. Weihs, and S. Portolan, arXiv:1305.1469.
- [36] D. Pagel, H. Fehske, J. Sperling, and W. Vogel, *Phys. Rev. A* **86**, 052313 (2012).
- [37] D. Deams, F. Bernard, N. J. Cerf, and M. I. Kolobov, *J. Opt. Soc. Am. B* **27**, 447 (2010).
- [38] O. Pfister, S. Feng, G. Jennings, R. Pooser, and D. Xie, *Phys. Rev. A* **70**, 020302 (2004).
- [39] A. Ferraro, M. G. A. Paris, M. Bondani, A. Allevi, E. Puddu, and A. Andreoni, *J. Opt. Soc. Am. B* **21**, 1241 (2004).
- [40] P. van Loock and S. L. Braunstein, *Phys. Rev. Lett.* **84**, 3482 (2000).
- [41] V. M. Axt and A. Stahl, *Z. Phys. B* **93**, 195 (1994).
- [42] S. Savasta and R. Girlanda, *Phys. Rev. Lett.* **77**, 4736 (1996).
- [43] S. Portolan, O. Di Stefano, S. Savasta, F. Rossi, and R. Girlanda, *Phys. Rev. B* **77**, 195305 (2008).
- [44] C. Ciuti, V. Savona, C. Piermarocchi, A. Quattropani, and P. Schwendimann, *Phys. Rev. B* **58**, 7926 (1998).
- [45] J. J. Hopfield, *Phys. Rev.* **112**, 1555 (1958).
- [46] V. Savona, F. Tassone, C. Piermarocchi, A. Quattropani, and P. Schwendimann, *Phys. Rev. B* **53**, 13051 (1996).
- [47] J. Sperling and W. Vogel, *Phys. Rev. A* **83**, 042315 (2011).
- [48] J. Sperling and W. Vogel, *Phys. Rev. A* **79**, 022318 (2009).
- [49] W. Vogel and D.-G. Welsch, *Quantum Optics*, 3rd ed. (Wiley-VCH, Weinheim, 2006).
- [50] A. A. Semenov and W. Vogel, *Phys. Rev. A* **81**, 023835 (2010).
- [51] D. Y. Vasylyev, A. A. Semenov, and W. Vogel, *Phys. Rev. Lett.* **108**, 220501 (2012).
- [52] L. Knöll, W. Vogel, and D.-G. Welsch, *Phys. Rev. A* **43**, 543 (1991).
- [53] A. A. Semenov and W. Vogel, *Phys. Rev. A* **80**, 021802(R) (2009).
- [54] P. Mai, B. Pressl, M. Sassermaun, Z. Vörös, G. Weihs, C. Schneider, A. Löffler, S. Höfling, and A. Forchel, *Appl. Phys. Lett.* **100**, 072109 (2012).
- [55] R.-C. Ge, S. Weiler, A. Ulhaq, S. M. Ulrich, M. Jetter, P. Michler, and S. Hughes, *Opt. Lett.* **38**, 1691 (2013).
- [56] H. Stolz (private communication).
- [57] J. DiGuglielmo, A. Samblowski, B. Hage, C. Pineda, J. Eisert, and R. Schnabel, *Phys. Rev. Lett.* **107**, 240503 (2011).

Equilibration and thermalization of the dissipative quantum harmonic oscillator in a nonthermal environment

D. Pagel, A. Alvermann,^{*} and H. Fehske*Institut für Physik, Ernst-Moritz-Arndt-Universität, 17487 Greifswald, Germany*

(Received 7 October 2012; revised manuscript received 19 December 2012; published 22 January 2013)

We study the dissipative quantum harmonic oscillator with general nonthermal preparations of the harmonic oscillator bath. The focus is on equilibration of the oscillator in the long-time limit and the additional requirements for thermalization. Our study is based on the exact solution of the microscopic model obtained by means of operator equations of motion, which provides us with the time evolution of the central oscillator density matrix in terms of the propagating function. We find a hierarchy of conditions for thermalization, together with the relation of the asymptotic temperature to the energy distribution in the initial bath state. We discuss the presence and absence of equilibration for the example of an inhomogeneous chain of harmonic oscillators, and we illustrate the general findings about thermalization for the nonthermal environment that results from a quench.

DOI: [10.1103/PhysRevE.87.012127](https://doi.org/10.1103/PhysRevE.87.012127)

PACS number(s): 05.30.—d

I. INTRODUCTION

Equilibration can be defined as the evolution of a system out of equilibrium toward a stationary state in the long-time limit. For quantum systems, the question arises how equilibration is possible in spite of the linear and unitary time evolution, how the stationary state depends on the initial conditions, and to which extent it can be described as a thermal state.

General arguments relate equilibration to dephasing of quantum states [1–5]. Starting from the expansion of an initial state $|\psi(0)\rangle = \sum_{n=1}^N \psi_n |n\rangle$ in the eigenstates $|n\rangle$ of the Hamiltonian $H = \sum_{n=1}^N E_n |n\rangle\langle n|$, the time evolution of an operator expectation value is given by

$$\begin{aligned} \langle A(t) \rangle &= \langle \psi(t) | A | \psi(t) \rangle \\ &= \sum_{m,n=1}^N \psi_m^* \psi_n e^{i(E_m - E_n)t} \langle m | A | n \rangle. \end{aligned} \quad (1)$$

In the thermodynamic limit $N \rightarrow \infty$, we can expect that only diagonal terms $m = n$ survive for $t \rightarrow \infty$, such that the long-time limit of the expectation value is

$$\lim_{t \rightarrow \pm\infty} \langle A(t) \rangle \simeq \text{tr}[\rho_\infty A] \quad (N \rightarrow \infty), \quad (2)$$

with the density matrix $\rho_\infty = \sum_{n=1}^N |\psi_n|^2 |n\rangle\langle n|$. This argument can be justified with the Riemann-Lebesgue lemma [6] that states

$$\lim_{t \rightarrow \pm\infty} \int_{-\infty}^{\infty} f(\omega) e^{i\omega t} d\omega = 0 \quad (3)$$

for any integrable function $f(\omega)$ [here, the density of states is $D(\omega)$]. Although this argument explains the origin of equilibration, not much is learned about the properties of the stationary state ρ_∞ . In particular, the question of thermalization is left open.

In this paper, we study equilibration and thermalization of dissipative quantum harmonic oscillators using the standard model of a central oscillator coupled to a harmonic oscillator bath. For this example we can determine the stationary state

ρ_∞ explicitly and analyze its dependence on the initial conditions completely. Most importantly, we allow for arbitrary nonthermal bath preparations in our study. Thermalization is subject to additional conditions in this more general situation, and we show how the temperature of the asymptotic stationary state is obtained from the initial energy distribution of the oscillator bath rather than from the initial bath temperature. We also include the case study of an interaction quench in an infinite harmonic chain, where undamped oscillations can prevent equilibration at strong damping.

The dissipative quantum harmonic oscillator is studied extensively in the literature [7–10], covering such diverse topics as Brownian motion [11–15], quantum fluctuations [16], driven dissipative systems [17], entanglement [18], the existence of local temperatures [19], or the second law of thermodynamics [20]. Reviews are given, e.g., in Refs. [21–23]. With an exact solution, this model is also an important example for the derivation of master equations [24–27], the discussion of fundamental statistical relations such as fluctuation-dissipation theorems [28] and their connection to detailed balance, and the Kubo-Martin-Schwinger condition [29], or for the assessment of numerical methods that provide a perspective for nonlinear models [30,31]. It appears, however, that the questions addressed here for nonthermal bath preparations require further analysis.

To obtain our results, we proceed as follows. After introduction of the model in Sec. II, we construct the exact solution for nonthermal initial states in Sec. III, including the propagating function in Sec. III D. Further details, including the extension to driven oscillators, are given in Appendixes A and B. The central results for equilibration and thermalization are formulated in Sec. IV. We discuss these results for the example of an infinite chain of harmonic oscillators in Sec. V before we conclude in Sec. VI.

II. THE MODEL

The Hamiltonian for the dissipative quantum harmonic oscillator,

$$H = H_S + H_B + H_{SB}, \quad (4)$$

*alvermann@physik.uni-greifswald.de

is the sum of the contribution of the central oscillator,

$$H_S = \frac{1}{2}[P^2 + \Omega^2 Q^2], \quad (5)$$

the contribution of the harmonic oscillator bath,

$$H_B = \frac{1}{2} \sum_{\nu=1}^N [P_\nu^2 + \omega_\nu^2 Q_\nu^2], \quad (6)$$

and the linear interaction term,

$$H_{SB} = Q \sum_{\nu=1}^N \lambda_\nu Q_\nu. \quad (7)$$

In these expressions, Q_ν, P_ν are position and momentum operators with canonical commutation relations, e.g., $[Q_\mu, P_\nu] = i\delta_{\mu\nu}$. Summations over Greek indices, used for bath oscillator operators Q_ν, P_ν , run from $1, \dots, N$. We suppress an index for the central oscillator operators.

The size of the coupling constants λ_ν is restricted by the positivity condition

$$\Omega^2 - \sum_{\nu=1}^N \frac{\lambda_\nu^2}{\omega_\nu^2} \geq 0. \quad (8)$$

It guarantees that the normal modes of the total Hamiltonian H have real frequencies, such that H is bounded from below [11]. A positive Hamiltonian can always be obtained through addition of the term $(1/2) \sum_{\nu=1}^N (\lambda_\nu/\omega_\nu)^2 Q^2$, which leads to renormalization of the central oscillator frequency [22]. We prefer the present form of the Hamiltonian since it allows for a more natural treatment of the harmonic chain in Sec. V.

Of primary interest to us is the central oscillator density matrix

$$\rho_S(t) = \text{tr}_B[\exp(-iHt)\rho(0)\exp(iHt)], \quad (9)$$

which is obtained from the initial state $\rho(0)$ through propagation with the total Hamiltonian H and subsequent evaluation of the partial trace tr_B over the bath degrees of freedom. A natural choice for $\rho(0)$ are factorizing initial conditions

$$\rho(0) = \rho_S(0) \otimes \rho_B(0), \quad (10)$$

which correspond to the picture that at $t = 0$ the previously isolated central oscillator is brought into contact with the oscillator bath.

The restriction to factorizing initial conditions is not essential for the following derivations, especially not for the long-time limit in Sec. IV, but it is a natural assumption that simplifies the presentation. For example, mixed central/bath oscillator terms drop out of the expressions for the central oscillator variance (see Sec. III B).

III. SOLUTION OF THE DISSIPATIVE QUANTUM OSCILLATOR FOR GENERAL INITIAL CONDITIONS

The central oscillator density matrix $\rho_S(t)$ can be obtained in various ways, e.g., through transformation of H to normal modes [7,11] or by using path integrals [21,32] based on the Feynman-Vernon influence functional formalism [33–35]. The arguably simplest approach is the direct solution of the Heisenberg equations of motion for the operators $Q(t)$ and $P(t)$, which reduces to the solution of a classical equation of motion. The initial conditions $\rho_S(0)$ and $\rho_B(0)$ enter only the

evaluation of central oscillator expectation values, such that we can allow for general initial bath states. The full solution is then given by the propagating function.

A. Reduction to the classical equation of motion

As further detailed in Appendix A, the central piece of information is the solution $u(t) \in \mathbb{R}$ of the classical equation of motion

$$\ddot{u}(t) = -\Omega^2 u(t) + \int_0^t K(t-\tau)u(\tau)d\tau, \quad (11)$$

which is subject to the following conditions:

- (i) $u(t)$ solves Eq. (11) for $t > 0$.
- (ii) $u(t) = 0$ for $t < 0$.
- (iii) The initial conditions are $u(0) = 0, \dot{u}(0) = 1$.

We introduced here the damping kernel

$$K(t) = \sum_{\nu=1}^N \frac{\lambda_\nu^2}{\omega_\nu} \sin \omega_\nu t. \quad (12)$$

The function $u(t)$ can be calculated as the Fourier transform [36]

$$u(t) = \frac{2}{\pi} \int_0^\infty \sin \omega t \text{Im} F(\omega + i0^+) d\omega \quad (13)$$

of the function

$$F(z) = \left(\Omega^2 - z^2 + \sum_{\nu=1}^N \frac{\lambda_\nu^2}{z^2 - \omega_\nu^2} \right)^{-1}, \quad (14)$$

writing $F(\omega + i0^+) = \lim_{\eta \rightarrow 0, \eta > 0} F(\omega + i\eta)$. We note that the positivity condition (8) implies that the poles of $F(z)$ occur on the real axis, such that $u(t)$ is a quasiperiodic function for finite N while $u(t) \rightarrow 0$ for $t \rightarrow \infty$ is possible in the thermodynamic limit $N \rightarrow \infty$. An explicit example for the computation of $u(t)$ is given for the harmonic chain in Sec. V [see Eq. (79)].

To proceed, we introduce the partial Fourier transforms

$$\tilde{u}(t, \omega) = e^{i\omega t} \int_0^t u(\tau) e^{-i\omega\tau} d\tau, \quad (15)$$

$$\tilde{v}(t, \omega) = e^{i\omega t} \int_0^t \dot{u}(\tau) e^{-i\omega\tau} d\tau = u(t) + i\omega \tilde{u}(t, \omega), \quad (16)$$

and define the matrices

$$\mathbf{U}(t) = \begin{pmatrix} U_{QQ}(t) & U_{QP}(t) \\ U_{PQ}(t) & U_{PP}(t) \end{pmatrix} = \begin{pmatrix} \dot{u}(t) & u(t) \\ \ddot{u}(t) & \dot{u}(t) \end{pmatrix}, \quad (17)$$

$$\mathbf{U}(t, \omega) = \begin{pmatrix} \text{Re} \tilde{u}(t, \omega) & \frac{\text{Im} \tilde{u}(t, \omega)}{\omega} \\ \text{Re} \tilde{v}(t, \omega) & \frac{\text{Im} \tilde{v}(t, \omega)}{\omega} \end{pmatrix}. \quad (18)$$

We now obtain the central oscillator operators from the matrix equation,

$$\begin{pmatrix} Q(t) \\ P(t) \end{pmatrix} = \mathbf{U}(t) \begin{pmatrix} Q(0) \\ P(0) \end{pmatrix} - \sum_{\nu=1}^N \lambda_\nu \mathbf{U}(t, \omega_\nu) \begin{pmatrix} Q_\nu(0) \\ P_\nu(0) \end{pmatrix}. \quad (19)$$

B. Central oscillator expectation values

Equation (19) gives the operators $Q(t)$ and $P(t)$ as linear combinations of the operators $Q(0), P(0)$ and $Q_\nu(0), P_\nu(0)$.

This allows us to express central oscillator expectation values for $t \geq 0$ in terms of the initial expectation values at $t = 0$.

The linear expectation values are given by the matrix equation

$$\mathbf{X}(t) \equiv \begin{pmatrix} \langle Q(t) \rangle \\ \langle P(t) \rangle \end{pmatrix} = \mathbf{U}(t)\mathbf{X}(0) + \mathbf{I}(t), \quad (20)$$

with the same shape as Eq. (19). In addition to the initial expectation values $\mathbf{X}(0)$, it contains the contribution

$$\mathbf{I}(t) = \begin{pmatrix} I_Q(t) \\ I_P(t) \end{pmatrix} = - \sum_{\nu=1}^N \lambda_{\nu} \mathbf{U}(t, \omega_{\nu}) \check{\mathbf{X}}_{\nu}, \quad (21)$$

where we mark the initial bath expectation values

$$\check{\mathbf{X}}_{\nu} = \begin{pmatrix} \langle Q_{\nu}(0) \rangle \\ \langle P_{\nu}(0) \rangle \end{pmatrix} \quad (22)$$

with a breve $\check{}$ as a notational convention. Note that if $\check{\mathbf{X}}_{\nu} \equiv 0$, e.g., for a thermal bath, the “noise term” $\mathbf{I}(t)$ vanishes. Then, position $\langle Q(t) \rangle$ and momentum $\langle P(t) \rangle$ of the central oscillator follow the classical equation of motion (11).

For the quadratic expectation values, we define the variance of operators A and B as

$$\Sigma_{AB} = \frac{1}{2} \langle AB + BA \rangle - \langle A \rangle \langle B \rangle, \quad (23)$$

which simplifies to $\Sigma_{AA} = \langle A^2 \rangle - \langle A \rangle^2$ for $A = B$, and we write $\Sigma_{AB}(t) = \Sigma_{A(t)B(t)}$. We combine the central oscillator variances into the real symmetric matrix,

$$\Sigma(t) = \begin{pmatrix} \Sigma_{QQ}(t) & \Sigma_{QP}(t) \\ \Sigma_{QP}(t) & \Sigma_{PP}(t) \end{pmatrix}, \quad (24)$$

and denote the initial bath variances with the matrix

$$\check{\Sigma}_{\nu\mu} = \begin{pmatrix} \Sigma_{Q_{\nu}Q_{\mu}}(0) & \Sigma_{Q_{\nu}P_{\mu}}(0) \\ \Sigma_{Q_{\mu}P_{\nu}}(0) & \Sigma_{P_{\nu}P_{\mu}}(0) \end{pmatrix}. \quad (25)$$

Note the index swap in the off-diagonal elements, and recall that mixed central oscillator and bath variances such as $\Sigma_{QQ_{\nu}}$ vanish for our choice (10) of factorizing initial conditions.

We now obtain with Eq. (19) the matrix equation

$$\Sigma(t) = \mathbf{U}(t)\Sigma(0)\mathbf{U}^T(t) + \mathbf{C}(t). \quad (26)$$

Similar to Eq. (20), the first term results from the time evolution of the central oscillator according to the classical equation of motion (11), and appears in the same form for an isolated oscillator. Only the second term,

$$\begin{aligned} \mathbf{C}(t) &= \begin{pmatrix} C_{QQ}(t) & C_{QP}(t) \\ C_{QP}(t) & C_{PP}(t) \end{pmatrix} \\ &= \sum_{\nu, \mu=1}^N \lambda_{\nu} \lambda_{\mu} \mathbf{U}(t, \omega_{\nu}) \check{\Sigma}_{\nu\mu} \mathbf{U}^T(t, \omega_{\mu}), \end{aligned} \quad (27)$$

depends on the initial bath oscillator variances $\check{\Sigma}_{\nu\mu}$. Mixed terms in $\mathbf{U}(t)$ and $\mathbf{U}(t, \omega_{\nu})$ do not appear for factorizing initial conditions.

C. The thermodynamic limit

Because $u(t)$ is a quasiperiodic function for a finite number N of bath oscillators, equilibration becomes possible only in

the thermodynamic limit $N \rightarrow \infty$. We assume that for $N \rightarrow \infty$, the density of states

$$D(\omega) = \frac{1}{N} \sum_{\nu=1}^N \delta(\omega - \omega_{\nu}) \quad (28)$$

converges to a continuous function. Note that $D(\omega) = 0$ for $\omega < 0$ since the bath oscillator frequencies are positive. The coupling constants appear in the damping kernel $K(t)$ and in Eq. (11) as λ_{ν}^2 , and must thus scale as $N^{-1/2}$. We assume that

$$\lambda_{\nu} = \lambda(\omega_{\nu})/\sqrt{N} \quad (29)$$

with a continuous function $\lambda(\omega)$, and we introduce the bath spectral function

$$\gamma(\omega) = D(\omega) \frac{\lambda(\omega)^2}{\omega} \quad (30)$$

with $\gamma(\omega) = 0$ for $\omega < 0$. The damping kernel is now given as

$$K(t) = \int_0^{\infty} \gamma(\omega) \sin \omega t d\omega, \quad (31)$$

and the positivity condition reads

$$\Omega^2 \geq \int_0^{\infty} \frac{\gamma(\omega)}{\omega} d\omega. \quad (32)$$

The function $F(z)$ in Eq. (13) for $u(t)$ can be written as

$$F(z) = \left(\Omega^2 - z^2 + \int_0^{\infty} \frac{\omega \gamma(\omega)}{z^2 - \omega^2} d\omega \right)^{-1}. \quad (33)$$

Under mild assumptions, the evaluation of the ω integral in this equation is possible by contour integration and results in

$$F(z) = [\Omega^2 - z^2 + \Gamma(z)]^{-1} \quad (34)$$

for $\text{Im } z > 0$, where the complex function $\Gamma(z)$ with $\gamma(\omega) = \mp(2/\pi) \text{Im } \Gamma(\pm\omega + i0^+)$ is the analytic continuation of $\gamma(\omega)$ into the upper half of the complex plane (see Sec. V for an example). For future use in Sec. IV we note the relation $\gamma(\omega)|F(\omega)|^2 = (2/\pi) \text{Im } F(\omega + i0^+)$ that follows from this representation. The analytic properties of $F(z)$ determine the behavior of $u(t)$ in the long-time limit, which is essential for equilibration [see condition (E0) in Sec. IV]: It is $u(t) \rightarrow 0$ for $t \rightarrow \infty$ if and only if $F(z)$ has no isolated poles.

The linear expectation values $\check{\mathbf{X}}_{\nu}$ enter Eq. (21) with the prefactors $\lambda_{\nu} \propto N^{-1/2}$. To obtain a finite result for the sum over N terms, also $\check{\mathbf{X}}_{\nu}$ has to scale as $N^{-1/2}$, which leads to the ansatz

$$\check{\mathbf{X}}_{\nu} = \frac{1}{\sqrt{N}} \check{\mathbf{X}}(\omega_{\nu}) \quad (35)$$

with a continuous vector-valued function $\check{\mathbf{X}}(\omega)$. Then, Eq. (21) becomes

$$\mathbf{I}(t) = - \int_0^{\infty} D(\omega) \lambda(\omega) \mathbf{U}(t, \omega) \check{\mathbf{X}}(\omega) d\omega. \quad (36)$$

The variances $\check{\Sigma}_{\nu\mu}$ enter the sum in Eq. (27) with the prefactors $\lambda_{\nu} \lambda_{\mu} \propto N^{-1}$. We must now distinguish between the N^2 off-diagonal terms $\nu \neq \mu$, which require an additional $1/N$ prefactor for convergence, and the N diagonal terms $\nu = \mu$.

Therefore, we make the ansatz

$$\check{\Sigma}_{\nu\mu} = \frac{1}{N} \check{\Sigma}^{(2)}(\omega_\nu, \omega_\mu) + \check{\Sigma}^{(1)}(\omega_\nu) \delta_{\nu\mu} \quad (37)$$

with continuous matrix-valued functions $\check{\Sigma}^{(2)}(\omega_1, \omega_2)$ and $\check{\Sigma}^{(1)}(\omega)$. Then, $\mathbf{C}(t)$ from Eq. (27) is the sum of the off-diagonal term

$$\begin{aligned} \mathbf{C}^{(2)}(t) = & \iint_0^\infty D(\omega_1) D(\omega_2) \lambda(\omega_1) \lambda(\omega_2) \\ & \times \mathbf{U}(t, \omega_1) \check{\Sigma}^{(2)}(\omega_1, \omega_2) \mathbf{U}^T(t, \omega_2) d\omega_1 d\omega_2 \end{aligned} \quad (38)$$

and the diagonal term

$$\mathbf{C}^{(1)}(t) = \int_0^\infty \omega \gamma(\omega) \mathbf{U}(t, \omega) \check{\Sigma}^{(1)}(\omega) \mathbf{U}^T(t, \omega) d\omega. \quad (39)$$

If the initial bath state is uncorrelated, such as for a thermal bath or a general product state $\rho_B(0) = \rho_B^1(0) \otimes \dots \otimes \rho_B^N(0)$, the off-diagonal term $\mathbf{C}^{(2)}(t)$ vanishes.

When we construct the propagating function in the next subsection, we will conveniently assume that the initial bath state $\rho_B(0)$ is a Gaussian state. For the long-time limit, which is the situation of interest here, this assumption can be justified in the thermodynamic limit on general grounds [37,38]. The principal mechanism is illustrated with counting arguments of the following kind: Consider an uncorrelated bath state, where only N diagonal terms contribute in any sum over the bath oscillators. If we consider a higher-order cumulant of bath operators, say $Q_3(\nu) = \langle Q_\nu^3 \rangle - 3\langle Q_\nu^2 \rangle \langle Q_\nu \rangle + 2\langle Q_\nu \rangle^3$ as mentioned before, it appears with a prefactor $\lambda_\nu^3 \propto N^{-3/2}$. Therefore, the total contribution of these cumulants scales as $N \times N^{-3/2} = N^{-1/2}$ and vanishes in the limit $N \rightarrow \infty$. Similar counting arguments can be given for cumulants involving two or more bath oscillators in the presence of correlations. Because higher-order cumulants vanish and only linear and quadratic bath expectation values survive the $N \rightarrow \infty$ and $t \rightarrow \infty$ limit, we can treat the bath state as Gaussian in any calculation of the central oscillator density matrix. For the formulation and proof of a strict result, which is involved even under some simplifying assumptions, see [38].

D. The propagating function

Knowledge of the expectation values $\mathbf{X}(t)$ and $\Sigma(t)$ does not suffice to obtain the central oscillator density matrix $\rho_S(t)$, unless we restrict ourselves completely to Gaussian oscillator states [cf. Eq. (43) below]. Otherwise, the general solution is given by the propagating function $J(\cdot)$ that, in position representation, expresses the density matrix $\rho_S(q, q', t) = \langle q | \rho_S(t) | q' \rangle$ for $t \geq 0$ as

$$\rho_S(q_f, q'_f, t) = \iint_{-\infty}^\infty J(q_f, q'_f, q_i, q'_i, t) \rho_S(q_i, q'_i, 0) dq_i dq'_i. \quad (40)$$

This expression must hold for all $\rho_S(0)$ and $t \geq 0$, and a fixed initial bath state $\rho_B(0)$.

The propagating function can be calculated using path integrals, and the result for a thermal bath is given, e.g., in Ref. [21]. Within our approach, it is more natural to construct the propagating function directly, using only that an initial Gaussian state of the joint central oscillator and bath system

remains a Gaussian state during time evolution with the bilinear Hamiltonian H . With respect to the final remarks in Sec. III C, we assume a Gaussian bath state $\rho_B(0)$. We can then consider the most general ansatz for $J(\cdot)$ that maps an initial Gaussian state $\rho_S(0)$ in Eq. (40) onto a Gaussian state $\rho_S(t)$ for $t \geq 0$, and we will find that the parameters of this ansatz are fully specified through the linear maps (20) and (26) of $\mathbf{X}(t)$ and $\Sigma(t)$. The result is valid for arbitrary $\rho_S(0)$ in Eq. (40), but we do not need to consider non-Gaussian $\rho_S(t)$ explicitly.

To translate this argument into equations, we work with the Wigner function [39,40]

$$W(q, p, t) = \frac{1}{2\pi} \int_{-\infty}^\infty \rho_S\left(q + \frac{s}{2}, q - \frac{s}{2}, t\right) e^{-ips} ds \quad (41)$$

instead of the density matrix $\rho_S(q, q', t)$ in position representation (see also Refs. [23,41] for a related calculation). The propagating function $J_W(\tilde{\mathbf{x}}, \mathbf{x}, t) = J_W(\tilde{q}, \tilde{p}, q, p, t)$ is defined by the relation

$$W(\tilde{\mathbf{x}}, t) = \int_{\mathbb{R}^2} J_W(\tilde{\mathbf{x}}, \mathbf{x}, t) W(\mathbf{x}, 0) d\mathbf{x}, \quad (42)$$

where we write $W(\mathbf{x}, t) = W(q, p, t)$ with $\mathbf{x} = (q, p)^T$ and $d\mathbf{x} = dq dp$ for abbreviation. Note that $W(\mathbf{x}, t)$ and $J_W(\tilde{\mathbf{x}}, \mathbf{x}, t)$ are real functions.

A Gaussian state to given $\mathbf{X}(t)$ and $\Sigma(t)$ has the Wigner function

$$W_g(\mathbf{x}, t) = \frac{\exp\left\{-\frac{1}{2}[\mathbf{x} - \mathbf{X}(t)] \cdot \Sigma^{-1}(t)[\mathbf{x} - \mathbf{X}(t)]\right\}}{2\pi \sqrt{\det \Sigma(t)}}, \quad (43)$$

and the most general expression for $J_W(\cdot)$ that respects this structure is an exponential function of the 14 linear and quadratic terms in the coordinates $q, p, \tilde{q}, \tilde{p}$. The normalization $\int_{\mathbb{R}^2} W(\mathbf{x}, t) d\mathbf{x} = 1$ of Wigner functions implies the condition

$$\int_{\mathbb{R}^2} J_W(\tilde{\mathbf{x}}, \mathbf{x}, t) d\tilde{\mathbf{x}} = 1 \quad (44)$$

on the propagating function, which fixes the prefactors of the five terms q^2, p^2, qp, q, p in the initial coordinates. This leaves nine free parameters that have to be fixed in accordance with the linear transformations (20) and (26) of expectation values. The final result is

$$\begin{aligned} J_W(\tilde{\mathbf{x}}, \mathbf{x}, t) &= \frac{\exp\left[-\frac{1}{2}[\tilde{\mathbf{x}} - \mathbf{U}(t)\mathbf{x} - \mathbf{I}(t)] \cdot \mathbf{C}^{-1}(t)[\tilde{\mathbf{x}} - \mathbf{U}(t)\mathbf{x} - \mathbf{I}(t)]\right]}{2\pi \sqrt{\det \mathbf{C}(t)}}, \end{aligned} \quad (45)$$

where the $4 + 3 + 2 = 9$ parameters are the entries of the 2×2 matrix $\mathbf{U}(t)$ from Eq. (17), the symmetric and positive-definite 2×2 matrix $\mathbf{C}(t)$ from Eq. (27), and the two-dimensional vector $\mathbf{I}(t)$ from Eq. (21).

To check that this expression indeed reproduces the transformations (20) and (26), we can express the expectation values at $t \geq 0$ in terms of those at $t = 0$ through the evaluation of simple Gaussian integrals. To give an example, it is

$$\begin{aligned} \langle Q(t) \rangle &= \int_{\mathbb{R}^2} \tilde{q} W(\tilde{\mathbf{x}}, t) d\tilde{\mathbf{x}} \\ &= \int_{\mathbb{R}^4} \tilde{q} J_W(\tilde{\mathbf{x}}, \mathbf{x}, t) W(\mathbf{x}, 0) d\tilde{\mathbf{x}} d\mathbf{x}. \end{aligned} \quad (46)$$

The integral of $\tilde{q} J_W(\tilde{\mathbf{x}}, \mathbf{x}, t)$ over $\tilde{\mathbf{x}}$ is a Gaussian integral with a linear term, and gives

$$\int_{\mathbb{R}^2} \tilde{q} J_W(\tilde{\mathbf{x}}, \mathbf{x}, t) d\tilde{\mathbf{x}} = U_{QQ}(t)q + U_{QP}(t)p + I_Q(t). \quad (47)$$

The final integration over \mathbf{x} in Eq. (46), which now involves the right-hand side of Eq. (47), generates the initial expectation values $\langle Q(0) \rangle$ and $\langle P(0) \rangle$. Therefore, we obtain the relation $\langle Q(t) \rangle = U_{QQ}(t)\langle Q(0) \rangle + U_{QP}(t)\langle P(0) \rangle + I_Q(t) = \tilde{u}(t)\langle Q(0) \rangle + u(t)\langle P(0) \rangle + I_Q(t)$ in accordance with Eq. (20). Following this recipe, we find that the given expression (45) for the propagating function $J_W(\cdot)$ reproduces the entire transformations (20) and (26) of the expectation values $\mathbf{X}(t)$, $\Sigma(t)$, as we required.

If $\mathbf{C}(t) \rightarrow 0$, we get a representation of the distribution $\delta(\tilde{\mathbf{x}} - \mathbf{U}(t)\mathbf{x} - \mathbf{I}(t))$ from Eq. (45). In particular, for $t = 0$, where $\mathbf{U}(0) = 1$, $\mathbf{I}(0) = 0$ in addition to $\mathbf{C}(0) = 0$, we have the correct result $J_W(\tilde{\mathbf{x}}, \mathbf{x}, 0) = \delta(\tilde{\mathbf{x}} - \mathbf{x})$ in Eq. (42).

We note that the conveniently simple derivation of $J_W(\cdot)$ relies on the use of Wigner functions. Of course, the expressions for $\rho_S(q_f, q'_f, t)$ in position representation often reported in the literature can be recovered from Eq. (45) (see Appendix B).

IV. EQUILIBRATION AND THERMALIZATION

The results from the preceding section allow us to study the behavior of the central oscillator density matrix $\rho_S(t)$ in the long-time limit $t \rightarrow \infty$. We can classify the behavior according to the general criteria of equilibration and thermalization. Equilibration means convergence to a stationary state as expressed in the following two conditions:

(E1) The central oscillator density matrix $\rho_S(t)$ converges for $t \rightarrow \infty$.

(E2) The stationary state $\rho_S^\infty = \lim_{t \rightarrow \infty} \rho_S(t)$ is independent of $\rho_S(0)$.

Note that ρ_S^∞ will depend on the initial bath state $\rho_B(0)$. Note further that the above definition of equilibration does not distinguish between stationary equilibrium states and stationary nonequilibrium states with finite heat flows. The latter cannot arise for a single bath with continuous initial conditions as in Eq. (37) such that condition (E1) is sufficient for the present study.

Equilibration (E1) implies convergence of central oscillator expectation values for $t \rightarrow \infty$. This, in turn, requires convergence of the matrix $\mathbf{U}(t)$ in Eqs. (20) and (26). Because the only stationary solution of the homogeneous differential Eq. (11) is $u(t) \equiv 0$, convergence of $\mathbf{U}(t)$ is equivalent to $\mathbf{U}(t) \rightarrow 0$ or $u(t) \rightarrow 0$ for $t \rightarrow \infty$. Therefore, we assume in this section the condition

(E0) $u(t) \rightarrow 0$ for $t \rightarrow \infty$

as the prerequisite for equilibration (E1). Under this assumption, we will be able to show convergence of expectation values and, building on this result, convergence of the central oscillator density matrix.

In the weak damping limit, condition (E0) is equivalent to $\gamma(\Omega) > 0$ (taking the thermodynamic limit for granted). This expresses the basic fact that equilibration occurs through energy exchange with the environment, which is not possible for an isolated oscillator with $\gamma(\Omega) = 0$. We note that a

small value of $\gamma(\Omega)$ can result in long transients that prevent equilibration over the observation time.

Thermalization additionally requires that the stationary state ρ_S^∞ is a thermal state, and we have the following three increasingly stronger properties:

(T1) The stationary state ρ_S^∞ is a thermal state.

(T2) The stationary state is a thermal state $\rho_S^\infty \propto e^{-H_S/T_\infty}$ of the central oscillator.

(T3) The temperature T_∞ of the stationary thermal state ρ_S^∞ is independent of the central oscillator frequency.

We will see that the stationary state is always Gaussian, which implies property (T1). Property (T2) reduces to an equipartition condition on the central oscillator variances that determine the Gaussian state, while property (T3) leads to a strong condition on the initial bath state.

A. Expectation values in the long-time limit

The assumption $\mathbf{U}(t) \rightarrow 0$ for $t \rightarrow \infty$ implies that the terms $\mathbf{U}(t)\mathbf{X}(0)$ in Eq. (20) and $\mathbf{U}(t)\Sigma(0)\mathbf{U}^T(t)$ in Eq. (26) drop out of the expressions for $\mathbf{X}(t)$ and $\Sigma(t)$ in the long-time limit. Only the terms $\mathbf{I}(t)$ and $\mathbf{C}(t)$, which depend exclusively on the initial bath preparation, can survive the $t \rightarrow \infty$ limit: All information about the initial central oscillator state is lost. We cannot immediately draw a conclusion about the long-time behavior because the functions $\tilde{u}(t, \omega)$ and $\tilde{v}(t, \omega)$ from Eqs. (15) and (16) do not converge for $t \rightarrow \infty$. Instead, we note that $\tilde{u}(t, \omega)$ behaves asymptotically as

$$\tilde{u}_{\text{as}}(t, \omega) \simeq e^{i\omega t} \int_0^\infty u(\tau) e^{-i\omega\tau} d\tau \quad (t \rightarrow \infty). \quad (48)$$

Similarly, it follows that $\tilde{v}(t, \omega) \simeq i\omega \tilde{u}_{\text{as}}(t, \omega)$ for $t \rightarrow \infty$ from Eq. (16). Consequently, the matrix $\mathbf{U}(t, \omega)$ behaves asymptotically as

$$\mathbf{U}(t, \omega) \simeq \begin{pmatrix} \text{Re } \tilde{u}_{\text{as}}(t, \omega) & \frac{\text{Im } \tilde{u}_{\text{as}}(t, \omega)}{\omega} \\ -\omega \text{Im } \tilde{u}_{\text{as}}(t, \omega) & \text{Re } \tilde{u}_{\text{as}}(t, \omega) \end{pmatrix} \quad (t \rightarrow \infty), \quad (49)$$

and remains oscillating for $t \rightarrow \infty$ even if $u(t) \rightarrow 0$.

The contributions to the term $\mathbf{I}(t)$ in Eq. (36), say to $\langle Q(t) \rangle$, are of the form

$$-\text{Re} \int_0^\infty D(\omega) \lambda(\omega) \tilde{u}_{\text{as}}(t, \omega) \check{X}_Q(\omega) d\omega. \quad (50)$$

The integrand depends on t through the factor $e^{i\omega t}$ from Eq. (48), such that the integral is the Fourier transform of an integrable (by assumption even continuous) function of ω . If we recall the Riemann-Lebesgue lemma (3), we see that $\mathbf{I}(t) \rightarrow 0$ for $t \rightarrow \infty$. Altogether, it follows that the position and momentum expectation values vanish in the long-time limit, i.e., $\mathbf{X}(t) \rightarrow 0$ for $t \rightarrow \infty$.

For the variances, a finite contribution can survive the $t \rightarrow \infty$ limit because the squares of the matrix elements of $\mathbf{U}(t, \omega)$ occur in $\mathbf{C}(t)$. For example, the diagonal term $\mathbf{C}^{(1)}(t)$ from Eq. (39) contributes to $\Sigma_{QQ}(t)$ the integral

$$C_{QQ}^{(1)}(t) = \int_0^\infty \omega \gamma(\omega) c_{QQ}(t, \omega) d\omega \quad (51)$$

of the function

$$c_{QQ}(t, \omega) = [\text{Re } \tilde{u}(t, \omega)]^2 \check{\Sigma}_{QQ}^{(1)}(\omega) + \frac{2[\text{Re } \tilde{u}(t, \omega)][\text{Im } \tilde{u}(t, \omega)]}{\omega} \check{\Sigma}_{QP}^{(1)}(\omega) + \frac{[\text{Im } \tilde{u}(t, \omega)]^2}{\omega^2} \check{\Sigma}_{PP}^{(1)}(\omega). \quad (52)$$

Here we write, using the notation from Eq. (24),

$$\mathbf{C}^{(1)}(t) = \begin{pmatrix} C_{QQ}^{(1)}(t) & C_{QP}^{(1)}(t) \\ C_{QP}^{(1)}(t) & C_{PP}^{(1)}(t) \end{pmatrix} \quad (53)$$

for the matrix elements of $\mathbf{C}^{(1)}(t)$ and

$$\check{\Sigma}^{(1)}(\omega) = \begin{pmatrix} \check{\Sigma}_{QQ}^{(1)}(\omega) & \check{\Sigma}_{QP}^{(1)}(\omega) \\ \check{\Sigma}_{QP}^{(1)}(\omega) & \check{\Sigma}_{PP}^{(1)}(\omega) \end{pmatrix} \quad (54)$$

for the matrix elements of $\check{\Sigma}^{(1)}(\omega)$ from Eq. (37).

The contribution from the first term in $c_{QQ}(t, \omega)$ is

$$\int_0^\infty \omega \gamma(\omega) [\text{Re } \tilde{u}_{\text{as}}(t, \omega)]^2 \check{\Sigma}_{QQ}^{(1)}(\omega) d\omega. \quad (55)$$

If we expand the square $[\text{Re } \tilde{u}_{\text{as}}(t, \omega)]^2$ according to

$$[\text{Re } e^{i\omega t} z]^2 = \frac{|z|^2}{2} + \frac{z_r^2 - z_i^2}{2} \cos 2\omega t - z_r z_i \sin 2\omega t \quad (56)$$

for a complex number z with $z_r = \text{Re } z$, $z_i = \text{Im } z$, we see that in the above integral a contribution $|\tilde{u}_{\text{as}}(t, \omega)|^2/2$ remains finite for $t \rightarrow \infty$, while the oscillatory terms with $\cos 2\omega t$, $\sin 2\omega t$ vanish according to the Riemann-Lebesgue lemma (3). Similar expressions are obtained for the remaining terms in $\mathbf{C}^{(1)}(t)$.

The off-diagonal term $\mathbf{C}^{(2)}(t)$ from Eq. (38) is given by a double Fourier integral and contains only oscillatory terms in the two frequencies ω_1 and ω_2 . Therefore, $\mathbf{C}^{(2)}(t) \rightarrow 0$ for $t \rightarrow \infty$.

We can now collect the finite contributions from the different terms in $\mathbf{C}^{(1)}(t)$ to find that the central oscillator variances converge to stationary values $\Sigma^\infty = \lim_{t \rightarrow \infty} \Sigma(t)$ in the long-time limit. They are given by

$$\Sigma_{QQ}^\infty = \int_0^\infty \gamma(\omega) \left| \int_0^\infty e^{i\tau\omega} u(\tau) d\tau \right|^2 \frac{\check{\xi}(\omega)}{\omega} d\omega, \quad (57)$$

$$\Sigma_{PP}^\infty = \int_0^\infty \gamma(\omega) \left| \int_0^\infty e^{i\tau\omega} u(\tau) d\tau \right|^2 \omega \check{\xi}(\omega) d\omega, \quad (58)$$

$$\Sigma_{QP}^\infty = 0, \quad (59)$$

where

$$\check{\xi}(\omega) = \frac{1}{2} (\omega^2 \check{\Sigma}_{QQ}^{(1)}(\omega) + \check{\Sigma}_{PP}^{(1)}(\omega)). \quad (60)$$

Comparison with Eqs. (13) and (34) gives the alternative expressions

$$\Sigma_{QQ}^\infty = \frac{2}{\pi} \int_0^\infty \text{Im } F(\omega + i0^+) \frac{\check{\xi}(\omega)}{\omega} d\omega, \quad (61)$$

$$\Sigma_{PP}^\infty = \frac{2}{\pi} \int_0^\infty \text{Im } F(\omega + i0^+) \omega \check{\xi}(\omega) d\omega. \quad (62)$$

Recall that $F(\omega + i0^+)$ is a continuous function according to our assumption $u(t) \rightarrow 0$.

As noted before, the values Σ^∞ are independent of the initial central oscillator state. Furthermore, the initial bath state $\rho_B(0)$ occurs only through the frequency-resolved energy distribution $\check{\xi}(\omega)$. In particular, the known equations for thermal baths [7] are recovered whenever $\check{\xi}(\omega) = E(T, \omega)$, where

$$E(T, \Omega) = \frac{\Omega}{2} \coth \frac{\Omega}{2T} \quad (63)$$

is the energy of a thermal oscillator at temperature T . Because there are no separate conditions on the two functions $\check{\Sigma}_{QQ}^{(1)}(\omega)$ and $\check{\Sigma}_{PP}^{(1)}(\omega)$, thermalization is possible also in nonthermal environments (see below).

Equations (57)–(59) follow directly if we assume a thermal bath from the outset, with initial conditions $\omega^2 \check{\Sigma}_{QQ}^{(1)}(\omega) = \check{\Sigma}_{PP}^{(1)}(\omega) = E(T, \omega)$ and $\check{\Sigma}_{QP}^{(1)}(\omega) = 0$. Equipartition of energy allows us to combine the terms in Eq. (52) to $c_{QQ}(t, \omega) = |\tilde{u}(t, \omega)|^2 E(T, \omega)/\omega^2$, which depends only on the modulus of $\tilde{u}(t, \omega)$. We can then drop the exponential factor $e^{i\omega t}$ from Eq. (48), and convergence of $\Sigma(t)$ is evident. This short cut is not available in the general case.

B. Equilibration of the central oscillator

If the initial bath state $\rho_B(0)$ and the central oscillator state $\rho_S(0)$ are both Gaussian states, the central oscillator density matrix $\rho_S(t)$ is Gaussian for all $t \geq 0$. Then, $\rho_S(t)$ is completely determined by the values of $\mathbf{X}(t)$ and $\Sigma(t)$, and their convergence suffices to establish equilibration (E1), and also (E2), in this case.

Otherwise, for non-Gaussian initial states $\rho_S(0)$, we can use the propagating function $J_W(\tilde{\mathbf{x}}, \mathbf{x}, t)$ from Eq. (45) to find $\rho_S(t)$ for $t \rightarrow \infty$. Recall that according to Sec. III C, we can assume that the initial bath state is Gaussian in the thermodynamic limit, which allows for the construction given in Sec. III D.

Equilibration follows now from the observation that $J_W(\tilde{\mathbf{x}}, \mathbf{x}, t)$ converges for $t \rightarrow \infty$ whenever $\mathbf{X}(t)$ and $\Sigma(t)$ converge. The long-time limit

$$J_W^\infty(\tilde{\mathbf{x}}) = \lim_{t \rightarrow \infty} J_W(\tilde{\mathbf{x}}, \mathbf{x}, t) = \frac{\exp[-\frac{1}{2} \tilde{\mathbf{x}} \cdot (\Sigma^\infty)^{-1} \tilde{\mathbf{x}}]}{2\pi \sqrt{\det \Sigma^\infty}} \quad (64)$$

is obtained through substitution of $\lim_{t \rightarrow \infty} \mathbf{I}(t) = 0$ and $\lim_{t \rightarrow \infty} \mathbf{C}(t) = \Sigma^\infty$ from Eqs. (57)–(59). Because $\mathbf{U}(t) \rightarrow 0$, the result does not depend on \mathbf{x} .

The long-time limit of the Wigner function $W_S^\infty(\mathbf{x}) = \lim_{t \rightarrow \infty} W_S(\mathbf{x}, t)$ follows immediately with Eq. (42): The integration over \mathbf{x} in the resulting expression

$$W_S^\infty(\tilde{\mathbf{x}}) = \int_{\mathbb{R}^2} J_W^\infty(\tilde{\mathbf{x}}) W_S(\mathbf{x}, 0) d\mathbf{x} = J_W^\infty(\tilde{\mathbf{x}}) \quad (65)$$

evaluates to 1 because $W_S(\mathbf{x}, 0)$ is normalized, such that $W_S^\infty(\mathbf{x})$ is equal to $J_W^\infty(\mathbf{x})$. In other words, the stationary state ρ_S^∞ is a Gaussian state (43) with parameters $\mathbf{X} = \mathbf{0}$ and $\Sigma = \Sigma^\infty$. These parameters depend on the initial bath state according to Eqs. (57) and (58), but they are independent of the initial central oscillator state. This proves equilibration (E1) and (E2) for general initial central oscillator states. In particular, the stationary state is Gaussian also for non-Gaussian initial

states. We note that the propagating function in position representation does not converge in the long-time limit (cf. Appendix B), which prevents an equally simple argument.

C. Thermalization of the central oscillator

Because the stationary state ρ_S^∞ in the long-time limit is a Gaussian state for which only Σ_{QQ}^∞ and Σ_{PP}^∞ are nonzero, it can always be interpreted as the thermal equilibrium state of some harmonic oscillator. This establishes the weakest thermalization property (T1).

The effective oscillator frequency Ω_∞ and temperature T_∞ associated with ρ_S^∞ are

$$\Omega_\infty^2 = \frac{\Sigma_{PP}^\infty}{\Sigma_{QQ}^\infty}, \quad T_\infty = \frac{\Omega_\infty}{2} \operatorname{arcoth}^{-1} [2\sqrt{\Sigma_{QQ}^\infty \Sigma_{PP}^\infty}]. \quad (66)$$

Generally, Ω_∞ is not equal to the central oscillator frequency Ω such that the stronger property (T2) is not fulfilled. By Eq. (66), the condition $\Omega_\infty = \Omega$ is equivalent to equipartition of kinetic and potential energy $\langle P^2 \rangle = \Sigma_{PP}^\infty = \Omega^2 \Sigma_{QQ}^\infty = \Omega^2 \langle Q^2 \rangle$. The violation of this condition arises from the integrations over ω in Eqs. (57) and (58) or (61) and (62), which cover a finite energy range and include values $\omega \neq \Omega$. Quantum corrections of this type are characteristic for strong damping [7].

Equipartition of energy is achieved in the limit of weak damping [$\gamma(\Omega) \rightarrow 0$], when according to Eq. (34) the function $(2/\pi) \operatorname{Im} F(\omega + i0^+)$ in Eqs. (61) and (62) converges to $2\delta(\omega^2 - \Omega^2) = [\delta(\omega + \Omega) + \delta(\omega - \Omega)]/\Omega$. Therefore, the values $\Omega^2 \Sigma_{QQ}^\infty = \Sigma_{PP}^\infty = \check{\mathcal{E}}(\Omega)$ are obtained. This establishes the stronger thermalization property (T2) in the weak damping limit.

For these values of $\Sigma_{QQ}^\infty, \Sigma_{PP}^\infty$, it is [cf. Eq. (63)]

$$\Omega_\infty^{(\text{WD})} = \Omega, \quad T_\infty^{(\text{WD})}(\Omega) = \frac{\Omega}{2} \operatorname{arcoth}^{-1} \frac{2\check{\mathcal{E}}(\Omega)}{\Omega}, \quad (67)$$

such that the stationary state ρ_S^∞ is a thermal equilibrium state of the central oscillator. The temperature $T_\infty(\Omega)$ is determined by the energy $\check{\mathcal{E}}(\Omega)$ of the bath oscillator at frequency Ω in the initial state. Note that the assumption (E0) implies $\gamma(\Omega) \neq 0$ and $D(\omega) \neq 0$, such that the value of $\check{\mathcal{E}}(\Omega)$ is defined. In particular, $\check{\mathcal{E}}(\Omega) \geq \Omega/2$ and the argument of $\operatorname{arcoth}(\cdot)$ is equal to or greater than 1.

Still, the asymptotic temperature $T_\infty = T_\infty^{(\text{WD})}(\Omega)$ from Eq. (67) is a function of Ω . The functional dependence is determined by the choice of $\check{\mathcal{E}}(\omega)$. If we demand, for the strongest thermalization property (T3), that T_∞ is independent of Ω , we have to solve Eq. (67) to obtain the condition

$$\check{\mathcal{E}}(\omega) = \frac{\omega}{2} \coth \frac{\omega}{2T_\infty}. \quad (68)$$

Note that this is a condition on the particular combination $\check{\mathcal{E}}(\omega)$ of initial bath variances $\check{\Sigma}_{QQ}^{(1)}(\omega)$ and $\check{\Sigma}_{PP}^{(1)}(\omega)$, and not on the individual functions. Therefore, any initial bath preparation with $\check{\mathcal{E}}(\omega) = E(T_0, \omega)$ results in the same stationary states as the thermal bath at temperature T_0 . One example for this additional freedom is the choice

$$\check{\Sigma}_{QQ}^{(1)}(\omega) = \frac{\coth(\omega/2T_0) - 1/2}{\omega}, \quad \check{\Sigma}_{PP}^{(1)}(\omega) = \omega/2, \quad (69)$$

and arbitrary $\check{\Sigma}_{QP}^{(1)}(\omega)$. It can be realized, e.g., by superposition of coherent oscillator states at different positions. This initial bath state is not a thermal state for $T_0 > 0$. In particular, it violates equipartition of energy $\omega^2 \check{\Sigma}_{QQ}^{(1)}(\omega) = \check{\Sigma}_{PP}^{(1)}(\omega)$. But since $\check{\mathcal{E}}(\omega) = E(T_0, \omega)$, we find that the stationary central oscillator state ρ_S^∞ is identical to that obtained with a thermal bath at temperature T_0 : Thermalization is well possible in nonthermal environments, even those far from thermal equilibrium.

D. Summary

In summary, we have a hierarchy of conditions for equilibration and thermalization:

(E1) and (E2) The central oscillator equilibrates whenever $u(t) \rightarrow 0$ for $t \rightarrow \infty$.

(T1) The stationary state is always a Gaussian and thermal state.

(T2) Equipartition of kinetic and potential energy occurs precisely at weak damping.

(T3) The asymptotic temperature T_∞ is independent of the central oscillator frequency under the additional condition (68) on $\check{\mathcal{E}}(\omega)$.

It is a special feature of linear systems such as the one studied here that equilibration depends only on the asymptotic behavior of the solution $u(t)$ of a classical equation of motion (11). Another feature is that the stationary state is always Gaussian such that equilibration implies thermalization, albeit only in the weak sense of property (T1). We noted earlier that in the situation studied here, with coupling to a single bath, a stationary state does not admit finite heat flows as would become possible for several baths with different preparations $\check{\mathcal{E}}(\omega)$. Therefore, conditions (E1) and (E2) capture the standard notion of thermodynamic equilibrium.

We note that a consistent definition of thermalization requires the strong property (T3). Suppose we deal with two central oscillators with frequencies $\Omega_1 \neq \Omega_2$. In the weak damping limit, the stationary state is the product state of two independent thermal states with respective temperatures $T_\infty(\Omega_1)$ and $T_\infty(\Omega_2)$. Such a state is only a thermal state of the combined system comprising the two oscillators if $T_\infty(\Omega_1) = T_\infty(\Omega_2)$. Therefore, thermalization of multiple oscillators, already in the weak sense (T1), requires the strong property (T3) and thus condition (68) [but recall that this condition can be fulfilled also for nonthermal environments as in Eq. (69)].

V. THE INFINITE HARMONIC CHAIN

As an example, for equilibration in a nonthermal environment we consider an infinite chain of harmonic oscillators (see Fig. 1). Oscillators in the right ($n \geq 1$) and left ($n \leq -1$) half of the chain, with frequency Ω_b , are coupled to their neighbors ($n \pm 1$) with spring constant k_b . They form the harmonic oscillator bath for the central oscillator at $n = 0$, with oscillator frequency Ω and coupling k to the oscillators at $n = \pm 1$. For $\Omega = \Omega_b$ and $k = k_b$ we obtain a homogeneous, translational invariant chain.

Related examples have been studied in numerous publications, see, e.g., [13,42–48]. The behavior for thermal initial conditions, e.g., in a homogeneous chain [42] or a

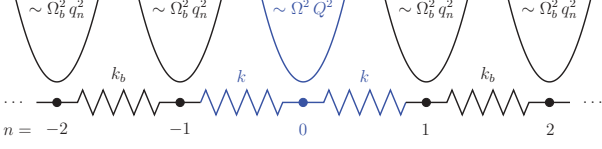


FIG. 1. (Color online) Sketch of the infinite harmonic chain as defined in Eqs. (70) and (71).

chain with a single heavy mass [13], is well understood. Equilibration in a harmonic chain with non-thermal initial conditions as discussed in Refs. [43,44] can be expressed in terms of our conditions from Sec. IV D. General arguments for the appearance of Gaussian states in the long-time limit are given in Refs. [38,46]. Still, a satisfactory and explicit analysis of equilibration and thermalization of the simple chain in non-thermal environments is missing. Some studies assume too quickly that equilibration implies thermalization, in the sense of our condition (T1), failing to note, e.g., that the appearance of Gaussian states is the general behavior of linear systems and unrelated to thermalization as expressed by condition (T3). According definitions of “temperature” have to be taken with care. In addition we must carefully analyze the role of undamped oscillatory behavior that prevents equilibration and, therefore, thermalization.

A. Mapping onto the central oscillator model

To address the harmonic chain within the formalism from Secs. II–IV, we must transform the Hamilton operator

$$H_B = \frac{1}{2} \sum_{n=1}^{\infty} [p_n^2 + \Omega_b^2 q_n^2] - k_b \sum_{n=1}^{\infty} q_n q_{n+1} \quad (70)$$

for the harmonic oscillator bath (with operators q_n and p_n for the oscillator at site $n \neq 0$) to normal modes. The same transformation has to be applied to the operator kq_1 in the coupling term

$$H_{SB} = -k Q(q_1 + q_{-1}) \quad (71)$$

between the central oscillator and the chain oscillators at $n = \pm 1$. It suffices to treat one of the two half-infinite chains explicitly, say the right chain $n \geq 1$ as in Eq. (70), and include a factor of 2 in $\gamma(\omega)$ to account for the left chain $n \leq -1$. Note that in doing so we implicitly assume identical initial conditions for both sides of the chain and thus exclude the possibility of stationary nonequilibrium states with finite heat flow between the right and left half-infinite chain.

The normal modes of H_B are the standing wave solutions $f_v(n) \propto \sin(\frac{\pi v n}{N+1})$ (for a finite chain of length N), and after a few lines of calculation we obtain the spectral function

$$\gamma(\omega) = \frac{2k^2}{\pi k_b^2} \sqrt{4k_b^2 - (\Omega_b^2 - \omega^2)^2} \quad (72)$$

for $|\Omega_b^2 - \omega^2| < 2k_b$

in the thermodynamic limit $N \rightarrow \infty$. It is $\gamma(\omega) = 0$ for $|\Omega_b^2 - \omega^2| > 2k_b$, and we impose the positivity condition $\Omega_b^2 \geq 2k_b \geq 0$ to exclude negative frequencies of the bath.

To proceed, it is convenient to introduce the dimensionless model parameters

$$\kappa_b = \frac{2k_b}{\Omega_b^2}, \quad \kappa = \frac{2k}{\Omega_b^2}, \quad \Omega_r = \frac{\Omega}{\Omega_b}, \quad (73)$$

and to use the normalized quantities

$$\bar{\omega} = \frac{\omega}{\Omega_b}, \quad \bar{t} = t\Omega_b, \quad \bar{u}(\bar{t}) = \Omega_b u(t). \quad (74)$$

Note that $0 \leq \kappa_b \leq 1$.

B. Conditions for equilibration in the harmonic chain

As discussed in Sec. IV, equilibration depends entirely on the decay of the function $u(t)$ for $t \rightarrow \infty$, and thus on the absence of poles in $F(z)$ from Eq. (33). To obtain $F(\omega)$, we use the representation (34) with the complex function

$$\Gamma(z) = \frac{k^2}{k_b^2} (z^2 - \Omega_b^2 \mp \sqrt{(\Omega_b^2 - z^2)^2 - 4k_b^2}), \quad (75)$$

where the branch cut of the root must be chosen along the positive real axis, and the minus (plus) sign applies for $\text{Re } z > 0$ ($\text{Re } z < 0$). Note that the positivity condition (8), which can now be rewritten as $\Omega^2 + \Gamma(i0^+) \geq 0$, requires that

$$\Omega_r^2 \geq \frac{\kappa^2}{\kappa_b^2} (1 - \sqrt{1 - \kappa_b^2}). \quad (76)$$

Before we can determine the function $u(t)$ with Eq. (13) we must consider the possibility of isolated poles of $F(z)$. According to Eq. (34) we have to compare the functions $\omega^2 - \Omega^2$ and $\text{Re } \Gamma(\omega + i0^+)$ in regions where $\text{Im } \Gamma(\omega + i0^+) = 0$. From the qualitative behavior of $\Gamma(\omega + i0^+)$, shown in Fig. 2, we deduce that isolated poles of $F(z)$ do not exist if and only if the inequalities

$$1 - \frac{\kappa_b^2 - \kappa^2}{\kappa_b} \leq \Omega_r^2 \leq 1 + \frac{\kappa_b^2 - \kappa^2}{\kappa_b} \quad (77)$$

are fulfilled. The first inequality excludes poles in the interval $\bar{\omega}^2 < 1 - \kappa_b$, the second inequality in the interval $\bar{\omega}^2 > 1 + \kappa_b$. Another more fundamental restriction is the positivity condition (76), which is however less restrictive than the present condition.

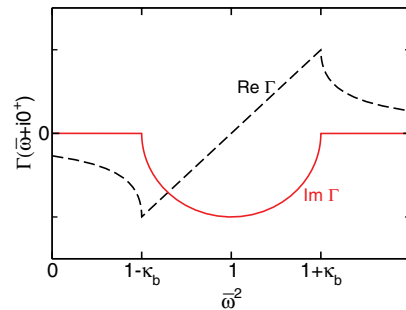


FIG. 2. (Color online) Real (dashed curve) and imaginary (solid curve) part of $\Gamma(\omega + i0^+)$ for $\kappa_b = 1/2$ and $\omega > 0$. For $\bar{\omega}^2 = \{1 - \kappa_b, 1, 1 + \kappa_b\}$ the function value is $\{-1, -i, 1\} \times (\kappa\Omega_b)^2/\kappa_b$, respectively.

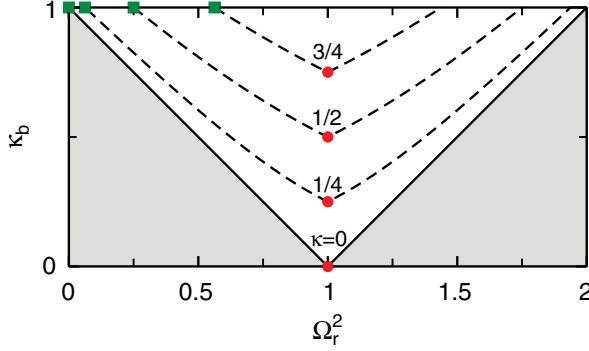


FIG. 3. (Color online) Diagram of the admissible parameter space for equilibration according to condition (77). The white triangular region above the solid black lines is the maximal set of allowed parameter combinations. Outside of this region, an isolated pole exists even in the weak damping limit $\kappa \rightarrow 0$. For $\kappa > 0$, the region of admissible parameters shrinks, as depicted by the dashed black curves. The parameter combinations of homogeneous chains ($\Omega_r = 1$) correspond to the cusps $\kappa_b = \kappa$ of the curves, marked with red dots. The parameter combinations of chains with a single heavy mass [13] correspond to the intersections of the curves with the $\kappa_b = 1$ line at $\Omega_r = \kappa$, marked with green squares. At these points, condition (77) coincides with the positivity condition (76).

The admissible parameter combinations for equilibration of the harmonic chain that follow from condition (77) are depicted in Fig. 3. We note the basic restrictions

$$\kappa \leq \kappa_b \quad \text{and} \quad |1 - \Omega_r^2| \leq \kappa_b. \quad (78)$$

The second inequality guarantees that the central oscillator frequency Ω_r lies within the interval $\bar{\omega} \in [\sqrt{1 - \kappa_b}, \sqrt{1 + \kappa_b}]$ where $\gamma(\bar{\omega}) > 0$. If this is fulfilled, equilibration is always possible for sufficiently small κ . Since $\kappa_b \leq 1$, it restricts the admissible parameters to the rectangle $(\kappa_b, \Omega_r^2) \in [0, 1] \times [0, 2]$.

Condition (77) is always fulfilled for the homogeneous chain (and we note that $\kappa = \kappa_b$ requires $\Omega_r = 1$). The chain studied by Ullersma corresponds to parameters $\kappa_b = 1$ and $\Omega_r = \kappa$ (Ω_r^2 equals the mass ratio μ in Ref. [13]). Condition (77) is fulfilled if $\Omega_r \leq 1$, i.e., only for a heavy mass. Both examples lie on the boundary of the admissible parameter space, with one or two of the inequalities in Eq. (77) becoming equalities.

C. Dynamical evolution of the harmonic chain

Depending on parameters, the harmonic chain features rich dynamical behavior. For parameter combinations that fulfill condition (77), the explicit result for $u(t)$ from Eq. (13) reads

$$\begin{aligned} \bar{u}(\bar{t}) = & \frac{2\kappa^2}{\pi} \int_{\sqrt{1-\kappa_b}}^{\sqrt{1+\kappa_b}} \sin \bar{\omega} \bar{t} \sqrt{\kappa_b^2 - (1 - \bar{\omega}^2)^2} \\ & \times \frac{1}{\kappa_b^2 (\bar{\omega}^2 - \Omega_r^2)^2 - 2\kappa^2 (\bar{\omega}^2 - 1) (\bar{\omega}^2 - \Omega_r^2) + \kappa^4} d\bar{\omega}. \end{aligned} \quad (79)$$

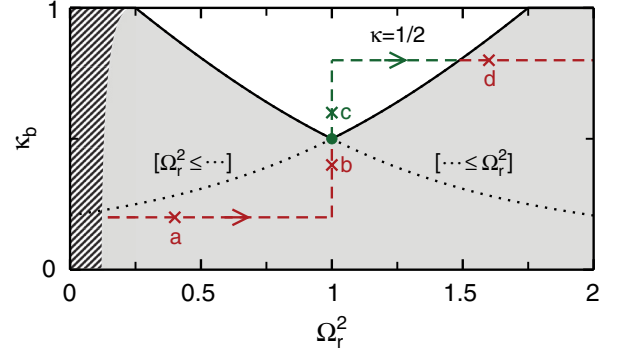


FIG. 4. (Color online) The (Ω_r^2, κ_b) parameter space of the infinite harmonic chain for $\kappa = 1/2$. The solid/dotted black curves give the boundary of the two regions defined by each of the inequalities from condition (77). The central oscillator equilibrates for parameters in the unshaded region above the solid curve, where the condition is fulfilled (note that $\kappa_b \leq 1$). For parameters lying between the solid and dotted curves, one of the two inequalities is violated and a single isolated pole of $F(z)$ exists. Below the dotted curve $F(z)$ has two isolated poles. The dashed region to the left indicates where the positivity condition (76) is violated, but such parameters already violate the first inequality in Eq. (77). Both conditions coincide at $\kappa_b = 1$, $\Omega_r = \kappa$. The dashed red/green lines indicate the path followed in the next Fig. 5; the crosses marked a–d indicate the parameters used in Fig. 6.

For parameter combinations violating condition (77) isolated poles of $F(z)$ occur and additional (undamped) sine functions $\xi_i \sin \Omega_i t$ must be added to this expression. According to Eq. (34), the poles of $F(z)$ are the solutions of $\Omega^2 - \Omega_i^2 + \Gamma(\Omega_i) = 0$, which gives a quadratic equation for the harmonic chain such that zero, one, or two (positive) poles are possible.

As an example let us consider the case $\kappa = 1/2$. The restrictions on the parameters arising from the positivity condition (76) and the stronger condition (77) are summarized in Fig. 4. We now follow the dashed path in this figure and plot the position $\Omega_{1/2}^2$ of isolated poles and their total weight $\xi = \xi_1 + \xi_2$ in Fig. 5. Only for parameter combinations in the white unshaded area in Fig. 4, which corresponds to the part between the dashed vertical lines in Fig. 5, condition (77) is fulfilled. Accordingly, only panel (c) in Fig. 6 (the parameter combination “c” in Figs. 4 and 5) shows a situation where $\bar{u}(\bar{t}) \rightarrow 0$ for $t \rightarrow \infty$. Otherwise, one (parameter combination “d”) or two (“a” and “b”) isolated poles exist if one or both inequalities from Eq. (77) are violated. Then, the amplitude of oscillations in $\bar{u}(\bar{t})$ remains finite in the long-time limit.

For strong damping situations ($\kappa \sim 1$) shown in Fig. 6 the function $u(t)$ deviates significantly from an exponentially decaying function, even in the absence of poles [panel (c)]. Exponential decay occurs only for weak damping $\kappa \ll \kappa_b$. For $|\Omega_r^2 - 1| \ll \kappa_b$ we have

$$\bar{u}(\bar{t}) = \frac{\sin(\Omega_r \bar{t})}{\Omega_r} \exp\left(-\frac{\kappa^2}{2\kappa_b} \bar{t}\right) \quad (\kappa \ll 1), \quad (80)$$

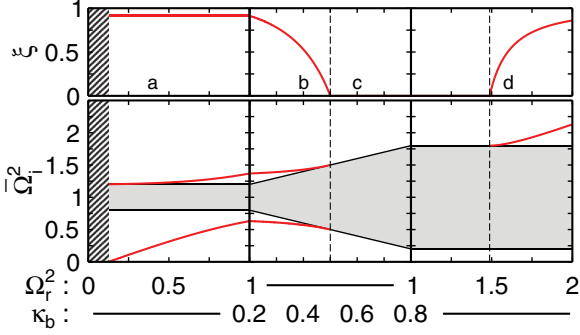


FIG. 5. (Color online) Position $\bar{\Omega}_i$ and total weight ξ of isolated poles of $F(z)$. We set $\kappa = 1/2$ and change Ω_r, κ_b along the dashed path from Fig. 4, i.e., from $\Omega_r = 0, \kappa_b = 0.2$ to $\Omega_r = 2, \kappa_b = 0.8$. The position of the poles is compared to the continuum of bath modes in the interval $\bar{\omega}^2 \in [1 - \kappa_b, 1 + \kappa_b]$, filling the gray area around $\bar{\Omega}_i^2 = 1$ in the plot. Between the two vertical dashed lines at $\Omega_r = 1, \kappa_b = 1/2$ (left) and $\kappa_b = 0.8, \Omega_r = 1.4875$ (right) no poles exist, in agreement with condition (77). For $\Omega_r^2 \lesssim 0.12628$, in the dashed region to the left, the positivity condition (76) is violated and one $\bar{\Omega}_i^2$ becomes negative.

as plotted in Fig. 7 (left panel). Note that the case $\gamma(\Omega) = 0$, with an undamped sine function in the weak damping limit, is excluded by the second inequality in Eq. (78).

For the homogeneous chain, with $\Omega_r = 1$ and $\kappa_b = \kappa$, the weak damping limit gives a different result. Since $\kappa_b = \kappa$, the width of the continuum of bath states shrinks to zero for $\kappa \rightarrow 0$ such that we do not obtain exponential decay of $u(t)$. Instead, it is

$$\bar{u}(\bar{t}) = J_0\left(\frac{\kappa \bar{t}}{2}\right) \sin \bar{t} \quad (\kappa \ll 1, \text{hom. chain}) \quad (81)$$

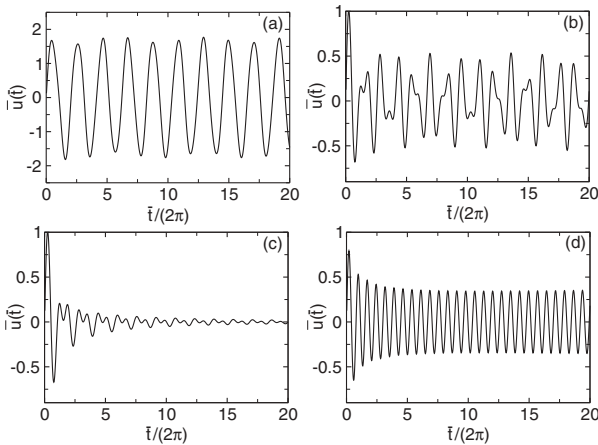


FIG. 6. Function $\bar{u}(\bar{t})$ for the harmonic chain with $\kappa = 1/2$. The parameters from panels (a)–(d) correspond to the crosses in Figs. 4 and 5. They are (a) $\kappa_b = 0.2, \Omega_r^2 = 0.4$ (two poles $\bar{\Omega}_1 = 0.48, \bar{\Omega}_2 = 1.10, \xi_1 = 0.82, \xi_2 = 0.10$); (b) $\kappa_b = 0.4, \Omega_r^2 = 1$ (two poles $\bar{\Omega}_1 = 0.76, \bar{\Omega}_2 = 1.20, \xi_1 = 0.26, \xi_2 = 0.26$); (c) $\kappa_b = 0.6, \Omega_r^2 = 1$ (no pole); (d) $\kappa_b = 0.8, \Omega_r^2 = 1.6$ (one pole $\bar{\Omega}_1 = 1.35, \xi_1 = 0.50$).

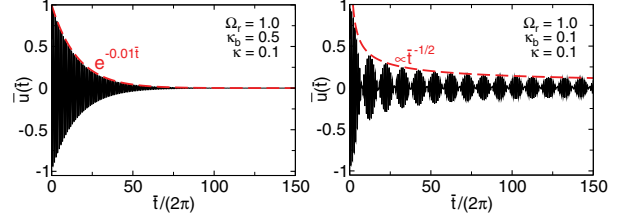


FIG. 7. (Color online) Function $\bar{u}(\bar{t})$ for the inhomogeneous (left panel, with $\Omega_r = 1, \kappa_b = 0.5, \kappa = 0.1$) and homogeneous (right panel, with $\Omega_r = 1, \kappa_b = 0.1, \kappa = 0.1$) harmonic chain at weak damping. The dashed red curves indicate the exponential decay from Eq. (80) (left panel) and the asymptotic decay $\propto 1/\sqrt{\bar{t}}$ of the Bessel function from Eq. (81) (right panel).

with the Bessel function $J_0(x)$ (cf. Refs. [42–44]). According to condition (77) isolated poles of $F(z)$ cannot occur in this situation. From the asymptotic behavior of the Bessel function we find that here $\bar{u}(\bar{t})$ decays only as $2(\pi\kappa\bar{t})^{-1/2}$ for $\bar{t} \gg 1$, as shown in the right panel of Fig. 7. Exponential decay in the weak damping limit is only achieved if the coupling κ of the central oscillator to the chain becomes small also in comparison to the width ($\sim \kappa_b$) of the continuum of bath s.

D. Thermalization after a quench

According to the previous discussion, the central oscillator in the harmonic chain equilibrates precisely for parameter combinations that fulfill condition (77). We now study, under these conditions, thermalization after a quench that generates a non-thermal environment for the central oscillator [cf. Eq. (84) below].

1. Initial conditions generated by the quench

We imagine that for $t < 0$ all oscillators are decoupled ($\kappa = \kappa_b = 0$) and in thermal equilibrium at temperature T_0 . Every oscillator has the same variance

$$\Omega_b^2 \check{\Sigma}_{qq}(n) = \check{\Sigma}_{pp}(n) = E(T_0, \Omega_b), \quad (82)$$

and we do not need to specify further initial expectation values if we are only interested in the stationary state in the long-time limit.

At $t = 0$, we quench the system by cranking up the coupling to finite values $\kappa, \kappa_b > 0$. Since $\check{\Sigma}_{qq}(n), \check{\Sigma}_{pp}(n)$ do not depend on n , transformation to the normal modes of the bath results in constant functions

$$\Omega_b^2 \check{\Sigma}_{QQ}^{(1)}(\omega) = \check{\Sigma}_{PP}^{(1)}(\omega) = E(T_0, \Omega_b) \quad (83)$$

for the initial bath variances at $t = 0$. The initial bath state is uncorrelated with $\check{\Sigma}^{(2)}(\omega_1, \omega_2) = 0$.

According to Sec. IV, the stationary state in the long-time limit depends only on the frequency-resolved energy $\check{\mathcal{E}}(\omega)$ of the initial bath state, which for the present example is given by the function

$$\check{\mathcal{E}}(\omega) = \frac{1 + (\omega/\Omega_b)^2}{2} E(T_0, \Omega_b). \quad (84)$$

This function acquires a dependence on ω through the dispersion of the bath modes after the quench, but it does not fulfill Eq. (68). We thus see that the thermal equilibrium state of uncoupled oscillators before the quench corresponds to a non-thermal state of the coupled chain of oscillators after the quench. According to condition (T3) from Sec. IV D we expect that the temperature T_∞ of the stationary state depends on the central oscillator frequency Ω_r even at weak coupling.

From Eqs. (57)–(59) or Eqs. (61) and (62), the variances in the long-time limit are obtained as

$$\Sigma_{\mathcal{Q}\mathcal{Q}}^\infty = \frac{1}{2\Omega_b^2} \left(1 + \frac{1}{\Omega_r^2 - \frac{\kappa^2}{\kappa_b^2} (1 - \sqrt{1 - \kappa_b^2})} \right) E(T_0, \Omega_b), \quad (85)$$

$$\Sigma_{\mathcal{P}\mathcal{P}}^\infty = \frac{1}{2} (1 + \Omega_r^2) E(T_0, \Omega_b). \quad (86)$$

We will give further results using normalized quantities

$$\bar{\Omega}_\infty = \Omega_\infty / \Omega_b, \quad \bar{T}_\infty = T_\infty / \Omega_b, \quad \bar{T}_0 = T_0 / \Omega_b. \quad (87)$$

choosing Ω_b as the unit of energy.

2. Thermalization (T2)

We recall that according to property (T1) the stationary state is always a thermal state of some harmonic oscillator Hamiltonian, such that we should check the stronger property (T2). From Eq. (66), the effective frequency associated with the stationary state is

$$\frac{\bar{\Omega}_\infty^2}{\Omega_r^2} = \frac{\Omega_r^2 + 1}{\Omega_r^2 + \left[1 - \frac{\kappa^2}{\Omega_r^2 \kappa_b^2} (1 - \sqrt{1 - \kappa_b^2}) \right]^{-1}}. \quad (88)$$

We observe that equipartition of energy, i.e., $\bar{\Omega}_\infty = \Omega_r$, can be achieved only in the weak damping limit $\kappa \rightarrow 0$. For $\kappa > 0$, it is always $\bar{\Omega}_\infty < \Omega_r$. This confirms the conditions given for property (T2) in Sec. IV D.

3. Thermalization (T3)

For weak damping, Eqs. (85) and (86) simplify to

$$\Omega^2 \Sigma_{\mathcal{Q}\mathcal{Q}}^\infty = \Sigma_{\mathcal{P}\mathcal{P}}^\infty = \frac{1}{2} (1 + \Omega_r^2) E(T_0, \Omega_b) \quad (\text{for } \kappa \rightarrow 0). \quad (89)$$

Equipartition of energy in the stationary state is evident, and the thermalization (T2) property fulfilled. To check property (T3), we calculate the temperature

$$\frac{2\bar{T}_\infty(\Omega)}{\Omega_r} = \text{arccoth}^{-1} \left[\frac{1}{2} \left(\Omega_r + \frac{1}{\Omega_r} \right) \coth \left(\frac{1}{2\bar{T}_0} \right) \right] \quad (90)$$

of the stationary state with Eq. (66) or the weak damping result (67). We see that $\bar{T}_\infty(\Omega_r)$ depends explicitly on the central oscillator frequency Ω_r , as depicted in Fig. 8. It is $\bar{T}_\infty = \bar{T}_0$ only for $\Omega_r = 1$. As discussed before, this results from the fact that $\check{\mathcal{E}}(\omega)$ after the quench violates condition (68).

We note that κ_b does not appear in Eq. (90). In the present example, the value of κ_b only determines the admissible values of Ω_r that lead to equilibration, as given by the second

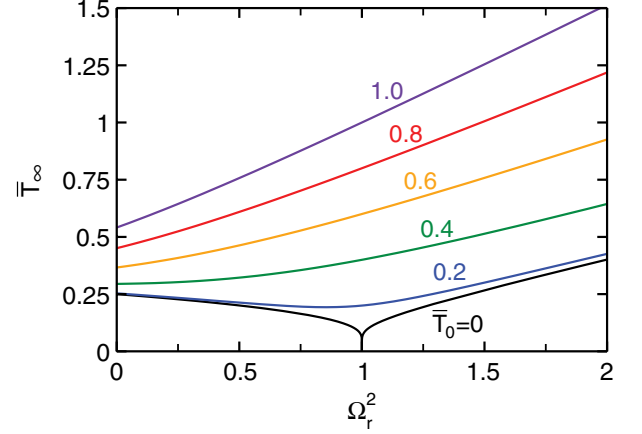


FIG. 8. (Color online) Temperature \bar{T}_∞ of the stationary thermal state at weak damping as given in Eq. (90). It is shown as a function of Ω_r for different temperatures $\bar{T}_0 = 0.2, \dots, 0.8$ of the initial state, as indicated. Note that \bar{T}_∞ does not depend on κ_b , but the admissible values of Ω_r for which equilibration occurs are restricted by the second condition in Eq. (78) (see also Fig. 3). In particular, it must be $0 \leq \Omega_r^2 \leq 2$.

inequality in Eq. (78). Once equilibration has been observed, the temperature of the stationary state at weak damping depends only on the value of $\check{\mathcal{E}}(\Omega)$ not on the functional dependence of the spectral function $\gamma(\omega)$.

4. The homogeneous chain

For the homogeneous chain with $\kappa_b = \kappa$, $\Omega_r = 1$, Eqs. (85) and (86) simplify to

$$\Sigma_{\mathcal{Q}\mathcal{Q}}^\infty = \frac{1}{2\Omega_b^2} \left(1 + \frac{1}{\sqrt{1 - \kappa^2}} \right) E(T_0, \Omega_b), \quad (91)$$

$$\Sigma_{\mathcal{P}\mathcal{P}}^\infty = E(T_0, \Omega_b). \quad (92)$$

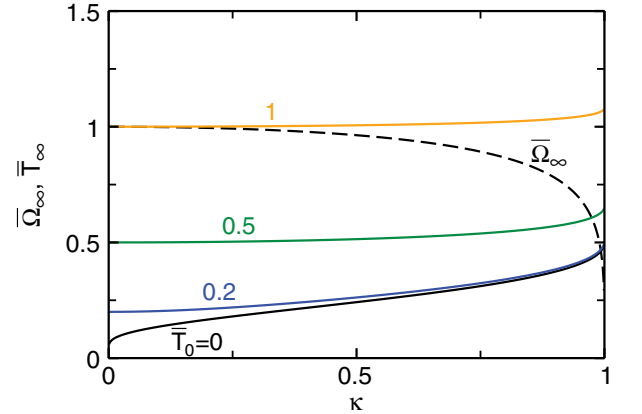


FIG. 9. (Color online) Frequency $\bar{\Omega}_\infty$ (dashed curve) and temperature \bar{T}_∞ (solid curves) for the homogeneous chain, from Eqs. (93) and (94), and shown as a function of κ . The temperature curves are plotted for $\bar{T}_0 = 0, 0.2, 0.5, 1$ as indicated.

Equipartition of energy is violated for any $\kappa > 0$, such that the effective frequency

$$\bar{\Omega}_\infty^2 = \frac{2}{1 + (1 - \kappa^2)^{-1/2}} \quad (93)$$

associated with the stationary state deviates from the central oscillator frequency (it is always $\bar{\Omega}_\infty \leq 1$). The temperature of the stationary state is

$$\frac{2\bar{T}_\infty}{\bar{\Omega}_\infty} = \operatorname{arcoth}^{-1} \left[\coth \left(\frac{1}{2\bar{T}_0} \right) \sqrt{\frac{1 + (1 - \kappa^2)^{-1/2}}{2}} \right]. \quad (94)$$

It is $\bar{T}_\infty > \bar{T}_0$ for $\kappa > 0$, for example $\bar{T}_\infty \rightarrow 1/2$ for $\kappa \rightarrow 1$ and $\bar{T}_0 \rightarrow 0$ (see Fig. 9).

The situation simplifies again in the weak damping limit $\kappa \rightarrow 0$, where we recover from Eqs. (91) and (92) the equilibration/thermalization result for the homogeneous chain formulated in Refs. [43,44]: At weak damping the central oscillator evolves into a stationary thermal state, with equipartition of energy $\Omega^2 \Sigma_{QQ}^\infty = \Sigma_{PP}^\infty = E(T_0, \Omega_b)$. Because of translational invariance this statement applies to every chain oscillator.

We note, however, that thermalization of the homogeneous chain is not perfect. As discussed in Sec. IV D, observation of a single oscillator in the homogeneous chain is not sufficient to establish thermalization of the entire chain. Thermalization fails for a finite chain segment consisting of two or more oscillators, because property (T3) is not fulfilled as seen in Eq. (90). Note that there is no possibility to check property (T3) directly for the homogeneous chain ($\Omega_r = 1$ is fixed here), such that results restricted to this situation have to be interpreted carefully [43,44].

VI. CONCLUSION

Our study of the dissipative quantum harmonic oscillator addresses equilibration and thermalization in nonthermal environments. Equilibration is the generic behavior, which is prevented only in situations in which the classical oscillator equation of motion possesses undamped oscillatory solutions. The infinite harmonic chain is an example for this behavior.

Thermalization of the central oscillator depends on additional conditions. Just as for thermal environments, equipartition of energy requires the weak damping limit but is independent of the precise initial conditions. The asymptotic temperature T_∞ is obtained from the energy distribution $\check{\mathcal{E}}(\omega)$ in the initial bath state, and generally depends on the central oscillator frequency Ω . If we demand that T_∞ is independent of Ω , another condition on $\check{\mathcal{E}}(\omega)$ follows. This condition is essential for simultaneous thermalization of several oscillators, when a thermal state of the combined system is obtained only if the same asymptotic temperature is assumed by each oscillator.

Part of the behavior discussed here generalizes to systems with nonlinear interactions. First, we note that equilibration is possible although the linear system is integrable. Equilibration occurs because, in a rough sense, the reduced density matrix of the central oscillator involves an average over conserved quantities of the joint oscillator-bath system. In other words, equilibration of small systems embedded in a large envi-

ronment does not require ergodicity. Second, because of the linearity and unitarity of quantum-mechanical time evolution, the stationary state depends explicitly on the initial (bath) state. But already for the linear system, some properties, such as equipartition of energy, are independent of the initial conditions. Furthermore, the stationary state depends only on the energy distribution $\check{\mathcal{E}}(\omega)$ in the initial bath state. Effectively, information is lost in the long-time limit and thermalization is possible for a large class of (nonthermal) initial states.

We discussed neither the generalization of the fluctuation-dissipation relation to the present nonthermal setting nor the role of stationary nonequilibrium states with finite heat flow that would require coupling to at least two baths with different preparations. Multitime correlation functions can be computed within the present formalism, which will allow for the analysis of both issues in the future.

ACKNOWLEDGMENTS

The authors wish to acknowledge helpful discussions with M. Cramer, G.-L. Ingold, and M. Thorwart. This work was supported by Deutsche Forschungsgemeinschaft through SFB 652 (B5) and AL1317/1-2.

APPENDIX A: OPERATOR EQUATIONS OF MOTION AND THEIR SOLUTION

The solution of the dissipative quantum harmonic oscillator model through operator equations of motion instead of transformation to normal modes of H allows for a simple treatment of general initial conditions and time-dependent coefficients. We list here the relevant steps of the derivation omitted in Sec. III, and we allow for a time-dependent central oscillator frequency $\Omega(t)$ (cf. Ref. [17] for a path integral calculation).

The Heisenberg equations of motion $\dot{A}(t) = i[H, A(t)]$ are

$$\dot{Q}(t) = P(t), \quad \dot{P}(t) = -\Omega^2(t)Q(t) - \sum_{\nu=1}^N \lambda_\nu Q_\nu(t) \quad (A1)$$

for the position and momentum operator of the central oscillator, and

$$\dot{Q}_\nu(t) = P_\nu(t), \quad \dot{P}_\nu(t) = -\omega_\nu^2 Q_\nu(t) - \lambda_\nu Q(t) \quad (A2)$$

for the bath oscillators.

We can read Eq. (A2) as an inhomogeneous linear equation for $Q_\nu(t)$. Using the Green function for the homogeneous equation $\ddot{Q}_\nu(t) = -\omega_\nu^2 Q_\nu(t)$, we find

$$Q_\nu(t) = \cos \omega_\nu t Q_\nu(0) + \frac{1}{\omega_\nu} \sin \omega_\nu t P_\nu(0) - \lambda_\nu \int_0^t \frac{1}{\omega_\nu} \sin \omega_\nu(t - \tau) Q(\tau) d\tau. \quad (A3)$$

Inserting this result into Eq. (A1) gives the equation of motion

$$\ddot{Q}(t) = -\Omega^2(t)Q(t) + \int_0^t K(t - \tau)Q(\tau) d\tau - N(t) \quad (A4)$$

for the central oscillator operator $Q(t)$, with the damping kernel $K(t)$ from Eq. (12) and the noise term

$$N(t) = \sum_{v=1}^N \lambda_v \left(\cos \omega_v t Q_v(0) + \frac{\sin \omega_v t}{\omega_v} P_v(0) \right). \quad (\text{A5})$$

Equation (A4) is an inhomogeneous linear integro-differential equation, which can be solved through solution of the classical equation of motion

$$\partial_t u(t, t') = -\Omega^2(t)u(t, t') + \int_{t'}^t K(t - \tau)u(\tau, t')d\tau. \quad (\text{A6})$$

We need the two solutions $u_1(t, t')$, $u_2(t, t')$ to the initial conditions $u_1(t, t) = 1$, $\partial_t u_1(t, t')|_{t=t'} = 0$ and $u_2(t, t) = 0$, $\partial_t u_2(t, t')|_{t=t'} = 1$. The solution of the operator equation of motion for $Q(t)$ is then given by

$$Q(t) = u_1(t, 0)Q(0) + u_2(t, 0)P(0) - \int_0^t u_2(t, \tau)N(\tau)d\tau, \quad (\text{A7})$$

and it is $P(t) = \dot{Q}(t)$.

With the partial Fourier transforms

$$\tilde{u}(t, \omega) = \int_0^t u_2(t, \tau)e^{i\omega\tau} d\tau, \quad (\text{A8})$$

$$\tilde{v}(t, \omega) = \int_0^t \partial_t u_2(t, \tau)e^{i\omega\tau} d\tau, \quad (\text{A9})$$

and the definition of matrices

$$\mathbf{U}(t) = \begin{pmatrix} u_1(t, 0) & u_2(t, 0) \\ \partial_t u_1(t, 0) & \partial_t u_2(t, 0) \end{pmatrix} \quad (\text{A10})$$

and $\mathbf{U}(t, \omega)$ as in Eq. (18), the operators $Q(t)$, $P(t)$ are given by the matrix Eq. (19).

For constant $\Omega(t) \equiv \Omega$, the function $u(t)$ used in Sec. III is recovered as $u(t) = u_2(t, 0)$, and it is $\dot{u}(t) = u_1(t, 0)$ [while $u_1(t, t') \neq \partial_t u_2(t, t')$ for time-dependent $\Omega(t)$]. Then, the partial Fourier transforms $\tilde{u}_2(t, \omega)$ and $\tilde{v}_2(t, \omega)$ are related by Eq. (16) and $\mathbf{U}(t)$ is given by the simpler expression (17). Equations (20) and (21) and Eqs. (26) and (27) for the calculation of expectation values and variances and Eq. (45) for the construction of the propagating function remain valid for time-dependent $\Omega(t)$.

APPENDIX B: PROPAGATING FUNCTION IN POSITION REPRESENTATION

The propagating function in position representation is the Fourier transform

$$J(q_f, q'_f, q_i, q'_i, t) = \frac{1}{2\pi} \iint_{-\infty}^{\infty} e^{i\tilde{p}(q_f - q'_f)} e^{-ip(q_i - q'_i)} \times J_W\left(\frac{q_f + q'_f}{2}, \tilde{p}, \frac{q_i + q'_i}{2}, p, t\right) d\tilde{p} dp \quad (\text{B1})$$

of Eq. (45). It results in the expression

$$J(Y, y, X, x, t) = \frac{|j_6|}{2\pi} \exp[j_1 x^2 + j_2 xy + j_3 y^2 + i((j_4 x + j_5 y)X + (j_6 x + j_7 y)Y + j_8 x + j_9 y)], \quad (\text{B2})$$

where we write $Y = (q_f + q'_f)/2$, $y = q_f - q'_f$, $X = (q_i + q'_i)/2$, $x = q_i - q'_i$ for abbreviation and drop the time argument in $j_k \equiv j_k(t)$. The nine real parameters j_1, \dots, j_9 in this expression are related to the parameters of $J_W(\tilde{\mathbf{x}}, \mathbf{x}, t)$ in Eq. (45) through

$$\begin{aligned} j_1 &= -\frac{C_{QQ}}{2U_{QP}^2}, & j_2 &= -\frac{C_{QP}}{U_{QP}} + C_{QQ} \frac{U_{PP}}{U_{QP}^2}, \\ j_3 &= -\frac{1}{2}C_{PP} - \frac{U_{PP}^2}{2U_{QP}^2}C_{QQ} + \frac{U_{PP}}{U_{QP}}C_{QP}, \\ j_4 &= \frac{U_{QQ}}{U_{QP}}, & j_5 &= U_{PQ} - \frac{U_{QQ}U_{PP}}{U_{QP}}, & j_6 &= -\frac{1}{U_{QP}}, \\ j_7 &= \frac{U_{PP}}{U_{QP}}, & j_8 &= \frac{1}{U_{QP}}I_Q, & j_9 &= I_P - \frac{U_{PP}}{U_{QP}}I_Q. \end{aligned} \quad (\text{B3})$$

Explicit insertion of $\mathbf{U}(t)$ from Eq. (17) or (A10) gives expressions that allow for direct comparison with the literature. For example, the expressions given in Ref. [17] are recovered for $\mathbf{I}(t) \equiv 0$ such that the terms $j_8 x$, $j_9 y$ vanish.

Obviously, the position representation leads to less convenient expressions for the propagating function, and obscures the clear formal structure of Eq. (45). In particular, the expressions (B3) are singular for $u(t) \rightarrow 0$, which gives a complicated representation of the δ distribution for the propagating function at $t = 0$ and $t \rightarrow \infty$ instead of the simple limit for $J_W(\tilde{\mathbf{x}}, \mathbf{x}, t)$ [cf. Eq. (64)].

- [1] T. Barthel and U. Schollwöck, *Phys. Rev. Lett.* **100**, 100601 (2008).
- [2] N. Linden, S. Popescu, A. J. Short, and A. Winter, *Phys. Rev. E* **79**, 061103 (2009).
- [3] P. Reimann, *Phys. Rev. Lett.* **101**, 190403 (2008).
- [4] P. Reimann, *New J. Phys.* **12**, 055027 (2010).
- [5] V. I. Yukalov, *Laser Phys. Lett.* **8**, 485 (2011).
- [6] T. W. Körner, *Fourier Analysis* (Cambridge University Press, Cambridge, 1989).
- [7] F. Haake and R. Reibold, *Phys. Rev. A* **32**, 2462 (1985).

- [8] G. W. Ford, J. T. Lewis, and R. F. O'Connell, *Phys. Rev. Lett.* **55**, 2273 (1985).
- [9] G. W. Ford, J. T. Lewis, and R. F. O'Connell, *Ann. Phys. (NY)* **185**, 270 (1988).
- [10] G. W. Ford and R. F. O'Connell, *Phys. Rev. B* **75**, 134301 (2007).
- [11] P. Ullersma, *Physica* **32**, 27 (1966).
- [12] P. Ullersma, *Physica* **32**, 56 (1966).
- [13] P. Ullersma, *Physica* **32**, 74 (1966).
- [14] P. Ullersma, *Physica* **32**, 90 (1966).
- [15] H. Grabert, *Chem. Phys.* **322**, 160 (2006).
- [16] K. E. Nagaev and M. Büttiker, *Europhys. Lett.* **58**, 475 (2002).

- [17] C. Zerbe and P. Hänggi, *Phys. Rev. E* **52**, 1533 (1995).
- [18] A. N. Jordan and M. Büttiker, *Phys. Rev. Lett.* **92**, 247901 (2004).
- [19] M. Hartmann, G. Mahler, and O. Hess, *Phys. Rev. E* **70**, 066148 (2004).
- [20] I. Kim and G. Mahler, *Phys. Rev. E* **81**, 011101 (2010).
- [21] H. Grabert, P. Schramm, and G.-L. Ingold, *Phys. Rep.* **168**, 115 (1988).
- [22] U. Weiss, *Quantum Dissipative Systems* (World Scientific, Singapore, 1999).
- [23] C. H. Fleming, A. Roura, and B. L. Hu, *Ann. Phys. (NY)* **326**, 1207 (2011).
- [24] W. G. Unruh and W. H. Zurek, *Phys. Rev. D* **40**, 1071 (1989).
- [25] B. L. Hu, J. P. Paz, and Y. Zhang, *Phys. Rev. D* **45**, 2843 (1992).
- [26] R. Karleins and H. Grabert, *Phys. Rev. E* **55**, 153 (1997).
- [27] H.-P. Breuer and F. Petruccione, *The Theory of Open Quantum Systems* (Oxford University Press, Oxford, 2002).
- [28] M. Campisi, P. Hänggi, and P. Talkner, *Rev. Mod. Phys.* **83**, 771 (2011).
- [29] C. H. Fleming and B. L. Hu, *Ann. Phys. (NY)* **327**, 1238 (2012).
- [30] M. Thorwart, P. Reimann, P. Jung, and R. Fox, *Chem. Phys.* **235**, 61 (1998).
- [31] M. Thorwart, P. Reimann, and P. Hänggi, *Phys. Rev. E* **62**, 5808 (2000).
- [32] H. Grabert, U. Weiss, and P. Talkner, *Z. Phys. B* **55**, 87 (1984).
- [33] R. P. Feynman and J. F. L. Vernon, *Ann. Phys. (NY)* **24**, 118 (1963).
- [34] A. Caldeira and A. Leggett, *Physica A* **121**, 587 (1983).
- [35] A. Caldeira and A. Leggett, *Ann. Phys. (NY)* **149**, 374 (1983).
- [36] B. Davies, *Integral Transforms and Their Applications*, 3rd ed. (Springer, New York, 2002).
- [37] M. Cramer, C. M. Dawson, J. Eisert, and T. J. Osborne, *Phys. Rev. Lett.* **100**, 030602 (2008).
- [38] M. Cramer and J. Eisert, *New J. Phys.* **12**, 055020 (2010).
- [39] E. Wigner, *Phys. Rev.* **40**, 749 (1932).
- [40] W. P. Schleich, *Quantum Optics in Phase Space* (Wiley-VCH, Berlin, 2001).
- [41] E. Calzetta, A. Roura, and E. Verdaguier, *Physica A* **319**, 188 (2003).
- [42] R. J. Rubin, *J. Math. Phys.* **1**, 309 (1960).
- [43] H. S. Robertson and M. A. Huerta, *Phys. Rev. Lett.* **23**, 825 (1969).
- [44] G. S. Agarwal, *Phys. Rev. A* **3**, 828 (1971).
- [45] M. A. Huerta, H. S. Robertson, and J. C. Nearing, *J. Math. Phys.* **12**, 2305 (1971).
- [46] M. Tegmark and H. S. Shapiro, *Phys. Rev. E* **50**, 2538 (1994).
- [47] M. Tegmark and L. Yeh, *Physica A* **202**, 342 (1994).
- [48] A. R. Usha Devi and A. K. Rajagopal, *Phys. Rev. E* **80**, 011136 (2009).

New Journal of Physics

The open access journal for physics

Nonequilibrium quantum fluctuation relations for harmonic systems in nonthermal environments

D Pagel^{1,3}, P Nalbach², A Alvermann¹, H Fehske¹
and M Thorwart²

¹ Institut für Physik, Ernst-Moritz-Arndt-Universität Greifswald,
Felix-Hausdorff-Straße 6, D-17489 Greifswald, Germany

² I. Institut für Theoretische Physik, Universität Hamburg, Jungiusstraße 9,
D-20355 Hamburg, Germany

E-mail: pagel@physik.uni-greifswald.de

New Journal of Physics **15** (2013) 105008 (20pp)

Received 31 May 2013

Published 8 October 2013

Online at <http://www.njp.org/>

doi:10.1088/1367-2630/15/10/105008

Abstract. We formulate exact generalized nonequilibrium fluctuation relations for the quantum mechanical harmonic oscillator coupled to multiple harmonic baths. Each of the different baths is prepared in its own individual (in general nonthermal) state. Starting from the exact solution for the oscillator dynamics we study fluctuations of the oscillator position as well as of the energy current through the oscillator under general nonequilibrium conditions. In particular, we formulate a fluctuation–dissipation relation for the oscillator position autocorrelation function that generalizes the standard result for the case of a single bath at thermal equilibrium. Moreover, we show that the generating function for the position operator fulfils a generalized Gallavotti–Cohen-like relation. For the energy transfer through the oscillator, we determine the average energy current together with the current fluctuations. Finally, we discuss the generalization of the cumulant generating function for the energy transfer to nonthermal bath preparations.

³ Author to whom any correspondence should be addressed.



Content from this work may be used under the terms of the [Creative Commons Attribution 3.0 licence](https://creativecommons.org/licenses/by/3.0/).

Any further distribution of this work must maintain attribution to the author(s) and the title of the work, journal citation and DOI.

Contents

1. Introduction	2
2. The model	4
2.1. The exact solution for the operator dynamics	4
2.2. Expectation values	6
2.3. The thermodynamic limit	6
3. Nonequilibrium fluctuation relation for the oscillator position	8
3.1. The symmetric correlation function	8
3.2. The antisymmetric correlation function	9
3.3. The generalized nonequilibrium fluctuation relation	10
4. Generating function for the position operator of the oscillator	10
5. Quantum mechanical energy transfer between nonequilibrium baths	12
6. Nonequilibrium fluctuations of the transferred energy	14
6.1. The first moment	15
6.2. The second moment	15
6.3. The generating function for the energy transfer	16
7. Summary	17
Acknowledgments	17
Appendix. Correlation functions of the fluctuating forces	17
References	19

1. Introduction

Fluctuation relations [1–7] build on the fundamental connection between the response of a physical system to a weak externally applied force and the fluctuations in the system without the external force. This connection was first observed for thermal equilibrium by William Sutherland [8, 9] and Albert Einstein [10–12]. They established the relation between the mobility of a Brownian particle, which is a quantity that measures the response to an external electric field, and the diffusion constant, which is a quantity that characterizes the fluctuating forces at equilibrium. The famous Johnson–Nyquist relation [13, 14] gives the corresponding connection between the electrical resistance of a circuit and charge fluctuations in the resistor. A more general relation has been derived by Callen and Welton [15] in form of the quantum fluctuation–dissipation theorem (FDT)

$$\Psi(\omega) = \frac{\hbar}{2i} \coth\left(\frac{\hbar\beta\omega}{2}\right) \Phi(\omega), \quad (1)$$

which relates the Fourier transform $\Psi(\omega)$ of the symmetric equilibrium correlation function of an observable to the Fourier transform $\Phi(\omega)$ of the (antisymmetric) response function of this observable in thermal equilibrium at temperature $T = (k_B\beta)^{-1}$. It was recognized by Green [16, 17] and Kubo [18] that the FDT in equation (1) is a particular case of the more general linear response theory which is an invaluable tool to model and understand experimental data in all fields of physics. However, often situations are encountered where the assumption of thermal equilibrium is invalid, for example, for systems strongly driven by external fields, charge currents in systems with large differences in the electric potential, heat currents in

systems with strong temperature gradients, or systems in solvents and disordered media which themselves are in metastable quasi-equilibria only. It has been a longstanding task in statistical physics to generalize linear response theory and FDTs to such nonequilibrium situations and, by this, to build a unifying theoretical framework of the spectral characteristics of environmental noise.

Generalized nonequilibrium fluctuation theorems have been formulated for classical nonstationary Markov processes [19] and for stationary Markov processes far away from thermal equilibrium [20, 21]. They relate the higher-order nonlinear response to higher-order correlation functions of stationary nonequilibrium fluctuations. A fully nonlinear, exact and universal classical fluctuation relation has been provided by Bochkov and Kuzovlev [22]. It gives the fluctuation relation at any order for systems that are in a thermal state in absence of external forces. It solely builds on the time-reversal invariance of the equations of motion and the assumption of a thermally equilibrated initial state. The quantum version was provided by Andrieux and Gaspard [23] and lead to fundamental insights [1] into the fact that work injected to or extracted from a system is not a quantum mechanical operator or observable, because it characterizes a process rather than a state of the system [24].

Recently, growing interest in nonequilibrium fluctuation relations arose from alternative formulations by Evans *et al* [25] and by Gallavotti and Cohen [26] for the statistics of nonequilibrium fluctuations in steady states and by Jarzynski [27] and Crooks [28] on the statistics of work performed by a transient time-dependent perturbation [1]. The reviews [1–7] summarize the actual progress in this field.

Most studies so far consider systems initially in thermal equilibrium, described by the canonical distribution

$$\rho_0 = \frac{1}{Z_0} e^{-\beta H_0} \quad (2)$$

with the system Hamiltonian H_0 and the partition function $Z_0 = \text{Tr}[e^{-\beta H_0}]$. In this work, we want to give up this assumption and formulate generalized nonequilibrium fluctuation relations for nonthermal initial states. To do so, we consider the dissipative quantum mechanical harmonic oscillator [29–37]. Building on our previous work in [38] we study a central oscillator coupled to an arbitrary number of harmonic baths each of which can be prepared in its own individual initial state. The fluctuations of the baths are thus still Gaussian, but not necessarily thermally distributed. Because the exact solution for the system dynamics is known, we can analytically calculate all observables and correlation functions of interest, and thus investigate the validity of nonthermal nonequilibrium fluctuation relations for this admittedly restricted model situation.

The structure of the paper is as follows. We introduce the model, its classical equation of motion and the basic notions in section 2. Then, in section 3, we calculate the symmetric and antisymmetric correlation functions of the oscillator position for the case of general nonthermal bath states. In section 3.3, we formulate the generalized nonequilibrium fluctuation relation for the oscillator position correlation functions. This constitutes one major result of this work. In section 4, we calculate the generating function for the position operator of the oscillator and show that it fulfils a generalized Gallavotti–Cohen relation under nonequilibrium conditions at arbitrary times. Section 5 is devoted to energy transfer and we present the derivation of the average energy current. In section 6, we calculate the energy current fluctuations and generalize the well-known cumulant generating function of the heat transfer for thermal baths to general bath preparations, before we summarize in section 7.

2. The model

In a system–bath model approach, we consider the one-dimensional harmonic oscillator bilinearly coupled to a finite number N_B of different and mutually uncoupled baths of harmonic oscillators. The total Hamiltonian is $H = H_S + H_B + H_{SB}$, where ($\hbar = 1$, $k_B = 1$ throughout the work)

$$H_S = \frac{1}{2}[P^2 + \Omega^2 Q^2] \quad (3)$$

is the contribution of the central oscillator with frequency Ω ,

$$H_B = \sum_{\alpha=1}^{N_B} H_B^\alpha, \quad H_B^\alpha = \sum_{\nu=1}^{N_\alpha} \frac{1}{2}[(P_\nu^\alpha)^2 + (\omega_\nu^\alpha Q_\nu^\alpha)^2] \quad (4)$$

is the contribution of the bath oscillators with frequencies ω_ν^α , and

$$H_{SB} = \sum_{\alpha=1}^{N_B} H_{SB}^\alpha, \quad H_{SB}^\alpha = Q \sum_{\nu=1}^{N_\alpha} \lambda_\nu^\alpha Q_\nu^\alpha + \sum_{\nu=1}^{N_\alpha} \frac{1}{2} \left(\frac{\lambda_\nu^\alpha}{\omega_\nu^\alpha} \right)^2 Q^2 \quad (5)$$

is the coupling part. In these expressions, the position and momentum operators Q_ν^α and P_ν^α fulfil the canonical commutation relation $[Q_\nu^\alpha, P_\mu^{\alpha'}] = i\delta_{\nu\mu}\delta_{\alpha\alpha'}$. The labels $\alpha, \alpha' = 1, \dots, N_B$ are used to identify a particular bath, while the indices $\nu, \mu = 1, \dots, N_\alpha$ identify a single oscillator from bath α .

The coupling term contains the counter term which serves to eliminate the potential renormalization due to the coupling of the oscillator to the baths [39, 40]. Throughout this work, we assume factorizing initial states $\rho(0) = \rho_S(0) \otimes_{\alpha=1}^{N_B} \rho_B^\alpha(0)$ corresponding to the choice of isolated systems that are brought into contact at $t = 0^+$. Notice, however, that we keep the initial distributions $\rho_B^\alpha(0)$ of the baths arbitrary and do not necessarily assume thermal equilibrium.

2.1. The exact solution for the operator dynamics

Starting from the Heisenberg equation of motion for the system and bath operators, one inserts the formal solution for the bath operator dynamics into the equation of motion of the central oscillator to obtain the quantum Langevin equation

$$\ddot{Q}(t) = -\Omega^2 Q(t) - \int_0^t d\tau K(t-\tau)\dot{Q}(\tau) - \eta(t) - K(t)Q(0) \quad (6)$$

with the damping or friction kernel

$$K(t) = \sum_{\alpha=1}^{N_B} K_\alpha(t), \quad K_\alpha(t) = \sum_{\nu=1}^{N_\alpha} \left(\frac{\lambda_\nu^\alpha}{\omega_\nu^\alpha} \right)^2 \cos \omega_\nu^\alpha t, \quad (7)$$

and the noise term

$$\eta(t) = \sum_{\alpha=1}^{N_B} \eta_\alpha(t), \quad \eta_\alpha(t) = \sum_{\nu=1}^{N_\alpha} \lambda_\nu^\alpha \left(Q_\nu^\alpha(0) \cos \omega_\nu^\alpha t + P_\nu^\alpha(0) \frac{\sin \omega_\nu^\alpha t}{\omega_\nu^\alpha} \right). \quad (8)$$

The noise term $\eta(t)$ together with the initial slip term $K(t)Q(0)$ appears as a fluctuating force in equation (6). Due to our choice of factorizing initial states, the noise terms of different baths are uncorrelated, i.e. $\langle \eta_\alpha(t)\eta_\beta(s) \rangle = \langle \eta_\alpha(t) \rangle \langle \eta_\beta(s) \rangle$ for $\alpha \neq \beta$. Nevertheless, the fluctuating forces

$\xi_\alpha(t) = \eta_\alpha(t) + K_\alpha(t)Q(0)$ including the initial slip term are correlated because of the coupling to the central oscillator [41]. These correlations vanish if the expectation values are calculated with respect to the nonfactorizing initial state that is obtained out of $\rho(0)$ through the unitary transformation with the displacement operator $\exp[iQ \sum_{\nu=1}^{N_\alpha} \lambda_\nu^\alpha P_\nu^\alpha / (\omega_\nu^\alpha)^2]$. At this point, we note that explicit expressions for the correlation functions of the fluctuating forces depend on the choice of the initial distributions $\rho_B^\alpha(0)$ and thus, the fluctuations are in general associated with a nonstationary Gaussian operator noise. Only in the limit of long times, these fluctuations become stationary again (see the appendix).

As is well established in the literature [29–37], the full solution for the central oscillator dynamics can be constructed from the solution $u(t) \in \mathbb{R}$ of the corresponding classical equation of motion

$$\ddot{u}(t) = -\Omega^2 u(t) - \int_0^t d\tau K(t-\tau)\dot{u}(\tau). \quad (9)$$

The relevant solution $u(t)$ is specified by $u(t) = 0$ for $t < 0$ and by the initial conditions $u(0) = 0$ and $\dot{u}(0) = 0$. It is given by the Fourier transform

$$u(t) = \frac{1}{2\pi} \int_{-\infty}^{\infty} d\omega e^{-i(\omega+i0^+)t} F(\omega+i0^+) = \frac{2}{\pi} \int_0^{\infty} d\omega \sin \omega t \operatorname{Im} F(\omega+i0^+) \quad (10)$$

of the function

$$F(z) = \left[\Omega^2 + \sum_{\alpha=1}^{N_B} \sum_{\nu=1}^{N_\alpha} \left(\frac{\lambda_\nu^\alpha}{\omega_\nu^\alpha} \right)^2 - z^2 + \sum_{\alpha=1}^{N_B} \sum_{\nu=1}^{N_\alpha} \frac{(\lambda_\nu^\alpha)^2}{z^2 - (\omega_\nu^\alpha)^2} \right]^{-1}. \quad (11)$$

Given $u(t)$, the solution for the dynamics of the central oscillator operators can be obtained from the matrix equation

$$\begin{pmatrix} Q(t) \\ P(t) \end{pmatrix} = \mathbf{U}(t) \begin{pmatrix} Q(0) \\ P(0) \end{pmatrix} - \sum_{\alpha=1}^{N_B} \sum_{\nu=1}^{N_\alpha} \lambda_\nu^\alpha \mathbf{U}(t, \omega_\nu^\alpha) \begin{pmatrix} Q_\nu^\alpha(0) \\ P_\nu^\alpha(0) \end{pmatrix}. \quad (12)$$

We here introduced the matrices

$$\mathbf{U}(t) = \begin{pmatrix} \dot{u}(t) & u(t) \\ \ddot{u}(t) & \dot{u}(t) \end{pmatrix}, \quad (13)$$

$$\mathbf{U}(t, \omega) = \begin{pmatrix} u_R(t, \omega) & \frac{u_I(t, \omega)}{\omega} \\ v_R(t, \omega) & \frac{v_I(t, \omega)}{\omega} \end{pmatrix}, \quad (14)$$

and denote by the respective index R or I the real or imaginary part of the partial Fourier transforms of the classical solution $u(t)$,

$$u(t, \omega) \equiv u_R(t, \omega) + i u_I(t, \omega) = e^{i\omega t} \int_0^t d\tau u(\tau) e^{-i\omega\tau}, \quad (15)$$

$$v(t, \omega) \equiv v_R(t, \omega) + i v_I(t, \omega) = e^{i\omega t} \int_0^t d\tau \dot{u}(\tau) e^{-i\omega\tau} = u(t) + i\omega u(t, \omega). \quad (16)$$

2.2. Expectation values

Equation (12) allows us to express central oscillator expectation values for $t \geq 0$ in terms of the initial ones at $t = 0$. The linear expectation values are given by the equation

$$\mathbf{X}(t) \equiv \begin{pmatrix} \langle Q(t) \rangle \\ \langle P(t) \rangle \end{pmatrix} = \mathbf{U}(t)\mathbf{X}(0) + \mathbf{I}(t), \quad (17)$$

where

$$\mathbf{I}(t) = - \sum_{\alpha=1}^{N_B} \sum_{\nu=1}^{N_\alpha} \lambda_\nu^\alpha \mathbf{U}(t, \omega_\nu^\alpha) \mathbf{X}_\nu^\alpha \quad (18)$$

depends on the initial bath expectation values $\mathbf{X}_\nu^\alpha = (\langle Q_\nu^\alpha(0) \rangle, \langle P_\nu^\alpha(0) \rangle)^T$.

For the quadratic expectation values we define the correlator of two operators A and B by

$$\Sigma_{AB} = \frac{1}{2} \langle AB + BA \rangle - \langle A \rangle \langle B \rangle, \quad (19)$$

and write $\Sigma_{AB}(t) \equiv \Sigma_{A(t)B(t)}$ for better readability. For correlators of operators related to bath oscillators at initial time, we define

$$\sigma_{A_\nu^\alpha B_\mu^\alpha} = \Sigma_{A_\nu^\alpha B_\mu^\alpha}(0) \quad (20)$$

and write

$$\Sigma_{\nu\mu}^\alpha = \begin{pmatrix} \sigma_{Q_\nu^\alpha Q_\mu^\alpha} & \sigma_{Q_\nu^\alpha P_\mu^\alpha} \\ \sigma_{P_\nu^\alpha Q_\mu^\alpha} & \sigma_{P_\nu^\alpha P_\mu^\alpha} \end{pmatrix}. \quad (21)$$

We then obtain with equation (12) the relation

$$\Sigma(t) \equiv \begin{pmatrix} \Sigma_{QQ}(t) & \Sigma_{QP}(t) \\ \Sigma_{QP}(t) & \Sigma_{PP}(t) \end{pmatrix} = \mathbf{U}(t)\Sigma(0)\mathbf{U}^T(t) + \mathbf{C}(t), \quad (22)$$

where

$$\mathbf{C}(t) = \sum_{\alpha=1}^{N_B} \sum_{\mu, \nu=1}^{N_\alpha} \lambda_\nu^\alpha \lambda_\mu^\alpha \mathbf{U}(t, \omega_\nu^\alpha) \Sigma_{\nu\mu}^\alpha \mathbf{U}^T(t, \omega_\mu^\alpha). \quad (23)$$

2.3. The thermodynamic limit

In the thermodynamic limit $N_\alpha \rightarrow \infty$ for all $\alpha = 1, \dots, N_B$ we can replace summations $(1/N_\alpha) \sum_{\nu=1}^{N_\alpha} f(\omega_\nu^\alpha)$ by integrations $\int_0^\infty d\omega D_\alpha(\omega) f(\omega)$ by introducing the densities of states of the baths,

$$D_\alpha(\omega) = \frac{1}{N_\alpha} \sum_{\nu=1}^{N_\alpha} \delta(\omega - \omega_\nu^\alpha), \quad (24)$$

that converge to continuous functions. Since the coupling constants λ_ν^α enter equations (7) and (11) as $(\lambda_\nu^\alpha)^2$, they have to scale as $1/\sqrt{N_\alpha}$ to obtain finite results for the sum over N_α terms. We thus introduce continuous functions $\lambda_\alpha(\omega)$ according to

$$\lambda_\nu^\alpha = \lambda_\alpha(\omega_\nu^\alpha) / \sqrt{N_\alpha}, \quad (25)$$

and define the bath spectral functions

$$\gamma_\alpha(\omega) = D_\alpha(\omega) \frac{\lambda_\alpha(\omega)^2}{\omega}. \quad (26)$$

Note that we here use the definition of the bath spectral function of [42] without the factor $\pi/2$, which corresponds to the definition of [30] with an additional $1/\omega$ factor.

The linear expectation values \mathbf{X}_v^α have to scale as $1/\sqrt{N_\alpha}$, because they appear in equation (18) with the prefactors $\lambda_{v,\alpha}^\alpha$. We introduce continuous functions $X_{\alpha,Q}(\omega)$ and $X_{\alpha,P}(\omega)$ according to

$$\mathbf{X}_v^\alpha = \frac{\mathbf{X}_\alpha(\omega_v^\alpha)}{\sqrt{N}} = \frac{1}{\sqrt{N}} \begin{pmatrix} X_{\alpha,Q}(\omega_v^\alpha) \\ X_{\alpha,P}(\omega_v^\alpha) \end{pmatrix}. \quad (27)$$

Moreover, we have to separate the N_α diagonal terms Σ_{vv}^α from the N_α^2 off-diagonal terms $\Sigma_{v\mu}^\alpha$ with $v \neq \mu$ that require an additional $1/N_\alpha$ prefactor for convergence in the thermodynamic limit. Hence, we define

$$\Sigma_{v\mu}^\alpha = \Sigma_\alpha^{(1)}(\omega_v^\alpha) \delta_{v\mu} + \frac{1}{N_\alpha} \Sigma_\alpha^{(2)}(\omega_v^\alpha, \omega_\mu^\alpha) \quad (28)$$

with continuous functions $\sigma_{\alpha,XY}^{(1)}(\omega)$ and $\sigma_{\alpha,XY}^{(2)}(\omega_1, \omega_2)$ ($X, Y = Q, P$) as the matrix entries of $\Sigma_\alpha^{(1)}(\omega)$ and $\Sigma_\alpha^{(2)}(\omega_1, \omega_2)$.

The function $F(z)$ in the thermodynamic limit can be obtained via contour integration with the result

$$\begin{aligned} F(z) &= \left(\Omega^2 + \sum_{\alpha=1}^{N_B} \int_0^\infty d\omega \frac{\gamma_\alpha(\omega)}{\omega} - z^2 + \sum_{\alpha=1}^{N_B} \int_0^\infty \frac{\omega \gamma_\alpha(\omega)}{z^2 - \omega^2} d\omega \right)^{-1} \\ &= \left(\Omega^2 - \sum_{\alpha=1}^{N_B} \Gamma_\alpha(i0^+) - z^2 + \sum_{\alpha=1}^{N_B} \Gamma_\alpha(z) \right)^{-1} \end{aligned} \quad (29)$$

for $\text{Im } z > 0$. The complex functions $\Gamma_\alpha(z)$ follow from analytic continuation of $\gamma_\alpha(\omega) = \mp(2/\pi) \text{Im } \Gamma_\alpha(\pm\omega + i0^+)$ into the upper half of the complex plane.

If the function $F(z)$ has no poles for $\text{Im } z > 0$, the classical function $u(t)$ from equation (10) is the inverse Fourier transform of a continuous function. We can use the Riemann–Lebesgue lemma

$$\lim_{t \rightarrow \pm\infty} \int_{-\infty}^\infty d\omega f(\omega) e^{i\omega t} = 0 \quad (30)$$

valid for any integrable function $f(\omega)$ and conclude, that $u(t) \rightarrow 0$ in the long-time limit $t \rightarrow \infty$. In turn, poles of $F(z)$ correspond to undamped oscillations in $u(t)$, such that the central oscillator will approach a stationary state only if isolated modes do not exist. The possibility of $\lim_{t \rightarrow \infty} u(t) \neq 0$, i.e. the existence of isolated poles in $F(z)$, is closely connected to a breaking of ergodicity in the sense of the mean-square of a stochastic observable [43–46]. Precise conditions for $\lim_{t \rightarrow \infty} u(t) = 0$, as well as a general discussion of equilibration and thermalization of the central oscillator, can be found in [38]. Throughout this work, we assume that $F(z)$ has no isolated poles, such that the classical solutions for $t \rightarrow \infty$ approach zero, i.e., $\mathbf{U}(t) \rightarrow 0$. Then, the central oscillator equilibrates and the asymptotic state is Gaussian with the expectation values in the long-time limit $\lim_{t \rightarrow \infty} \mathbf{X}(t) = 0$ and $\lim_{t \rightarrow \infty} \Sigma(t) = \Sigma^\infty$ [38].

3. Nonequilibrium fluctuation relation for the oscillator position

The results from the previous section allow us to derive a generalized nonequilibrium fluctuation relation of the form of equation (1). For this, we determine the symmetric and the antisymmetric correlation functions of the central oscillator position Q . Their Fourier transforms are then shown to obey a generalized nonequilibrium fluctuation relation in form of a characteristic proportionality relation.

3.1. The symmetric correlation function

We define the symmetric correlation function of the central oscillator position as

$$\Psi(t, s) = \frac{1}{2} \langle Q(t)Q(t+s) + Q(t+s)Q(t) \rangle. \quad (31)$$

Inserting the solution for $Q(t)$ from equation (12) and performing the thermodynamic limit $N_\alpha \rightarrow \infty$, we obtain

$$\begin{aligned} \Psi(t, s) = & \langle Q(t) \rangle \langle Q(t+s) \rangle + \dot{u}(t)\dot{u}(t+s)\Sigma_{QQ}(0) + u(t)u(t+s)\Sigma_{PP}(0) \\ & + (\dot{u}(t)u(t+s) + u(t)\dot{u}(t+s))\Sigma_{QP}(0) + \Psi^{(1)}(t, s) + \Psi^{(2)}(t, s) \end{aligned} \quad (32)$$

with the two functions

$$\begin{aligned} \Psi^{(1)}(t, s) = & \sum_{\alpha=1}^{N_B} \int_0^\infty d\omega \omega \gamma_\alpha(\omega) \left\{ u_R(t, \omega)u_R(t+s, \omega)\sigma_{\alpha,QQ}^{(1)}(\omega) + u_I(t, \omega)u_I(t+s, \omega) \frac{\sigma_{\alpha,PP}^{(1)}(\omega)}{\omega^2} \right. \\ & \left. + [u_R(t, \omega)u_I(t+s, \omega) + u_R(t+s, \omega)u_I(t, \omega)] \frac{\sigma_{\alpha,QP}^{(1)}(\omega)}{\omega} \right\} \end{aligned} \quad (33)$$

and

$$\begin{aligned} \Psi^{(2)}(t, s) = & \sum_{\alpha=1}^{N_B} \int_0^\infty d\omega_1 \int_0^\infty d\omega_2 D_\alpha(\omega_1)D_\alpha(\omega_2)\lambda_\alpha(\omega_1)\lambda_\alpha(\omega_2) \\ & \times \left\{ u_R(t, \omega_1)u_R(t+s, \omega_2)\sigma_{\alpha,QQ}^{(2)}(\omega_1, \omega_2) + u_I(t, \omega_1)u_I(t+s, \omega_2) \frac{\sigma_{\alpha,PP}^{(2)}(\omega_1, \omega_2)}{\omega_1\omega_2} \right. \\ & \left. + [u_R(t, \omega_1)u_I(t+s, \omega_2) + u_R(t+s, \omega_1)u_I(t, \omega_2)] \frac{\sigma_{\alpha,QP}^{(2)}(\omega_1, \omega_2)}{\omega_2} \right\}. \end{aligned} \quad (34)$$

In the long-time limit $t \rightarrow \infty$ the terms involving $u(t)$, $\dot{u}(t)$ and $\langle Q(t) \rangle$ vanish according to our assumption of continuity of $F(z)$. For the remaining terms $\Psi^{(1)}(t, s)$ and $\Psi^{(2)}(t, s)$ we rewrite the partial Fourier transform of equation (15) as $u(t+s, \omega) = e^{i\omega s} [u(t, \omega) - \int_0^s d\tau u(t+\tau) e^{-i\omega\tau}]$. Since $u(t)$ vanishes at long times, the partial Fourier transform $u(t+s, \omega)$ behaves asymptotically as

$$u_{\text{as}}(t+s, \omega) \simeq e^{i\omega(t+s)} u(\omega), \quad (35)$$

where

$$u(\omega) = \int_0^\infty d\tau u(\tau) e^{-i\omega\tau} \quad (36)$$

is the full Fourier transform of the function $u(t)$.⁴ Using this asymptotic behaviour in the expressions for $\Psi^{(1)}(t, s)$ and $\Psi^{(2)}(t, s)$ we see that the off-diagonal term $\Psi^{(2)}(t, s)$ contains only oscillatory terms in the two frequencies ω_1 and ω_2 . If we recall the Riemann–Lebesgue lemma, equation (30), we conclude, that $\Psi^{(2)}(t, s)$ vanishes in the long-time limit. Following the same line of reasoning we find that the only non-zero term in the limit $t \rightarrow \infty$ comes from $\Psi^{(1)}(t, s)$ and involves $|u(\omega)|^2$ while the arising oscillating terms vanish. In particular,

$$\Psi(s) \equiv \lim_{t \rightarrow \infty} \Psi(t, s) = \sum_{\alpha=1}^{N_B} \int_0^{\infty} d\omega \gamma_{\alpha}(\omega) |u(\omega)|^2 \frac{\mathcal{E}_{\alpha}(\omega)}{\omega} \cos \omega s, \quad (37)$$

where

$$\mathcal{E}_{\alpha}(\omega) = \frac{1}{2} [\omega^2 \sigma_{\alpha, QQ}^{(1)}(\omega) + \sigma_{\alpha, PP}^{(1)}(\omega)] \quad (38)$$

denotes the frequency-resolved energy distribution functions of the initial bath states.

We next Fourier transform equation (37) and obtain

$$\Psi(\omega) = \int_{-\infty}^{\infty} ds e^{i\omega s} \Psi(s) = \pi \sum_{\alpha=1}^{N_B} \gamma_{\alpha}(\omega) |u(\omega)|^2 \frac{\mathcal{E}_{\alpha}(\omega)}{\omega}. \quad (39)$$

3.2. The antisymmetric correlation function

The antisymmetric correlation function of the oscillator position Q is given by

$$\Phi(t, s) = \frac{1}{i} \langle Q(t)Q(t+s) - Q(t+s)Q(t) \rangle. \quad (40)$$

Inserting the solution $Q(t)$ of equation (12), using the property $\langle [Q_{\nu}^{\alpha}(0), P_{\mu}^{\alpha}(0)] \rangle = i\delta_{\nu\mu}$ and performing the thermodynamic limit $N_{\alpha} \rightarrow \infty$, we obtain

$$\begin{aligned} \Phi(t, s) &= \dot{u}(t)u(t+s) - u(t)\dot{u}(t+s) \\ &+ \sum_{\alpha=1}^{N_B} \int_0^{\infty} d\omega \gamma_{\alpha}(\omega) [u_R(t, \omega)u_I(t+s, \omega) - u_R(t+s, \omega)u_I(t, \omega)], \end{aligned} \quad (41)$$

which is independent of the initial bath preparation as expected [39].

Similar to the calculation of the symmetric correlation function, we obtain for the antisymmetric response function in the long-time limit

$$\Phi(s) \equiv \lim_{t \rightarrow \infty} \Phi(t, s) = \sum_{\alpha=1}^{N_B} \int_0^{\infty} d\omega \gamma_{\alpha}(\omega) |u(\omega)|^2 \sin \omega s. \quad (42)$$

Its Fourier transform readily follows as

$$\Phi(\omega) = \int_{-\infty}^{\infty} ds e^{i\omega s} \Phi(s) = i\pi \sum_{\alpha=1}^{N_B} \gamma_{\alpha}(\omega) |u(\omega)|^2. \quad (43)$$

⁴ We use the same symbol u for the function and its Fourier transform for ease of readability. Time arguments are denoted as t , τ or s , while frequency arguments are denoted by ω .

3.3. The generalized nonequilibrium fluctuation relation

To formulate the general nonequilibrium fluctuation relation, we compare equations (39) and (43) and obtain for general initial preparations and an arbitrary number N_B of independent harmonic baths the relation

$$\Psi(\omega) = \frac{1}{i} \frac{\sum_{\alpha=1}^{N_B} \gamma_{\alpha}(\omega) \mathcal{E}_{\alpha}(\omega)}{\omega \sum_{\alpha=1}^{N_B} \gamma_{\alpha}(\omega)} \Phi(\omega). \quad (44)$$

This is one major result of the present work and illustrates that the relation is crucially determined by the frequency-resolved energy distributions $\mathcal{E}_{\alpha}(\omega)$ of the initial bath states defined in equation (38) and the bath spectral functions $\gamma_{\alpha}(\omega)$ given in equation (26). A comparison with the thermal FDT in equation (1) shows that in the considered nonthermal situation we have to exchange the thermal energy distribution

$$\mathcal{E}_{\text{th}}(\omega, T) = \frac{\omega}{2} \coth \frac{\omega}{2T} \quad (45)$$

with the average of the individual energy distributions of the baths weighted with their spectral functions.

In the case when all baths are initially distributed thermally at the same temperature T according the thermal equilibrium Bose–Einstein distribution function, we have $\mathcal{E}_{\alpha}(\omega) = \mathcal{E}_{\text{th}}(\omega, T)$ for all $\alpha = 1, \dots, N_B$. This reproduces the equilibrium FDT equation (1) [39].

A natural question then is under which initial bath preparations the central oscillator thermalizes, i.e. reaches a stationary state which is thermally distributed with a given temperature T . By comparing equations (44) and (1), we obtain the condition

$$\frac{\sum_{\alpha} \gamma_{\alpha}(\omega) \mathcal{E}_{\alpha}(\omega)}{\sum_{\alpha} \gamma_{\alpha}(\omega)} = \mathcal{E}_{\text{th}}(\omega, T) \quad (46)$$

for which the fluctuations of the central oscillator for $t \rightarrow \infty$ are thermal. This condition certainly is satisfied whenever all baths are thermal and have equal temperature, but can also be satisfied for other nonthermal initial bath preparations. In turn, if this condition is satisfied, the quantity

$$T^{-1} = \frac{2}{\omega} \operatorname{arccoth} \left(\frac{2 \sum_{\alpha} \gamma_{\alpha}(\omega) \mathcal{E}_{\alpha}(\omega)}{\omega \sum_{\alpha} \gamma_{\alpha}(\omega)} \right) \quad (47)$$

is a constant, i.e. independent of ω . It is then tempting to understand this quantity as an ‘effective’ temperature characterizing the general initial bath preparation. However, the above condition does not guarantee true thermalization of the central oscillator, which is essential for a meaningful notion of temperature. For a more detailed discussion of this question, see [38].

4. Generating function for the position operator of the oscillator

In this section we show that the dissipative oscillator model allows us to study the connection between transient and steady state fluctuation relations. We calculate the generating function for the central oscillator position operator and show that it fulfils a Gallavotti–Cohen symmetry relation [26] valid for arbitrary times and a Gaussian initial state of the central oscillator. This additional Gaussian assumption is not necessary in the long-time limit and we obtain an exact result for the steady state fluctuation relation.

We define the generating function for the position operator according to

$$Z_Q(\xi, t) = \langle e^{i\xi Q(t)} \rangle. \quad (48)$$

With that, all the cumulants $\langle\langle Q^n(t) \rangle\rangle$ of the position operator follow by performing the respective derivative

$$\langle\langle Q^n(t) \rangle\rangle = \left. \frac{\partial^n \ln Z_Q(\xi, t)}{\partial (i\xi)^n} \right|_{\xi=0}. \quad (49)$$

For instance, we have $\langle\langle Q(t) \rangle\rangle = \langle Q(t) \rangle$ and $\langle\langle Q^2(t) \rangle\rangle = \Sigma_{QQ}(t)$.

It is convenient to represent the generating function in terms of the Wigner function of the central oscillator

$$W_S(q, p, t) = \frac{1}{2\pi} \int_{-\infty}^{\infty} ds \left\langle q + \frac{s}{2} \middle| \rho_S(t) \middle| q - \frac{s}{2} \right\rangle e^{-ips}, \quad (50)$$

such that

$$Z_Q(\xi, t) = \int_{\mathbb{R}^2} d\mathbf{x} W_S(\mathbf{x}, t) e^{i\xi q}, \quad (51)$$

where we write $W_S(\mathbf{x}, t) = W_S(q, p, t)$ with $\mathbf{x} = (q, p)^T$ and $d\mathbf{x} = dq dp$ for abbreviation. The Wigner function $W_S(\mathbf{x}, t)$ at time $t \geq 0$ can be obtained from the propagating function $J_W(\mathbf{x}, \bar{\mathbf{x}}, t) = J_W(q, p, \bar{q}, \bar{p}, t)$ in Wigner representation, that is defined by the relation

$$W_S(\mathbf{x}, t) = \int_{\mathbb{R}^2} d\bar{\mathbf{x}} J_W(\mathbf{x}, \bar{\mathbf{x}}, t) W_S(\bar{\mathbf{x}}, 0), \quad (52)$$

and can be evaluated to [38]

$$J_W(\mathbf{x}, \bar{\mathbf{x}}, t) = \frac{\exp \left\{ -\frac{1}{2} [\mathbf{x} - \mathbf{U}(t)\bar{\mathbf{x}} - \mathbf{I}(t)] \cdot \mathbf{C}^{-1}(t) [\mathbf{x} - \mathbf{U}(t)\bar{\mathbf{x}} - \mathbf{I}(t)] \right\}}{2\pi \sqrt{\det \mathbf{C}(t)}} \quad (53)$$

with $\mathbf{U}(t)$, $\mathbf{I}(t)$ and $\mathbf{C}(t)$ from equations (13), (18) and (23). Performing the Gaussian integral over \mathbf{x} we obtain

$$Z_Q(\xi, t) = \int_{\mathbb{R}^2} d\bar{\mathbf{x}} W_S(\bar{\mathbf{x}}, 0) \exp \left\{ -\frac{\xi^2}{2} \mathbf{e}_1 \cdot \mathbf{C}(t) \mathbf{e}_1 + i\xi [\mathbf{U}(t)\bar{\mathbf{x}} + \mathbf{I}(t)] \cdot \mathbf{e}_1 \right\}, \quad (54)$$

where $\mathbf{e}_1 = (1, 0)^T$.

In the long-time limit $t \rightarrow \infty$, where $\mathbf{U}(t) \rightarrow 0$ according to our assumption of continuity of $F(z)$, the integration in equation (54) evaluates to one because the initial Wigner function is normalized. We then obtain

$$Z_Q^\infty(\xi) \equiv \lim_{t \rightarrow \infty} Z_Q(\xi, t) = \exp \left\{ -\frac{\xi^2}{2} \Sigma_{QQ}^\infty \right\} \quad (55)$$

with $\Sigma_{QQ}^\infty = \lim_{t \rightarrow \infty} \Sigma_{QQ}(t)$. The results obeys the symmetry $Z_Q^\infty(\xi) = Z_Q^\infty(-\xi)$.

For finite times, we can restrict ourselves to Gaussian initial states of the central oscillator

$$W_S(\bar{\mathbf{x}}, 0) = \frac{\exp \left\{ -\frac{1}{2} [\bar{\mathbf{x}} - \mathbf{X}(0)] \cdot \Sigma^{-1}(0) [\bar{\mathbf{x}} - \mathbf{X}(0)] \right\}}{2\pi \sqrt{\det \Sigma(0)}}, \quad (56)$$

and obtain

$$\begin{aligned} Z_Q(\xi, t) &= \exp \left\{ -\frac{\xi^2}{2} \mathbf{e}_1 \cdot \boldsymbol{\Sigma}(t) \mathbf{e}_1 + i\xi \mathbf{X}(t) \cdot \mathbf{e}_1 \right\} \\ &= \exp \left\{ -\frac{\xi^2}{2} \Sigma_{QQ}(t) + i\xi \langle Q(t) \rangle \right\}. \end{aligned} \quad (57)$$

In order to see when the Gallavotti–Cohen relation is fulfilled, we calculate

$$Z_Q(-\xi + iA, t) = \exp \left\{ -\frac{\xi^2}{2} \Sigma_{QQ}(t) + i\xi [A \Sigma_{QQ}(t) - \langle Q(t) \rangle] + \frac{A}{2} [A \Sigma_{QQ}(t) - 2\langle Q(t) \rangle] \right\}. \quad (58)$$

Hence, the relation $Z_Q(-\xi + iA, t) = Z_Q(\xi, t)$ is fulfilled at any arbitrary time t , if

$$A \equiv A(t) = 2 \frac{\langle Q(t) \rangle}{\Sigma_{QQ}(t)}. \quad (59)$$

This implies that the oscillator fluctuates symmetrically around its momentary position average $\langle Q(t) \rangle$ since $Z_{Q-\langle Q \rangle}(-\xi, t) = Z_{Q-\langle Q \rangle}(\xi, t)$. On the other hand, however, the symmetry point for the generating function of the position operator, which in the stationary state is $\xi = 0$, is shifted by the momentary position expectation value scaled by the momentary position variance, i.e. $Z_Q(-\xi + iA/2, t) = Z_Q(\xi + iA/2, t)$. Note that this relation holds in general and also when the central oscillator has not yet reached its equilibrium state. This transient fluctuation relation is linked with the steady state fluctuation relation from above by realizing that $\lim_{t \rightarrow \infty} A(t) = 0$.

5. Quantum mechanical energy transfer between nonequilibrium baths

We now study the quantum mechanical transfer of energy between nonequilibrium baths. To keep the discussion simple, we concentrate on the case of the energy transfer between two baths, i.e. $N_B = 2$, and denote them as left ($\alpha = l$) and right ($\alpha = r$) reservoir. In particular, we are interested in the form of the expectation value of the energy current operator which can be defined for instance for the left junction according to [47–52]

$$I(t) = -\frac{dH_B^l(t)}{dt} = \frac{1}{2} \sum_{\nu=1}^{N_l} \lambda_\nu^l \{P_\nu^l(t), Q(t)\} \quad (60)$$

with the anticommutator defined as $\{A, B\} = AB + BA$.

For the calculation of the expectation value $\langle I(t) \rangle$ we need the solutions of the Heisenberg equations of motion for the left bath operators,

$$Q_\nu^l(t) = \cos \omega_\nu^l t Q_\nu^l(0) + \frac{\sin \omega_\nu^l t}{\omega_\nu^l} P_\nu^l(0) - \lambda_\nu^l \int_0^t d\tau \frac{\sin \omega_\nu^l(t-\tau)}{\omega_\nu^l} Q(\tau), \quad (61a)$$

$$P_\nu^l(t) = \dot{Q}_\nu^l(t). \quad (61b)$$

We insert these equations and the solution equation (12) for $Q(t)$ into equation (60) and perform the thermodynamic limit to obtain $\langle I(t) \rangle = \langle I_1(t) \rangle + \langle I_2(t) \rangle + \langle I_3(t) \rangle$ with

$$\langle I_1(t) \rangle = \int_0^\infty d\omega D_1(\omega) \lambda_1(\omega) \omega \sin \omega t X_{1,Q}(\omega) \langle Q(t) \rangle + \langle I_1^{(1)}(t) \rangle + \langle I_1^{(2)}(t) \rangle, \quad (62a)$$

$$\langle I_2(t) \rangle = - \int_0^\infty d\omega D_1(\omega) \lambda_1(\omega) \cos \omega t X_{1,P}(\omega) \langle Q(t) \rangle + \langle I_2^{(1)}(t) \rangle + \langle I_2^{(2)}(t) \rangle, \quad (62b)$$

$$\langle I_3(t) \rangle = \int_0^\infty d\omega \omega \gamma_1(\omega) \int_0^t d\tau \cos \omega \tau \Psi(t, \tau). \quad (62c)$$

In these equations, $\Psi(t, \tau)$ is the symmetric position autocorrelation function given in equation (31) and the diagonal and nondiagonal contributions to $\langle I_1(t) \rangle$ and $\langle I_2(t) \rangle$ are

$$\langle I_1^{(1)}(t) \rangle = - \int_0^\infty d\omega \omega^2 \gamma_1(\omega) \sin \omega t \left[u_R(t, \omega) \sigma_{1,QQ}^{(1)}(\omega) + \frac{u_1(t, \omega)}{\omega} \sigma_{1,QP}^{(1)}(\omega) \right], \quad (63a)$$

$$\begin{aligned} \langle I_1^{(2)}(t) \rangle = & - \int_0^\infty d\omega_1 \int_0^\infty d\omega_2 D_1(\omega_1) D_1(\omega_2) \lambda_1(\omega_1) \lambda_1(\omega_2) \omega_1 \sin \omega_1 t \\ & \times \left[u_R(t, \omega_2) \sigma_{1,QQ}^{(2)}(\omega_1, \omega_2) + \frac{u_1(t, \omega_2)}{\omega_2} \sigma_{1,QP}^{(2)}(\omega_1, \omega_2) \right], \end{aligned} \quad (63b)$$

and

$$\langle I_2^{(1)}(t) \rangle = \int_0^\infty d\omega \omega \gamma_1(\omega) \left[\cos \omega t u_1(t, \omega) \sigma_{1,QP}^{(1)}(\omega) + \cos \omega t \frac{u_1(t, \omega)}{\omega} \sigma_{1,PP}^{(1)}(\omega) \right], \quad (64a)$$

$$\begin{aligned} \langle I_2^{(2)}(t) \rangle = & \int_0^\infty d\omega_1 \int_0^\infty d\omega_2 D_1(\omega_1) D_1(\omega_2) \lambda_1(\omega_1) \lambda_1(\omega_2) \\ & \times \left[\cos \omega_2 t u_R(t, \omega_1) \sigma_{1,QP}^{(2)}(\omega_1, \omega_2) + \cos \omega_1 t \frac{u_1(t, \omega_2)}{\omega_2} \sigma_{1,PP}^{(2)}(\omega_1, \omega_2) \right]. \end{aligned} \quad (64b)$$

To perform the long-time limit, we follow the line of reasoning of section 3.1. The terms containing the linear expectation value $\langle Q(t) \rangle$ vanish. The off-diagonal terms $\langle I_1^{(2)}(t) \rangle$ and $\langle I_2^{(2)}(t) \rangle$ contain oscillatory terms in the two frequencies ω_1 and ω_2 only, such that $\langle I_1^{(2)}(t) \rangle, \langle I_2^{(2)}(t) \rangle \rightarrow 0$ for $t \rightarrow \infty$. The remaining diagonal terms can be simplified algebraically using the asymptotic behaviours equation (35) of the partial Fourier transform $u(t, \omega)$ and equation (37) of the symmetric correlation function $\Psi(t, \tau)$ and by applying the Riemann–Lebesgue lemma equation (30). We finally obtain the expectation value of the energy current from the left reservoir to the central oscillator in the long-time limit as

$$I_\infty \equiv \lim_{t \rightarrow \infty} \langle I(t) \rangle = - \int_0^\infty d\omega \gamma_1(\omega) \left[u_1(\omega) \mathcal{E}_l(\omega) + \frac{\pi}{2} \sum_{\alpha=l,r} \gamma_\alpha(\omega) |u(\omega)|^2 \mathcal{E}_\alpha(\omega) \right]. \quad (65)$$

We can rewrite this expression into the final form

$$I_\infty = \frac{\pi}{2} \int_0^\infty d\omega \gamma_l(\omega) \gamma_r(\omega) |u(\omega)|^2 [\mathcal{E}_l(\omega) - \mathcal{E}_r(\omega)] \quad (66)$$

by using, that the Fourier transform $u(\omega)$ in equation (36) is the inverse of the Fourier transform in equation (10), such that $u_1(\omega) = -\text{Im} F(\omega + i0^+) = -(\pi/2)[\gamma_l(\omega) + \gamma_r(\omega)]|u(\omega)|^2$.

Expression (66) generalizes equation (4.2) of [49] and reproduces it for the special case of thermal baths. Obviously, the asymptotic energy current vanishes exactly, if $\gamma_r(\omega) = 0$ for only one bath, or if $\mathcal{E}_r(\omega) = \mathcal{E}_l(\omega)$ for equal bath preparations.

For two thermal baths with $\mathcal{E}_\alpha(\omega) = \mathcal{E}_{\text{th}}(\omega, T_\alpha)$, and $T_l = T_r + \Delta T$ where $\Delta T \ll T_l$, we can expand the energy distribution function as

$$\mathcal{E}_l(\omega) = \mathcal{E}_r(\omega) + \left[\frac{\omega}{2T_r} \sinh^{-1} \frac{\omega}{2T_r} \right]^2 \Delta T + \mathcal{O}(\Delta T^2), \quad (67)$$

where $\sinh^{-1}x = 1/\sinh x$. Thus, we obtain the linear response result

$$I_\infty^{(\text{lin})} = \Delta T \frac{\pi}{2} \int_0^\infty d\omega \gamma_l(\omega) \gamma_r(\omega) |u(\omega)|^2 \frac{\omega^2}{4T_r^2} \sinh^{-2} \frac{\omega}{2T_r} + \mathcal{O}(\Delta T^2) \quad (68)$$

growing linearly with the difference ΔT of the temperatures of the left and right bath.

6. Nonequilibrium fluctuations of the transferred energy

In this section, we consider the energy which is transferred from one bath (say, the left) to the central oscillator in presence of the second bath (say, the right). Moreover, we are interested in the fluctuations of the transferred energy. We note in passing that we use the more general term of ‘energy’ instead of ‘heat’ since the definition of heat in the strict sense requires purely thermal environments.

The energy that is transferred from the left bath to the rest of the system until time t is obtained from the difference of the energy of the left bath between times t and 0. This involves the measurement of the observable H_B^1 at two different times. Following the idea of two-time quantum measurements, the corresponding generating function can be written as [50–52]

$$Z(\xi, t) = \langle e^{i\xi H_B^1} e^{-i\xi H_B^1(t)} \rangle', \quad (69)$$

where the prime indicates that the expectation value has to be taken with respect to the projected density matrix

$$\rho'(0) = \sum_a |\phi_a\rangle \langle \phi_a | \rho(0) | \phi_a\rangle \langle \phi_a|. \quad (70)$$

Here $|\phi_a\rangle$ is an eigenstate of the operator H_B^1 , i.e. $H_B^1 |\phi_a\rangle = a |\phi_a\rangle$. Writing the generating function as a series in powers of $i\xi$, we obtain [50, 52]

$$\ln Z(\xi, t) = \sum_{n=1}^{\infty} \frac{(i\xi)^n}{n!} \langle \langle W^n(t) \rangle \rangle, \quad (71)$$

where $\langle \langle W^n(t) \rangle \rangle$ denotes the n th order cumulant of the operator

$$W(t) = \int_0^t d\tau I(\tau) = H_B^1(0) - H_B^1(t). \quad (72)$$

In the following, we calculate the moments of the energy transfer operator $W(t)$ entering equation (71). In particular, we are interested in the long-time limit of these quantities.

6.1. The first moment

Using equations (61a) and (61b) the linear expectation value of the energy transfer operator follows as

$$\begin{aligned} \langle W(t) \rangle = & -\frac{1}{2} \sum_{\nu=1}^{N_1} \left\langle \lambda_{\nu}^1 \int_0^t d\tau \left(\omega_{\nu}^1 \sin \omega_{\nu}^1 \tau \{Q_{\nu}^1(0), Q(\tau)\} - \cos \omega_{\nu}^1 \tau \{P_{\nu}^1(0), Q(\tau)\} \right) \right. \\ & \left. + \frac{(\lambda_{\nu}^1)^2}{2} \int_0^t \int_0^t d\tau d\bar{\tau} \cos \omega_{\nu}^1 (\tau - \bar{\tau}) \{Q(\tau), Q(\bar{\tau})\} \right\rangle. \end{aligned} \quad (73)$$

In the long-time limit $t \rightarrow \infty$, we expect from the definition in equation (72) and from the result $\langle I(t) \rangle \rightarrow I_{\infty}$ of the last section that $\langle W(t) \rangle$ grows linearly with time. It is thus useful to consider $\langle W(t) \rangle / t$ instead of $\langle W(t) \rangle$.

The explicit calculation of $\langle W(t) \rangle / t$ in the long-time limit is achieved by inserting the solution $Q(t)$ from equation (12), performing the thermodynamic limit according to section 2.3, and analytically carrying out the remaining time integrations. The result is

$$\begin{aligned} \lim_{t \rightarrow \infty} \frac{1}{t} \langle W(t) \rangle = & - \left\{ \int_0^{\infty} d\omega \gamma_l(\omega) u_l(\omega) \mathcal{E}_l(\omega) + \frac{\pi}{2} \sum_{\alpha=l,r} \int_0^{\infty} d\omega \gamma_l(\omega) \gamma_{\alpha}(\omega) |u(\omega)|^2 \mathcal{E}_{\alpha}(\omega) \right\} \\ = & \frac{\pi}{2} \int_0^{\infty} d\omega \gamma_l(\omega) \gamma_r(\omega) |u(\omega)|^2 [\mathcal{E}_l(\omega) - \mathcal{E}_r(\omega)]. \end{aligned} \quad (74)$$

As expected, this expression coincides with the expectation value of the energy current operator given in equation (66).

6.2. The second moment

The second moment of the energy transfer operator is

$$\begin{aligned} \langle W^2(t) \rangle = & \left\langle \left[\sum_{\nu=1}^{N_1} \left\{ \frac{\lambda_{\nu}^1}{2} \int_0^t d\tau \left(\omega_{\nu}^1 \sin \omega_{\nu}^1 \tau \{Q_{\nu}^1(0), Q(\tau)\} - \cos \omega_{\nu}^1 \tau \{P_{\nu}^1(0), Q(\tau)\} \right) \right. \right. \right. \\ & \left. \left. \left. + \frac{(\lambda_{\nu}^1)^2}{4} \int_0^t \int_0^t d\tau d\bar{\tau} \cos \omega_{\nu}^1 (\tau - \bar{\tau}) \{Q(\tau), Q(\bar{\tau})\} \right\} \right]^2 \right\rangle. \end{aligned} \quad (75)$$

Expanding the square yields a sum of terms containing expectation values of products of four operators. We may reorder the operator products using the commutators

$$[Q_{\nu}^1(0), Q(t)] = -i \frac{\lambda_{\nu}^1}{\omega_{\nu}^1} u_l(t, \omega_{\nu}^1), \quad [P_{\nu}^1(0), Q(t)] = i \lambda_{\nu}^1 u_r(t, \omega_{\nu}^1). \quad (76)$$

A general expectation value of a product of four operators can be ascribed to a sum of products of expectation values of one or two operators for Gaussian states. The assumption of a Gaussian bath state is justified in the thermodynamic and long-time limit on general grounds [53, 54]. In [38] it is shown that the state of the central oscillator becomes Gaussian for $t \rightarrow \infty$, independent of its initial preparation, if the classical solution $u(t)$ vanishes asymptotically—the situation of interest here.

For an explicit result, we insert the solution $Q(t)$ from equation (12), perform the thermodynamic limit, use the results for the position correlation functions from section 3 and

carry out the remaining time integrals in the long-time limit. The result for the second order cumulant then reads

$$\lim_{t \rightarrow \infty} \frac{\langle\langle W^2(t) \rangle\rangle}{t} = \frac{\pi^3}{2} \int_0^\infty d\omega \gamma_l^2(\omega) \gamma_r^2(\omega) |u(\omega)|^4 [\mathcal{E}_l(\omega) - \mathcal{E}_r(\omega)]^2 + \frac{\pi}{2} \int_0^\infty d\omega \gamma_l(\omega) \gamma_r(\omega) |u(\omega)|^2 \left[2\mathcal{E}_l(\omega) \mathcal{E}_r(\omega) - \frac{\omega^2}{2} \right]. \quad (77)$$

This expression generalizes the result for the second moment given in equation (9) in [50, 51]. Equation (77) reduces to this equation for the special case of thermal baths with $\mathcal{E}_\alpha(\omega) = \mathcal{E}_{\text{th}}(\omega, T_\alpha) = \omega f_\alpha(\omega) + \omega/2$ which then lead to the expressions $f_\alpha(\pm\omega) = 1/[\exp(\pm\omega/T_\alpha) - 1]$ in [50, 51].

6.3. The generating function for the energy transfer

We have seen that the well-known results [50, 52] for the first and second moment of the heat transfer operator for the special case of thermal baths are well reproduced by our more general results. The generalization follows by the corresponding replacements of the thermal distribution functions of the baths by the general initial distributions. Hence we can now follow the same line of reasoning and generalize the steady state expression of the cumulant generating function for the heat transfer given in equation (8) in [50, 51] with the result

$$G(\xi) \equiv \lim_{t \rightarrow \infty} \frac{\ln Z(\xi, t)}{t} = -\frac{1}{2\pi} \int_0^\infty d\omega \ln \left\{ 1 + \pi^2 \gamma_l(\omega) \gamma_r(\omega) \frac{|u(\omega)|^2}{\omega^2} \times \left[\left(2\mathcal{E}_l(\omega) \mathcal{E}_r(\omega) - \frac{\omega^2}{2} \right) (1 - \cos \xi \omega) - i\omega (\mathcal{E}_l(\omega) - \mathcal{E}_r(\omega)) \sin \xi \omega \right] \right\}. \quad (78)$$

We observe that $G(\xi)$ fulfils the symmetry relation

$$G(\xi) = G(-\xi + iA), \quad (79)$$

where $A = \beta_r - \beta_l$ with

$$\beta_\alpha = \frac{2}{\omega} \operatorname{arcoth} \left(\frac{2\mathcal{E}_\alpha(\omega)}{\omega} \right). \quad (80)$$

Since the constants β_α should be independent of ω the existence of the symmetry (79) implies a condition on the initial bath preparation. In particular, the energy distribution functions should be thermal, i.e. $\mathcal{E}_\alpha(\omega) = \mathcal{E}_{\text{th}}(\omega, T_\alpha)$. Note that this is a condition on the combination $\mathcal{E}_\alpha(\omega)$ of the initial bath variances $\sigma_{\alpha, QQ}^{(1)}(\omega)$ and $\sigma_{\alpha, PP}^{(1)}(\omega)$, not on the individual functions (see equation (38)). It can be fulfilled for nonthermal bath preparations as well [38].

From the relation (79) it follows that the probability distribution of the transferred energy,

$$P(W) = \int_{-\infty}^\infty \frac{d\xi}{2\pi} \lim_{t \rightarrow \infty} Z(\xi, t) e^{-i\xi W}, \quad (81)$$

fulfils the steady state fluctuation theorem

$$P(W) = e^{AW} P(-W). \quad (82)$$

We remark that the exchange fluctuation relation (82) can only be proven rigorously when the initial preparation is indeed free of correlations and also the interaction of the system and the bath is switched off at some final time [1, 55, 56]. The role of initial system–bath correlations for the nonequilibrium fluctuation relations is still an open problem. According to that the result in equation (78) and the corresponding symmetry relation (79) are formulated and valid in the long-time limit only. For transient times $t < \infty$, we expect additional contributions to the steady state fluctuation theorem in equation (82) [1, 55, 56].

7. Summary

Most studies related to fluctuation relations so far consider the special case when the systems are initially in thermal equilibrium, but do not restrict their analyses to a specific model. In the present study, we give up the assumption of initial thermal states and allow for nonthermal bath preparations. The price we have to pay for this generalization is the restriction to an analytically solvable model for which we obtain exact generalized nonequilibrium fluctuation relations. On the one hand, we can give the explicit expressions for the symmetric and antisymmetric autocorrelation functions of the central oscillator position. Then, a generalized nonequilibrium fluctuation relation follows which only involves the bath spectral functions and the frequency-resolved energy distribution of the initial bath states. The general expression also contains the special case of a single thermal bath and coincides with the well-known equilibrium FDT. Moreover, we discuss the conditions under which the generating function of the oscillator position fulfils a Gallavotti–Cohen relation at arbitrary times. This relation reflects the fact that the oscillator position fluctuates symmetrically around its momentary average position. On the other hand, we have elucidated the quantum mechanical energy transfer through the central oscillator by calculating the time-dependent energy current and the second moment of the current fluctuations. Based on this result we generalize the cumulant generating function for energy transfer, which is well-known for thermal baths, to the nonthermal situation.

Acknowledgments

We acknowledge support by the DFG through SFB 652 (project B5), SFB 925 (project C8) and SFB 668 (project B16).

Appendix. Correlation functions of the fluctuating forces

We here give the correlation functions of the fluctuating operator-valued forces in the quantum Langevin equation (6). By this, we illustrate some subtleties of the nonthermal initial bath preparations with respect to stationarity and ergodicity.

The statistics of the operator-valued noise forces $\eta_\alpha(t)$ is determined through their respective moments and explicitly depends on the initial preparation of the baths. For the common thermal bath preparation the linear expectation values

$$\langle \eta_\alpha(t) \rangle = \sum_{\nu=1}^{N_\alpha} \lambda_\nu^\alpha \left(\langle Q_\nu^\alpha(0) \rangle \cos \omega_\nu^\alpha t + \langle P_\nu^\alpha(0) \rangle \frac{\sin \omega_\nu^\alpha t}{\omega_\nu^\alpha} \right) \quad (\text{A.1})$$

vanish because $\langle Q_v^\alpha(0) \rangle = \langle P_v^\alpha(0) \rangle = 0$ for thermal bath states $\rho_B^\alpha(0) \propto e^{-\beta_\alpha H_B^\alpha}$, i.e. the random noise forces are not biased. In the considered case with nonthermal bath preparations the expectation values $\langle \eta_\alpha(t) \rangle$, in general, are finite. This leads to a finite shift of the central oscillator. In the thermodynamic limit, where

$$\langle \eta_\alpha(t) \rangle = \int_0^\infty d\omega D_\alpha(\omega) \lambda_\alpha(\omega) \left(X_{\alpha,Q}(\omega) \cos \omega t + X_{\alpha,P}(\omega) \frac{\sin \omega t}{\omega} \right), \quad (\text{A.2})$$

we can use the Riemann–Lebesgue lemma (30) to find $\lim_{t \rightarrow \infty} \langle \eta_\alpha(t) \rangle = 0$. In conclusion, for transient times $t < \infty$ the generalization of the initial preparation from thermal to general nonthermal states introduces a shift of the central oscillator which vanishes in the long-time limit.

The correlations of the noise forces are given by

$$\begin{aligned} S_{\eta_\alpha \eta_\beta}(t, s) &= \frac{1}{2} \langle \eta_\alpha(t) \eta_\beta(s) + \eta_\beta(s) \eta_\alpha(t) \rangle - \langle \eta_\alpha(t) \rangle \langle \eta_\beta(s) \rangle \\ &= \sum_{\nu, \mu=1}^{N_\alpha} \lambda_\nu^\alpha \lambda_\mu^\alpha \left(\cos(\omega_\nu^\alpha t) \cos(\omega_\mu^\alpha s) \sigma_{Q_\nu^\alpha Q_\mu^\alpha} + [\cos(\omega_\nu^\alpha t) \sin(\omega_\mu^\alpha s) \right. \\ &\quad \left. + \cos(\omega_\nu^\alpha s) \sin(\omega_\mu^\alpha t)] \frac{\sigma_{Q_\nu^\alpha P_\mu^\alpha}}{\omega_\mu^\alpha} + \sin(\omega_\nu^\alpha t) \sin(\omega_\mu^\alpha s) \frac{\sigma_{P_\nu^\alpha P_\mu^\alpha}}{\omega_\nu^\alpha \omega_\mu^\alpha} \right) \delta_{\alpha, \beta}. \end{aligned} \quad (\text{A.3})$$

Of course, $S_{\eta_\alpha \eta_\beta}(t, s) = 0$ for $\alpha \neq \beta$ due to our assumption of factorizing states. Starting again with the thermal bath preparation, where $(\omega_\nu^\alpha)^2 \sigma_{Q_\nu^\alpha Q_\mu^\alpha} = \sigma_{P_\nu^\alpha P_\mu^\alpha} = \mathcal{E}_{\text{th}}(\omega_\nu^\alpha, T_\alpha) \delta_{\nu, \mu}$ and $\sigma_{Q_\nu^\alpha P_\mu^\alpha} = 0$ we obtain

$$S_{\eta_\alpha \eta_\beta}^{\text{th}}(t, s) = S_{\eta_\alpha \eta_\beta}^{\text{th}}(t - s, 0) = \sum_\nu^{N_\alpha} \left(\frac{\lambda_\nu^\alpha}{\omega_\nu^\alpha} \right)^2 \cos \omega_\nu^\alpha(t - s) \mathcal{E}_{\text{th}}(\omega_\nu^\alpha, T_\alpha) \delta_{\alpha, \beta}. \quad (\text{A.4})$$

This expression depends on $t - s$ only, i.e. it is time-homogeneous. In the thermal case, the fluctuating forces constitute a stationary Gaussian process. For a nonthermal bath preparation, the correlation functions $S_{\eta_\alpha \eta_\beta}(t, s)$, in general, are not time-homogeneous. Performing the thermodynamic limit, the correlation function in equation (A.3) assumes the form

$$\begin{aligned} S_{\eta_\alpha \eta_\beta}(t, s) &= \int_0^\infty d\omega \frac{\gamma_\alpha(\omega)}{\omega} \left[\omega^2 \cos(\omega t) \cos(\omega s) \sigma_{\alpha, QQ}^{(1)}(\omega) + \omega \sin \omega(t + s) \sigma_{\alpha, QP}^{(1)}(\omega) \right. \\ &\quad \left. + \sin(\omega t) \sin(\omega s) \sigma_{\alpha, PP}^{(1)}(\omega) \right] \delta_{\alpha, \beta} + \int_0^\infty d\omega_1 \int_0^\infty d\omega_2 D_\alpha(\omega_1) D_\alpha(\omega_2) \lambda_\alpha(\omega_1) \lambda_\alpha(\omega_2) \\ &\quad \times \left(\cos(\omega_1 t) \cos(\omega_2 s) \sigma_{\alpha, QQ}^{(2)}(\omega_1, \omega_2) + [\cos(\omega_1 t) \sin(\omega_2 s) \right. \\ &\quad \left. + \cos(\omega_1 s) \sin(\omega_2 t)] \frac{\sigma_{\alpha, QP}^{(2)}(\omega_1, \omega_2)}{\omega_2} + \sin(\omega_1 t) \sin(\omega_2 s) \frac{\sigma_{\alpha, PP}^{(2)}(\omega_1, \omega_2)}{\omega_1 \omega_2} \right) \delta_{\alpha, \beta}. \end{aligned} \quad (\text{A.5})$$

In the limit $t \rightarrow \infty$ and/or $s \rightarrow \infty$, the nondiagonal parts with double frequency integrals as well as the term involving $\sigma_{\alpha, QP}^{(1)}(\omega)$ vanish. The remaining terms

$$\int_0^\infty d\omega \frac{\gamma_\alpha(\omega)}{\omega} \left[\omega^2 \cos(\omega t) \cos(\omega s) \sigma_{\alpha, QQ}^{(1)}(\omega) + \sin(\omega t) \sin(\omega s) \sigma_{\alpha, PP}^{(1)}(\omega) \right] \delta_{\alpha, \beta} \quad (\text{A.6})$$

disappear as well if only one of the two variables t or s independently approaches infinity. A finite contribution to $S_{\eta_\alpha \eta_\beta}(t, s)$ is obtained when t and s simultaneously approach infinity, such that

$$\lim_{t \rightarrow \infty} S_{\eta_\alpha \eta_\beta}(t, t+s) = \int_0^\infty d\omega \frac{\gamma_\alpha(\omega)}{\omega} \mathcal{E}_\alpha(\omega) \cos(\omega s) \delta_{\alpha, \beta}. \quad (\text{A.7})$$

We note that this result is identical to the thermal result in equation (A.4), provided that $\mathcal{E}_\alpha(\omega)$ is replaced by the corresponding expression for the thermal state of a single bath.

In contrast to $\eta_\alpha(t)$, the statistical properties of the fluctuating forces $\xi_\alpha(t)$ including the initial slip term explicitly depend on the initial preparation of the total system including the central oscillator. For the random forces $\xi_\alpha(t)$ to be not biased and to have time-homogeneous correlations, the total system should be prepared in the state $\rho(0) \propto \rho_S(0) \prod_{\alpha=1}^{N_B} e^{-\beta_\alpha (H_B^\alpha + H_{SB}^\alpha)}$, where the bath contains shifted oscillators, see [41] for a detailed discussion. In the nonthermal situation, we have

$$\langle \xi_\alpha(t) \rangle = \langle \eta_\alpha(t) \rangle + \langle Q(0) \rangle \sum_{\nu=1}^{N_\alpha} \left(\frac{\lambda_\nu^\alpha}{\omega_\nu^\alpha} \right)^2 \cos \omega_\nu^\alpha t \quad (\text{A.8})$$

and

$$S_{\xi_\alpha, \xi_\beta}(t, s) = S_{\eta_\alpha, \eta_\beta}(t, s) + \Sigma_{QQ}(0) \sum_{\nu=1}^{N_\alpha} \sum_{\mu=1}^{N_\beta} \left(\frac{\lambda_\nu^\alpha \lambda_\mu^\beta}{\omega_\nu^\alpha \omega_\mu^\beta} \right)^2 \cos(\omega_\nu^\alpha t) \cos(\omega_\mu^\beta s). \quad (\text{A.9})$$

Performing the thermodynamic limit one notes that the additional contributions from the initial slip term vanish in the long-time limit $t \rightarrow \infty$ and/or $s \rightarrow \infty$. We remark that the stationarity of the correlation functions in the long-time limit is a consequence of the thermodynamic limit and does not rely on ergodicity.

References

- [1] Campisi M, Hänggi P and Talkner P 2011 *Rev. Mod. Phys.* **83** 771
- [2] Jarzynski C 2011 *Annu. Rev. Condens. Matter Phys.* **2** 329
- [3] Esposito M, Harbola U and Mukamel S 2009 *Rev. Mod. Phys.* **81** 1665
- [4] Jarzynski C 2008 *Eur. Phys. J. B* **64** 331
- [5] Marconi U M B, Puglisi A, Rondoni L and Vulpiani A 2008 *Phys. Rep.* **461** 111
- [6] Seifert U 2008 *Eur. Phys. J. B* **64** 423
- [7] Rondoni L and Mejía-Monasterio C 2007 *Nonlinearity* **20** R1
- [8] Sutherland W 1902 *Phil. Mag.* **3** 161
- [9] Sutherland W 1905 *Phil. Mag.* **9** 781
- [10] Einstein A 1905 *Ann. Phys.* **17** 549
- [11] Einstein A 1906 *Ann. Phys.* **19** 289
- [12] Einstein A 1906 *Ann. Phys.* **19** 371
- [13] Johnson J B 1928 *Phys. Rev.* **32** 97

- [14] Nyquist H 1928 *Phys. Rev.* **32** 110
- [15] Callen H B and Welton T A 1951 *Phys. Rev.* **83** 34
- [16] Green M S 1952 *J. Chem. Phys.* **20** 1281
- [17] Green M S 1954 *J. Chem. Phys.* **22** 398
- [18] Kubo R 1957 *J. Phys. Soc. Japan* **12** 570
- [19] Hänggi P and Thomas H 1975 *Z. Phys. B* **22** 295
- [20] Hänggi P 1978 *Helv. Phys. Acta* **51** 202
- [21] Hänggi P and Thomas H 1982 *Phys. Rep.* **88** 207
- [22] Bochkov G N and Kuzovlev Y E 1977 *Zh. Eksp. Teor. Fiz.* **72** 238
Bochkov G N and Kuzovlev Y E 1977 *Sov. Phys.—JETP* **45** 125 (Engl. transl.)
- [23] Andrieux D and Gaspard P 2008 *Phys. Rev. Lett.* **100** 230404
- [24] Talkner P and Hänggi P 2007 *J. Phys. A: Math. Theor.* **40** F569
- [25] Evans D J, Cohen E G D and Morriss G P 1993 *Phys. Rev. Lett.* **71** 2401
- [26] Gallavotti G and Cohen E G D 1995 *Phys. Rev. Lett.* **74** 2694
- [27] Jarzynski C 1997 *Phys. Rev. Lett.* **78** 2690
- [28] Crooks G E 1999 *Phys. Rev. E* **60** 2721
- [29] Ullersma P 1966 *Physica* **32** 27
Ullersma P 1966 *Physica* **32** 56
Ullersma P 1966 *Physica* **32** 74
Ullersma P 1966 *Physica* **32** 90
- [30] Haake F and Reibold R 1985 *Phys. Rev. A* **32** 2462
- [31] Ford G W, Lewis J T and O'Connell R F 1985 *Phys. Rev. Lett.* **55** 2273
- [32] Ford G W, Lewis J T and O'Connell R F 1988 *Ann. Phys., NY* **185** 270
- [33] Grabert H, Schramm P and Ingold G-L 1988 *Phys. Rep.* **168** 115
- [34] Zerbe C and Hänggi P 1995 *Phys. Rev. E* **52** 1533
- [35] Thorwart M, Reimann P and Hänggi P 2000 *Phys. Rev. E* **62** 5808
- [36] Grabert H 2006 *Chem. Phys.* **322** 160
- [37] Ford G W and O'Connell R F 2007 *Phys. Rev. B* **75** 134301
- [38] Pagel D, Alvermann A and Fehske H 2013 *Phys. Rev. E* **87** 012127
- [39] Weiss U 2008 *Quantum Dissipative Systems* 3rd edn (Singapore: World Scientific)
- [40] Hänggi P 1997 *Stochastic Dynamics (Lecture Notes in Physics vol 484)* ed L Schimansky-Geier and T Pöschel (Berlin: Springer) pp 15–22
- [41] Hänggi P and Ingold G L 2005 *Chaos* **15** 026105
- [42] Caldeira A O and Leggett A J 1983 *Ann. Phys., NY* **149** 374
- [43] Papoulis A 1991 *Probability, Random Variables and Stochastic Processes* 3rd edn (New York: McGraw-Hill)
- [44] Lutz E 2004 *Phys. Rev. Lett.* **93** 190602
- [45] Bao J D, Hänggi P and Zhuo Y Z 2005 *Phys. Rev. E* **72** 061107
- [46] Bao J D, Zhuo Y Z, Oliveira F A and Hänggi P 2006 *Phys. Rev. E* **74** 061111
- [47] Zürcher U and Talkner P 1990 *Phys. Rev. A* **42** 3278
- [48] Segal D, Nitzan A and Hänggi P 2003 *J. Chem. Phys.* **119** 6840
- [49] Dhar A and Roy D 2006 *J. Stat. Phys.* **125** 805
- [50] Saito K and Dhar A 2007 *Phys. Rev. Lett.* **99** 180601
- [51] Saito K and Dhar A 2008 *Phys. Rev. Lett.* **101** 049902 (erratum)
- [52] Agarwalla B K, Li B and Wang J-S 2012 *Phys. Rev. E* **85** 051142
- [53] Cramer M, Dawson C M, Eisert J and Osborne T J 2008 *Phys. Rev. Lett.* **100** 030602
- [54] Cramer M and Eisert J 2010 *New J. Phys.* **12** 055020
- [55] Campisi M, Talkner P and Hänggi P 2010 *Phys. Rev. Lett.* **105** 140601
- [56] Campisi M, Talkner P and Hänggi P 2011 *Phys. Rev. E* **83** 041114

Nonclassical light from few emitters in a cavity

D. Pagel, A. Alvermann, and H. Fehske

Institut für Physik, Ernst-Moritz-Arndt-Universität, 17487 Greifswald, Germany

(Received 16 February 2015; published 9 April 2015)

We study the characteristics of the light generated by a few emitters in a cavity at strong light-matter coupling. By means of the Glauber $g^{(2)}$ function we can identify clearly distinguished parameter regimes with super-Poissonian and sub-Poissonian photon statistics. We establish a relation between the emission characteristics for one and multiple emitters and explain its origin in terms of the photon-dressed emitter states. Cooperative effects lead to the generation of nonclassical light already at reduced light-matter coupling if the number of emitters is increased. Our results are obtained with a full input-output formalism and master equation valid also at strong light-matter coupling. We compare the behavior obtained with and without counterrotating light-matter-interaction terms in the Hamiltonian and find that the generation of nonclassical light is robust against such modifications. Finally, we contrast our findings with the predictions of the quantum optical master equation and find that it fails entirely at predicting regimes with different photon statistics.

DOI: [10.1103/PhysRevA.91.043814](https://doi.org/10.1103/PhysRevA.91.043814)

PACS number(s): 42.50.Ar, 42.50.Pq, 03.65.Yz

I. INTRODUCTION

Two-level emitters interacting with a cavity photon mode are widely studied in quantum optics with respect to spontaneous emission and superradiance [1–4], cooperativity and lasing [5–7], and the emission of nonclassical light [8–10]. For sufficiently weak light-matter coupling, when the photon dressing of emitter states is negligibly small, the emitter-cavity system can be studied with the quantum optical master equation, usually in combination with the rotating-wave approximation [11]. The quantum optical master equation fails at strong light-matter coupling to the extent that it predicts unphysical emission at zero temperature if the number of photons in the ground state is finite [12–14].

The correct theoretical description of systems with (ultra)strong light-matter coupling [15–18] has attracted increasing interest recently [19–24]. Essentially, the quantum optical master equation has to be replaced by a master equation expressed in the photon-dressed emitter eigenstates [24–29]. While the master equation remains Markovian, which is justified because of the weak emitter-environment and cavity-environment couplings [11,25], it now requires full diagonalization of the interacting emitter-cavity Hamiltonian. Such an equation was used in recent studies of photon blockade effects [19], spontaneous conversion of virtual to real photons [20,21], and the emission of nonclassical light from a single emitter [22].

In this paper we study the emission of a few emitters in a cavity, with particular focus on the photon statistics of the emitted light. Our goal is the characterization of temperature and coupling regimes where nonclassical light [30,31] is generated. A major result will be the identification of two clearly distinguished neighboring regimes with pronounced sub-Poissonian and super-Poissonian photon statistics at strong coupling.

Our results are obtained with the full input-output formalism [32–35] and master equation [24–29] without further approximations. To understand the relevance of the different approximations involved in traditional quantum optics treatments we make two comparisons. First, we compare the results that are obtained when the counterrotating light-matter

interaction terms are included in the Hamiltonian to those when they are dropped. Second, we contrast the results obtained with the full master equation with results from the quantum optical master equation. The latter comparison will clearly show the necessity of using the correct master equation already at weak coupling if the photon statistics is of interest. This issue has been studied conclusively for a single emitter in Ref. [22], which also contains Glauber function plots for few emitters in the supplemental material but omits the further analysis of the situation that we give here.

This paper is organized as follows. In Sec. II we introduce the physical situation under study together with the master equation used for its analysis. In Sec. III we discuss the emission spectra in relation to the energy spectra of the emitter-cavity Hamiltonian, while the statistics of the emitted photons is studied in Sec. IV. We conclude in Sec. V. The appendixes collect further information on the theoretical approach. Appendix A gives details of the input-output formalism. In Appendix B we derive the master equation, and we give a few analytical results for the photon statistics in Appendix C.

II. THE PHYSICAL SITUATION

The interaction of N two-level emitters with a single cavity photon mode is described by the Dicke model [36],

$$H = \omega_c a^\dagger a + \omega_x \sum_{j=1}^N \sigma_+^{(j)} \sigma_-^{(j)} + g \sum_{j=1}^N (a^\dagger \sigma_-^{(j)} + a \sigma_+^{(j)}) + g' \sum_{j=1}^N (a \sigma_-^{(j)} + a^\dagger \sigma_+^{(j)}), \quad (1)$$

where the operator $a^{(\dagger)}$ annihilates (creates) a cavity photon with frequency ω_c and $\sigma_-^{(j)}$ ($\sigma_+^{(j)}$) is the corresponding lowering (raising) operator for the j th emitter with transition energy ω_x . Throughout this work, we consider the resonant case $\omega_0 = \omega_c = \omega_x$. We allow for different emitter-photon coupling strengths for the corotating (g) and counterrotating (g') interaction terms. Changing g' relative to g interpolates

between the Tavis-Cummings (TC) limit ($g' = 0$) without and the Dicke limit ($g' = g$) with counterrotating terms. Both situations can be realized experimentally [37,38]. The rotating-wave approximation consists in replacing the Dicke by the TC limit.

Dissipation arises from the coupling of the emitters and the cavity to the environment. For a bosonic environment the coupling terms are of the form

$$H_I = -iS \sum_v \lambda_v (b_v - b_v^\dagger), \quad (2)$$

where S is a (Hermitian) emitter or cavity operator and $b_v^{(\dagger)}$ are bosonic operators for the environment photons (at frequencies ω_v with coupling constants λ_v). As the operator S we choose the field operator $X = -iX_0(a - a^\dagger)$ for the coupling of the cavity and the transition operator $\sigma_y^{(j)} = i(\sigma_+^{(j)} - \sigma_-^{(j)})$ for the coupling of the j th emitter to the environment.

At sufficiently weak coupling to the environment, the emitter-cavity system density matrix ρ obeys a Markovian master equation [24–29],

$$\begin{aligned} \frac{d}{dt}\rho(t) = & -i[H, \rho(t)] - i\frac{1}{2} \sum_\omega \xi(\omega)[S_\omega^\dagger S_\omega, \rho(t)] \\ & + \frac{1}{2} \sum_\omega \chi(\omega)\{[S_\omega \rho(t), S_\omega^\dagger] + [S_\omega, \rho(t)S_\omega^\dagger]\}, \end{aligned} \quad (3)$$

where

$$S_\omega = \sum_{m,n} |m\rangle \langle m|S|n\rangle \langle n| \delta_{E_n - E_m, \omega} \quad (4)$$

is the projection of S onto transitions between eigenstates $|m\rangle$, $|n\rangle$ of H with energy difference $\omega_{nm} = E_n - E_m$ (see Appendix B for a derivation). For the sake of notational simplicity we state the master equation for a single coupling term (2). Multiple coupling terms lead to additional contributions of the same form.

The functions $\chi(\omega)$ and $\xi(\omega)$ in Eq. (3) follow from the environment spectral function

$$\gamma(\omega) = 2\pi \sum_v \lambda_v^2 \delta(\omega - \omega_v) \quad (5)$$

and its analytical continuation $\Gamma(\omega)$ into the upper half plane, with $\gamma(\omega) = \mp \text{Im} \Gamma(\pm\omega + i0^+)$. For a thermal environment with inverse temperature $\beta = 1/T$ we get

$$\chi(\omega) = \begin{cases} \gamma(\omega)[n(\omega, T) + 1] & \text{if } \omega > 0, \\ \gamma(-\omega)n(-\omega, T) & \text{if } \omega < 0, \end{cases} \quad (6)$$

and

$$\xi(\omega) = \begin{cases} \text{Re} \Gamma(\omega + i0^+)[n(\omega, T) + 1] & \text{if } \omega > 0, \\ -\text{Re} \Gamma(-\omega + i0^+)n(-\omega, T) & \text{if } \omega < 0, \end{cases} \quad (7)$$

with the Bose-Einstein distribution function

$$n(\omega, T) = \frac{1}{e^{\beta\omega} - 1}. \quad (8)$$

Note that in the zero-temperature limit $n(\omega, T) \rightarrow 0$ such that the master equation (3) contains only dissipative terms for transitions $|n\rangle \rightarrow |m\rangle$ with positive energy $\omega_{nm} > 0$; that is, dissipation correctly leads to energy decrease. In particular, the

problem of unphysical emission from the ground state encountered for the quantum optical master equations is resolved.

In the present work we assume an Ohmic spectral function $\gamma_c(\omega) = \gamma\omega/\omega_0$ for the cavity-environment coupling and use $\gamma = 10^{-2}\omega_0$ in all numerical computations. To reduce the number of free parameters we assume the same spectral function $\gamma_x^{(j)}(\omega) = \gamma_c(\omega)$ for the emitter-environment couplings. The respective environment temperatures are also identical.

A. Solution of the master equation

As we show in Appendix B, the master equation (3) splits into two equations of motion,

$$\begin{aligned} \frac{d}{dt}\rho_{m,n}(t) = & \sum_{k \neq n} \chi(\omega_{kn}) S_{n,k} \rho_{k,k}(t) \\ & - \sum_{k \neq n} \chi(\omega_{nk}) S_{k,n} \rho_{m,n}(t), \end{aligned} \quad (9)$$

$$\frac{d}{dt}\rho_{m,n}(t) = -(Z_m + Z_n^*)\rho_{m,n}(t) \quad (m \neq n), \quad (10)$$

for the matrix elements $\rho_{m,n}(t) = \langle m|\rho(t)|n\rangle$ of the density operator. In these equations, $S_{n,k} = |n|S|k\rangle|^2$ and

$$Z_n = \frac{1}{2} \sum_{k \neq n} [\chi(\omega_{nk}) + i\xi(\omega_{nk})] S_{k,n} + iE_n. \quad (11)$$

The general solution of Eq. (10) is

$$\rho_{m,n}(t) = e^{-(Z_m + Z_n^*)t} \rho_{m,n}(0) \quad (m \neq n). \quad (12)$$

Because $\text{Re} Z_n > 0$ for all n , the off-diagonal elements of $\rho(t)$ decay exponentially. Hence, the stationary state fulfills

$$\rho_{m,n}^\infty \equiv \lim_{t \rightarrow \infty} \rho_{m,n}(t) = \rho_{n,n}^\infty \delta_{m,n}. \quad (13)$$

The diagonal elements $\rho_{n,n}^\infty$ are determined by the stationary solution of the Pauli master equation (9). If the system is coupled to a thermal environment as in Eqs. (6) and (7), the stationary solution of Eq. (9) is the thermal state $\rho^\infty \propto e^{-\beta H}$ of the system corresponding to the temperature $T = 1/\beta$ of the environment.

The emission spectrum and photon statistics can now be computed through a standard input-output formalism (see Appendix A), which leads to the projected cavity-environment coupling operator

$$\dot{X}_- = -i \sum_{m,n>m} (E_n - E_m) |m\rangle \langle m|X|n\rangle \langle n| \quad (14)$$

describing the emission. The correlation functions of \dot{X}_- and $\dot{X}_+ = (\dot{X}_-)^\dagger$ characterize the properties of the emitted light. The emission spectrum of the cavity is

$$S(\omega) = \lim_{t \rightarrow \infty} \frac{\gamma_c(\omega)}{\pi} \text{Re} \int_0^\infty e^{-i\omega\tau} \langle \dot{X}_+(t+\tau) \dot{X}_-(t) \rangle d\tau, \quad (15)$$

and the second-order Glauber function [39] reads

$$g^{(2)}(\tau) = \lim_{t \rightarrow \infty} \frac{\langle \dot{X}_+(t) \dot{X}_+(t+\tau) \dot{X}_-(t+\tau) \dot{X}_-(t) \rangle}{\langle \dot{X}_+(t) \dot{X}_-(t) \rangle^2}. \quad (16)$$

Note that evaluation of Eqs. (15) and (16) requires diagonalization of the Hamiltonian H .

Because the stationary state ρ^∞ from Eq. (13) is diagonal in the eigenbasis $|n\rangle$ of H , we can evaluate the τ integration in Eq. (15) analytically as

$$S(\omega) = \frac{\gamma_c(\omega)}{\pi} \sum_{m < n} |\langle m | \dot{X}_- | n \rangle|^2 \rho_{n,n}^\infty \times \frac{\text{Re}(Z_m + Z_n)}{[\omega - \text{Im}(Z_n - Z_m)]^2 + [\text{Re}(Z_m + Z_n)]^2}. \quad (17)$$

The emission spectrum $S(\omega)$ is the sum of Lorentz peaks with width $\text{Re}(Z_n + Z_m)$ at the respective transition energies $\text{Im}(Z_n - Z_m)$, which, according to Eq. (11), are shifted relative to the transition energies $E_n - E_m$ of the closed system by a Lamb shift that results from coupling to the environment.

B. Quantum optical master equation

It is instructive to compare the master equation (3) to the quantum optical master equation [11]

$$\frac{d}{dt} \rho(t) = -i[H, \rho(t)] - i \sum_{\pm} \frac{\xi_{\pm}}{2} [S_{\pm}^{\dagger} S_{\pm}, \rho(t)] + \sum_{\pm} \frac{\chi_{\pm}}{2} \{[S_{\pm} \rho(t), S_{\pm}^{\dagger}] + [S_{\pm}, \rho(t) S_{\pm}^{\dagger}]\}, \quad (18)$$

which is obtained by replacing the projected operators S_{ω} with the ‘‘bare’’ operators $S_{\pm} = \sum_{\omega \geq 0} S_{\omega}$ and by assuming $\chi(\pm\omega) \approx \chi_{\pm}$, $\xi(\pm\omega) \approx \xi_{\pm}$ in the vicinity of a typical transition energy ω . Note that $S_+ = -iX_0 a$ for the cavity-environment coupling and $S_+ = -i\sigma_-^{(j)}$ for the emitter-environment coupling. Evidently, this approximation can be valid only for weak light-matter coupling $g, g' \ll \omega_c, \omega_x$, when the dressing of emitter states by cavity photons can be neglected. Because the quantum optical master equation does not distinguish between energy-increasing and energy-decreasing transitions, which are equally contained in the unprojected operator S because of Hermiticity, it can lead to unphysical predictions such as emission out of the ground state. Furthermore, because failure to observe the above distinction is tantamount to a high-temperature approximation, one will expect that the quantum optical master equation fails at the prediction of nonthermal photon statistics at low temperatures. Therefore, we use the more general master equation (3).

III. THE EMITTED LIGHT

The first characterization of the light generated in the cavity is provided by the emission spectrum. Because the emission spectrum depends on the (Lamb-shifted) energy spectrum of the Dicke Hamiltonian, we start with a discussion of the eigenvalues of H for a few emitters before we turn to the actual function $S(\omega)$ obtained from numerical solution of the master equation (3).

A. Energy spectrum of the Hamiltonian

To construct the energy spectrum of H we notice first that the eigenstates of N uncoupled two-level emitters can be classified as angular momentum eigenstates with total angular momentum $J = N/2, N/2 - 1, \dots \geq 0$. Since H commutes with the total angular momentum operator, states

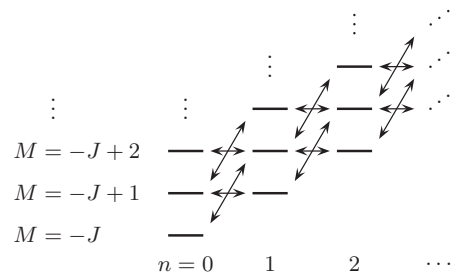


FIG. 1. Schematic energy-level pattern for the construction of the spectrum of the Dicke model. Horizontal arrows depict the corotating interaction terms in Eq. (1) (coupling constant g); diagonal arrows depict the counterrotating terms (g').

with different J do not mix even at finite coupling $g, g' \neq 0$. For fixed J , the J_z quantum number M can assume the values $M = -J, -J + 1, \dots, J$, and a corresponding emitter eigenstate has energy $(M + N/2)\omega_x$. Note that for $N \geq 3$ the classification in terms of J, M is not exhaustive since different emitter states can have identical values. However, these states give the same contribution to the emission spectrum. The cavity photon eigenstates are Fock states $|n\rangle$ with energies $n\omega_c$.

For given J we can arrange the eigenstates of the uncoupled emitter-cavity system as the rungs of a ladder diagram as in Fig. 1. Working at resonance $\omega_c = \omega_x = \omega_0$, the energy $(M + N/2 + n)\omega_0$ of each state is given by the total number of emitter and cavity excitations. The corotating light-matter interaction terms in H preserve the number of excitations and connect states at the same energy level (horizontal arrows in Fig. 1). The counterrotating terms change the number of excitations by two (diagonal arrows in Fig. 1). This simple scheme explains many properties of the energy spectra of H shown in Fig. 2.

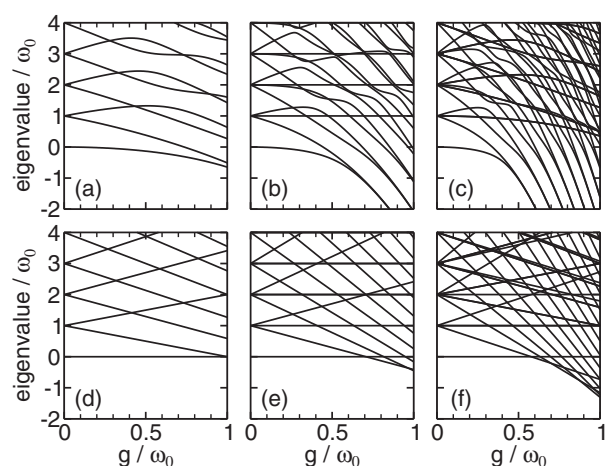


FIG. 2. Eigenvalues of H in Eq. (1) for (a)–(c) $g' = g$ and (d)–(f) $g' = 0$ as functions of the coupling strength g . (a) and (b) show the results for one emitter, whereas the number of emitters is $N = 2$ in (b) and (e) and $N = 3$ in (c) and (f).

For $N = 1$ it is $J = 1/2$, and we recover the Jaynes-Cummings ladder [40] for $g' = 0$. The lowest level ($M = -1/2, n = 0$) does not couple to any other state and hence leads to the g -independent eigenvalue zero of H [see Fig. 2(d)]. Every other level consists of two ladder rungs. They lead to the eigenvalues $n\omega_0 \pm \sqrt{n}g$ for $n \geq 1$. For $g' = g$ corrections arise from coupling between states at different heights in the ladder, but the energy-level pattern remains discernible [Fig. 2(a)].

For $N = 2$ [see Figs. 2(b) and 2(e)] we have either triplet ($J = 1$) or singlet ($J = 0$) emitter states. For $g' = 0$, the triplet states lead to the eigenvalue zero ($n = 0$), the two eigenvalues $\omega_0 \pm \sqrt{2}g$ ($n = 1$), and the three eigenvalues $n\omega_0, n\omega_0 \pm \sqrt{2}\sqrt{2n-1}g$ for $n \geq 2$. The singlet states do not couple with each other and lead to the g -independent eigenvalues $(n+1)\omega_0$ for $n \geq 0$. It follows that the eigenvalues $n\omega_0$ for $n \geq 2$ are twofold degenerate (one triplet, one singlet state). This degeneracy is lifted for $g' = g$, but the energies of the singlet states remain fixed.

For $N = 3$ we have quadruplet ($J = 3/2$) and doublet ($J = 1/2$) emitter states. The ladder scheme for the doublet is equal to that for $N = 1$ and hence leads to the same energy spectrum, apart from the fact that all energies are shifted up by ω_0 when going from $N = 1$ to $N = 3$. Notice that the doublet states are twofold degenerate because the angular momentum classification of the emitter states is not unique in this case. The quadruplet states lead to one (starting at zero for $g = 0$), two (at ω_0), three (at $2\omega_0$), and four (at $n\omega_0$ with $n \geq 3$) additional eigenvalues in Fig. 2(f). Because of the close vicinity of many states in the energy spectrum the corrections resulting from the counterrotating terms for $g' = g$ are large. This trend continues if N is increased further.

B. The emission spectrum

In Fig. 3 we show the emission spectrum $S(\omega)$ for $N = 2$ emitters at different coupling strengths g and environment temperatures T . These data, as well as those for the Glauber function $g^{(2)}(t)$ shown later, have been computed with a maximal number of 10^2 cavity photons in the numerical diagonalization of H , which is sufficient for the given parameter combinations.

For low temperatures $T \ll \omega_0$, only the first possible transition into the ground state contributes to the emission spectrum. It leads to the single peak in panels (i) and (iii) of Fig. 3. With increasing temperature, transitions involving higher excited states begin to contribute. For example, the two peaks in panels (ii) and (iv) correspond to the transition from the second to the first excited state and from the third excited state to the ground state. As could be deduced already from Figs. 2(b) and 2(e), the transitions tend to have smaller energies in the TC limit than in the Dicke limit, which leads to the redshift of the emission peaks in panel (v) relative to those in panel (ii). However, at not too strong coupling the low-lying states still have comparable energies, and the emission spectra look similar. The situation changes at ultrastrong coupling when the corotating and counterrotating terms are of equal magnitude [panels (iii) and (vi)]. In addition to the markedly different peak energies the peak height has now decreased by

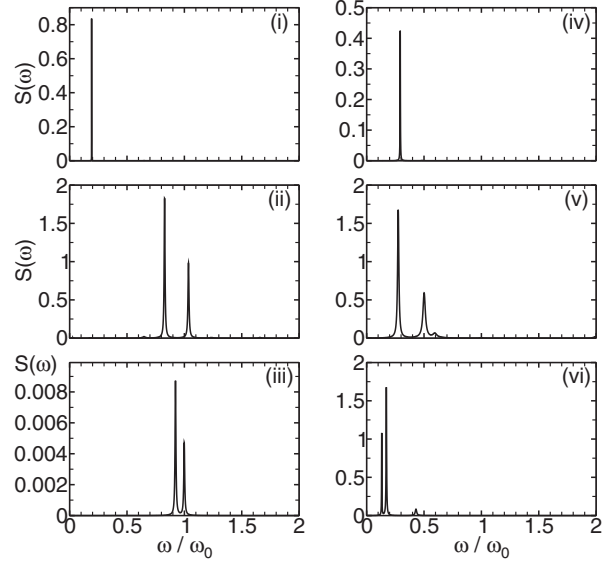


FIG. 3. Emission spectra $S(\omega)$ for $N = 2$ emitters, for (left) $g' = g$ and (right) $g' = 0$. The emitter-cavity coupling strength and the environment temperature are $g = 0.5\omega_0, T = 0.07\omega_0$ in panels (i) and (iv), $g = 0.7\omega_0, T = 0.23\omega_0$ in panels (ii) and (v), and $g = 0.8\omega_0, T = 0.1\omega_0$ in panels (iii) and (vi).

two orders of magnitude in the Dicke limit but not in the TC limit.

The decrease of peak height can be recognized in the ω -integrated emission spectrum

$$\int_{-\infty}^{\infty} \frac{S(\omega)}{\gamma_c(\omega)} d\omega = \langle \dot{X}_+ \dot{X}_- \rangle \quad (19)$$

shown in Fig. 4. The equality with the given expectation value follows directly from Eq. (17). Only in the Dicke limit, but not in the TC limit, does the total emission become small again at ultrastrong coupling and low temperatures. Still, one sees that both plots agree nicely for not too strong coupling ($g/\omega_0 \lesssim 0.5$). This observation sets the upper limit of the coupling strength (here, for $N = 2$ emitters) below which the presence

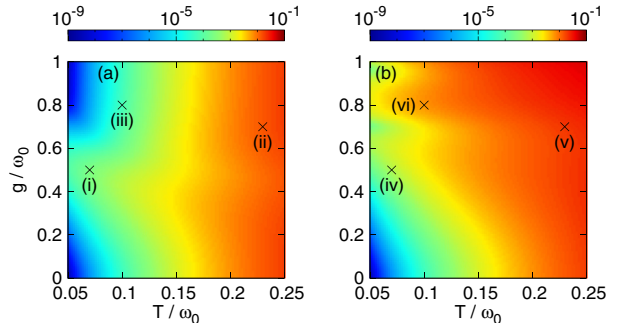


FIG. 4. (Color online) Expectation value $\langle \dot{X}_+ \dot{X}_- \rangle$ for $N = 2$ emitters as a function of temperature T and coupling strength g . Results are given for (a) $g' = g$ and (b) $g' = 0$. Crosses mark the parameters used in Fig. 3.

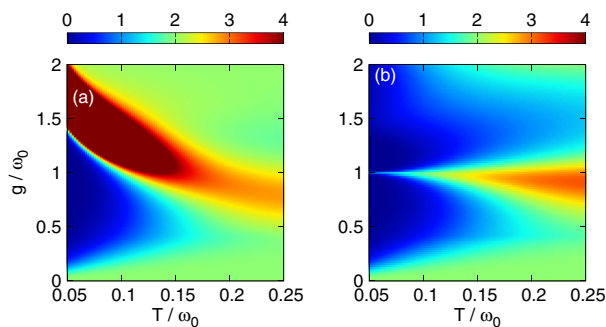


FIG. 5. (Color online) Glauber function $g^{(2)}(0)$ at zero time delay for one emitter ($N = 1$) as a function of temperature T and coupling strength g . Results are given for (a) $g' = g$ and (b) $g' = 0$. Note that all values $g^{(2)}(0) \geq 4$ are assigned the same [dark red (dark gray)] color in the density plots.

or absence of counterrotating interaction terms does not affect the light emission significantly. We will find the same behavior for the Glauber function.

IV. NONCLASSICAL LIGHT

A basic decision on the possible generation of nonclassical light is possible with the Glauber function $g^{(2)}(0)$ at zero time delay. For $g^{(2)}(0) = 1$ the emitted photons have a Poissonian distribution, while $g^{(2)}(0) > 1$ indicates super-Poissonian statistics. Thermal light has $g^{(2)}(0) = 2$. By contrast, $g^{(2)}(0) < 1$ indicates nonclassical light with sub-Poissonian photon statistics. Further information on photon (anti)bunching is provided by the full time-dependent function $g^{(2)}(t)$.

A. Photon statistics for one emitter

The Glauber function $g^{(2)}(0)$ for one emitter ($N = 1$) is shown in Fig. 5. Two distinct regions can be identified in the Dicke limit in Fig. 5(a) (where $g' = g$). A triangular region with $g^{(2)}(0) < 1$, which stretches out along the vertical axis, indicates the emission of nonclassical light with sub-Poissonian photon statistics at low temperatures and moderate to strong light-matter coupling. It lies below an elongated region with strongly super-Poissonian photon statistics [$g^{(2)}(0) \gg 2$] at larger coupling, which extends diagonally towards higher temperatures. Both regions are embedded in the background of thermal light with $g^{(2)}(0) \approx 2$. The situation is distinctly different in the TC limit ($g' = 0$) in Fig. 5(b), where the super-Poissonian region is pushed back in favor of a second sub-Poissonian region that continues towards ultrastrong coupling. Note, however, that the emission of nonclassical light in the first sub-Poissonian region is observed equally in both limits.

B. Photon statistics for few emitters

The distinctive features of the Glauber function persist for multiple emitters (see Fig. 6), but the regions are shifted to smaller couplings g as the number of emitters increases from one to three.

The obvious similarity between $g^{(2)}(0)$ for $N = 1, 2, 3$ emitters visible in Figs. 5 and 6 can be expressed as an

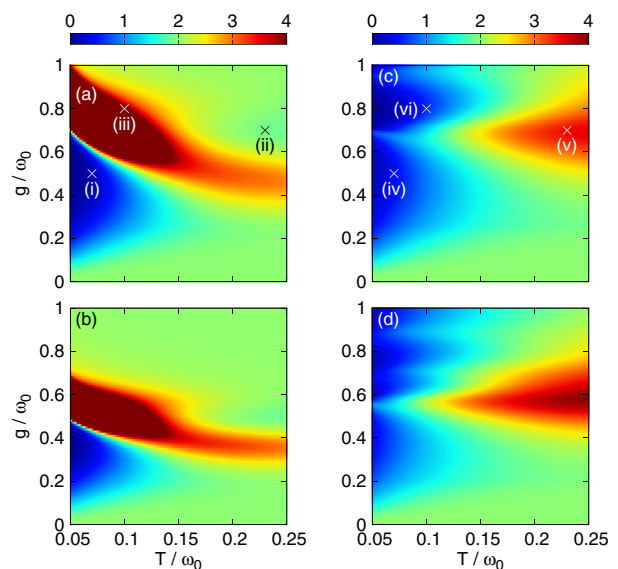


FIG. 6. (Color online) Glauber function $g^{(2)}(0)$ at zero time delay as a function of temperature T and coupling strength g for (top) $N = 2$ emitters and (bottom) $N = 3$ emitters. Results are given for (a) and (b) $g' = g$ and (c) and (d) $g' = 0$. Note that all values $g^{(2)}(0) \geq 4$ are assigned the same [dark red (dark gray)] color in the density plots.

approximate relation between the respective emitter-cavity coupling g . In the Dicke limit ($g' = g$) we find that the features of $g^{(2)}(0)$ are closely reproduced under the scaling $g \propto 1/N$. In the TC limit ($g' = 0$) features are reproduced under the scaling $g \propto 1/\sqrt{N}$. Interestingly, the proper scaling of g depends on the presence of counterrotating interaction terms in the Hamiltonian. This difference is in contrast to the semiclassical theory where the mean cavity photon number in the steady state scales $\propto N$ in both the Dicke and TC limits. Not surprisingly, the Glauber function $g^{(2)}(0)$ is more sensitive to the details of light-matter coupling than the semiclassical theory that neglects quantum correlations in favor of a mean-field approximation.

Our arguments in favor of the above scaling relations depend on several observations, which we now develop for the TC limit ($g' = 0$). Without counterrotating interaction terms the Hamiltonian H commutes with the operator $N_t = a^\dagger a + \sum_{j=1}^N \sigma_+^{(j)} \sigma_-^{(j)}$, which counts the total number of excitations. Hence, H is block diagonal with blocks of the form $n_t \omega_0 \mathbb{I} + g\mathbf{C}$, where n_t denotes the eigenvalue of N_t , \mathbb{I} is the identity matrix, and the matrix block \mathbf{C} contains the g -independent matrix elements of the corotating interaction terms in H . From this form of the blocks it is evident that the eigenvectors of H do not depend on g , that is, the matrix elements of \hat{X}_\pm that enter Eq. (16) are constant. The dependence of $g^{(2)}(0)$ on g results purely from the eigenvalues, which determine the occupation of the states in the stationary (thermal) state and the prefactors of \hat{X}_\pm . If we can show that the eigenvalues scale approximately as $g\sqrt{N}$, the above relation follows.

Let us focus on the low-lying states that give the dominant contribution in the interesting temperature regimes. These states can be found in the ladder diagram of states in Fig. 7.

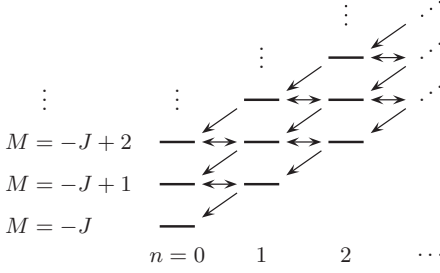


FIG. 7. Schematic energy-level pattern. Horizontal arrows depict the corotating interaction terms in Eq. (1) (coupling constant g); diagonal arrows illustrate the action of the cavity photon annihilation operator a .

They must be connected to the ground state at energy zero by a diagonal arrow that gives the action of the operator a , i.e., of \dot{X}_- .

For the denominator $\langle \dot{X}_+ \dot{X}_- \rangle$ of $g^{(2)}(0)$ from Eq. (16) states which are separated by one vertical step in the ladder diagram contribute. The energy of the most relevant first excited state is given by $E_1 = \omega_0 \pm g\sqrt{N}$, which has the postulated scaling. This scaling of the first excited state for a few emitters has been verified experimentally in Ref. [41].

For the numerator $\langle \dot{X}_+ \dot{X}_+ \dot{X}_- \dot{X}_- \rangle$ of $g^{(2)}(0)$, where each operator appears twice, states which are separated by two vertical steps on the ladder contribute. Now the second excited state is most relevant, which is the linear combination of the two ($N = 1$) or three ($N \geq 2$) vertical rungs that occur for $n_t = 2$ excitations. The corresponding 2×2 or 3×3 matrix from the above block decomposition of H is

$$\begin{pmatrix} 2\omega_0 & \sqrt{2}g \\ \sqrt{2}g & 2\omega_0 \end{pmatrix}, \quad \begin{pmatrix} 2\omega_0 & \sqrt{2}g & 0 \\ \sqrt{2}g & 2\omega_0 & \sqrt{2N}g \\ 0 & \sqrt{2N}g & 2\omega_0 \end{pmatrix}. \quad (20)$$

Diagonalization gives the energies $E_2 = 2\omega_0 \pm \sqrt{2}g$ for $N = 1$, while $E_2 \in \{2\omega_0, 2\omega_0 \pm \sqrt{2}\sqrt{N+1}g\}$ for $N \geq 2$. With the approximation $\sqrt{N+1} \approx \sqrt{N}$, which is good enough for a rule of thumb, this is again the postulated scaling. Put together, the energies that enter the computation of $g^{(2)}(0)$ scale roughly as $g\sqrt{N}$, which concludes our argument in favor of the observed relation “ $g \propto 1/\sqrt{N}$ ” in the TC limit.

In the Dicke limit $g' = g$ the block decomposition of H is not possible because of the counterrotating interaction terms. The eigenvectors of H now depend on g , and the previous argument cannot be easily translated. However, inspection of the energy spectra in Fig. 2 strongly suggests that the observed relation is still related to an approximate relation between the eigenvalues of H for different N , now with the scaling $g \propto 1/N$.

C. Photon statistics from the quantum optical master equation

Results for the Glauber function obtained with the quantum optical master equation (18) are shown in Fig. 8 in the Dicke limit $g' = g$. In stark contrast to the results from Figs. 5 and 6 the quantum optical master equation does not predict the emission of nonclassical light with sub-Poissonian

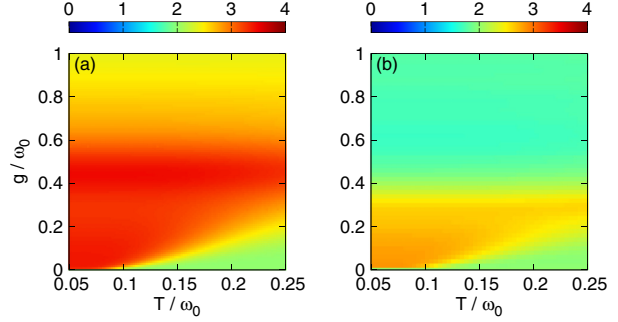


FIG. 8. (Color online) Glauber function $g^{(2)}(0)$ computed with the quantum optical master equation (18), shown as a function of temperature T and coupling strength g for $g' = g$. Results are given for (a) $N = 1$ emitter and (b) $N = 2$ emitters.

photon statistics in any part of the parameter space. The situation does not improve in the TC limit $g' = 0$, where $[H, N_t] = 0$ and the quantum optical master equation gives the stationary (thermal) state $\propto e^{-\beta\omega_0 N_t}$, leading to $g^{(2)}(0) = \langle a^\dagger a^\dagger a a \rangle / \langle a^\dagger a \rangle^2 = 2$ independent of the number of emitters N , the coupling strength g , or the temperature T , thus always predicting the emission of thermal light. While it may not be surprising that the quantum optical master equation fails because the weak-coupling condition $g \ll \omega_{x,c}$ is not satisfied, it is remarkable that it fails to capture any features from the previous Glauber function plots in Figs. 5 and 6. This failure highlights the importance of using the correct master equation not only for strong light-matter coupling but also if one is interested in properties following from higher-order correlation functions, such as the photon statistics obtained from the second-order Glauber function.

D. Photon bunching and antibunching

A further property to distinguish classical and nonclassical light is the time-coincidence statistics of the emitted photons, which can be deduced from the time-dependent Glauber function $g^{(2)}(t)$. For classical light, $g^{(2)}(t)$ has a nonpositive initial slope at $t = 0$. This indicates photon bunching, i.e., that the probability of observing two photons at equal times is larger than the probability of observing them at different times. Conversely, a positive slope indicates photon antibunching, which is possible only for nonclassical light. In the long-time limit, $\lim_{t \rightarrow \infty} g^{(2)}(t) = 1$ in all cases.

In Fig. 9 we plot $g^{(2)}(t)$ for the parameter combinations marked in the two upper panels in Fig. 6. We see that $g^{(2)}(t)$ is always a strictly monotonic function of t . Therefore, in the present situation photon bunching and antibunching coincide precisely with super-Poissonian and sub-Poissonian photon statistics. Only if $1 \leq g^{(2)}(0) \leq 2$ in panel (ii) the function $g^{(2)}(t)$ shows small oscillations, but the overall decay is still indicative of photon bunching.

V. CONCLUSIONS

Our analysis of the light generated by a few emitters in a cavity reveals a nontrivial dependence of the photon statistics on the light-matter coupling and temperature. Clearly

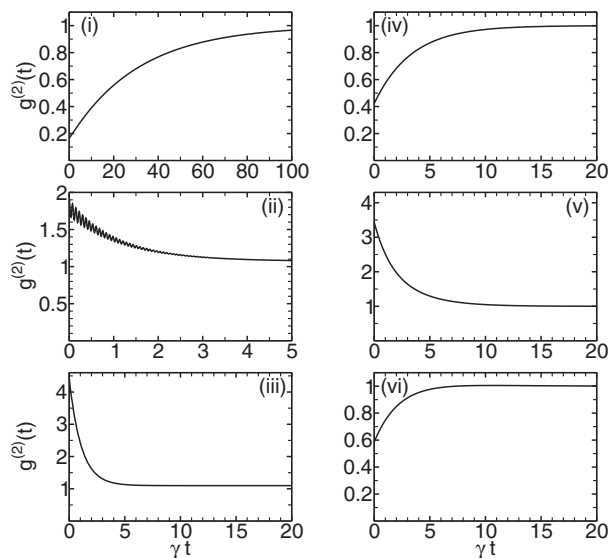


FIG. 9. Glauber function $g^{(2)}(t)$ as a function of time for $N = 2$ emitters, for (left) $g' = g$ and (right) $g' = 0$. The emitter-cavity coupling strength and the bath temperature are $g = 0.5\omega_0$, $T = 0.07\omega_0$ in panels (i) and (iv), $g = 0.7\omega_0$, $T = 0.23\omega_0$ in panels (ii) and (v), and $g = 0.8\omega_0$, $T = 0.1\omega_0$ in panels (iii) and (vi).

identifiable parameter regimes with sub- and super-Poissonian photon statistics appear at strong and ultrastrong coupling and lie immediately next to each other. Tuning the light-matter coupling or changing the temperature can thus have a tremendous effect on the photon statistics. As a general trend we find strong signatures of nonclassical light at strong coupling. Thermal photon statistics, on the other hand, requires weak coupling or high temperatures: It is the exception rather than the rule at low temperatures.

The photon statistics, and to a lesser degree also the total emission, is strongly influenced by the presence of counterrotating light-matter interaction terms in the Hamiltonian. These terms are responsible for the prevalence of super-Poissonian over sub-Poissonian light at ultrastrong coupling. Not surprisingly, the convenient rotating-wave approximation (i.e., identification of the Dicke limit by the TC limit) gives the wrong prediction when the coupling becomes too large. Nevertheless, the scenarios with and without counterrotating terms are surprisingly similar at not too strong coupling, which shows that generation of nonclassical light is not a peculiar effect arising from the fine-tuning of interaction terms in the Hamiltonian but a rather robust feature.

We have provided an approximate rule to relate the emission of a few emitters to the emission of a single emitter under appropriate scaling of the coupling constant. In accordance with this rule, the features of the Glauber function observed for one emitter occur at comparably smaller values of the individual emitter-cavity coupling in the case of a few emitters. The reason is that all emitters interact with the same cavity mode, which magnifies the effects of resonant emission and (re)absorption of cavity photons. Broadly speaking, generation of nonclassical light is easier with more emitters because the

required coupling of each individual emitter to the cavity mode can be reduced.

Our analysis of strong light-matter coupling required the use of the full input-output formalism and of the full master equation, which carefully distinguishes between transitions at different energies. If this correct treatment is replaced by the standard quantum optical master equation, results change completely. Especially, the prediction of nonclassical light does not survive the additional approximations made in the replacement. While the quantum optical master equation could not be expected to work at strong coupling, its outright failure at describing any of the distinctive features observed in the photon statistics shows that using the right master equation is essential in all situations, perhaps apart from extremely weak coupling. The price one has to pay is full diagonalization of the Hamiltonian.

We here focus on the system at thermal equilibrium. Future work should address emission if the system is driven coherently through external photon sources. This will require the addition of explicitly time-dependent periodic terms to the Hamiltonian and thus combination of the present master equation with the Floquet formalism. By contrast, a perturbative expansion in the driving strength is sufficient only for weak off-resonant driving, but then the possible new effects would be weak too.

ACKNOWLEDGMENTS

This work was supported by Deutsche Forschungsgemeinschaft through Sonderforschungsbereich 652 (project B5).

APPENDIX A: THE INPUT-OUTPUT FORMALISM

We follow standard input-output theory [19,42]. The interaction Hamiltonian in Eq. (2) for the cavity-environment coupling in the continuum limit is

$$H_I = -iX \int D(\omega)\lambda(\omega)(b_\omega - b_\omega^\dagger)d\omega, \quad (\text{A1})$$

where $D(\omega)$ is the environment density of states and $\lambda_c(\omega)$ is the cavity-environment coupling function; that is, the environment spectral function is $\gamma_c(\omega) = 2\pi D(\omega)\lambda_c(\omega)^2$. H_I together with the free Hamiltonian $\int D(\omega)\omega b_\omega^\dagger b_\omega d\omega$ of the environment photons and the commutator $[b_\omega, b_{\omega'}^\dagger] = \delta(\omega - \omega')$ leads to the equation of motion

$$\dot{b}_\omega = -i\omega b_\omega + \lambda(\omega)X \quad (\text{A2})$$

for the field quadratures of the environment. For $t_0 < t < t_1$, the formal solution of Eq. (A2) is

$$\begin{aligned} b_\omega(t) &= e^{-i\omega(t-t_0)}b_\omega(t_0) + \lambda(\omega) \int_{t_0}^t e^{-i\omega(t-t')}X(t')dt' \\ &= e^{-i\omega(t-t_1)}b_\omega(t_1) - \lambda(\omega) \int_t^{t_1} e^{-i\omega(t-t')}X(t')dt'. \end{aligned} \quad (\text{A3})$$

We define input (output) field operators

$$b_{\text{in(out)}}(t) = \int D(\omega)\lambda(\omega)e^{-i\omega(t-t_{0(1)})}b_\omega(t_{0(1)})d\omega \quad (\text{A4})$$

and make use of the spectral function $\gamma_c(\omega) = \gamma\omega/\omega_0$ to obtain the input-output relation

$$b_{\text{out}}(t) = b_{\text{in}}(t) + i \frac{\gamma}{\omega_0} \dot{X}_-(t), \quad (\text{A5})$$

where \dot{X}_- denotes the positive frequency component of \dot{X} ; that is, \dot{X}_- acts as a lowering operator. The explicit definition of \dot{X}_- in the system-energy eigenbasis is given in Eq. (14).

APPENDIX B: THE MARKOVIAN MASTER EQUATION

We consider the dissipative dynamics of the system density matrix in the weak system-environment coupling limit. For strong coupling within the system the quantum optical master equation predicts unphysical emission from the ground state [14]. Going one step back in the derivation of the quantum optical master equation, the second-order time-convolutionless projection operator method [25] gives a time-local master equation leading to consistent results including the counterrotating terms [43,44]. Nevertheless, this master equation does not, in general, generate positive dynamics [45,46]. This problem was resolved by a recently derived master equation in the system eigenbasis [24–29], and we here recapitulate its derivation.

The total Hamiltonian is the sum of the contribution of the system H , the contribution of the reservoir H_R , and the interaction H_I . We note that the interaction Hamiltonian in Eq. (2) is of the general form $H_I = SR$, where S (R) is a Hermitian system (reservoir) operator. A more general coupling $H_I = \sum_n S_n R_n$ can also be considered but leads to the same qualitative results. The dynamics of the density operator $\hat{\rho}_T(t)$ of the total system in the interaction picture is described by the von Neumann equation,

$$\frac{d}{dt} \hat{\rho}_T(t) = -i[\hat{H}_I(t), \hat{\rho}_T(t)]. \quad (\text{B1})$$

As a notational convenience, we mark operators in the interaction picture with a hat. The interaction Hamiltonian and the density operator in the interaction picture are defined as

$$\hat{\rho}_T(t) = U_0^\dagger(t,0) \rho_T(t) U_0(t,0), \quad (\text{B2})$$

$$\hat{H}_I(t) = U_0^\dagger(t,0) H_I U_0(t,0), \quad (\text{B3})$$

where the time-evolution operator of the uncoupled system and reservoir is

$$U_0(t,s) = e^{-i(H+H_R)(t-s)}. \quad (\text{B4})$$

In the limit of weak system-reservoir coupling several approximations are performed. First of all, within the Born approximation, initial factorization of the density operator is assumed, $\rho_T(0) = \rho(0)\rho_R$, and the back-action of the system onto the reservoir is neglected, $\rho_T(t) = \rho(t)\rho_R$. Second, the Markov approximation is performed by replacing $\rho(\tau)$ at retarded times τ with $\rho(t)$ at the local time t . Third, assuming

that the reservoir correlation time is small compared to the relaxation time of the system, the time integration is extended to infinity to arrive at the Born-Markov equation of motion

$$\frac{d}{dt} \hat{\rho}(t) = - \int_0^\infty \text{Tr}_R\{[\hat{H}_I(t), [\hat{H}_I(t-\tau), \hat{\rho}(t)\rho_R]]\} d\tau, \quad (\text{B5})$$

where $\text{Tr}_R\{\cdot\}$ denotes the partial trace over the reservoir degrees of freedom and $\langle R \rangle = 0$ is assumed. We further assume a thermal reservoir state $\rho_R \propto e^{-\beta H_R}$ and define the reservoir correlation function

$$C(\tau) = \text{Tr}_R\{e^{iH_R\tau} R e^{-iH_R\tau} R \rho_R\} = C(-\tau)^* \quad (\text{B6})$$

to evaluate the traces in Eq. (B5). This yields the master equation

$$\frac{d}{dt} \hat{\rho}(t) = \int_0^\infty [\hat{S}(t-\tau) \hat{\rho}(t), \hat{S}(t)] C(\tau) d\tau + \text{H.c.}, \quad (\text{B7})$$

where H.c. denotes the Hermitian conjugate.

We introduce the transition operators in Eq. (4) that are the discrete Fourier components of the interaction picture $\hat{S}(t)$, i.e.,

$$\hat{S}(t) = \sum_\omega e^{-i\omega t} S_\omega. \quad (\text{B8})$$

Equivalently, $[H, S_\omega] = -\omega S_\omega$. In addition, we introduce the even and odd Fourier transforms of the reservoir correlation function,

$$\chi(\omega) = \int_{-\infty}^\infty C(\tau) e^{i\omega\tau} d\tau = \chi(\omega)^*, \quad (\text{B9})$$

$$\xi(\omega) = \frac{1}{i} \int_{-\infty}^\infty C(\tau) \text{sgn}(\tau) e^{i\omega\tau} d\tau = \xi(\omega)^*. \quad (\text{B10})$$

For a thermal photon reservoir with spectral function $\gamma(\omega)$ the functions $\chi(\omega)$ and $\xi(\omega)$ are given in Eqs. (6) and (7). With these definitions we find

$$\frac{d}{dt} \hat{\rho}(t) = \frac{1}{2} \sum_{\omega, \omega'} \{\chi(\omega') + i\xi(\omega')\} e^{i(\omega-\omega')t} [S_{\omega'} \hat{\rho}(t), S_\omega^\dagger] + \text{H.c.} \quad (\text{B11})$$

Equation (B11) is the standard Born-Markov master equation in the system energy eigenbasis. It contains the dissipative parts proportional to $\chi(\omega)$ and the Lamb-shift terms proportional to $\xi(\omega)$. Because Eq. (B11) is not of Lindblad type, it does not, in general, preserve the positivity of the density operator.

Inspecting Eq. (B11), we recognize that it contains oscillating terms proportional to $e^{\pm i(\omega-\omega')t}$. If we assume that the relaxation of the system is slow compared with all oscillations $e^{\pm i(\omega-\omega')t}$, we can neglect the contribution from terms with $\omega' \neq \omega$. This approximation is called secular or rotating-wave approximation, and the master equation in the Schrödinger picture simplifies to the result given in Eq. (3). This equation is the Lindblad master equation that includes the Lamb shift of the unperturbed system energies E_n as well as reservoir induced dissipation effects to lowest order in the system-reservoir interaction strength.

As is already known in the literature, special care has to be taken if the spectrum of H is degenerate [24,47]. But even if the eigenvalues E_n are nondegenerate, we may have situations where energy differences are degenerate, i.e., $E_n - E_m = E_k - E_l$ for $n \neq m \neq k \neq l$. The consequences of these two different types of degeneracy can be understood when we decompose the density matrix into blocks. In particular, we write $\hat{\rho}_{nm}$ (\mathbf{S}_{mn}) for the matrix containing the elements $\langle k|\hat{\rho}|l\rangle$ ($\langle k|S|l\rangle$) with $E_k = E_n$ and $E_l = E_m$. The master equation (3) in this block notation reads

$$\begin{aligned} \frac{d}{dt}\hat{\rho}_{mn}(t) = & \sum_{k,l} \chi(E_k - E_m)\mathbf{S}_{mk}\hat{\rho}_{kl}(t)\mathbf{S}_{ln}^\dagger \delta_{E_k - E_m, E_l - E_n} \\ & - \frac{1}{2} \sum_k \varphi(E_n - E_k)^* \hat{\rho}_{mn}(t)\mathbf{S}_{nk}^\dagger \mathbf{S}_{kn} \\ & - \frac{1}{2} \sum_k \varphi(E_m - E_k)\mathbf{S}_{mk}^\dagger \mathbf{S}_{km} \hat{\rho}_{mn}(t), \quad (\text{B12}) \end{aligned}$$

where the summations run only over different system energies, and the complex function $\varphi(x) = \chi(x) + i\xi(x)$ is introduced. We see that the last two lines in this equation are block diagonal. For $m = n$, the Kronecker delta in the first line evaluates to δ_{E_k, E_l} such that diagonal blocks couple only to diagonal blocks. For $m \neq n$, the first line contains only terms with $k \neq l$, such that nondiagonal blocks do not couple to diagonal ones. Nevertheless, a nondiagonal block $\hat{\rho}_{mn}$ couples to another nondiagonal block $\hat{\rho}_{kl}$ with $k \neq l \neq m \neq n$ if the respective transition energies are degenerate. Thus, energy-level degeneracy introduces a block structure implying that a diagonal density matrix element couples to nondiagonal elements within diagonal blocks, whereas energy transition degeneracy leads to a coupling of nondiagonal blocks to different nondiagonal blocks. We remark that both subtleties have their origin in the rotating-wave approximation. On the one hand, this approximation leads to the Lindblad structure of Eq. (3). On the other hand, it results in strict Kronecker deltas between the two transition energies ω' and ω .

Consider a situation where each degeneracy in the spectrum of H as well as in their differences is lifted by a small ϵ parameter. Then, each block contains only a single element, implying that the equations for the diagonal density matrix elements no longer couple to nondiagonal elements. In addition, any nondiagonal element of the density matrix evolves independently from all other elements. This behavior does not change when we let each $\epsilon \rightarrow 0$. In this limit, the equations become independent of the ϵ parameters but are different from the $\epsilon = 0$ case. In particular, for every nonzero $\epsilon \rightarrow 0$ we get the two equations (9) and (10) for the diagonal and nondiagonal density matrix elements.

We remark that in real physical systems one will never have perfectly equal or equidistant energies because each small perturbation will lift the degeneracies. In the theoretical description we may argue that the Lamb shift lifts degeneracies. Nevertheless, we have to keep in mind that with Eqs. (9) to (11) we cannot study effects that rely on degenerate energies or degenerate transitions; for example, the perfectly harmonic oscillator or a system composed of completely uncoupled identical subsystems is not correctly described.

APPENDIX C: ANALYTICAL RESULTS IN THE TAVIS-CUMMINGS LIMIT

In this section we derive analytical results for the Glauber $g^{(2)}(0)$ function in the TC limit ($g' = 0$) for a single emitter ($N = 1$).

According to the argumentation in Sec. IV B, the dominant contribution to the denominator of $g^{(2)}(0)$ in Eq. (16) at low temperatures is that of the first excited state with energy $E_1 = \omega_0 - g$. Specifically, the denominator $\langle \dot{X}_+ \dot{X}_- \rangle$ is approximated by

$$\frac{1}{2}(\omega_0 - g)^2 e^{-\beta(\omega_0 - g)}. \quad (\text{C1})$$

In this expression the exponential $e^{-\beta(\omega_0 - g)}$ is the thermal population of the first excited state, and the prefactor $(\omega_0 - g)^2/2$ is the squared transition matrix element of \dot{X}_- between the first excited state and the ground state.

The most relevant state for the numerator of $g^{(2)}(0)$ at low temperatures is the lowest eigenstate with energy $E_2 = 2\omega_0 - \sqrt{2}g$ of the 2×2 matrix given in Eq. (20). To evaluate the matrix elements of the operators \dot{X}_\pm we have to consider the four possible transition sequences $|2, -\rangle \rightarrow |1, \pm\rangle \rightarrow |0\rangle \rightarrow |1, \pm\rangle \rightarrow |2, -\rangle$, where $|0\rangle$ denotes the ground state and $|n, \pm\rangle$ are the two eigenstates with energies $E_n = n\omega_0 \pm \sqrt{n}g$. This yields the expression

$$\begin{aligned} & \left\{ \frac{3 + \sqrt{8}}{8} [\omega_0 - (\sqrt{2} - 1)g]^2 (\omega_0 - g)^2 \right. \\ & + \frac{1}{4} [\omega_0 - (\sqrt{2} - 1)g] (\omega_0^2 - g^2) [\omega_0 - (\sqrt{2} + 1)g] \\ & \left. + \frac{3 - \sqrt{8}}{8} [\omega_0 - (\sqrt{2} + 1)g]^2 (\omega_0 + g)^2 \right\} e^{-\beta(2\omega_0 - \sqrt{2}g)} \quad (\text{C2}) \end{aligned}$$

approximating the numerator of $g^{(2)}(0)$.

The results belonging to Eqs. (C1) and (C2) are plotted in Fig. 10(a). Compared to the exact numerical results in Fig. 5(b), a good agreement appears for $0.2 \lesssim g/\omega_0 < 0.4$ and low temperatures. For high values of $g \gtrsim 0.4\omega_0$ the first excited state becomes closer and closer to the ground state, such that

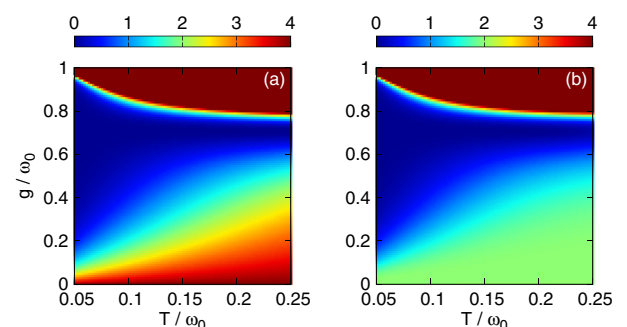


FIG. 10. (Color online) Analytical results for the Glauber function $g^{(2)}(0)$ for one emitter ($N = 1$) as a function of temperature T and coupling strength g in the TC limit. Shown are (a) the result following from Eqs. (C1) and (C2) and (b) the result refined for $g \leq \omega_0$ as explained in the text.

the finite temperature leads to significant contributions from transitions not involving the ground state. For this reason, the upper part of Fig. 10(a) is not well reproduced. In contrast, the lower part of Fig. 10(a) is not in accordance with the exact numerical results because our assumption of low temperatures $T \ll g < \omega_0$ does not include the limit $g \rightarrow 0$.

To improve the results in regions with $g \ll \omega_0$ we additionally have to take into account the transition sequences $|1, +\rangle \rightarrow |0\rangle \rightarrow |1, +\rangle$ for the denominator and $|2, +\rangle \rightarrow$

$|1, \pm\rangle \rightarrow |0\rangle \rightarrow |1, \pm\rangle \rightarrow |2, +\rangle$ for the numerator. The result is shown in Fig. 10(b), where the agreement with the exact results in Fig. 5(b) is now very good for all temperatures and $g \lesssim 0.4\omega_0$. Note that at $g \simeq 0.4\omega_0$ a crossing of the eigenvalues of the second and third excited states occurs, as can be seen in Fig. 2(d). This indicates that the role of these states in the calculation of $g^{(2)}(0)$ is interchanged. The impact of these eigenvalue crossings would analytically be reproduced if we include contributions to $g^{(2)}(0)$ from higher excited states.

-
- [1] R. Bonifacio, P. Schwendimann, and F. Haake, *Phys. Rev. A* **4**, 302 (1971).
 - [2] M. Gross and S. Haroche, *Phys. Rep.* **93**, 301 (1982).
 - [3] D. Meiser and M. J. Holland, *Phys. Rev. A* **81**, 063827 (2010).
 - [4] V. M. Bastidas, C. Emary, B. Regler, and T. Brandes, *Phys. Rev. Lett.* **108**, 043003 (2012).
 - [5] A. Auffèves, D. Gerace, S. Portolan, A. Drezet, and M. F. Santos, *New J. Phys.* **13**, 093020 (2011).
 - [6] F. P. Laussy, A. Laucht, E. del Valle, J. J. Finley, and J. M. Villas-Bôas, *Phys. Rev. B* **84**, 195313 (2011).
 - [7] E. Mascarenhas, D. Gerace, M. F. Santos, and A. Auffèves, *Phys. Rev. A* **88**, 063825 (2013).
 - [8] G. S. Agarwal and K. Tara, *Phys. Rev. A* **43**, 492 (1991).
 - [9] V. V. Temnov and U. Woggon, *Opt. Express* **17**, 5774 (2009).
 - [10] N. Quesada, *Phys. Rev. A* **86**, 013836 (2012).
 - [11] H. J. Carmichael, *Statistical Methods in Quantum Optics I* (Springer, Berlin, 1999).
 - [12] C. Ciuti, G. Bastard, and I. Carusotto, *Phys. Rev. B* **72**, 115303 (2005).
 - [13] C. Ciuti and I. Carusotto, *Phys. Rev. A* **74**, 033811 (2006).
 - [14] T. Werlang, A. V. Dodonov, E. I. Duzzioni, and C. J. Villas-Bôas, *Phys. Rev. A* **78**, 053805 (2008).
 - [15] R. J. Thompson, G. Rempe, and H. J. Kimble, *Phys. Rev. Lett.* **68**, 1132 (1992).
 - [16] R. Miller, T. E. Northup, K. M. Birnbaum, A. Boca, A. D. Boozer, and H. J. Kimble, *J. Phys. B* **38**, S551 (2005).
 - [17] K. Słowik, R. Filter, J. Straubel, F. Lederer, and C. Rockstuhl, *Phys. Rev. B* **88**, 195414 (2013).
 - [18] A. L. Grimsmo and S. Parkins, *Phys. Rev. A* **87**, 033814 (2013).
 - [19] A. Ridolfo, M. Leib, S. Savasta, and M. J. Hartmann, *Phys. Rev. Lett.* **109**, 193602 (2012).
 - [20] R. Stassi, A. Ridolfo, O. Di Stefano, M. J. Hartmann, and S. Savasta, *Phys. Rev. Lett.* **110**, 243601 (2013).
 - [21] L. Garziano, A. Ridolfo, R. Stassi, O. Di Stefano, and S. Savasta, *Phys. Rev. A* **88**, 063829 (2013).
 - [22] A. Ridolfo, S. Savasta, and M. J. Hartmann, *Phys. Rev. Lett.* **110**, 163601 (2013).
 - [23] D. Pagel, H. Fehske, J. Sperling, and W. Vogel, *Phys. Rev. A* **88**, 042310 (2013).
 - [24] F. Beaudoin, J. M. Gambetta, and A. Blais, *Phys. Rev. A* **84**, 043832 (2011).
 - [25] H.-P. Breuer and F. Petruccione, *The Theory of Open Quantum Systems* (Oxford University Press, Oxford, 2002).
 - [26] R. Alicki, D. A. Lidar, and P. Zanardi, *Phys. Rev. A* **73**, 052311 (2006).
 - [27] G. Schaller and T. Brandes, *Phys. Rev. A* **78**, 022106 (2008).
 - [28] G. Schaller, *Open Quantum Systems Far from Equilibrium*, Lecture Notes in Physics Vol. 881 (Springer, Heidelberg, 2014).
 - [29] G. S. Agarwal, *Quantum Optics* (Cambridge University Press, Cambridge, 2013).
 - [30] S. Singh, *Opt. Commun.* **44**, 254 (1983).
 - [31] L. Mandel and E. Wolf, *Optical Coherence and Quantum Optics* (Cambridge University Press, Cambridge, 1995).
 - [32] M. J. Collett and C. W. Gardiner, *Phys. Rev. A* **30**, 1386 (1984).
 - [33] C. W. Gardiner and M. J. Collett, *Phys. Rev. A* **31**, 3761 (1985).
 - [34] R. Graham, *Z. Phys. B* **76**, 265 (1989).
 - [35] S. Savasta and R. Girlanda, *Phys. Rev. A* **53**, 2716 (1996).
 - [36] R. H. Dicke, *Phys. Rev.* **93**, 99 (1954).
 - [37] F. Dimer, B. Estienne, A. S. Parkins, and H. J. Carmichael, *Phys. Rev. A* **75**, 013804 (2007).
 - [38] M. P. Baden, K. J. Arnold, A. L. Grimsmo, S. Parkins, and M. D. Barrett, *Phys. Rev. Lett.* **113**, 020408 (2014).
 - [39] R. J. Glauber, *Phys. Rev.* **130**, 2529 (1963).
 - [40] E. T. Jaynes and F. W. Cummings, *Proc. IEEE* **51**, 89 (1963).
 - [41] J. M. Fink, R. Bianchetti, M. Baur, M. Göppl, L. Steffen, S. Filipp, P. J. Leek, A. Blais, and A. Wallraff, *Phys. Rev. Lett.* **103**, 083601 (2009).
 - [42] C. Gardiner and P. Zoller, *Quantum Noise* (Springer, Berlin, 2004).
 - [43] S. De Liberato, D. Gerace, I. Carusotto, and C. Ciuti, *Phys. Rev. A* **80**, 053810 (2009).
 - [44] I. Carusotto, S. De Liberato, D. Gerace, and C. Ciuti, *Phys. Rev. A* **85**, 023805 (2012).
 - [45] R. Dümcke and H. Spohn, *Z. Phys. B* **34**, 419 (1979).
 - [46] R. Alicki, *Phys. Rev. A* **40**, 4077 (1989).
 - [47] M. Jakob and S. Stenholm, *Phys. Rev. A* **69**, 042105 (2004).

Entangled light from driven dissipative microcavities

D. Pagel* and H. Fehske

Institut für Physik, Ernst-Moritz-Arndt-Universität Greifswald, 17487 Greifswald, Germany

(Received 11 June 2015; published 19 August 2015)

We study the generation of entangled light in planar semiconductor microcavities. The focus is on a particular pump configuration where the dissipative internal polariton dynamics leads to the emission of entangled light in a W state. Our study is based on the nonlinear equations of motion for the polariton operators derived within the dynamics-controlled truncation formalism. They include the losses through the cavity mirrors, the interaction with lattice vibrations, and the external laser driving in a Langevin approach. We find that the generated entanglement is robust against decoherence under realistic experimental conditions. Our results show that pair correlations in solid-state devices can be used to stabilize the nonlocal properties of the emitted radiation.

DOI: [10.1103/PhysRevA.92.022342](https://doi.org/10.1103/PhysRevA.92.022342)

PACS number(s): 03.67.Bg, 42.50.Dv, 71.36.+c

I. INTRODUCTION

Quantum entanglement is known as the essential resource for quantum information processing [1–3]. It is defined as a nonlocal correlation that cannot be interpreted in terms of classical joint probabilities [4–6]. The most fundamental examples of nonequivalent forms are Greenberger-Horne-Zeilinger (GHZ) and W states [7,8]. The identification and quantification of entanglement is commonly based on entanglement witnesses [9–14]. The generation and control of entangled states still is a challenging task for quantum computation. In the optical domain, the implementation of quantum algorithms relies on the availability of efficient sources for entangled photons.

The generation of entangled photons is usually based on parametric down conversion in nonlinear crystals [15,16] or biexciton decay in quantum dots [17,18]. Optically excited semiconductor microcavities [19–23] are alternative candidates for the efficient generation of entangled light on the micrometer scale [23–28]. The exciting laser field with frequency near the fundamental band gap coherently generates electron-hole pairs (excitons). The dynamical evolution of excitons is governed by the Coulomb interaction, and the efficient coupling to the cavity photons leads to mixed exciton-photon modes—so-called polaritons [29–31]. The external laser can be tuned to stimulate parametric scattering processes between polaritons which may cause entanglement [32,33]. A moving polariton induces an electric polarization as a source of light that carries the initial (internal) polariton entanglement [22]. Then, depending on the explicit pump configuration, branch or frequency entanglement [23,32], polarization entanglement [28], multipartite entanglement [33], and hyperentangled photon pairs in multiple coupled microcavities [27] can be generated. A very recent interesting development in the generation of entanglement considers a microcavity coupled to a mechanical oscillator and shows that such a hybrid system creates exciton-mechanical mode entanglement [34].

In this work, we demonstrate that a semiconductor microcavity can be used to entangle light in a W -state configuration. Beyond that, such a setup allows one to analyze the internal polariton entanglement properties in the presence

of dissipation. Specifically, we consider a microcavity that is either continuously driven or excited by Gaussian pump pulses. In previous work [33], we introduced the specific pump arrangement for the creation of entangled light in a W state and used multipartite entanglement witnesses to verify the nonlocal correlations. Here, the inclusion of decoherence, induced by the losses through the cavity mirrors, and the coupling to lattice vibrations, within the dynamics-controlled truncation formalism, allows us to study the emitted light under realistic experimental conditions. Most notably, we show that the entanglement of the generated light is robust against dephasing.

We proceed as follows. In Sec. II we briefly recapitulate the equations of motion obtained within the dynamics-controlled truncation formalism and review the explicit pump configuration. The tomographic reconstruction of the state of the emitted radiation is performed in Sec. III, including the analytical solution in the limit of continuous pumping in Sec. III A and the numerical solution for Gaussian pump pulses in Sec. III B. Further details for the derivation of the analytical result can be found in the Appendix. We finally conclude in Sec. IV.

II. THEORETICAL DESCRIPTION OF PARAMETRIC EMISSION

The theoretical description of the dynamical processes in semiconductor microcavities is frequently based on an explicit bosonization of the whole system Hamiltonian [22,24,35]. Alternatively, one can derive equations of motion for generalized Hubbard (transition) operators and truncate these equations at a certain order of the external field. This approach is called a dynamics-controlled truncation scheme [36–39]. The structure of the equations of motion is similar in both approaches. However, the nonlinear coupling coefficients due to fermionic phase-space filling differ [38]. In this work, we adopt the dynamics-controlled truncation formalism because the resulting coefficients are expected to more closely match the experimental data [27,28]. Combining this method with the quantum Langevin approach allows for the evaluation of correlation functions needed for the tomographic reconstruction of the state of the emitted light modes [26,28]. It is thus well suited to study the generation of entangled light in semiconductor microcavities under realistic experimental conditions.

*pagel@physik.uni-greifswald.de

A. Nonlinear system dynamics

We begin with the equations of motion for the semiconductor exciton and cavity photon operators that are derived within the dynamics-controlled truncation formalism [38,39],

$$\frac{d}{dt}a_{\mathbf{k}} = -i\omega_{\mathbf{k}}^c a_{\mathbf{k}} + i\Omega_R b_{\mathbf{k}}, \quad (1a)$$

$$\frac{d}{dt}b_{\mathbf{k}} = -i\omega_{\mathbf{k}}^x b_{\mathbf{k}} + i\Omega_R a_{\mathbf{k}} - iR_{\mathbf{k}}^{NL}, \quad (1b)$$

where $R_{\mathbf{k}}^{NL} = R_{\mathbf{k}}^{sat} + R_{\mathbf{k}}^{xx}$,

$$R_{\mathbf{k}}^{sat} = \frac{\Omega_R}{n_{sat}} \sum_{\mathbf{k}_1, \mathbf{k}_2} b_{\mathbf{k}_1 + \mathbf{k}_2 - \mathbf{k}}^\dagger b_{\mathbf{k}_1} a_{\mathbf{k}_2}, \quad (2a)$$

$$R_{\mathbf{k}}^{xx} = V_{xx} \sum_{\mathbf{k}_1, \mathbf{k}_2} b_{\mathbf{k}_1 + \mathbf{k}_2 - \mathbf{k}}^\dagger b_{\mathbf{k}_1} b_{\mathbf{k}_2}. \quad (2b)$$

In these equations, $a_{\mathbf{k}}$ ($b_{\mathbf{k}}$) annihilates a cavity photon (semiconductor exciton) with in-plane wave vector \mathbf{k} and energy $\omega_{\mathbf{k}}^c$ ($\omega_{\mathbf{k}}^x$). Ω_R is the dipole coupling strength between excitons and photons—the so-called Rabi frequency. In addition, n_{sat} denotes the exciton saturation density and V_{xx} is the exciton-exciton coupling strength.

The unitary Hopfield transformation to polaritons [29],

$$\begin{pmatrix} p_{1\mathbf{k}} \\ p_{2\mathbf{k}} \end{pmatrix} = \begin{pmatrix} X_{1\mathbf{k}} & C_{1\mathbf{k}} \\ X_{2\mathbf{k}} & C_{2\mathbf{k}} \end{pmatrix} \begin{pmatrix} b_{\mathbf{k}} \\ a_{\mathbf{k}} \end{pmatrix}, \quad (3)$$

which is tuned to diagonalize the linear part of the equations of motion (1), leads to the equations of motion in the polariton basis,

$$\frac{d}{dt}p_{1\mathbf{k}} = -i\omega_{1\mathbf{k}} p_{1\mathbf{k}} - iR_{1\mathbf{k}}^{NL}, \quad (4a)$$

$$\frac{d}{dt}p_{2\mathbf{k}} = -i\omega_{2\mathbf{k}} p_{2\mathbf{k}} - iR_{2\mathbf{k}}^{NL}, \quad (4b)$$

with $R_{j\mathbf{k}}^{NL} = X_{j\mathbf{k}} R_{\mathbf{k}}^{NL}$. Here, $p_{j\mathbf{k}}$ annihilates a polariton with dispersion $\omega_{j\mathbf{k}}$ in the lower ($j = 1$) or upper ($j = 2$) branch.

B. External driving and dissipation

To include losses through the mirrors, the interaction with lattice vibrations and the external laser driving, we couple the system dynamics to the environment. As shown in Ref. [38], combining the dynamics-controlled truncation scheme with the nonequilibrium quantum Langevin approach, the incoherent system dynamics decouples from parametric scattering processes. In particular, we have to add the damping rates $\Gamma_{j\mathbf{k}}^{(tot)}$ and Langevin noise source operators \mathcal{F} with proper statistics and moments to the equations of motion (4). This yields

$$\frac{d}{dt}p_{1\mathbf{k}} = -i\tilde{\omega}_{1\mathbf{k}} p_{1\mathbf{k}} - iR_{1\mathbf{k}}^{NL} + \mathcal{F}_{p_{1\mathbf{k}}}, \quad (5a)$$

$$\frac{d}{dt}p_{2\mathbf{k}} = -i\tilde{\omega}_{2\mathbf{k}} p_{2\mathbf{k}} - iR_{2\mathbf{k}}^{NL} + \mathcal{F}_{p_{2\mathbf{k}}}, \quad (5b)$$

where $\tilde{\omega}_{j\mathbf{k}} = \omega_{j\mathbf{k}} - i\Gamma_{j\mathbf{k}}^{(tot)}/2$. The operators \mathcal{F} are characterized by vanishing expectation values, $\langle \mathcal{F}_\mu \rangle = 0$, where

$\mu = p_{j\mathbf{k}}^{(\dagger)}$, and by the second-order moments

$$\langle \mathcal{F}_\mu(t) \mathcal{F}_\nu(t') \rangle = 2\langle D_{\mu\nu}(t) \rangle \delta(t - t') \quad (6)$$

with diffusion coefficients

$$2\langle D_{\mu\nu}(t) \rangle = \frac{d}{dt} \langle \mu(t) \nu(t) \rangle - \langle \dot{\mu}(t) \nu(t) + \mu(t) \dot{\nu}(t) \rangle. \quad (7)$$

In Eq. (7), the dot denotes the time-derivative following from Eqs. (4), i.e., without noise source operators \mathcal{F} .

Equations of motion for the expectation values $\langle \mu(t) \nu(t) \rangle$ —the so-called polariton photoluminescence—are given in Ref. [38]. They are derived in the framework of a second-order Born-Markov approach. Important for us is the final result: Due to the decoupling of incoherent dynamics and parametric processes the diffusion coefficients in Eq. (6) can be used as input when we calculate multitime correlation functions of polariton operators. We stress that the damping rates $\Gamma_{j\mathbf{k}}^{(tot)}$ follow from this treatment too.

C. Explicit pump scenario

Let us now consider the experimental setup introduced in Ref. [33], where four pump lasers drive the lower polariton branch at wave vectors $\mathbf{k}_{p1} = (k_p, k_p)$, $\mathbf{k}_{p2} = (-k_p, k_p)$, $\mathbf{k}_{p3} = (-k_p, -k_p)$, and $\mathbf{k}_{p4} = (k_p, -k_p)$ (see Fig. 1). The incident angles of all pumps are below the magic angle [21,40] such that single-pump scattering processes (signal at \mathbf{k} and idler at $2\mathbf{k}_{pn} - \mathbf{k}$) are negligible. The multipump parametric processes (signal at \mathbf{k} and idler at $\mathbf{k}_{pn} + \mathbf{k}_{pm} - \mathbf{k}$ with $n \neq m$) share a common idler mode at $\mathbf{k}_i = (0, 0)$. The four corresponding signal modes at $\mathbf{k}_{s1} = (0, 2k_p)$, $\mathbf{k}_{s2} = (-2k_p, 0)$, $\mathbf{k}_{s3} = (0, -2k_p)$, and $\mathbf{k}_{s4} = (2k_p, 0)$ have been shown to be entangled [33].

To obtain the equations of motion for the signal and idler modes, we introduce a simplified notation. In particular, because all scattering processes are within the lower polariton branch, we omit the branch index. In addition, we introduce $Y_x = Y_{1\mathbf{k}_x}$ for every quantity $Y = P, \omega, \Gamma^{(tot)}, \tilde{\omega}, R^{NL}, X, C$ and define $\gamma_x = \Gamma_x^{(tot)}/2$ for $x = i, s1, \dots, s4, p1, \dots, p4$. Because of the particular pump-signal-idler configuration, we have $\omega_{sn} \equiv \omega_s$, $\gamma_{sn} \equiv \gamma_s$, $X_{sn} \equiv X_s$, $C_{sn} \equiv C_s$, $\omega_{pn} \equiv \omega_p$, $X_{pn} \equiv X_p$, and $C_{pn} \equiv C_p$ for $n = 1, \dots, 4$.

Assuming classical pump fields $\langle p_{j\mathbf{k}_{pn}} \rangle = \mathcal{P}_n \in \mathbb{C}$, which imply a coherent driving, and identical pumps $\mathcal{P}_n \equiv \mathcal{P}$, we retain only terms containing the semiclassical pump amplitude \mathcal{P} twice. Introducing the vectors $\mathbf{P} = (p_i, p_{s1}^\dagger, \dots, p_{s4}^\dagger)^T$ and $\mathbf{F} = (F_{p_i}, F_{p_{s1}^\dagger}, \dots, F_{p_{s4}^\dagger})^T$, the equation of motion for the signal and idler modes takes the form:

$$\frac{d}{dt} \mathbf{P}(t) = \mathbf{M}(t) \mathbf{P}(t) + \mathbf{F}(t), \quad (8)$$

where

$$\mathbf{M} = \begin{pmatrix} -i\tilde{\omega}_i & -ig_s \mathcal{P}^2 & -ig_s \mathcal{P}^2 & -ig_s \mathcal{P}^2 & -ig_s \mathcal{P}^2 \\ ig_s (\mathcal{P}^*)^2 & i\tilde{\omega}_s^* & 0 & 0 & 0 \\ ig_s (\mathcal{P}^*)^2 & 0 & i\tilde{\omega}_s^* & 0 & 0 \\ ig_s (\mathcal{P}^*)^2 & 0 & 0 & i\tilde{\omega}_s^* & 0 \\ ig_s (\mathcal{P}^*)^2 & 0 & 0 & 0 & i\tilde{\omega}_s^* \end{pmatrix}, \quad (9)$$

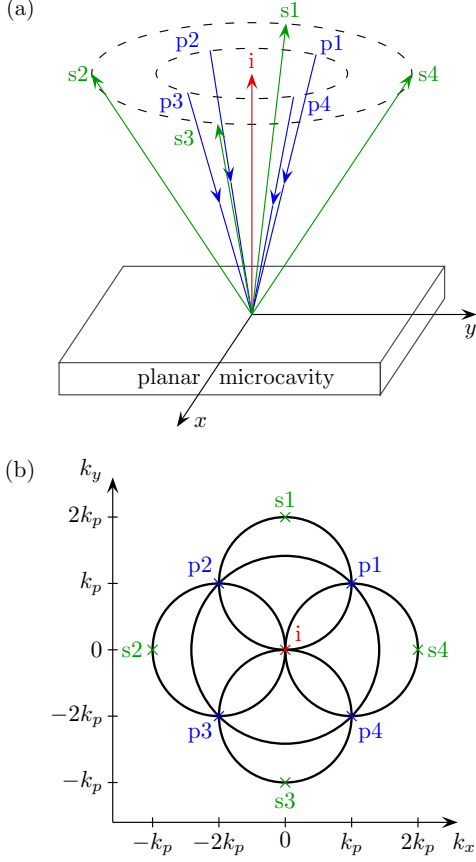


FIG. 1. (Color online) Sketch of the considered pump-signal-idler configuration in (a) position space and (b) momentum space. The circles in panel (b) display the possible energy- and momentum-conserving scattering processes within the lower branch, where two pumped polaritons scatter into pairs of signal and idler polaritons. Specifically, mixed-pump scattering processes of oppositely arranged (neighboring) pumps with $|\mathbf{k}_{pn} + \mathbf{k}_{pm}| = 0$ ($|\mathbf{k}_{pn} + \mathbf{k}_{pm}| = 2k_p$) contribute to the circle(s) with radius $\sqrt{2}k_p$ (k_p).

and

$$g_s = 2X_i X_s X_p \left(\frac{\Omega_R}{n_{sat}} C_p + V_{xx} X_p \right). \quad (10)$$

We note that the matrix \mathbf{M} depends on time solely, because the pump amplitude \mathcal{P} is time dependent.

D. State of emitted field

Defining the matrix \mathbf{G} of Green's functions as the solution of the homogeneous equation,

$$\frac{d}{dt} \mathbf{G}(t, t') = \mathbf{M}(t) \mathbf{G}(t, t'), \quad (11)$$

with the initial condition $\mathbf{G}(t, t) = \mathbb{I}$ (\mathbb{I} is the 5×5 identity matrix), the solution of the inhomogeneous

Eq. (8) is

$$\mathbf{P}(t) = \mathbf{G}(t, 0) \mathbf{P}(0) + \int_0^t \mathbf{G}(t, \tau) \mathbf{F}(\tau) d\tau. \quad (12)$$

It allows for the calculation of multitime correlation functions.

As a basis for the tomographic reconstruction of the measured signal and idler photon density matrix we choose the four states $|1_i, 1_{sn}\rangle$ ($n = 1, \dots, 4$), where $|1_x\rangle$ denotes the state of a photon in channel $x = i, s1, \dots, s4$. This choice can experimentally be realized by the postselection of events, where a click in the idler detector occurs, which takes out the vacuum component. Then the matrix elements of the measured photon density matrix $\rho_{i,sm;i,sn} = \langle 1_i, 1_{sm} | \rho | 1_i, 1_{sn} \rangle$ are given by

$$\begin{aligned} \rho_{i,sm;i,sn} &= \frac{1}{\mathcal{N}} \int_{T_d} \int_{T_d} \langle p_i^\dagger(t_1) p_{sm}^\dagger(t_2) p_{sn}(t_2) p_i(t_1) \rangle dt_1 dt_2 \\ &= \frac{1}{\mathcal{N}} \int_{T_d} \int_{T_d} [\langle p_i^\dagger(t_1) p_i(t_1) \rangle \langle p_{sm}^\dagger(t_2) p_{sn}(t_2) \rangle \\ &\quad + \langle p_i^\dagger(t_1) p_{sm}^\dagger(t_2) \rangle \langle p_{sn}(t_2) p_i(t_1) \rangle] dt_1 dt_2, \end{aligned} \quad (13)$$

where the second line follows from a Wick factorization. In this equation \mathcal{N} is a normalization constant and T_d is the detector window.

III. RESULTS

The equations from the last section allow us to study the tomographic reconstruction of the state of the emitted signal and idler fields in different situations. If the semiconductor microcavity is continuously pumped, the equations of motion can be solved analytically through transformation into the pump rotating frame. For Gaussian pump pulses—the usual experimental situation—the equations have to be solved numerically.

A. Analytical modeling

To obtain analytical results for the stationary state in the long-time limit we assume a continuous pumping, i.e., $\mathcal{P} = \bar{\mathcal{P}} e^{-i\omega_p t}$, with $\bar{\mathcal{P}} \in \mathbb{R}$. We define $\Delta = g_s \bar{\mathcal{P}}^2$ for abbreviation and perform a transformation into the pump rotating frame:

$$\bar{p}_{sn}^\dagger = p_{sn}^\dagger e^{-2i\omega_p t}, \quad \bar{F}_{p_{sn}^\dagger} = F_{p_{sn}^\dagger} e^{-2i\omega_p t}. \quad (14)$$

Defining

$$\mathbf{T}(t) = \begin{pmatrix} 1 & 0 & 0 & 0 & 0 \\ 0 & e^{-2i\omega_p t} & 0 & 0 & 0 \\ 0 & 0 & e^{-2i\omega_p t} & 0 & 0 \\ 0 & 0 & 0 & e^{-2i\omega_p t} & 0 \\ 0 & 0 & 0 & 0 & e^{-2i\omega_p t} \end{pmatrix}, \quad (15)$$

$$\bar{\mathbf{P}}(t) = \mathbf{T}(t) \mathbf{P}(t), \quad \text{and} \quad \bar{\mathbf{F}}(t) = \mathbf{T}(t) \mathbf{F}(t) \quad (16)$$

brings the equation of motion (8) to the form

$$\frac{d}{dt} \bar{\mathbf{P}}(t) = \bar{\mathbf{M}} \bar{\mathbf{P}}(t) + \bar{\mathbf{F}}(t), \quad (17)$$

with the time-independent matrix

$$\begin{aligned} \bar{\mathbf{M}} &= \mathbf{T}^{-1}(t)\mathbf{M}(t)\mathbf{T}(t) - 2i\omega_p \begin{pmatrix} 0 & 0 & 0 & 0 & 0 \\ 0 & 1 & 0 & 0 & 0 \\ 0 & 0 & 1 & 0 & 0 \\ 0 & 0 & 0 & 1 & 0 \\ 0 & 0 & 0 & 0 & 1 \end{pmatrix} \\ &= \begin{pmatrix} -\gamma_i & -i\Delta & -i\Delta & -i\Delta & -i\Delta \\ i\Delta & -\gamma_s & 0 & 0 & 0 \\ i\Delta & 0 & -\gamma_s & 0 & 0 \\ i\Delta & 0 & 0 & -\gamma_s & 0 \\ i\Delta & 0 & 0 & 0 & -\gamma_s \end{pmatrix} - i\omega_i \mathbb{I}. \end{aligned} \quad (18)$$

According to $\bar{\mathbf{G}}(t, t') = \mathbf{T}^{-1}(t)\mathbf{G}(t, t')\mathbf{T}(t')$, the Green's functions become a matrix exponential

$$\bar{\mathbf{G}}(t, t') = \exp\{\bar{\mathbf{M}}(t - t')\} = \bar{\mathbf{G}}(t - t'). \quad (19)$$

In order to calculate the populations and correlators in the long-time limit needed for the tomographic state reconstruction, we assume the condition $\gamma_s \gamma_i > 4\Delta^2$ to be fulfilled. This guarantees that all eigenvalues of $\bar{\mathbf{M}}$ have negative real parts; i.e., the corresponding Green's functions converge in the long-time limit. In addition, we assume a (dimensionless) uniform noise background N_b , characterized by $\langle \mathcal{F}_{p_x}(t)\mathcal{F}_{p_y}(t') \rangle = \langle \mathcal{F}_{p_x}^\dagger(t)\mathcal{F}_{p_y}^\dagger(t') \rangle = 0$, $\langle \mathcal{F}_{p_x}^\dagger(t)\mathcal{F}_{p_y}(t') \rangle = N_b \Gamma_x \delta_{x,y} \delta(t - t')$, and $\langle \mathcal{F}_{p_x}(t)\mathcal{F}_{p_y}^\dagger(t') \rangle = (N_b + 1) \Gamma_x \delta_{x,y} \delta(t - t')$, with $x, y = i, s1, \dots, s4$. As shown in the Appendix, the tomographic reconstruction is

$$\rho = \frac{X}{4} \begin{pmatrix} 1 & 1 & 1 & 1 \\ 1 & 1 & 1 & 1 \\ 1 & 1 & 1 & 1 \\ 1 & 1 & 1 & 1 \end{pmatrix} + \frac{1-X}{4} \begin{pmatrix} 1 & 0 & 0 & 0 \\ 0 & 1 & 0 & 0 \\ 0 & 0 & 1 & 0 \\ 0 & 0 & 0 & 1 \end{pmatrix}, \quad (20)$$

with $X \in [0, 1]$. The state ρ in Eq. (20) is a mixture of a pure (fully entangled) W state and a (not entangled) identity state. In the four-partite case under study, full entanglement means that neither subsystem can be separated. The parameter X is the weight of the W state in the mixture ρ . For $X = 1$, ρ is fully entangled. Contrariwise, ρ is fully separable for $X = 0$. Clearly the state ρ is entangled for any finite $X > 0$. In this sense, X can be taken as an entanglement measure, which quantifies the violation of a corresponding Bell inequality.

Figure 2 shows X as a function of Δ/γ and N_b for $\gamma = \gamma_i = \gamma_s$. We note that the parameter Δ is proportional to the pump intensity, which, however, is limited by the stationarity condition $4\Delta^2 < \gamma_i \gamma_s$. Obviously, the fully entangled pure W state is obtained for vanishing noise background. This result is in accordance with the discussion in our previous article [33], where losses through the cavity mirrors and the coupling to lattice vibrations are neglected. Interestingly, even for a finite noise background $N_b > 0$ the pure W state can be generated if the pump power is high enough. Lowering the pump power at fixed N_b leads to a decrease of entanglement.

B. Numerical solution

Numerically, we can also study the case of Gaussian pump pulses. In practice, we solve Eq. (11) for Gaussian pump pulses, having an intensity maximum at 4 ps and a width of 1 ps, and calculate the populations and correlators

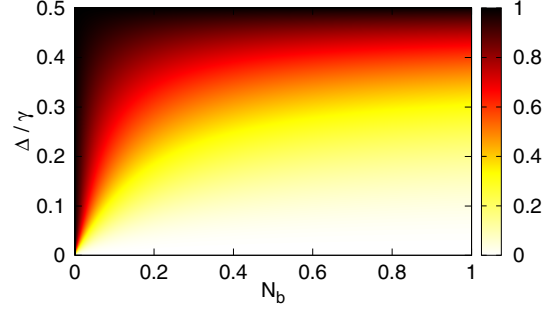


FIG. 2. (Color online) Amount of entanglement in the state ρ [Eq. (20)], quantified by X as a function of Δ/γ and N_b , for $\gamma = \gamma_i = \gamma_s$.

to do the tomography. Thereby we choose a reasonable detection window of $T_d = 120$ ps, allowing for technically feasible experiments with standard photodetectors. Again, the tomographic reconstruction results in a state of the form (20); i.e., it is fully characterized by a single parameter X . The amount of entanglement quantified by X is shown in Fig. 3(a) in dependence on the pump intensity at various temperatures, while Fig. 3(b) gives X as a function

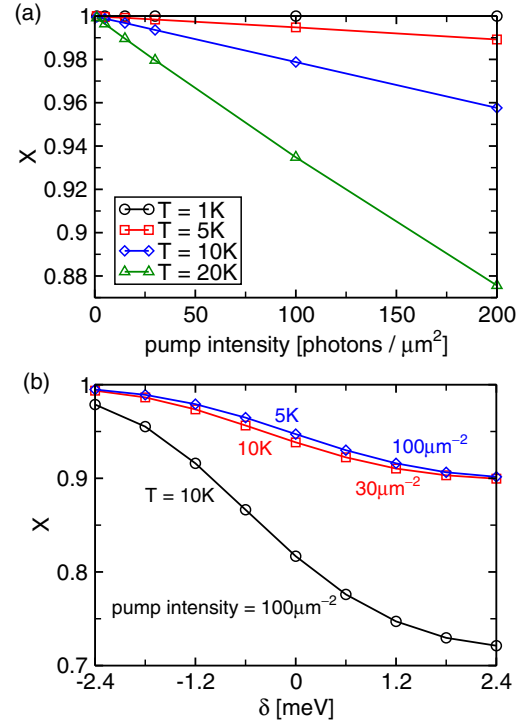


FIG. 3. (Color online) Entanglement of the numerically reconstructed signal density matrix as a function of the pump intensity (a) and the detuning $\delta = \omega_0^c - \omega_0^x$ (b). The results in panel (a) are calculated for different environment temperatures but fixed detuning $\delta = -2.4$ meV, whereas data in panel (b) are obtained for different environment temperatures and pump intensities. Other parameters of the investigated sample can be found in Ref. [21].

of the detuning $\delta = \omega_0^c - \omega_0^x$. The remaining system parameters are fixed in accordance with Refs. [21,25,26], where a specific semiconductor microcavity sample was investigated.

Compared to the analytical solution in the last section, we have set the uniform noise background N_b to 0. Noise enters the equations through the pump-induced photoluminescence [41] that depends on the temperature of the reservoirs. The choice $N_b = 0$ is the reason why the numerical results in Fig. 3(a) tend to 1 for vanishing pump intensity. Contrary to the long-time behavior for continuous pumps, an increase in the pump intensity leads to a decrease of the entanglement. This behavior is even more pronounced for higher reservoir temperatures. The reason for this is a temperature-dependent background, created by the pump-induced photoluminescence, on top of which parametric scattering, i.e., entanglement generation, takes place. Increasing the temperature at a fixed pump intensity leads to a higher background at a fixed number of parametric scattering processes and hence to a lower degree of entanglement. Nevertheless, the generated entanglement is surprisingly robust [see the range of X in Fig. 3(a)], even in the full simulation which includes the losses through the cavity mirrors and the coupling to lattice vibrations.

When one keeps the environment temperature and the pump intensity fixed, the entanglement decreases if the detuning is increased [see Fig. 3(b)]. This happens as a consequence of the suppression of exciton and photon mixing for positive detuning, which weakens the polariton parametric scattering strength. Increasing the environment temperature or the pump intensity leads to a decrease of entanglement, but the functional δ dependence remains similar. Interestingly, even for large

positive detuning a finite amount of entanglement is generated by the microcavity.

IV. CONCLUSIONS

We have studied the generation of multipartite entangled light in semiconductor microcavities within the dynamics-controlled truncation scheme. If one includes the losses through the cavity mirrors and the coupling to lattice vibrations, this formalism allows for a decoupling of the incoherent system dynamics (pump-induced photoluminescence) from the parametric scattering processes as the source of entanglement. After calculation of particular multitime correlation functions, the state of the emitted signal and idler fields is obtained through tomographic reconstruction. The resulting multipartite entanglement between the four signal channels for both continuous pumping and Gaussian pump pulses is robust against decoherence under realistic experimental conditions. This observation shows that the emitted photons carry the initial polariton entanglement. Since polaritons are quasiparticles composed of cavity photons and semiconductor excitons, they can sustain pair correlations over long times and distances inside such solid-state devices. In this sense, the emitted photons serve as a probe of the internal entanglement properties.

ACKNOWLEDGMENTS

The authors would like to thank Z. Vörös and S. Portolan for valuable discussions; D.P. acknowledges the hospitality at the Photonics group at the University of Innsbruck. This work was supported by the Deutsche Forschungsgemeinschaft (Germany) through the Collaborative Research Center 652, Project B5.

APPENDIX: EXPLICIT SOLUTION FOR CONTINUOUS PUMPING

Here, we evaluate the stationary populations and correlations in the long-time limit. We start with the diagonalization of the matrix $\bar{\mathbf{M}}$ from Eq. (18). The eigenvalues of $\bar{\mathbf{M}}$ are

$$\lambda_1 = \lambda_2 = \lambda_3 = -\gamma_s - i\omega_i, \quad \lambda_{4/5} = -\frac{1}{2}(\gamma_i + \gamma_s \pm \sqrt{(\gamma_i - \gamma_s)^2 + 16\Delta^2}) - i\omega_i. \quad (\text{A1})$$

To simplify the notation, we introduce $\Omega = \sqrt{(\gamma_i - \gamma_s)^2 + 16\Delta^2}$, $\lambda = -\gamma_s - i\omega_i$, and $\lambda_{\pm} = \lambda - \lambda_{4/5} = (\gamma_i - \gamma_s \pm \Omega)/2$, with $\lambda_+ > 0$ and $\lambda_- < 0$. With these definitions, the matrix \mathbf{V} of eigenvectors is

$$\mathbf{V} = \frac{1}{\sqrt{2\Omega\lambda_+|\lambda_-|}} \begin{pmatrix} 0 & 0 & 0 & -\sqrt{2|\lambda_-|}\lambda_+ & \sqrt{2\lambda_+|\lambda_-|} \\ -\sqrt{\Omega\lambda_+|\lambda_-|} & -\sqrt{\Omega\lambda_+|\lambda_-|} & -\sqrt{\Omega\lambda_+|\lambda_-|} & \sqrt{2|\lambda_-|}i\Delta & \sqrt{2\lambda_+}i\Delta \\ 0 & 0 & \sqrt{\Omega\lambda_+|\lambda_-|} & \sqrt{2|\lambda_-|}i\Delta & \sqrt{2\lambda_+}i\Delta \\ 0 & \sqrt{\Omega\lambda_+|\lambda_-|} & 0 & \sqrt{2|\lambda_-|}i\Delta & \sqrt{2\lambda_+}i\Delta \\ \sqrt{\Omega\lambda_+|\lambda_-|} & 0 & 0 & \sqrt{2|\lambda_-|}i\Delta & \sqrt{2\lambda_+}i\Delta \end{pmatrix}, \quad (\text{A2})$$

such that

$$\mathbf{V}^{-1}\bar{\mathbf{M}}\mathbf{V} = \lambda\mathbb{I} - \begin{pmatrix} 0 & 0 & 0 & 0 & 0 \\ 0 & 0 & 0 & 0 & 0 \\ 0 & 0 & 0 & 0 & 0 \\ 0 & 0 & 0 & \lambda_+ & 0 \\ 0 & 0 & 0 & 0 & \lambda_- \end{pmatrix}. \quad (\text{A3})$$

The matrix $\overline{\mathbf{G}}$ of the Green's functions is given by

$$\overline{\mathbf{G}}(t) = e^{\lambda t} \mathbf{V} \begin{pmatrix} 1 & 0 & 0 & 0 & 0 \\ 0 & 1 & 0 & 0 & 0 \\ 0 & 0 & 1 & 0 & 0 \\ 0 & 0 & 0 & e^{-\lambda+t} & 0 \\ 0 & 0 & 0 & 0 & e^{-\lambda-t} \end{pmatrix} \mathbf{V}^{-1} = e^{\lambda t} \begin{pmatrix} G_{i,i}(t) & G_{i,s}(t) & G_{i,s'}(t) & G_{i,s}(t) & G_{i,s}(t) \\ G_{i,s}^*(t) & G_{s,s}(t) & G_{s,s'}(t) & G_{s,s'}(t) & G_{s,s'}(t) \\ G_{i,s}^*(t) & G_{s,s'}(t) & G_{s,s}(t) & G_{s,s'}(t) & G_{s,s'}(t) \\ G_{i,s}^*(t) & G_{s,s'}(t) & G_{s,s'}(t) & G_{s,s}(t) & G_{s,s'}(t) \\ G_{i,s}^*(t) & G_{s,s'}(t) & G_{s,s'}(t) & G_{s,s'}(t) & G_{s,s}(t) \end{pmatrix}, \quad (\text{A4})$$

with matrix elements

$$G_{i,i}(t) = e^{-\frac{1}{2}(\gamma_i - \gamma_s)t} \left(\cosh \frac{\Omega}{2} t - \frac{\gamma_i - \gamma_s}{\Omega} \sinh \frac{\Omega}{2} t \right), \quad (\text{A5a})$$

$$G_{i,s}(t) = -2i \frac{\Delta}{\Omega} e^{-\frac{1}{2}(\gamma_i - \gamma_s)t} \sinh \frac{\Omega}{2} t, \quad (\text{A5b})$$

$$G_{s,s}(t) = \frac{3}{4} + \frac{e^{-\frac{1}{2}(\gamma_i - \gamma_s)t}}{4} \left(\cosh \frac{\Omega}{2} t + \frac{\gamma_i - \gamma_s}{\Omega} \sinh \frac{\Omega}{2} t \right), \quad (\text{A5c})$$

$$G_{s,s'}(t) = G_{s,s}(t) - 1. \quad (\text{A5d})$$

Convergence of these functions requires $\gamma_i + \gamma_s > \Omega$, i.e., $\gamma_i \gamma_s > 4\Delta^2$.

Introduction of the uniform noise background N_b allows for the evaluation of the idler and signal populations in the long-time limit. This yields

$$\begin{aligned} N_{i,i}^\infty &\equiv \lim_{t \rightarrow \infty} \langle p_i^\dagger(t) p_i(t) \rangle = \int_0^\infty 2e^{-2\gamma_s t} \{ N_b \gamma_i G_{i,i}^2(\tau) + 4(N_b + 1) \gamma_s |G_{i,s}(\tau)|^2 \} d\tau \\ &= \frac{N_b \gamma_i}{\gamma_i + \gamma_s} \frac{\gamma_s (\gamma_i + \gamma_s) - 4\Delta^2}{\gamma_i \gamma_s - 4\Delta^2} + \frac{(N_b + 1) \gamma_s}{\gamma_i + \gamma_s} \frac{4\Delta^2}{\gamma_i \gamma_s - 4\Delta^2}, \end{aligned} \quad (\text{A6})$$

$$N_{s,s}^\infty \equiv \lim_{t \rightarrow \infty} \langle p_s^\dagger(t) p_s(t) \rangle = \frac{(N_b + 1) \gamma_i}{\gamma_i + \gamma_s} \frac{\Delta^2}{\gamma_i \gamma_s - 4\Delta^2} + \frac{3N_b}{4} + \frac{N_b \gamma_s}{4(\gamma_i + \gamma_s)} \frac{\gamma_i (\gamma_i + \gamma_s) - 4\Delta^2}{\gamma_i \gamma_s - 4\Delta^2}, \quad (\text{A7})$$

and the correlators become

$$N_{s,s'}^\infty \equiv \lim_{t \rightarrow \infty} \langle P_s^\dagger(t) P_{s'}(t) \rangle = \frac{(N_b + 1) \gamma_i}{\gamma_i + \gamma_s} \frac{\Delta^2}{\gamma_i \gamma_s - 4\Delta^2} - \frac{N_b}{4} + \frac{N_b \gamma_s}{4(\gamma_i + \gamma_s)} \frac{\gamma_i (\gamma_i + \gamma_s) - 4\Delta^2}{\gamma_i \gamma_s - 4\Delta^2}, \quad (\text{A8})$$

$$N_{i,s}^\infty \equiv \lim_{t, t' \rightarrow \infty} \langle P_i^\dagger(t) P_s^\dagger(t') \rangle = \frac{i(2N_b + 1) \gamma_i \gamma_s \Delta}{(\gamma_i + \gamma_s)(\gamma_i \gamma_s - 4\Delta^2)}. \quad (\text{A9})$$

Finally, the tomographic reconstruction results in the state

$$\rho = \frac{1}{4} \frac{N_{i,i}^\infty N_{s,s'}^\infty + |N_{i,s}^\infty|^2}{N_{i,i}^\infty N_{s,s}^\infty + |N_{i,s}^\infty|^2} \begin{pmatrix} 1 & 1 & 1 & 1 \\ 1 & 1 & 1 & 1 \\ 1 & 1 & 1 & 1 \\ 1 & 1 & 1 & 1 \end{pmatrix} + \frac{1}{4} \left(1 - \frac{N_{i,i}^\infty N_{s,s'}^\infty + |N_{i,s}^\infty|^2}{N_{i,i}^\infty N_{s,s}^\infty + |N_{i,s}^\infty|^2} \right) \begin{pmatrix} 1 & 0 & 0 & 0 \\ 0 & 1 & 0 & 0 \\ 0 & 0 & 1 & 0 \\ 0 & 0 & 0 & 1 \end{pmatrix}, \quad (\text{A10})$$

such that the value of X in Eq. (20) becomes

$$X = \frac{N_{i,i}^\infty N_{s,s'}^\infty + |N_{i,s}^\infty|^2}{N_{i,i}^\infty N_{s,s}^\infty + |N_{i,s}^\infty|^2}. \quad (\text{A11})$$

-
- [1] R. Horodecki, P. Horodecki, M. Horodecki, and R. Horodecki, *Rev. Mod. Phys.* **81**, 865 (2009).
[2] O. Gühne and G. Tóth, *Phys. Rep.* **474**, 1 (2009).
[3] M. A. Nielsen and I. L. Chuang, *Quantum Computation and Quantum Information* (Cambridge University Press, Cambridge, UK, 2010).
[4] A. Einstein, B. Podolsky, and N. Rosen, *Phys. Rev.* **47**, 777 (1935).
[5] E. Schrödinger, *Naturwissenschaften* **23**, 807 (1935).
[6] R. F. Werner, *Phys. Rev. A* **40**, 4277 (1989).
[7] D. M. Greenberger, M. A. Horne, and A. Zeilinger, *Going Beyond Bells Theorem in Bells Theorem, Quantum Theory, and Conceptions of the Universe* (Kluwer Academic, Dordrecht, 1989).
[8] W. Dür, G. Vidal, and J. I. Cirac, *Phys. Rev. A* **62**, 062314 (2000).
[9] M. Horodecki, P. Horodecki, and R. Horodecki, *Phys. Lett. A* **223**, 1 (1996).
[10] M. Horodecki, P. Horodecki, and R. Horodecki, *Phys. Lett. A* **283**, 1 (2001).

- [11] F. G. S. L. Brandao, *Phys. Rev. A* **72**, 022310 (2005).
- [12] J. Sperling and W. Vogel, *Phys. Rev. A* **83**, 042315 (2011).
- [13] J. Sperling and W. Vogel, *Phys. Rev. Lett.* **111**, 110503 (2013).
- [14] A. Reusch, J. Sperling, and W. Vogel, *Phys. Rev. A* **91**, 042324 (2015).
- [15] P. G. Kwiat, K. Mattle, H. Weinfurter, A. Zeilinger, A. V. Sergienko, and Y. Shih, *Phys. Rev. Lett.* **75**, 4337 (1995).
- [16] V. M. Axt and T. Kuhn, *Rep. Prog. Phys.* **67**, 433 (2004).
- [17] O. Benson, C. Santori, M. Pelton, and Y. Yamamoto, *Phys. Rev. Lett.* **84**, 2513 (2000).
- [18] U. Hohenester, C. Sifel, and P. Koskinen, *Phys. Rev. B* **68**, 245304 (2003).
- [19] C. Weisbuch, M. Nishioka, A. Ishikawa, and Y. Arakawa, *Phys. Rev. Lett.* **69**, 3314 (1992).
- [20] R. Houdré, C. Weisbuch, R. P. Stanley, U. Oesterle, P. Pellandini, and M. Illegems, *Phys. Rev. Lett.* **73**, 2043 (1994).
- [21] W. Langbein, *Phys. Rev. B* **70**, 205301 (2004).
- [22] C. Ciuti, G. Bastard, and I. Carusotto, *Phys. Rev. B* **72**, 115303 (2005).
- [23] C. Ciuti, *Phys. Rev. B* **69**, 245304 (2004).
- [24] C. Ciuti, P. Schwendimann, and A. Quattropani, *Phys. Rev. B* **63**, 041303 (2001).
- [25] S. Savasta, O. Di Stefano, V. Savona, and W. Langbein, *Phys. Rev. Lett.* **94**, 246401 (2005).
- [26] S. Portolan, O. Di Stefano, S. Savasta, and V. Savona, *Europhys. Lett.* **88**, 20003 (2009).
- [27] S. Portolan, L. Einkemmer, Z. Vörös, G. Weihs, and P. Rabl, *New J. Phys.* **16**, 063030 (2014).
- [28] L. Einkemmer, Z. Vörös, G. Weihs, and S. Portolan, *Phys. Status Solidi B* **252**, 1749 (2015).
- [29] J. J. Hopfield, *Phys. Rev.* **112**, 1555 (1958).
- [30] T. Östreich, K. Schönhammer, and L. J. Sham, *Phys. Rev. B* **58**, 12920 (1998).
- [31] F. Tassone and Y. Yamamoto, *Phys. Rev. B* **59**, 10830 (1999).
- [32] D. Pagel, H. Fehske, J. Sperling, and W. Vogel, *Phys. Rev. A* **86**, 052313 (2012).
- [33] D. Pagel, H. Fehske, J. Sperling, and W. Vogel, *Phys. Rev. A* **88**, 042310 (2013).
- [34] E. A. Sete, H. Eleuch, and C. R. Ooi, [arXiv:1504.06318](https://arxiv.org/abs/1504.06318).
- [35] T. Usui, *Prog. Theor. Phys.* **23**, 787 (1960).
- [36] V. M. Axt and A. Stahl, *Z. Phys. B* **93**, 195 (1994).
- [37] S. Savasta and R. Girlanda, *Phys. Rev. Lett.* **77**, 4736 (1996).
- [38] S. Portolan, O. Di Stefano, S. Savasta, F. Rossi, and R. Girlanda, *Phys. Rev. B* **77**, 035433 (2008).
- [39] S. Portolan, O. Di Stefano, S. Savasta, F. Rossi, and R. Girlanda, *Phys. Rev. B* **77**, 195305 (2008).
- [40] P. G. Savvidis, J. J. Baumberg, R. M. Stevenson, M. S. Skolnick, D. M. Whittaker, and J. S. Roberts, *Phys. Rev. Lett.* **84**, 1547 (2000).
- [41] F. Rossi, T. Meier, P. Thomas, S. W. Koch, P. E. Selbmann, and E. Molinari, *Phys. Rev. B* **51**, 16943 (1995).

Bibliography

- [1] H. J. Carmichael, *Statistical Methods in Quantum Optics 1*, Springer, Berlin, 1999.
- [2] H.-P. Breuer and F. Petruccione, *The Theory of Open Quantum Systems*, Oxford University Press, Oxford, 2007.
- [3] L. K. Grover, *Phys. Rev. Lett.* **79**, 325 (1997).
- [4] P. Shor, *SIAM J. Comput.* **26**, 1484 (1997).
- [5] R. P. Feynman, *Int. J. Theor. Phys.* **21**, 467 (1982).
- [6] S. Lloyd, *Science* **273**, 1073 (1996).
- [7] M. A. Nielsen and I. L. Chuang, *Quantum Computation and Quantum Information*, Cambridge University Press, Cambridge, 2010.
- [8] U. Weiss, *Quantum Dissipative Systems*, World Scientific, Singapore, 2012.
- [9] L. M. K. Vandersypen, M. Steffen, G. Breyta, C. S. Yannoni, M. H. Sherwood, and I. L. Chuang, *Nature* **414**, 883 (2001).
- [10] J. I. Cirac and P. Zoller, *Physics Today* **57**, 38 (2004).
- [11] J. Du, N. Xu, X. Peng, P. Wang, S. Wu, and D. Lu, *Phys. Rev. Lett.* **104**, 030502 (2010).
- [12] R. Sánchez and M. Büttiker, *Phys. Rev. B* **83**, 085428 (2011).
- [13] N. Linden, S. Popescu, and P. Skrzypczyk, *Phys. Rev. Lett.* **105**, 130401 (2010).
- [14] M. Campisi, F. Zhan, P. Talkner, and P. Hänggi, *Phys. Rev. Lett.* **108**, 250601 (2012).
- [15] G. Schaller, *Open Quantum Systems Far from Equilibrium*, volume 881 of *Lecture Notes in Physics*, Springer, Heidelberg, 2014.
- [16] A. Einstein, B. Podolsky, and N. Rosen, *Phys. Rev.* **47**, 777 (1935).
- [17] E. Schrödinger, *Naturwiss.* **23**, 807 (1935).
- [18] R. Horodecki, P. Horodecki, M. Horodecki, and R. Horodecki, *Rev. Mod. Phys.* **81**, 865 (2009).
- [19] R. F. Werner, *Phys. Rev. A* **40**, 4277 (1989).
- [20] J. S. Bell, *Physics (Long Island City, N.Y.)* **1**, 195 (1964).

- [21] D. M. Greenberger, M. A. Horne, and A. Zeilinger, *Going Beyond Bells Theorem in Bells Theorem, Quantum Theory, and Conceptions of the Universe*, Kluwer Academic, Dordrecht, 1989.
- [22] W. Dür, G. Vidal, and J. I. Cirac, *Phys. Rev. A* **62**, 062314 (2000).
- [23] M. Horodecki, P. Horodecki, and R. Horodecki, *Phys. Lett. A* **223**, 1 (1996).
- [24] M. Horodecki, P. Horodecki, and R. Horodecki, *Phys. Lett. A* **283**, 1 (2001).
- [25] V. Vedral, M. B. Plenio, M. A. Rippin, and P. L. Knight, *Phys. Rev. Lett.* **78**, 2275 (1997).
- [26] G. Vidal, *J. Mod. Opt.* **47**, 355 (2000).
- [27] F. G. S. L. Brandao, *Phys. Rev. A* **72**, 022310 (2005).
- [28] J. Sperling and W. Vogel, *Physica Scripta* **83**, 045002 (2011).
- [29] J. Sperling and W. Vogel, *Phys. Rev. Lett.* **111**, 110503 (2013).
- [30] P. G. Kwiat, K. Mattle, H. Weinfurter, A. Zeilinger, A. V. Sergienko, and Y. Shih, *Phys. Rev. Lett.* **75**, 4337 (1995).
- [31] V. M. Axt and T. Kuhn, *Rep. Prog. Phys.* **67**, 433 (2004).
- [32] S. Gerke, J. Sperling, W. Vogel, Y. Cai, J. Roslund, N. Treps, and C. Fabre, *Phys. Rev. Lett.* **114**, 050501 (2015).
- [33] O. Benson, C. Santori, M. Pelton, and Y. Yamamoto, *Phys. Rev. Lett.* **84**, 2513 (2000).
- [34] U. Hohenester, C. Sifel, and P. Koskinen, *Phys. Rev. B* **68**, 245304 (2003).
- [35] C. Weisbuch, M. Nishioka, A. Ishikawa, and Y. Arakawa, *Phys. Rev. Lett.* **69**, 3314 (1992).
- [36] W. Langbein, *Phys. Rev. B* **70**, 205301 (2004).
- [37] C. Ciuti, G. Bastard, and I. Carusotto, *Phys. Rev. B* **72**, 115303 (2005).
- [38] R. Houdré, C. Weisbuch, R. P. Stanley, U. Oesterle, P. Pellandini, and M. Ilegems, *Phys. Rev. Lett.* **73**, 2043 (1994).
- [39] C. Ciuti, *Phys. Rev. B* **69**, 245304 (2004).
- [40] C. Ciuti, P. Schwendimann, and A. Quattropani, *Phys. Rev. B* **63**, 041303 (2001).
- [41] S. Savasta, O. Di Stefano, V. Savona, and W. Langbein, *Phys. Rev. Lett.* **94**, 246401 (2005).
- [42] S. Portolan, O. Di Stefano, S. Savasta, and V. Savona, *Europhys. Lett.* **88**, 20003 (2009).

-
- [43] S. Portolan, L. Einkemmer, Z. Vörös, G. Weihs, and P. Rabl, *New J. Phys.* **16**, 063030 (2014).
- [44] F. Tassone and Y. Yamamoto, *Phys. Rev. B* **59**, 10830 (1999).
- [45] B. M. Terhal and P. Horodecki, *Phys. Rev. A* **61**, 040301 (2000).
- [46] T. Usui, *Prog. Theor. Phys.* **23**, 787 (1960).
- [47] G. Rochat, C. Ciuti, V. Savona, C. Piermarocchi, A. Quattropani, and P. Schwendimann, *Phys. Rev. B* **61**, 13856 (2000).
- [48] J. J. Hopfield, *Phys. Rev.* **112**, 1555 (1958).
- [49] J. von Neumann, *Mathematische Grundlagen der Quantenmechanik*, Springer, Berlin, 1996.
- [50] P. G. Savvidis, J. J. Baumberg, R. M. Stevenson, M. S. Skolnick, D. M. Whittaker, and J. S. Roberts, *Phys. Rev. Lett.* **84**, 1547 (2000).
- [51] J. Sperling and W. Vogel, *Phys. Rev. A* **79**, 022318 (2009).
- [52] J. Sperling and W. Vogel, *Phys. Rev. A* **83**, 042315 (2011).
- [53] A. A. Semenov and W. Vogel, *Phys. Rev. A* **81**, 023835 (2010).
- [54] D. Y. Vasylyev, A. A. Semenov, and W. Vogel, *Phys. Rev. Lett.* **108**, 220501 (2012).
- [55] L. Knöll, W. Vogel, and D.-G. Welsch, *Phys. Rev. A* **43**, 543 (1991).
- [56] A. A. Semenov and W. Vogel, *Phys. Rev. A* **80**, 021802(R) (2009).
- [57] T. Barthel and U. Schollwöck, *Phys. Rev. Lett.* **100**, 100601 (2008).
- [58] N. Linden, S. Popescu, A. J. Short, and A. Winter, *Phys. Rev. E* **79**, 061103 (2009).
- [59] P. Reimann, *Phys. Rev. Lett.* **101**, 190403 (2008).
- [60] P. Reimann, *New J. Phys.* **12**, 055027 (2010).
- [61] V. I. Yukalov, *Laser Phys. Lett.* **8**, 485 (2011).
- [62] F. Haake and R. Reibold, *Phys. Rev. A* **32**, 2462 (1985).
- [63] G. W. Ford, J. T. Lewis, and R. F. O'Connell, *Phys. Rev. Lett.* **55**, 2273 (1985).
- [64] G. W. Ford, J. T. Lewis, and R. F. O'Connell, *Ann. Phys. (N.Y.)* **185**, 270 (1988).
- [65] C. Zerbe and P. Hänggi, *Phys. Rev. E* **52**, 1533 (1995).
- [66] G. W. Ford and R. F. O'Connell, *Phys. Rev. B* **75**, 134301 (2007).

- [67] U. Weiss, *Quantum Dissipative Systems*, World Scientific, Singapore, 1999.
- [68] P. Ullersma, *Physica* **32**, 27 (1966).
- [69] P. Ullersma, *Physica* **32**, 74 (1966).
- [70] R. J. Rubin, *J. Math. Phys.* **1**, 309 (1960).
- [71] H. S. Robertson and M. A. Huerta, *Phys. Rev. Lett.* **23**, 825 (1969).
- [72] G. S. Agarwal, *Phys. Rev. A* **3**, 828 (1971).
- [73] M. A. Huerta, H. S. Robertson, and J. C. Nearing, *J. Math. Phys.* **12**, 2305 (1971).
- [74] E. Wigner, *Phys. Rev.* **40**, 749 (1932).
- [75] U. M. B. Marconi, A. Puglisi, L. Rondoni, and A. Vulpiani, *Phys. Rep.* **461**, 111 (2008).
- [76] M. Esposito, U. Harbola, and S. Mukamel, *Rev. Mod. Phys.* **81**, 1665 (2009).
- [77] M. Campisi, P. Hänggi, and P. Talkner, *Rev. Mod. Phys.* **83**, 771 (2011).
- [78] C. Jarzynski, *Annu. Rev. Condens. Matter Phys.* **2**, 329 (2011).
- [79] W. Sutherland, *Phil. Mag.* **3**, 161 (1902).
- [80] A. Einstein, *Ann. Phys.* **17**, 549 (1905).
- [81] H. B. Callen and T. A. Welton, *Phys. Rev.* **83**, 34 (1951).
- [82] M. S. Green, *J. Chem. Phys.* **22**, 398 (1954).
- [83] R. Kubo, *J. Phys. Soc. Jpn.* **12**, 570 (1957).
- [84] R. J. Glauber, *Physics Reports* **131**, 2766 (1963).
- [85] S. Singh, *Optics Communications* **44**, 254 (1983).
- [86] L. Mandel and E. Wolf, *Optical Coherence and Quantum Optics*, Cambridge University Press, Cambridge, 1995.
- [87] M. J. Collett and C. W. Gardiner, *Phys. Rev. A* **30**, 1386 (1984).
- [88] C. W. Gardiner and M. J. Collett, *Phys. Rev. A* **31**, 3761 (1985).
- [89] R. Graham, *Z. Phys. B* **76**, 265 (1989).
- [90] F. Beaudoin, J. M. Gambetta, and A. Blais, *Phys. Rev. A* **84**, 043832 (2011).
- [91] R. Alicki, D. A. Lidar, and P. Zanardi, *Phys. Rev. A* **73**, 052311 (2006).
- [92] G. Schaller and T. Brandes, *Phys. Rev. A* **78**, 022106 (2008).
- [93] G. S. Agarwal, *Quantum Optics*, Cambridge University Press, Cambridge, 2013.

- [94] R. H. Dicke, *Phys. Rev.* **93**, 99 (1954).
- [95] F. Dimer, B. Estienne, A. S. Parkins, and H. J. Carmichael, *Phys. Rev. A* **75**, 013804 (2007).
- [96] M. P. Baden, K. J. Arnold, A. L. Grimsmo, S. Parkins, and M. D. Barrett, *Phys. Rev. Lett.* **113**, 020408 (2014).
- [97] V. M. Axt and A. Stahl, *Z. Phys. B* **93**, 195 (1994).
- [98] S. Savasta and R. Girlanda, *Phys. Rev. Lett.* **77**, 4736 (1996).
- [99] S. Portolan, O. Di Stefano, S. Savasta, F. Rossi, and R. Girlanda, *Phys. Rev. B* **77**, 035433 (2008).
- [100] S. Portolan, O. Di Stefano, S. Savasta, F. Rossi, and R. Girlanda, *Phys. Rev. B* **77**, 195305 (2008).
- [101] D. F. V. James, P. G. Kwiat, W. J. Munro, and A. G. White, *Phys. Rev. A* **64**, 052312 (2001).

Scientific Contributions

Publications

- (a) *Strongly entangled light from planar microcavities*, D. Pagel, H. Fehske, J. Sperling, and W. Vogel, *Phys. Rev. A* **86**, 052313 (2012). Copyright (2012) by the American Physical Society.
- (b) *Equilibration and thermalization of the dissipative quantum harmonic oscillator in a nonthermal environment*, D. Pagel, A. Alvermann, and H. Fehske, *Phys. Rev. E* **87**, 012127 (2013). Copyright (2013) by the American Physical Society.
- (c) *Nonequilibrium quantum fluctuation relations for harmonic systems in nonthermal environments*, D. Pagel, P. Nalbach, A. Alvermann, H. Fehske, and M. Thorwart, *New J. Phys.* **15**, 105008 (2013). Copyright (2013) by the IOP Publishing Ltd and the Deutsche Physikalische Gesellschaft.
- (d) *Multipartite entangled light from driven microcavities*, D. Pagel, H. Fehske, J. Sperling, and W. Vogel, *Phys. Rev. A* **88**, 042310 (2013). Copyright (2013) by the American Physical Society.
- (e) *Nonclassical light from few emitters in a cavity*, D. Pagel, A. Alvermann, and H. Fehske, *Phys. Rev. A* **91**, 043814 (2015). Copyright (2015) by the American Physical Society.
- (f) *Entangled light from driven dissipative microcavities*, D. Pagel and H. Fehske, *Phys. Rev. A* **92**, 022342 (2015). Copyright (2015) by the American Physical Society.

Conferences and Workshops

- (a) *Equilibration of the harmonic oscillator from non-thermal initial states*, •D. Pagel, A. Alvermann, and H. Fehske, poster at the DPG Spring Meeting, Dresden, 2011
- (b) *Equilibration and thermalisation of the harmonic oscillator from non-thermal initial states*, •D. Pagel, A. Alvermann, and H. Fehske, poster at the International Conference on Correlation Effects in Radiation Fields (CERF), Rostock, 2011
- (c) *Strong bipartite and multipartite entanglement from planar microcavities*, •D. Pagel, H. Fehske, J. Sperling, and W. Vogel, poster at the DPG Spring Meeting, Regensburg, 2013
- (d) *Dissipative dynamics and energy transfer of a harmonic oscillator coupled to non-thermal baths*, •D. Pagel, A. Alvermann, H. Fehske, P. Nalbach, and M. Thorwart, talk at the DPG Spring Meeting, Dresden, 2014

- (e) *Computing the Markovian dynamics of periodically driven systems*, •D. Pagel, A. Alvermann, and H. Fehske, talk at the DPG Spring Meeting, Berlin, 2015

Erklärung

Hiermit erkläre ich, dass diese Arbeit bisher von mir weder an der Mathematisch-Naturwissenschaftlichen Fakultät der Ernst-Moritz-Arndt-Universität Greifswald noch einer anderen wissenschaftlichen Einrichtung zum Zwecke der Promotion eingereicht wurde. Ferner erkläre ich, dass ich diese Arbeit selbständig verfasst und keine anderen als die darin angegebenen Hilfsmittel und Hilfen benutzt und keine Textabschnitte eines Dritten ohne Kennzeichnung übernommen habe.

(Daniel Pagel)

Greifswald, 7. Juli 2015

Acknowledgement

Over the past four years I have received support and encouragement from a great number of individuals. I extend my deepest gratitude to Prof. Dr. Holger Fehske for his support over the past years as I moved from an idea to a completed study. Dr. Andreas Alvermann has been a mentor, colleague, and friend. His guidance has made this a thoughtful and rewarding journey. My special appreciation belongs to Dr. Jan Sperling for his friendship and feedback on various aspects of this project. I wish to express my sincere thanks to all of the work group members for their help and support. I would like to thank Dr. Thomas Meyer and Jens Schleede for their patience in the face of diverse numerical and technical obstacles. During writing my colleges Dr. Marc Bogaczyk, Dr. Hans Höft, and Dr. André Schella spent numerous hours listening to me talk about my research. Finally, I wish to thank my family for the unceasing encouragement, support and attention.